Alma Mater Studiorum – Università di Bologna

DOTTORATO DI RICERCA IN

Scienze Biotecnologiche e Farmaceutiche

Ciclo XXXII

Settore Concorsuale: 05/G1

Settore Scientifico Disciplinare: BIO/14

UNRAVELING THE PATHOPHYSIOLOGICAL MECHANISMS OF VISCERAL PAIN IN THE MURINE MODEL OF FABRY DISEASE

Presentata da: Martina Masotti

Coordinatore Dottorato

Chiar.ma Prof.ssa Maria Laura Bolognesi

Supervisore

Prof. Marco Caprini

Esame finale anno 2020

INDEX

ABBREVIATIONS 1
SUMMARY 7
1 INTRODUCTION 9
1.1 Fabry Disease 9
1.1.1 Etiology 9
1.1.1.1 GLA gene 9
1.1.1.2 Structure and function of α-Galactosidase A 10
1.1.1.3 Globotriaosylceramide 3 13
1.1.2 Epidemiology 14
1.1.3 Inheritance 14
1.1.4 Diagnosis 15
1.1.5 Clinical manifestations of Fabry disease 16
1.1.5.1 Classic phenotype 16
1.1.5.2 Atypical variants 19
1.1.6 Therapies for Fabry disease 19
1.1.6.1 Enzyme Replacement Therapy 19
1.1.6.2 Pharmacological Chaperone Therapy 21
1.1.6.3 Substrate reduction therapy 21
1.1.6.4 Gene therapy 22
1.1.7 A murine model of Fabry disease: the α-Galactosidase A knock-out mouse 23
1.2 The gastrointestinal system 26
1.2.1 Gross anatomy of human and murine lower gastrointestinal tract 27
1.2.2 Histology of human and murine lower gastrointestinal tract 28
1.2.3 The Enteric Nervous System 31
1.2.3.1 Organization of neural pathways 31
1.2.3.1.1 The intrinsic innervation of the gastrointestinal tract 32
1.2.3.1.1.1 The enteric plexi 32
1.2.3.1.1.2 Gastrointestinal wall innervation 33
1.2.3.1.2 The extrinsic innervation of the gastrointestinal tract 34
1.2.3.1.2.1 Vagal innervation 34
1.2.3.1.2.2 Thoracolumbar innervation 37
1.2.3.1.2.3 Pelvic innervation 38
1.2.3.2 Functionally defined enteric neurons 38
1.2.3.2.1 Intrinsic Primary Afferent Neurons 39

1.2.3.2.2 Motor neurons ... 40
1.2.3.2.3 Interneurons ... 41
1.2.3.3 Gatrointestinal pain: visceral nociception and hypersensitivity ... 41
1.2.3.3.1 Transient Receptor Potential channels: the role as molecular sensors ... 42
1.2.3.3.1.1 TRPV1 ... 44
1.2.3.3.1.2 TRPV4 ... 45
1.2.3.3.1.3 TRPA1 ... 46
1.2.3.3.1.4 TRPM8 ... 46
1.2.3.3.2 Evaluation of visceral sensitivity ... 47
1.2.3.4 Enteric Glial Cells ... 49
1.3 Gastrointestinal symptoms of Fabry disease ... 51
1.3.1 Correlation between non-specific gastrointestinal symptoms and Fabry disease ... 52
1.3.2 Pathophysiology of Fabry disease gastrointestinal symptoms ... 53
2 AIM ... 56
3 MATERIALS AND METHODS ... 58
3.1 Animals and maintenance ... 58
3.2 Genotyping ... 58
3.3 Tissue collection and sample preparation ... 60
4.1 Macroscopic damage assessment of mice colon ... 61
4.2 Histomorphological analysis of mice colon ... 62
4.2.1 Hematoxylin and Eosin staining ... 62
4.2.2 Immunohistochemical analysis ... 62
4.2.3 Immunofluorescence analysis ... 63
4.3 Data acquisition and evaluation ... 64
4.3.1 Microscopic damage assessment ... 64
4.3.2 Evaluation of myenteric plexus area and nuclear density ... 65
4.3.3 Evaluation of Gb3 accumulation and PGP9.5-Gb3 colocalization ... 65
4.3.4 Evaluation of mucosal nerve fiber density ... 66
4.3.5 Analysis of PGP9.5/NF-L colocalization ... 66
4.4 Determination of serum cytokine levels ... 66
4.5 Assessment of colon sensitivity by colorectal distension ... 67
4.5.1 Evaluation of the VisceroMotor Response and intraluminal pressure ... 67
4.5.2 Evaluation of the Abdominal Withdrawal Reflex ... 68
4.6 Statistical analysis ... 70
4.7 Primary cultures of enteric nervous system cells ... 71
4.7.1 Animals and maintenance ... 71
4.7.2 Primary cell cultures of Enteric Nervous System from mouse embryos ... 71

4.7.2.1 Mice breeding and embryos collection 71
4.7.2.2 Dissection of embryos intestines 71
4.7.2.3 Mechanical dissociation and enzymatic digestion of embryos intestines 72
4.7.2.4 Cell plating and maintenance 72
4.7.3 Primary cell cultures of enteric neurons from mouse embryos 72
4.7.3.1 Plating of embryonic enteric glial cells derived from rat 72
4.7.3.2 Coating of coverslips 73
4.7.3.3 Cell plating and maintenance 73
4.7.4 Enteric Glial Cell cultures derived from adult mouse 73
4.7.4.1 Coating of plates 73
4.7.4.2 Intestine collection 74
4.7.4.3 Dissection 74
4.7.4.4 Mechanical dissociation and enzymatic digestion 74
4.7.4.5 Ganglia collection and glial cell expansion 75
4.7.5 Immunofluorescence staining 75
4.7.6 Data acquisition 76
5 RESULTS 77
5.1 Genotyping of α-Gal A (+/0) and α-Gal A (-/0) mice 77
5.2 Macroscopic and microscopic damage assessment in α-Gal A (-/0) mice colon 78
5.3 Determination of serum cytokine levels in α-Gal A (-/0) mice 79
5.4 Evaluation of myenteric plexus area and nuclear density in α-Gal A (-/0) mice colon 79
5.5 Evaluation of PGP9.5 and NF-L co-localization 81
5.6 Evaluation of Gb3 deposits in α-Gal A (-/0) mice colon 83
5.7 Evaluation of mucosal nerve fiber density in α-Gal A (-/0) mice colon 85
5.8 Assessment of colon sensitivity of α-Gal A (-/0) mice by colorectal distension 87
5.9 Evaluation of TRPV1, TRPV4, TRPA1 and TRPM8 expression in α-Gal A (-/0) and α-Gal A (+/0) mice colon: optimization of IF protocols 90
5.10 Primary cultures of enteric nervous system cells: optimization of protocols 94
5.10.1 Primary cell cultures of Enteric Nervous System from E14 mouse embryos intestine 94
5.10.2 Primary cell cultures of enteric neurons from E14 mouse embryos intestine 96
5.10.3 Enteric Glia Cells cultures from adult mouse intestine 98
6 DISCUSSION 101
7 REFERENCES 111

ABBREVIATIONS

5-HT, 5-hydroxytryptamine, serotonin

Ach, acetylcholine

AF, Alexa fluor

AITC, allyl isothiocyanate

ANOVA, analysis of variance

ANS, autonomic nervous system

APPI-MS, atmospheric pressure photoionization-mass spectrometry

AraC, cytosine arabinoside

ASIC, acid sensing ion channel

ATP, adenosine triphosphate

AUC, area under the curve

AWR, abdominal withdrawal reflex

BCR, B-cell receptor

bp, base pairs

BSA, bovine serum albumin

CD, Chron's disease

CD77, globotriaosylceramide 3

CGRP, calcitonin gene-related peptide

ChAT, choline acetyltransferase

CHO, chinese hamster ovary mammalian cells

CNS, central nervous system

CRD, colorectal distension

C-terminal, carboxy-terminal

CV, coefficient of variation

Cy, cyanine dyes

DAB, 3,3-diaminobenzidine tetrahydrochloride

DAPI, 4′,6-diaminobenzidine-2-phenylindole

DIV, day in vitro

DMEM, Dulbecco's modified Eagle's medium

DNA, deoxyribonucleic acid

dNTPs, deoxynucleotide triphosphates

DRG, dorsal root ganglia

DSS, dextran sulfate sodium

E, embryonic day

EDTA, ethylenediaminetetraacetic acid

EGCs, enteric glial cells

EMG, electromyographic

ENS, enteric nervous system

EPANs, extrinsic primary afferent neurons

EQ-5D, EuroQoL five-dimension

ER, endoplasmic reticulum

ERT, enzyme replacement therapy

ESCs, embryonic stem cells

EtBr, ethidium bromide

Fab, fragment antigen-binding

FBS, fetal bovine serum

FD, Fabry disease

FDA, US Food and Drug Administration

FGIDs, functional gastrointestinal disorders

GALT, gut-associated lymphoid tissue

Gb3, globotriaosylceramide 3

GFAP, glial fibrillary acidic protein

GFR, glomerular filtration rate

GI, gastrointestinal

GLA, alpha-Galactosidase A gene

GPCRs, G-protein-coupled receptors

GSLs, glycosphingolipids

GVC, Ganciclovir

H&E, hematoxylin and eosin

HBSS, Hank's balanced salt solution

HEPES, 4-(2-hydroxyethyl)-1-piperazineethanesulfonic acid

HRLM, high-resolution light microscopy

HRP, horseradish peroxidase

HR-QoL, health-related quality of life

IBD, inflammatory bowel disease

IBS, irritable bowel syndrome

ICCs, interstitial cells of Cajal

IEB, intestinal epithelial barrier

IENFD, intra-epidermal nerve fiber density

IF, immunofluorescence

IFNγ, interferon gamma

IGLEs, intraganglionic laminar endings

IHC, immunohistochemistry

IL, interleukin

IMAs, intramuscular arrays

IPANs, intrinsic primary afferent neurons

kb, kilobase

kDa, kilodalton

KO, knock-out

L-Glu, L-Glutamine

LM/MP, longitudinal muscle/myenteric plexus

LSDs, lysosomal storage diseases

lyso-Gb3, globotriaosylsphingosine

M6PR, mannose-6-phosphate receptor

MALDI-TOF, Matrix Assisted Laser Desorption Ionization Time-of-Flight

MAP2, microtubule-associated protein 2

MMC, migrating myoelectric complexes

mRNA, messenger RNA

NC, neuronal crest

NeoR, Neomycin resistance

NFD, nerve fiber density

NF-L, neurofilament light polypeptide

NF-κB, nuclear factor kappa B

NO, nitric oxide

NOS, nitric oxide synthases

N-terminal, amino-terminal

OCT, optimal cutting temperature

PAR2, protease activated receptor 2

PBS, phosphate-buffered saline

PCR, polymerase chain reaction

PCT, pharmacological chaperone therapy

PE, phycoerythrin

PFA, paraformaldehyde

PGP9.5, protein gene product 9.5

PNS, peripheral nervous system

PS, Penicillin and Streptomycin

RNA, ribonucleic acid

ROI, region of interest

RT, room temperature

S100β, S100 calcium-binding protein beta

SEM, standard error of mean

SFN, small fiber neuropathy

SNPs, single nucleotide polymorphism

SOM, somastatin

Sox10, SRY-related HMG-box 10 transcription factor

SP, substance P

STC, slow transit constipation

TAE, tris base, acetic acid, EDTA

TEM, transmission electron microscopy

TK, thymidine kinase

TLR, Toll-like receptor

TNBS, 2,4,6-trinitrobenzene sulfonic acid

TNFα, tumor necrosis factor alpha

Tris, tris(hydroxymethyl)aminomethane

TRPA, transient receptor potential ankyrin

TRPC, transient receptor potential canonical or classical

TRPM, transient receptor potential melastatin

TRPP, transient receptor potential polycystin

TRPs, transient receptor potential channels

TRPV, transient receptor potential vanilloid

Tuj-1, beta III Tubulin

UC, ulcerative colitis

VHS, visceral hypersensitivity

VIP, vasoactive intestinal peptide

VMR, visceromotor response

VtS, verotoxins

WT, wild-type

α-Gal A (-/0), hemizygous male mouse for α-Gal A gene deletion, knock-out mouse

α-Gal A (+/0), hemizygous male mouse for α-Gal A gene, wild-type mouse

α-Gal A, alpha-Galactosidase A enzyme

α-SMA, alpha-smooth muscle actin

SUMMARY

Fabry disease (FD) is a rare, progressive, multi-organ, X-linked inherited, metabolic storage disorder characterized by a deficient or absent activity of the lysosomal enzyme α-Galactosidase A (α-Gal A). This deficiency causes a progressive accumulation of glycosphingolipids (GSLs), primarily globotriaosylceramide 3 (Gb3), in nearly all organ systems. Gastrointestinal (GI) symptoms are among the earliest and most frequent symptoms of FD, affecting the half of adults and up to 60% of children. Registry data from the Fabry Outcome Survey show that a severe and debilitating abdominal pain is the most common GI complaint, being experienced by up to one third of patients. It has been hypothesized that the pathophysiological mechanisms accounting for GI symptoms of FD are mainly three: dysfunction of the autonomic nervous system (ANS) responsible for gut motility, vasculopathy affecting GI circulation, and tissue inflammation related to Gb3 accumulation. However, the pathophysiology of these symptoms is complex and multifactorial and the exact mechanisms of pain perception and the structural/functional modifications occurring in the GI wall are still poorly understood. The α-Gal A (-/0) mouse, the murine model of FD, has already provided proof to be a useful and reliable model to study FD neuropathy, suggesting that it could be a good model also for investigating visceral pain. In this study, we aim at understanding the molecular mechanisms underpinning the GI symptoms of FD. For this purpose, we used the α-Gal A (-/0) male mouse to characterize anatomical, morphological and molecular features of the colon tract. Our results show that α-Gal A (-/0) mice display a thickening of the colonic muscular layer compared to controls, even if no other macroscopic and microscopic sign of inflammation was detected. We demonstrated that this increase is due to a hypertrophic state of myenteric plexus ganglia, caused by a severe accumulation of Gb3 in myenteric neurons. In addition, we displayed that α-Gal A (-/0) mice present a decreased density of mucosal nerve fibers, which are also more fragmented, scattered and swelled, compared to α-Gal A +/0 controls. Furthermore, we assessed colon sensitivity of α-Gal A (-/0) mice by studying the visceromotor response (VMR), the abdominal withdrawal reflex (AWR) and the intraluminal pressure in response to colorectal distension (CRD). α-Gal A (-/0) mice resulted to present visceral hyperalgesia, by showing greater VMR values and obtaining higher AWR scores. Conversely, we did not reveal differences in terms of intraluminal pressure between α-Gal A (-/0) and α-Gal A (+/0) mice. Subsequently, we optimized the IF protocols to stain transient receptor potential (TRP) cation channel subfamily V member 1 (TRPV1), TRPV4, TRPA1 and TRPM8 pain-related ion channels in the α-Gal A (-/0) and α-Gal A (+/0) mice colonic wall. Their immunoreactivity was detected at level of myenteric and submucosal plexus ganglia. Nevertheless, further studies are required to assess the presence of differences in terms of molecular and functional expression between

α-Gal A (-/0) and α-Gal A (+/0) mice. Finally, we optimized the protocols to obtain three different types of primary cultures from mouse intestine: a mixed culture containing both enteric neurons and glia, a co-culture system with enteric glial cells (EGCs) which allow to obtain an enriched culture of enteric neurons, and finally, an enriched culture of EGCs. In summary, we revealed alterations that are likely to be part of the pathophysiological causes at the basis of gut motor dysfunctions experienced by FD patients, and that imply the α-Gal A (−/0) male mouse represents a reliable model for translational studies on visceral pain and GI symptoms in FD. Moreover, we have provided the optimization of useful protocols for the molecular and functional analysis of α-Gal A (−/0) mice enteric nervous system (ENS) cells. Therefore, together with further studies, this work could help identify new therapeutic targets for the treatment of visceral pain in FD.

1 INTRODUCTION

1.1 Fabry Disease

1.1.1 Etiology

FD is a rare, X-linked genetic, progressive and multisystem disorder caused by mutations in the GLA gene, which encodes for the lysosomal enzyme acid hydrolase α-Gal A, enzyme involved in GSLs catabolism (Brady et al., 1967; Kint, 1970). The first description of FD was made in 1898. Working independently of each other, William Anderson and Johannes Fabry described patients with "angiokeratoma corporis diffusum", the red-purple maculopapular skin lesions that are now recognized as a characteristic feature of the disorder (Anderson, 1898; Fabry, 1898). Alterations of the GLA gene product, caused mostly by single amino acid substitutions, leads to its early degradation within the endoplasmic reticulum and inhibit the intracellular trafficking of the enzyme to the destination organelle, the lysosome (Ishii et al., 2007). This leads to a decrease or even complete absence of enzymatic activity. The α-galactosidase deficiency results in a progressive accumulation, in the affected cells and in body fluids, of GSLs, mainly of Gb3, a neutral GSL involved in cellular signalling, as well as its deacylated and soluble derivative globotriaosylsphingosine (lyso-Gb3) (Duve, 1975). The pathophysiological alterations of tissues associated with Gb3 and lyso-Gb3 accumulation lead to the manifestations of FD in many organ systems, including the heart, kidneys, skin, nervous and GI system (Germain, 2010).

1.1.1.1 GLA gene

The GLA gene has been mapped to the region q22.1 of the X chromosome (Figure 1) (Bishop et al., 1988). The coding part of the gene consists of 1290 base pairs (bp), is divided into eight exons, ranging in size from 92 to 291 bp, and encodes a polypeptide of 429 amino acids (Kornreich et al., 1990). Newborn screenings revealed a high number of abnormal variants of GLA gene, resulting in the wide variability of FD in terms of symptoms and penetrance (Spada et al., 2006; Wittmann et al., 2012). Indeed, over 900 mutations of different type have been reported in GLA gene, the majority of which make the enzyme non-functional (Figure 2) (Human Gene Mutation Database (HGMD) at the Institute of Medical Genetics in Cardiff, Public database, GLA gene, 2017; Gal, 2010; Stenson et al., 2017). Missense mutations are the most common type in GLA gene and they have been classified in three groups: 1) mutations that alter the active site of the enzyme by changing residues that either form the active centre itself or are essential for its correct three-dimensional structure; 2) buried mutations that affect residues which are distant from the active site and influence the folding and stability of the protein; 3) mutations that do not fall into either of the above categories, although their

negative effect on the catabolic function of the molecule is clear (Garman and Garboczi, 2004). For example, it has been reported that the disruption of an important disulphide bond, caused by an amino acid substitution (Cysteine 56 is replaced by Glycine, Phenylalanine, or Tyrosine), leads to the loss of enzymatic activity. Similarly, the elimination of an *N*-carbohydrate attachment site, due to a mutation in the signal sequence (Asparagin 215 is replaced by Serine), affects the correct secretion of the protein (Garman and Garboczi, 2004).

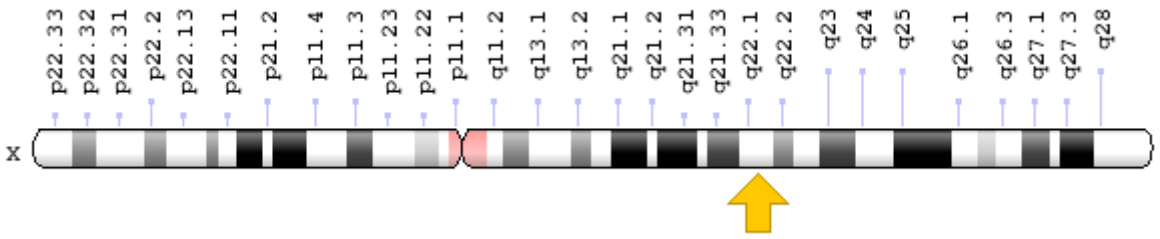

Figure 1. Locus of GLA gene on the X chromosome. The image shows the structure of the short (*p*) and long (*q*) arms of X chromosome, which is divided in different regions and chromosomal bands (*numbers*). The GLA gene is located in the locus q22.1 of the long arm of the X chromosome (*yellow arrow*), in particular in the region 2, band 2, sub-band 1. From National Institute of Health (NIH), Genetics home reference, GLA gene, 2019.

Mutation type	Number of mutations	Mutation data by type (register
Missense/nonsense	533	Get mutations
Splicing	36	Get mutations
Regulatory	4	Get mutations
Small deletions	110	Get mutations
Small insertions	38	Get mutations
Small indels	11	Get mutations
Gross deletions	31	Get mutations
Gross insertions/duplications	4	Get mutations
Complex rearrangements	6	Get mutations
Repeat variations	0	No mutations
Get all mutations by type		Available to subscribers QIAGEN
Public total (HGMD Professional 2019.1 total)	**773** (967)	

Figure 2. Known mutations of GLA gene. The figure lists the known mutations of the GLA gene (967) by type: missense/nonsense, splicing, regulatory, small deletions, small insertions, small indels, gross deletions, gross insertions/duplications, complex rearrangements, repeat variations. From The Human Gene Mutation Database (HGMD) at the Institute of Medical Genetics in Cardiff website, Public database, GLA gene, 2017.

1.1.1.2 Structure and function of α-Galactosidase A

Alpha-Gal A is a lysosomal enzyme that catalyses the removal of galactose residues from oligosaccharides, glycoproteins and glycolipids during the catabolism of macromolecules (Figure 3). In Fabry patients, the absence of functional α-Gal A causes to the accumulation of galactosylated

substrates, primarily Gb3, in many cellular compartments such as lysosomes, endoplasmic reticulum (ER), cell membrane and nucleus (Askari et al., 2007) in several cell types, such as capillary endothelial cells, renal (podocytes, tubular cells, glomerular endothelial, mesangial and interstitial cells), cardiac (cardiomyocytes and fibroblasts) and neuronal cells (Desnick et al., 2001). Alpha-Gal A is synthetized as a pre-pro-protein. Generally, the prefix "pre" indicates the presence of sequences that act as leader (signal peptide), needed for protein sorting (or targeting), whereas the prefix "pro" suggests the presence of sequences required for the folding of pro-protein. The pre-pro-protein is moved to the double phospholipids layer of rough endoplasmic reticulum, where the loss of the signal peptide leads to the formation of the pro-protein, which moves to the smooth endoplasmic reticulum, where a group of different molecular chaperones determines its correct folding (Bekri, 2006). Subsequently, the precursor reaches the Cis-Golgi, where undergoes several post translational modifications, such as glycosylations, phosphorylations and sulphations, which are requested for the protein correct folding and targeting to the lysosomes (Ioannou et al., 1992). This process, which results in the formation of the mature protein (101 kDa), requires several days after synthesis (Bishop and Desnick, 1981; Lemansky et al., 1987).

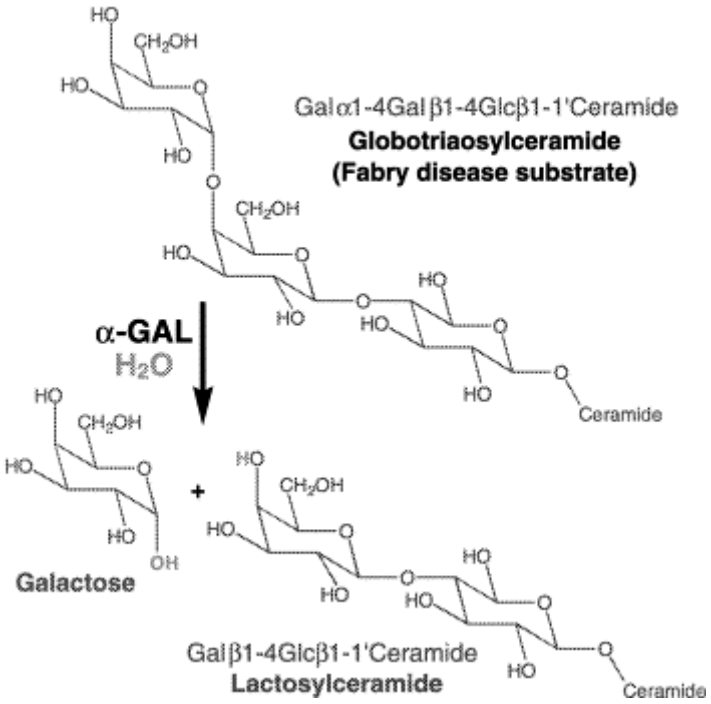

Figure 3. The enzymatic reaction catalysed by α-Gal A. Physiologically, Gb3 is cleaved by α-Gal A to form lactosylceramide and galactose. In FD, this reaction is prevented by the lack or decrease of α-Gal A activity, which leads to Gb3 accumulation in lysosomes and other cellular compartments. From Garman and Garboczi, 2004.

The structure of α-Gal A was determined by X-ray crystallography (Garman and Garboczi, 2004). As shown in Figure 4, the mature protein is a homodimeric glycoprotein in which each monomer is composed of two domains:

- eight β/α domains containing the active site;
- C-terminal domain containing eight antiparallel β strands assembled in two sheets forming a β sandwich.

Human α-Gal A contains three sites of glycosylation: N139, which is generally associated with complex carbohydrates, N192 and N215 (Ioannou et al., 1998). Since oligomannosyl carbohydrates contain mannose-6-phosphate, the lysosomal targeting signal, N-linked carbohydrates at N192 and N215 are responsible for targeting the glycoprotein to lysosomes (Ghosh et al, 2003). Indeed, mutation of N215 to Serine eliminates the carbohydrate attachment site, leading to an unsuccessful trafficking of the enzyme to lysosomes (Ioannou et al., 1998).

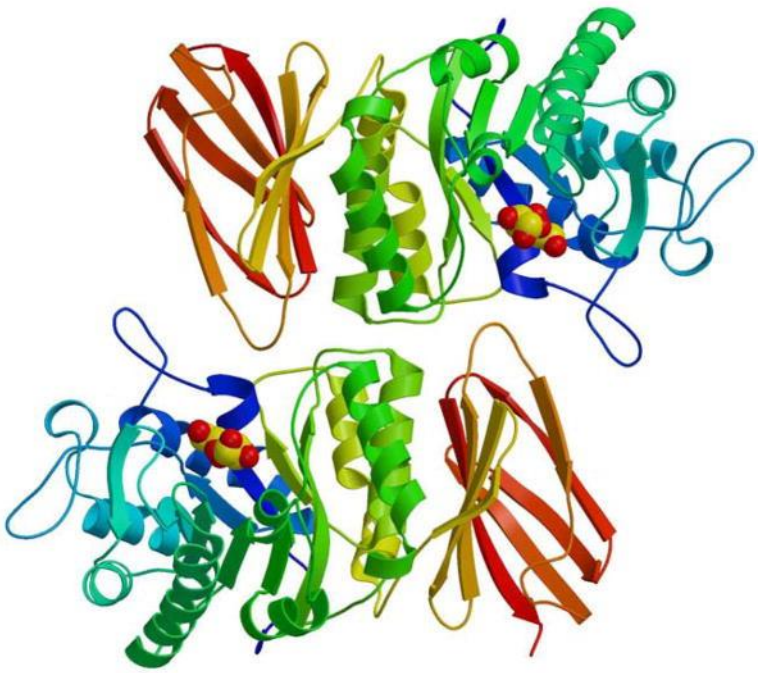

Figure 4. The structure of α-Gal A. The structure of the human α-Gal A is shown in ribbon representation. *N*- and *C*-terminals are displayed in *blue* and *red*, respectively. The active site is identified by the catalytic product galactose, represented in sphere Corey-Pauling-Koltun (CPK) format. The mature protein is a homodimeric glycoprotein, with each monomer containing two domains, a $(\beta/\alpha)_8$ barrel containing the active site (*blue to yellow*) and a *C*-terminal antiparallel β domain (*yellow to red*). From Garman, 2007.

1.1.1.3 Globotriaosylceramide 3

Gb3, also known as CD77 or trihexosylceramide, is a globoside belonging to the GSLs, a subtype of glycolipids (Adlercreutz et al., 2010). GSLs are a heterogeneous class of amphipathic compounds characterized by complex glycan structures linked to a ceramide backbone by a β-glycosidic bond and they are the most represented class of glycolipids in cells (Merrill Jr, 2011). It has been established that even if GSLs are dispensable for cellular life (Ichikawa et al., 1994), they are indeed collectively required for the development of multicellular organisms (Figure 5) (Yamashita et al., 1999), by modulating membrane-protein function and contributing to cell-cell communication (D'Angelo et al., 2013). For several GSLs, modulatory effects on specific plasma membrane receptors have been displayed, demonstrating their involvement in environment "sensing" and in cell identity establishment/maintenance (Hakomori, 2008). Indeed, it has been displayed that Gb3 is present on the cell surface, with the two hydrocarbon chains of the ceramide moiety embedded in the plasma membrane and the oligosaccharides located on the extracellular surface, where they present points of recognition for extracellular molecules or surfaces of neighboring cells (Bekri et al., 2006).

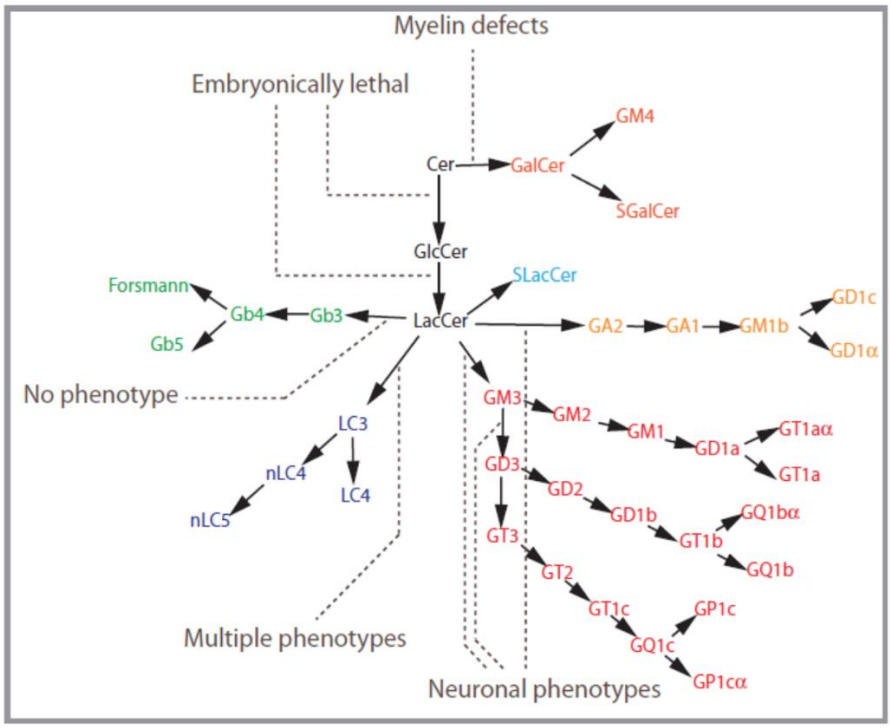

Figure 5. Scheme of GSLs metabolism. The image shows the different GSLs pathways: globo series GSLs (*green*); lacto/neolacto series GSLs (*blue*); ganglio series GSLs (*red*); asialo series GSLs (*light orange*); gala series GSLs (*dark orange*). The phenotypic consequences of different genetic manipulations of GSL synthetic pathway in mice are also indicated. Metazoan and especially vertebrates need GSLs to correctly complete their development, even if ablation of significant subparts of the GSL synthetic pathways causes milder phenotypes in animal models. This is thought to be due to a compensatory potential of the remaining GSLs, but it was also suggested to be the consequence of involvement of those GSLs in very specific physiological roles. Modified from D'Angelo et al., 2013.

Gb3 is also expressed on B cells, where it plays a role as a regulator of B-cell receptor (BCR)-mediated apoptosis in human B cells (Mangeney et al., 1991; Taga et al., 1997). Gb3 is known for being the receptor of verotoxins (VTs), members of the bacterial shigatoxin family expressed by some bacterial serotypes of Escherichia coli and Shigella dysenteriae (Frankel et al., 2000). Moreover, Gb3 has also been found to be expressed on the cell surface in some malignant tumours such as colorectal adenoma, Burkitt's lymphoma, breast cancer and testicular carcinoma (Hakomori, 2001; Kovbasnjuk et al., 2005; Mangeney et al., 1993; Johansson et al., 2009; Kang et al., 1995). It is noteworthy that, as observed by Kovbasnjuk and colleagues, there is a correlation between Gb3 and metastasis in colorectal adenoma. Indeed, normal human colonic epithelial cells lack Gb3 expression whereas colon cancer cells overexpress it (Kovbasnjuk et al., 2005).

1.1.2 Epidemiology

The incidence of FD is underestimated due to the rarity and high variability of symptoms and their manifestations. For this reason, diagnosis is often delayed. Recent data on cohorts of male patients indicate an incidence of approximately 1:17000 to 1:117000 depending on the cohort of patients, which is a wide range (Bokhari et al., 2019). Classic FD mutations have been seen in approximately 1:22000 to 1:40000 males and atypical presentations have been associated with about 1:1000 to 1:3000 males and 1:6000 to 1:40000 females (Bokhari et al., 2019). The disease has been diagnosed in all racial and ethnic groups. In Italy, for example, Spada and co-workers (2006) used enzymatic diagnosis on dried blood spots in three pilot studies (Spada et al., 2006). The results showed that the prevalence of the disease is approximately 1:3100 in males. In Australia the prevalence of FD have been displayed to be 1:4100 in males (Mechtler et al., 2012), whereas in Taiwan ranges from 1 in 1250 to 1 in 4000 in two different cohorts (Hwu et al., 2009; Lin et al., 2009). In Austria it resulted to be 1 in 3000 males, whereas in USA 1 in 7800 males in the state of Washington and 1 in 2900 males in Missouri (Hopkins et al., 2015).

1.1.3 Inheritance

FD is an X-linked disorder, neither recessive nor dominant (Happle, 2006). Whereas in males one altered copy of the gene in each cell is sufficient to cause disease onset, in female patients this is not always true. Heterozygous females show a high penetrance, with at least 70% of patients displaying the disease symptoms (Dobyns, 2006). This is due to the X-chromosome inactivation process, which is known as lyonization, which leads females to show a mosaic of cells expressing genes from maternal origin or paternal origin (Lyon, 1961). For this reason, it may no longer be appropriate to define FD as a "recessive disease" and heterozygous female patients as "carriers", but it could be

preferable to define FD as a genetic disorder which follows an "X-linked inheritance" (Germain, 2006; Germain et al., 2010).

1.1.4 Diagnosis

FD symptoms heterogeneity makes diagnosis very difficult. All clinical manifestations need biochemical and genetic confirmation (Linthorst et al., 2005). The measurement of α-Gal A activity and the genetic test are the two most used procedures for FD diagnosis. Enzymatic activity is usually measured in plasma, leukocytes or dried blood spots by using the synthetic substrate 4-methylumbelliferyl-α-d-galactopyranoside (Desnick et al., 1973). Blood tests to measure α-Gal A activity are mainly used in males, since these assays have limitations in the diagnosis of females (Gal et al., 2011) (Figure 6). Female patients may have indeed a normal α-Gal A activity. In one study using dried whole blood spots to measure α-Gal A activity, 8 out of 21 females with documented FD had false negative results (Linthorst et al., 2005). For this reason, in female patients, genetic analysis is also needed when the enzyme assays give a negative result. Genetic test is conducted on genomic DNA and total RNA, which can be extracted from peripheral blood leukocytes or cultured skin fibroblasts (Shabbeer et al., 2005). Alpha-Gal A coding regions and adjacent intronic regions are sequenced. Plasma or urinary levels of Gb3 or lyso-Gb3 are important diagnostic biomarkers as well (Auray-Blais et al., 2008; Germain, 2010). FD can also be diagnosed prenatally via cultured amniotic fluid cells and by chorionic villus sampling at 9-10 weeks, or by amniocentesis at approximately 15 weeks (Desnick, 2007).

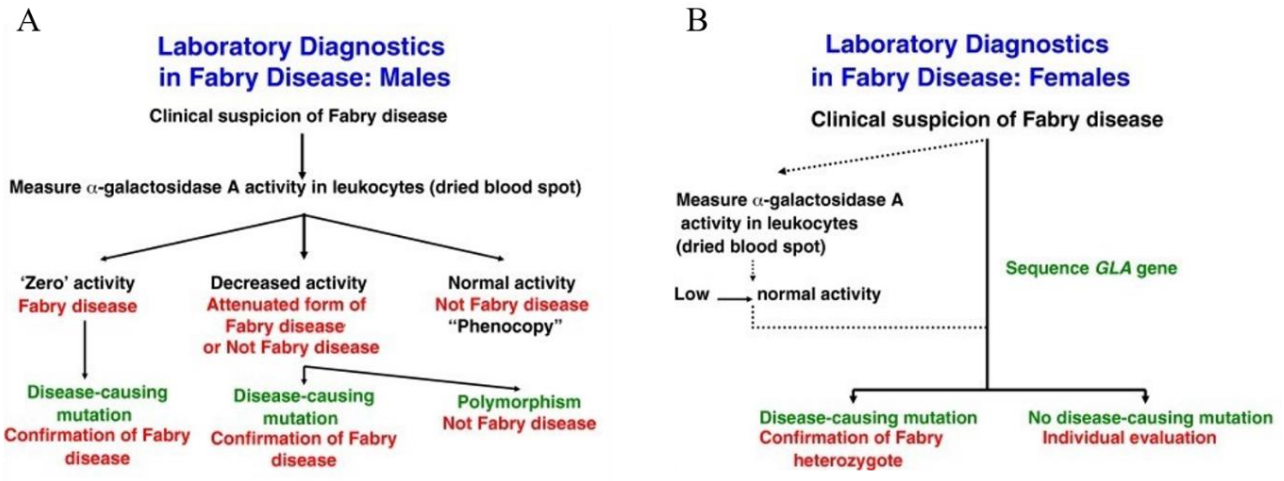

Figure 6. The differential diagnostic process in FD patients. (A) Male with classic FD phenotype can be easily diagnosed based on the absence of α-Gal A activity. (B) Whereas patients with attenuated forms may present considerable residual α-Gal A activity, but still exhibiting levels below the normal range, thus the genetic test can be done to analyse the types of GLA gene mutation/s. In most female patients, DNA sequencing is required when the α-Gal A activity level results normal. Modified from Gal et al., 2011.

There are others approaches for the diagnosis such as the analysis of the tissue glycolipid composition, the use of the atmospheric pressure photoionization mass spectrometry (APPI-MS) for the analysis of Gb3 molecular species and the Matrix Assisted Laser Desorption Ionization Time-of-Flight (MALDI-TOF) imaging of biomarkers, but they are currently used only for research purposes (Hozumi et al., 1990; Delobel et al., 2006; Touboul et al., 2007).

1.1.5 Clinical manifestations of Fabry disease

Lysosomal storage diseases (LSDs) such as FD usually present a wide spectrum of clinical manifestations with high variable severity. For this reason, patients are generally distinguished based on their disease phenotype. The "classic" severe phenotype generally affects males, it targets several organs and is characterized by a low or very little α-Gal A activity. There are also patients who display a residual α-Gal A activity (1-20 % of normal levels) and experience a milder or "later-onset" variant (atypical variants), with manifestations circumscribed mainly to one organ, the heart ("cardiac variant") (Elleder et al., 1990; Nakao et al., 1995) or kidneys ("renal variant") (Nakao et al., 2003). Since homozygous mutations are very rare, the majority of female Fabry patients are generally heterozygous and experience a wide range of symptoms. Because of lyonization, the ratio between normal cells and mutant cells determines the phenotype of the female patient. Nevertheless, heterozygous females may display an unfavorably skewed X inactivation resulting in a high severity of disease manifestations (Morrone et al., 2003; Dobrovolny et al., 2005), which most often associated to heart disease and stroke (Wilcox et al., 2008). Age at onset of symptoms in females is generally older (Wilcox et al., 2008).

1.1.5.1 Classic phenotype

Patients with classical FD display signs and symptoms affecting several organs, and manifestations usually start at early age, during the first 10 ten years of life (Rozenfeld, 2009). One of the earliest symptoms is pain, which is experienced by 60-80% of affected boys and girls (Hopkin et al., 2008; Hoffmann et al., 2007). This has been demonstrated to be due to neuronal damage involving peripheral somatic (Dutsch et al., 2002) and autonomic (Cable et al., 1982) nervous system, with onset occurring at an earlier age in boys than in girls (Hopkin et al., 2008; Ramaswami et al., 2006; Desnick and Brady, 2004; Zarate and Hopkin, 2008). The fingertips, palms, toes, and soles of the feet are the sites commonly affected by pain in FD. However, pain may arise in any body area, such as the joints, teeth, or shoulders (Üçeyler et al., 2014). Two types of pain have been described: episodic crises ("Fabry crises") characterized by agonizing burning pain originating in the extremities and radiating inwards to the limbs and other parts of the body, and chronic pain characterized by burning

and tingling paraesthesias (Charrow, 2009). Fabry crises may last from hours to several days and may be worsened by fever, exercise, fatigue, stress, and rapid changes in temperature (Hilz et al., 2000). Pain may disappear in adulthood, and it is important to search for a medical history of acroparesthesia in childhood in order to diagnose new adult patients (Naleschinski et al., 2009). Neuropathic pain has been recently defined in 2011 as "pain caused by a lesion or disease of the somatosensory system" (the system allowing for the perception of touch, pressure, pain, temperature, position, movement and vibration) (Colloca et al., 2017). In FD patients, pain is thought to be predominantly neuropathic, because of its commonly reported neuropathic features and reports of Gb3 deposits in the dorsal root ganglion (DRG) neurons, which may induce the frequently experienced "shooting pains" (Kahn, 1973; Gadoth and Sandbank, 1983). Patients present a predominantly length-dependent decrease in the density of small, thinly myelinated Aδ nerve fibers (mediating pricking pain, cold perception) and unmyelinated C nerve fibers (mediating "slow" pain, warmth, and heat perception) (Liguori et al., 2010; Üçeyler et al., 2013), impairment which correlates well with the increased heat and cold pain perception experienced by FD patients (Hilz et al., 2004; Üçeyler et al., 2013). Recent experimental studies have suggested that some of the spontaneous types of pain in patients with FD may be explained by hyperexcitability of peripheral nociceptive neurons mediated by upregulation of sodium ion channels (Nav1.8), TRPV1 (Lakomá et al., 2014), or a lyso-Gb3-dependent increase in calcium (Ca^{2+}) influx (Choi et al., 2015). GI complaints appear in childhood and, in contrast to pain, remain present during adulthood (Sheth et al., 1981). They include abdominal pain, diarrhea, constipation, bloating, nausea, and vomiting. They may worsen after meals and be cause of anorexia (Hoffmann et al., 2007). This kind of symptoms may be related to the accumulation of Gb3 in the autonomic ganglia of the gut and mesenteric blood vessels (Eng et al., 2006). Since they are really common, GI symptoms of FD are frequently underestimated (Sheth et al., 1981), and when there is no suspicion of the disease in the family, patients are frequently diagnosed as celiac, chronic inflammatory bowel disease, irritable bowel syndrome (IBD), or Crohn's disease, and the correct diagnosis can be delayed for years (Tielemans et al., 2013; Tokuda et al., 2007; Chitkara et al., 2005; Hyams et al., 2000; Cremonini and Talley, 2005). The most visible early clinical feature of FD is angiokeratoma (skin lesions) and clusters of small reddish purple, raised skin lesions, which are typically found on the buttocks, groin, umbilicus and upper thighs. Histologically, they are small superficial angiomas induced by cumulative damage of the vascular endothelial cells of the skin with vessel dilatation in the dermis that increase in number and size with age and can occur singly or in groups (Germain, 2002; Mohrenschlager et al., 2003; Orteu et al., 2007).

Organ system	Sign/Symptom
Nervous system	Acroparesthesias
	Nerve deafness
	Heat intolerance
	Hearing loss, tinnitus
Gastrointestinal tract	Nausea, vomiting, diarrhoa
	Postprandial bloating and pain, early satiety
	Difficulty gaining weight
Skin	Angiokeratomas
	Hypohidrosis
Eyes	Corneal and lenticular opacities
	Vasculopathy (retina, conjunctiva)
Kidneys	Microalbuminuria, proteinuria
	Impaired concentration ability
	Hyperfiltration
	Increased urinary Gb3 excretion
Heart	Impaired heart rate variability
	Arrhythmias
	ECG abnormalities (shortened PR interval)
	Mild valvular insufficiency

Table 1. Early signs and symptoms of Fabry disease. Modified from Germain, 2010.

At skin level, Fabry patients are also characterized by absence of sweating (anhidrosis) (Kang et al., 1987) or a decreased ability to sweat (hypohidrosis) (Orteu et al., 2007), with decreased skin impedance (Gupta et al., 2008) that results in a significant problem because can cause heat (Shelley et al., 1995) and exercise intolerance (Eng et al., 2006; Germain, 2002). Another characteristic feature is represented by corneal changes known as "cornea verticillata", which is rarely of visual significance (Sodi et al., 2006). Early symptoms of cardiac and cerebrovascular abnormalities may be present during adolescence in both males and females. Signs of involvement of the sinus node and conduction system (e.g. shortened PR interval, arrhythmias, impaired heart rate variability, and mild valvular insufficiency) have been demonstrated (Kampmann et al., 2008). Finally, another early clinical sign of FD disease is renal involvement, represented by microalbuminuria and proteinuria developing as early as in the second decade of life (Gubler et al., 1978; Sessa et al., 2001; Tondel et al., 2008). Histologically, potentially irreversible changes to glomeruli, interstitial tubules and vascular structures happen before the first appearance of microalbuminuria in children (Tondel et al., 2008). Podocyte foot process effacement has been reported, indicating focal segmental glomerulosclerosis. A decrease in glomerular filtration rate (GFR) is uncommon at pediatric ages but may occur as early as adolescence (Germain, 2002; Ramaswami et al., 2010). Despite the absence of major organ dysfunction, these symptoms, individually or in combination, may cause significant morbidity limiting children's physical, school and social life (Ries et al., 2005). Psychiatric studies

revealed a high incidence of severe depression (Cole et al., 2007) that is related to the degree to which symptoms interfere with normal life. The main complications of FD are more evident after the age of 30 when kidney, heart and/or cerebrovascular manifestations start (Macdermot et al., 2001). These symptoms are the most frequent cause of death and reduce life expectancy by 20 years, compared with the healthy population (Rozenfeld, 2009). Table 1 summarizes the earliest signs and symptoms of FD classic phenotype.

1.1.5.2 Atypical variants

Atypical variants have few or none of the hallmark symptoms of classical FD, but have manifestations confined predominantly to one organ system (Elleder et al., 1990; von Scheidt et al., 1991). Presenting much later in life (fourth to sixth decades) than patients with classical disease, they are often identified serendipitously. In the cardiac variant, clinical symptoms are limited to heart and present in the sixth or seventh decade of life. This phenotype is characterized by left ventricular concentric hypertrophy and by the lack of angiokeratoma, acroparesthesias, hypohydrosis, or corneal opacities. Patients may display proteinuria, but renal function is generally not affected. Mutations detected in cardiac variant patients are generally missense mutations or intronic alterations that decrease mRNA levels (Nakao et al., 1995). In renal variant, patients experience end-stage renal disease at ages similar to those of patients with classic phenotype, but lack the other classical manifestations. The majority of these cases are initially diagnosed as chronic glomerulonephritis (Nagao et al., 1991).

1.1.6 Therapies for Fabry disease

Different therapeutic approaches have been attempted to treat FD and other LSDs (Parenti et al., 2013). Different strategies were shown to be efficient from a clinical point of view, such as enzyme replacement therapy (ERT), pharmacological chaperone therapy (PCT), substrate reduction therapy and gene therapy. Only ERT and PCT have been approved for clinical use (Germain, 2010; Markham, 2016). Other therapies are still undergoing clinical trials (substrate reduction therapy, gene therapy).

1.1.6.1 Enzyme Replacement Therapy

ERT has been introduced in 2001 as a life-long treatment and it is now the first-line therapy for FD. This approach provides an exogenous source of α-Gal A by replacing the deficient enzyme in cells and thus helping to slow down disease progression (Germain, 2010). The recombinant enzyme expresses the mannose-6-phosphate receptor (M6PR) target, so that it can be picked up by the M6PR expressed on membrane surface and transported to lysosomes by the endocytic pathway (Figure 7) (Parenti et al., 2013).

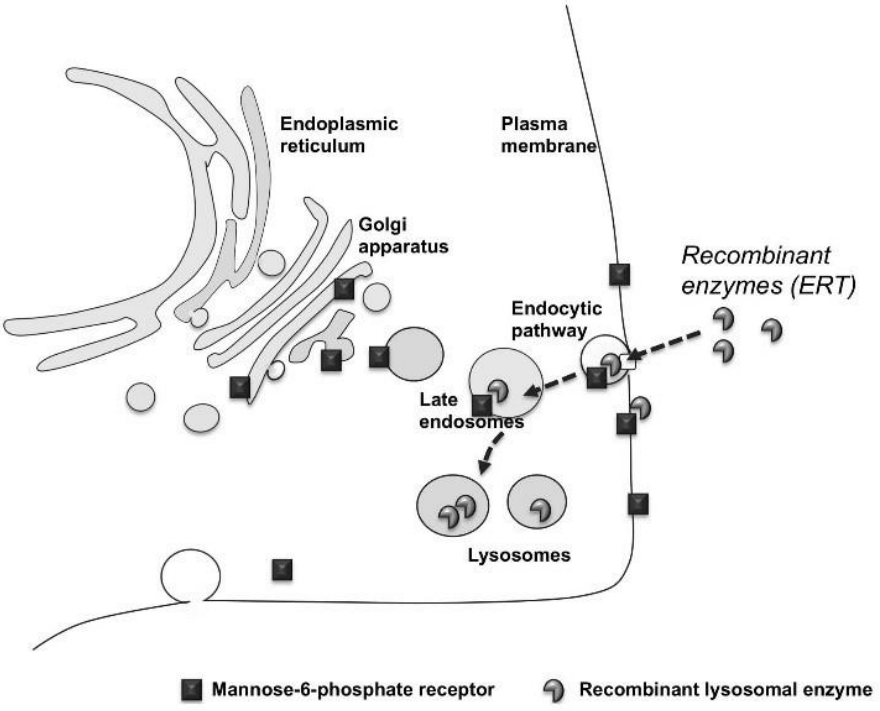

Figure 7. Comprehensive mechanism of ERT action. The recombinant lysosomal enzyme binds to the mannose or M6PR available at the plasma membrane of cells. The enzymes are thus internalized by the cells and delivered to lysosomes through the endocytic route (*dotted lines*). From Parenti et al., 2013.

There are currently two commercially available ERT preparations: agalsidase alfa (Replagal®, Shire HGT, Inc., Cambridge, MA, USA) and agalsidase beta (Fabrazyme®, Sanofi Genzyme, Cambridge, MA, USA) (Lee et al., 2003; Sakuraba et al., 2006). Many studies suggest that the two proteins are biochemically, structurally, and functionally equivalent (Lee et al., 2003), to the extent that no difference in clinical effect has been observed with the same dose (Vedder et al., 2007). ERT is administered by periodical intravenous infusions. The former is given at 0.2 mg/kg body weight every other week and is approved in many countries throughout the world, included European Union, but not by the US Food and Drug Administration (FDA) (Ortiz et al., 2018). The latter is administered at 1.0 mg/kg body weight once every 2 weeks and is approved in Europe, in the USA, and in many other countries (Ortiz et al., 2018). Agalsidase beta is produced by recombinant DNA technology in a Chinese Hamster Ovary (CHO) mammalian cell expression system, whereas agalsidase alfa is produced in human fibrosarcoma cells (Desnick and Schuchman, 2012). Both polypeptides have the same primary structure, but the glycosylation pattern is variable according to cell culture origin. Quality of life of patients receiving ERT is improved. It has been indeed demonstrated that pain, GI (Hoffmann et al., 2007), cardiac (Hughes et al., 2008) and renal (Feriozzi et al., 2009; Germain et al., 2007) manifestations are significantly reduced. The major drawback of this therapy is that neither Agalsidase alfa nor Agalsidase beta have been shown to cross the blood-brain barrier (Burlina and

Politei 2016). Initiation timing is crucial for ERT therapy because some early pathological changes are potentially reversible by ERT (Tøndel et al., 2013). Importantly, the impact of ERT is reduced if extensive irreversible pathological changes (e.g. fibrosis) have already occurred in organs (Weidemann et al., 2013). The importance of early initiation of ERT has been highlighted in treatment guidelines for paediatric patients with FD. ERT is recommended for all symptomatic pediatric patients, regardless of their sex and the severity of their symptoms. Treatment should be considered for asymptomatic boys with classical FD mutations by age 8-10 years. Asymptomatic girls need to have regular, ongoing monitoring that is maintained throughout their lives with clinical vigilance for non-specific signs such as pain and GI signs that could indicate the onset of active disease (Hopkin et al., 2016).

1.1.6.2 Pharmacological Chaperone Therapy

PCT is based on the concept that loss-of-function diseases are often due to missense mutations that cause misfolding (abnormal conformation) of mutant proteins without affecting the catalytic activity. The result is the degradation of the aberrant protein (Parenti et al., 2015). Migalastat, a small-molecule pharmacological chaperone, reversibly binds to the active site of α-Gal A. In patients with FD, migalastat stabilises specific mutant forms of the enzyme helping their folding and promoting their trafficking to lysosomes (Fan et al., 1999; Yam et al., 2005; Benjamin et al., 2009; Germain and Fan, 2009; Khanna et al., 2010; Germain et al., 2016). PCT has several advantages, compared to ERT: it can be administered orally, increasing the compliance of the treatment; PCT is non-immunogenic and would not be expected to have tolerability issues similar to those described for ERT; since it is a small molecule, it can diffuse freely across membranes and reach therapeutic concentrations in different tissues and systems, including brain; it can induce the production of more sustained and stable enzyme levels, mimicking the natural production. However, PCT can be used only for chaperone-responsive mutations (“amenable mutations”) (Parenti et al., 2015).

1.1.6.3 Substrate reduction therapy

This therapy is based on the principle of decreasing the production of the pathologic substrate by inhibiting the glucosylceramide synthase, which catalyses the first step in the synthesis GSLs. This treatment has been evaluated in vitro studies as well as in murine models (Abe et al., 2000; Heare et al., 2006; Brogden et al., 2017) and currently is under investigation in different clinical trials (NIH, ClinicalTrials.gov, Interventional Studies Fabry disease, 2019). This treatment is successful only in patients retaining sufficient levels of functional enzyme (Bruni et al., 2007).

1.1.6.4 Gene therapy

Gene therapy is an attractive strategy for treating patients affected by LSDs, and is commonly viewed as the therapeutic approach with the greatest potential for complete and long-term correction of enzymatic alterations (Sands and Davidson, 2006; Cardone, 2007). Gene therapy is based on the principle of delivering the normal copy of the defective gene that synthesizes the functional enzyme by means of the recipient's cells. LSDs appear to be amenable to this therapy for several reasons. First, these disorders are monogenic; second, if lysosomal enzymes are secreted from a small number of transduced cells they can be taken up, via the M6PR, by adjacent affected cells, thus avoiding the necessity of transferring the gene to all cells; third, even a small increases of enzymatic activity (up to 10%) may be sufficient for clinical benefit and partial phenotypic correction (Parenti et al., 2013). The available strategies are two: *ex vivo* (cell-based delivery) and *in vivo* (direct delivery) gene therapy (Figure 8). The first one consists in the transplantation of transduced stem cells into patients (e.g. bone marrow stem cells).

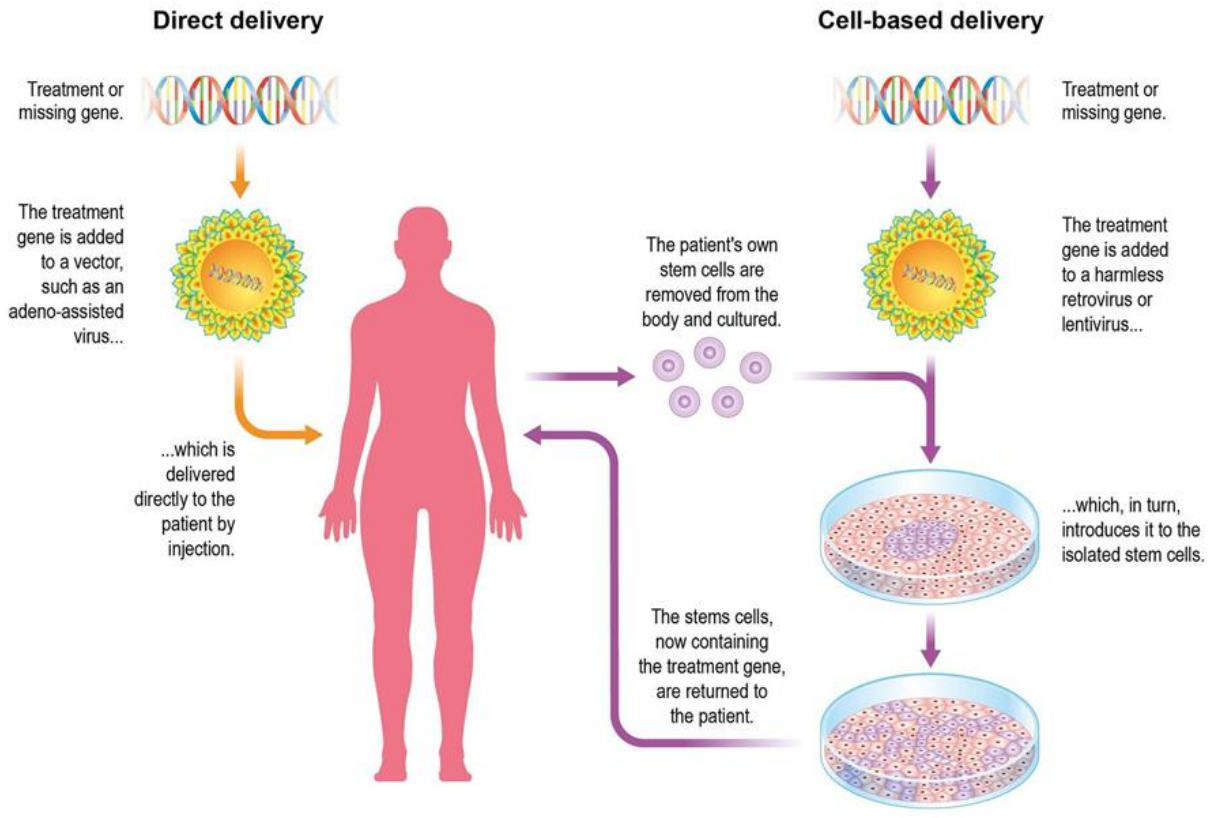

Figure 8. Direct and cell-based delivery of gene therapy. The image displays the *ex vivo* (*right*) and *in vivo* (*left*) strategies for gene therapy. In both of them, the gene of interest is cloned into viral vectors. With direct delivery, the vector is injected into the parenchyma or intravenous system of the patient. With cell-based delivery, patients (or donors) stem cells are isolated, cultured and transduced with the viral vector. Transduced stem cells are finally re-injected into patients. From © Peter Bull Art Studio.

Stem cells are harvested from either donors or patients, transduced *in vitro* with a viral vector (derived from adenoviruses, herpes simplex viruses or adeno-associated virus) to express the therapeutic gene at normal or supra-normal levels, and finally infused into the patients, where they can proliferate and restore the healthy phenotype (Parenti et al., 2013; Penati et al., 2017). The second strategy is based on the injection of the gene transfer vector directly into the tissue or circulation of the patient. (Parenti et al., 2013). Gene therapy is currently under investigation humans with promising results. For example, the lentivirus-mediated gene therapy AVR-RD-01 developed by the company AVROBIO has been recently approved by FDA (From Fabry disease news, 2019), and patients are currently under recruitment for as Phase 2 trial that will assess efficacy and safety of the therapy on classically affected Fabry patients (NCT03454893). The therapy follows the *ex vivo* strategy: patient's hematopoietic stem cells are extracted and genetically modified by adding a functional copy of the GLA gene coding for α-Gal A. The modified cells are then infused back into the patient via a one-time procedure.

1.1.7 A murine model of Fabry disease: the α-Galactosidase A knock-out mouse

As stated before, animal models allow researchers to both study and evaluate biological and behavioural processes and create a suitable model of a disease. Among rodents (rats, mice, gerbils, guinea pigs, and hamsters), mice are the most used because of their genome similarity with humans, availability, ease of handling, high reproductive rate, and relatively low cost of use (Simmons, 2008). In Ohshima et al. (1997) the authors described the generation of the α-Gal knock-out (KO) mouse by using gene targeting. This approach is based on disrupting α-Gal A gene by homologous recombination (Capecchi's method). Neomycin resistance (NeoR) and thymidine kinase (TK) genes were cloned through restriction enzymes digestion into the target gene sequence (GLA gene) in order to replace the target gene and create the targeting vector (Ohshima et al. 1996; Ohshima et al. 1997). 7.5 kb of α-Gal A genomic sequence was subcloned in the pPNT vector, creating the targeting construct (Figure 9). The 1.5 kb of 5′ flanking fragment consisting of *Kpn*I-*Bam*HI fragment, and the 6 kb of *Eco*RI-*Eco*RI fragment were subcloned into *Xho*I site and *Eco*RI site of pPNT, respectively. J1 embryonic stem cells (ESCs) transfection was made by electroporation (24 hours). After 8-10 days, clones of interest were selected by G418 and Ganciclovir (GVC), expanded and analysed. In particular, recombinant ESCs where GLA gene had been KO resulted to be Neo- and GCV-resistant, whereas the cells where a recombination in a wrong place occurred resulted to be Neo-resistant but GCV-sensitive. Genomic DNA from these clones was digested with *Eco*RI and hybridized with 5′ flanking probe isolated from the 0.5 kb of *Sac*I-*Kpn*I fragment. The digestion resulted in 7.5 kb-long fragments for wild-type (WT) alleles and 8 kb-long fragments for the mutated ones. In order to

demonstrate the single integration event, hybridization with neomycin phosphotransferase gene-specific probe (neo probe) was carried out, using the same membrane after stripping the 5′ flanking probe (Ohshima et al., 1996). Targeted ESCs were injected into blastocysts, to give rise to a "mixed" inner cell mass. Blastocysts were then implanted into a surrogate mother where they developed into mosaic embryos. Heterozygous (+/-) female mice for α-Gal A gene deletion were generated by mating male chimeras with C57BL/6 females; hemizygous (-/0) α-Gal A mutant male mice were generated by mating heterozygous females and C57BL/6 male mice (Ohshima et al., 1997). In Figure 10 a schematic representation of gene targeting in mice is shown.

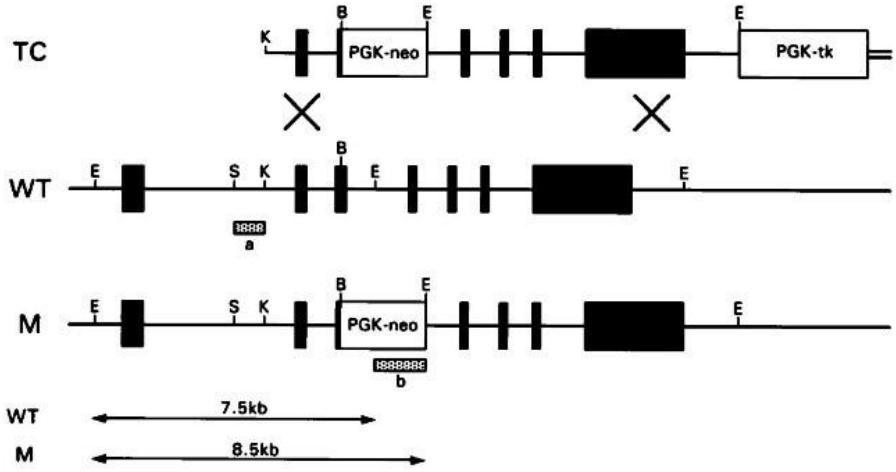

Figure 9. Schematic representation of the targeting vector and the wild-type and mutated alleles of α-Gal A gene. The hatched bars indicate 5′ flanking probe and neomycin resistance gene (neo) probe used to identify targeted clones. Restriction enzyme sites are as follows: K, KpnI; B, BamHI; E, EcoRI; S, SacI. TC, targeting construct; WT, wild type; M, mutate. Modified from Ohshima et al., 1997.

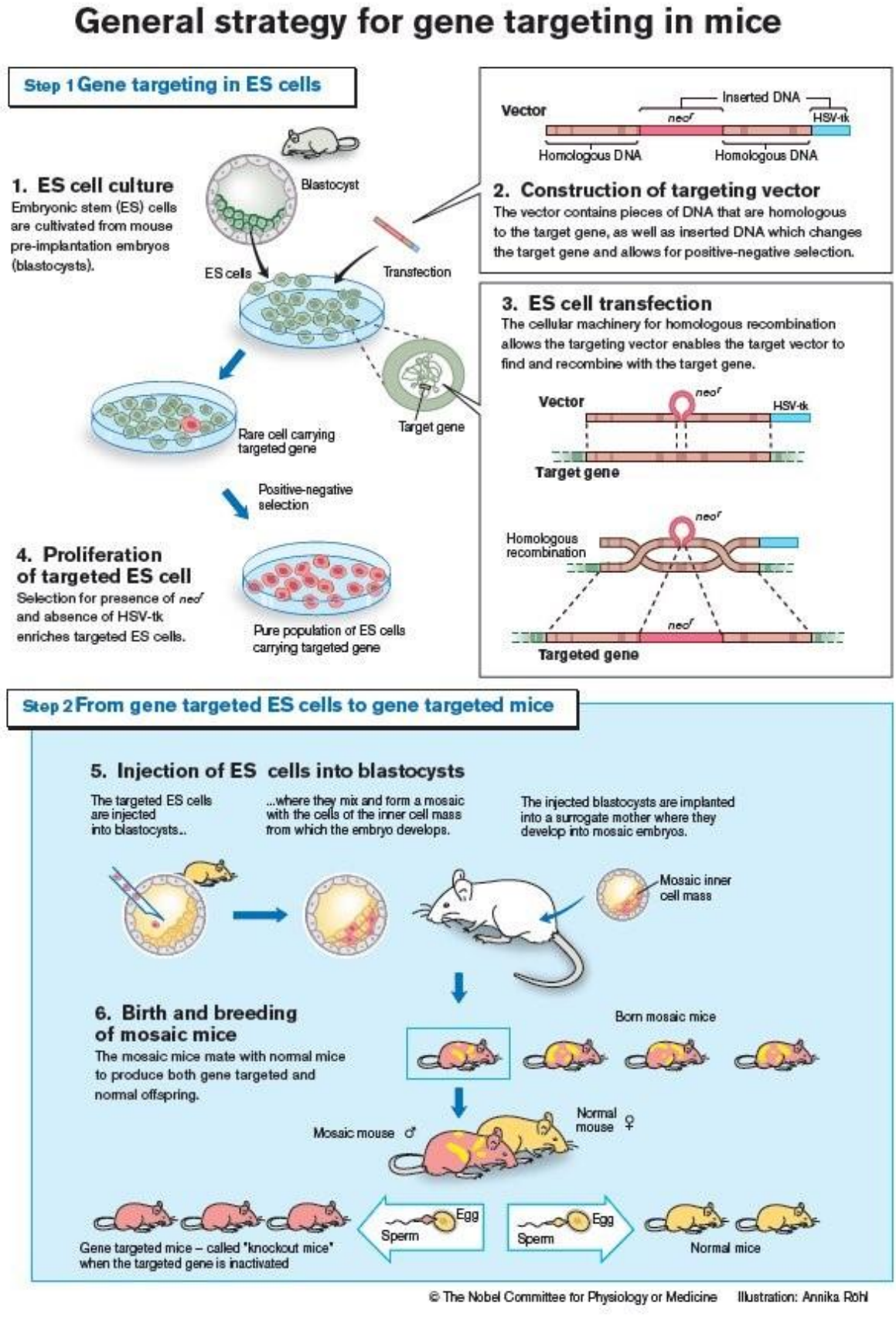

Figure 10. Schematic representation of gene targeting strategy in mice. From Animal and the Partner.

1.2 The gastrointestinal system

The GI system consists of oral cavity and salivary glands, esophagus, stomach, small intestine (duodenum, jejunum, and ileum), or upper GI tract, and large intestine (cecum, colon, and rectum), or lower GI tract. The GI tract is involved in the digestion process, which begins in the oral cavity and terminates in the small intestine. The functions of the upper GI tract include transport of the swallowed food bolus, enzymatic digestion, and absorption of nutrients, in addition to protective barrier function against the external environment; whereas the lower GI tract is involved in fecal material dehydration and storage, as well as in water and salt reabsorption.

The whole GI tract is histologically composed of four layers (Figure 11), which may be more or less prominent and/or display specialized features depending on the function of segment (Pathway medicine, gastrointestinal medicine, GI tract histology):

1. The mucosa is the innermost layer and is itself made of three layers. The epithelium morphology and architecture changes along the different segments of the GI system according to the function of the tract (digestion, absorption, secretion). The lamina propria consists of an underlying layer of loose connective tissue that supports the epithelium, and often contains clusters of Gut-Associated Lymphoid Tissue (GALT). The muscularis mucosae is a thin layer of smooth muscle that actuates local motions of the GI mucosa.
2. The submucosa is a large layer of collagenous tissue that contains blood and lymphatic vessels, nerves, and mucous secreting glands. The nerve fibers within the submucosa form the Submucosal Plexus.
3. The muscularis propria is a wide smooth muscle layer consisting of the circular (inner) and longitudinal (outer) sub-layers. It is responsible for the peristaltic movement and is controlled by the Myenteric Plexus, which is located between the two muscular layers.
4. Intraperitoneal parts of the GI tract are covered with serosa (most of the stomach, first part of the duodenum, the small intestine, caecum and appendix, transverse colon, sigmoid colon and rectum). The serous membrane is composed of two layers: a secretory epithelial layer, known as mesothelium, produces a lubricating serous fluid with the consistency of the mucus and the function to reduce friction derived by muscle movement; a connective tissue layer underneath provides blood vessels and nerve fibers to the mesothelium as well as adhesion to the gut. Retroperitoneal parts are instead covered with adventitia (oral cavity, esophagus, pylorus of the stomach, distal duodenum, ascending colon, descending colon and anal canal). These segments are fixed in position. The adventitia consists of a layer of collagenous tissue that

allow the passage of large blood vessels and nerves that support and modulate the entire GI tract.

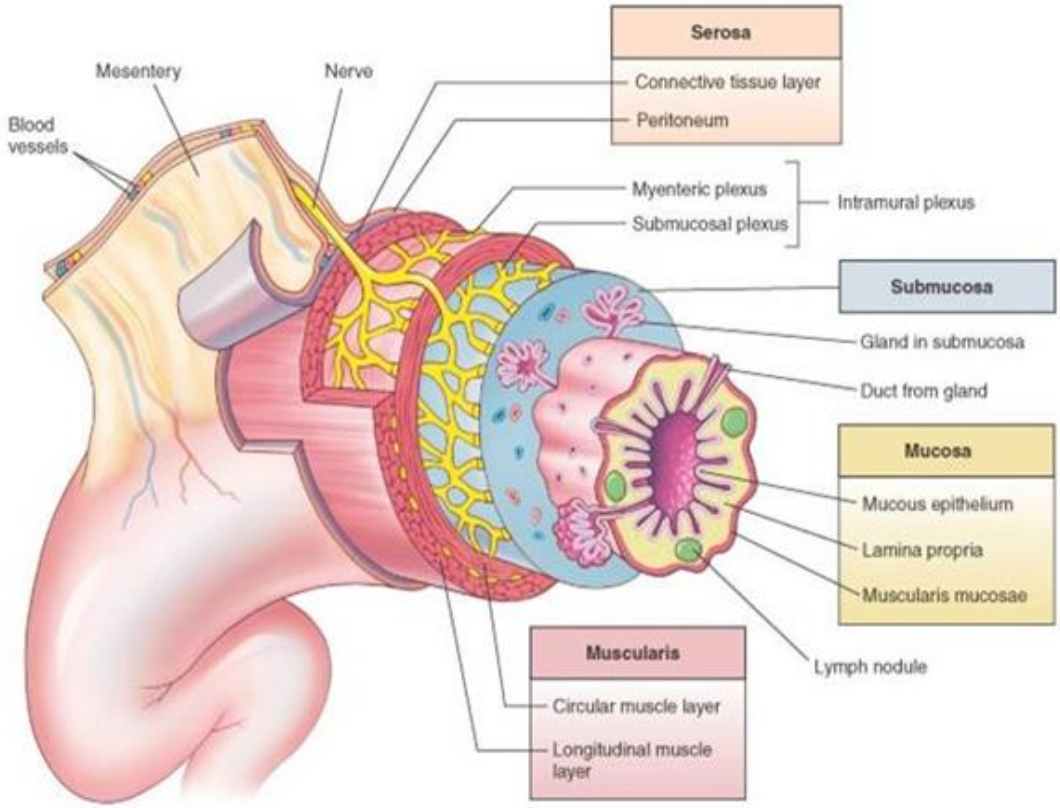

Figure 11. Layers of GI tract. The image shows the four layers of GI wall (mucosa, submucosa, muscularis propria and serosa/adventitia) and their respective sub-layers (*boxes*). The position of glands, lymph glands, nerves, plexi and blood vessels is also represented. From Gastrointestinal Tract Histology.

1.2.1 Gross anatomy of human and murine lower gastrointestinal tract

Human and mouse GI tract are anatomically similar, but despite this, there are prominent differences due to diverging diets, feeding patterns, body sizes and metabolic requirements. Large intestine of both human and mouse is divided in cecum, colon and rectum (Treuting and Dintzis, 2012) (Figure 12). The anatomic division of human colon is based on configuration and location. The human right colon includes the appendix, cecum, ascending colon and the first half of transverse colon, corresponding to the cecum and proximal colon of the mouse. In mice, the appendix is absent and the cecum represents up to one-third of the large intestine resulting much larger in size compared to human. The mouse cecum carries out a rumen-like function so its size is diet-dependent: it contains a high concentration of bacteria, thus serving as a fermentation vat. The fermentation is needed to produce Vitamin K, free fatty acids and some of the B vitamins, which are recaptured through coprophagy. This difference from humans reflects murine adaptation to extract nutrients from the

relatively larger proportion of indigestible food components in their diet. The mid and distal colon of mice correspond to the human left colon, which begins at the midline of the transverse colon including the descending colon and rectum, and ends at the external anal orifice. The rectum is short in mice and is easily prolapsed under some pathological conditions. Mice colon also lacks taenia coli and haustra and hence has a smooth serosal appearance. The differences between mouse and human in the anatomy of GI tract also determine a difference in the gut microbiota composition (Nguyen et al., 2015).

1.2.2 Histology of human and murine lower gastrointestinal tract

Human and mouse large intestine are histologically similar in basal GI wall structure: mucosa, submucosa, muscularis propria and serosa (Treuting and Dintzis 2012). Whereas the human colonic mucosa presents transverse folds throughout, the mouse large intestine mucosa displays specific regional differences: it shows transverse folds at the cecum and proximal colon level, a flat mid-section and longitudinal folds distally. Both species lack villi in large intestine, but display tubular glands perpendicularly oriented to the long axis of the gut. These glands, named crypts of Lieberkühn, are lined by epithelium consisting of absorptive enterocytes, Goblet cells and enteroendocrine cells. Goblet cells are responsible of the production of mucin, which is required to lubricate the passage of the bowel content. In mice, Goblet cells are more abundant in cecum and proximal colon compared to distal colon, whereas in humans their number increases from cecum to rectum. Paneth cells are specialized epithelial cells present at the base of the crypts of Lieberkühn.

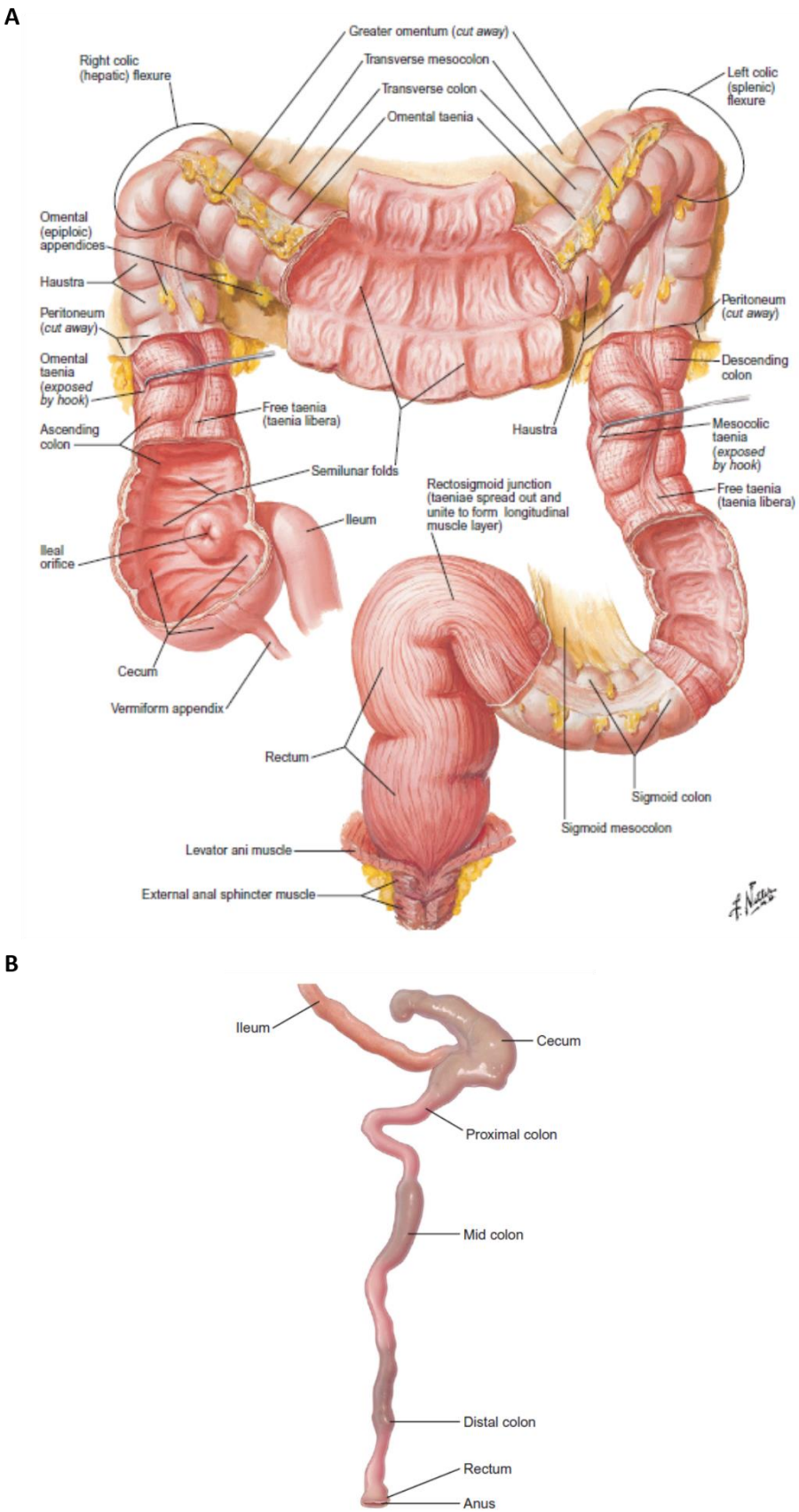

Figure 12. Gross anatomy of human and mouse large intestine. The figure displays the gross anatomy of human and mouse large intestine. In both species, the large intestine is divided in cecum, colon and rectum but important anatomic and histological differences exist due to diverging diets, feeding patterns, body sizes and metabolic requirements. Modified from Treuting and Dintzis 2012.

They are responsible of the secretion of antimicrobial peptides and proteins that were discovered to modulate homeostatic balance with colonizing microbiota and innate immune protection from enteric pathogens (Clevers and Bevins, 2013). In humans, these cells are present in the appendix and cecum but are absent from distal colon, whereas mice colon totally lack them (Treuting and Dintzis 2012). GALT is present in both mice and humans. Peyer's patches are large organized areas of lymphocytes that may be found in the cecum submucosa and are visible by eye from the serosal surface (Scudamore, 2014). Lymphocytes may also be present as small aggregates (cryptopatches) or isolated lymphoid follicles in the lamina propria of the whole intestine (Pabst et al., 2005). In humans, the appendix submucosa presents several lymphoid follicles, with lymphoid infiltrates extending into the lamina propria (Treuting and Dintzis 2012). The human submucosa present copious adipose tissue, which is absent in mice. For this reason, the mucosa and submucosa of mice are thinner and prone to herniation compared to human. In both species, the muscularis propria displays the longitudinal and circular sublayers. The mouse muscular layers thickness increases from cecum to distal colon. The ENS in both species is organized in two main aggregates of ganglion cell and nerve fibers called plexi, which are present into the submucosa (submucosal or Meissner's plexus) and between the longitudinal and circular layer of muscularis propria (myenteric or Auerbach's plexus). Figure 13 shows the histological structure of the mouse colonic wall, whereas Table 2 summarizes the anatomic and histological differences between human and mouse large intestine.

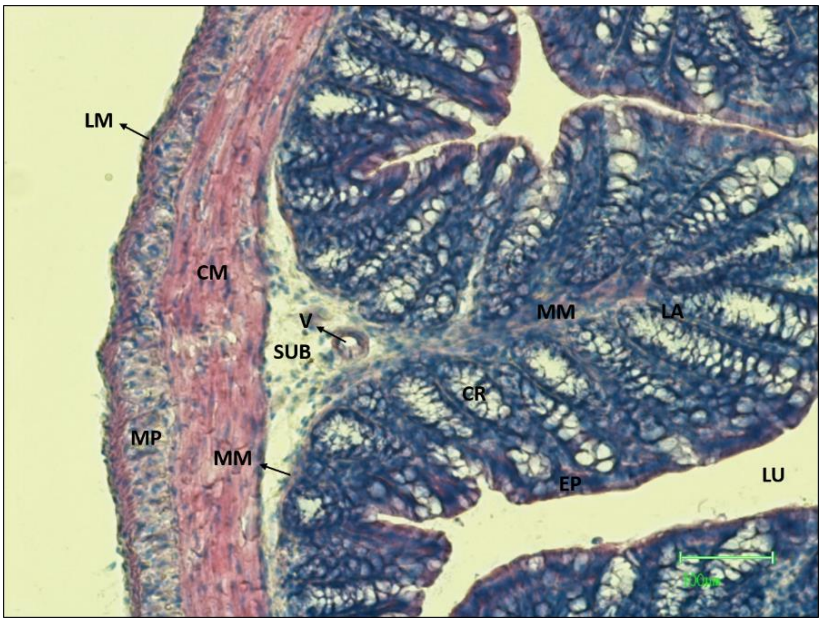

Figure 13. Histological structure of mouse colonic wall. The image shows the histological structure of a WT mouse colonic wall in a transverse frozen section stained in our laboratory with Haematoxylin and Eosin (H&E) and magnified to 10x. The mucosa is the innermost layer of the GI wall and is itself made of three sublayers: epithelium (EP), lamina propria (LA) and muscularis mucosae (MM). The mucosa lacks villi in large intestine, but displays tubular glands called crypts of Lieberkühn (CR) that are perpendicularly oriented to the long axis of the gut. In mice, the submucosa (SUB) is very thin (one vessel is also shown, V). The muscularis propria consists of the circular (CM) and longitudinal (LM) sub-layers, between which the myenteric plexus (MP) is located. The intestinal lumen (LU) is also shown.

	Feature	Mouse	Human
Gross	Cecum to rectum	14 cm	1.00–1.05 m
	Taenia coli and haustra	None; smooth serosa; may have fecal pellets	Yes
	Appendix	No appendix; significant cecal GALT	Vermiform
	Cecum	Fully functional blind sac, 3–4 cm; no villi; transverse mucosal folds; thin submucosa and muscular tunics; straight crypts; may have simple branching at base; size dependent on diet, flora	Portion of the proximal colon lying below the ileocecal valve
	Functional cecum	Yes; fermentation, vitamins K and B	No
	Corprophagy	Yes	No
	Ascending/right	Ascending/proximal transverse fold in mucosa, from cecum to pylorus	Colon from ileocecal valve superior to the hepatic flexure
	Transverse	Very short; lumen narrows; no transverse folds	Connects the hepatic to the splenic flexure
	Descending/left	Fecal pellets may be seen	Splenic flexure inferior to left lower quadrant; S-shaped sigmoid colon extends from descending colon to peritoneal reflection; sigmoid colon may be redundant
	Rectum	Short rectum; very prone to prolapse; squamous epithelium	Distal 8–15 cm of extraperitoneal colon, lies within the pelvis
	Anus	At base of tail	Anal canal is ~4 cm, pelvic floor to anal opening
	Circumanal glands	Modified sebaceous glands	Apocrine glands
Tissue	Mucosa	Pregnant and lactating mice have physiologic mucosal thickening	No changes with pregnancy
	Lamina propria	Lymphocytes, plasma cells, macrophages, eosinophils, mast cells	Same
	Submucosa	Thin	Contains adipose tissue, arterioles, venules, lymphatics, and Meissner's plexus
	Muscularis mucosae	Thin muscularis mucosae	Variable thickness; traversed by lymphoid follicles; poorly developed in appendix
	Muscular tunics	Muscular tunics thicken distally	Auerbach's plexus between the two muscle bands
	Cecum	Abundant lymphoid tissue at tip	Paneth cells may be present
	Proximal colon	Transverse mucosal folds	Histologically indistinguishable
	Mid colon	Flat mucosa	Histologically indistinguishable
	Distal colon	Longitudinal mucosal folds	Histologically indistinguishable
	Rectum	Indistinguishable from distal colon	Histologically indistinguishable
	Anus	Keratinized squamous epithelium	Stratified squamous epithelium
Cells	Absorptive colonocytes	Yes	Yes
	Mucous/goblet cells	Yes	Yes
	Enteroendocrine cells	Yes	Yes
	Paneth cells	No	Yes
	Microfold (M) cells	Yes	Yes

Table 2. Anatomic and histological differences between human and murine large intestine. The table summarizes the existing differences between human and mouse large intestine due to diverging diets, feeding patterns, body sizes and metabolic requirements From Treuting and Dintzis, 2012.

1.2.3 The Enteric Nervous System

1.2.3.1 Organization of neural pathways

The GI tract differs from other organs since it is controlled by an intrinsic nervous system called ENS, which, however, is not completely independent (Bayliss and Starling, 1899). The organization of ENS does not follow the anatomic conventional rules of ANS. Conventionally, CNS communicates with the effector tissues via pre and post ganglionic neurons, and sensory information flow from the periphery to the CNS through spinal and cranial primary afferent neurons. Neuronal control of GI function instead is an integrated system involving interactions between local enteric reflexes, reflexes that pass through sympathetic ganglia and reflexes that pass from the gut and back through the CNS (Furness, 2012). The total number of enteric neurons in humans is huge, ranging from 400 to 600 million, which is greater than the total of all sympathetic and parasympathetic ganglia combined and approximately equal to the number of neurons in the spinal cord (Furness, 2006). The ENS consists of aggregates of neurons, enteric ganglia and the neural connections between ganglia and the nerve

fibers innervating the effector tissues, such as the smooth musculature of the gut, epithelial cells, blood vessels and endocrine cells (Furness, 2012). The ENS has several functions: determining the propulsion movement of GI tract, controlling gastric secretion, modulating movement of fluid across the epithelium, changing local blood flow, modifying nutrient uptake, interacting with immune and endocrine systems of the gut (Furness, 2006) as well as contributing to maintain GI barrier integrity (Toumi et al., 2003; Savidge et al., 2007). The importance of ENS is highlighted by the high number of neuropathies that are caused by an impairment of its roles and which can be classified as: congenital or developmental neuropathies (e.g. Hirschsprung disease); sporadic and acquired neuropathies (e.g. Chagas disease); neuropathies associated with other disease states (e.g. Diabetic gastroparesis, Enteric neuropathy of Parkinson disease) and iatrogenic or drug-induced neuropathies (e.g. Opioid-induced constipation) (Furness, 2012).

1.2.3.1.1 The intrinsic innervation of the gastrointestinal tract

1.2.3.1.1.1 The enteric plexi

The ENS is organized in two major sets of ganglia. The myenteric plexus was first described by Auerbach in 1862 (Auerbach, 1862a, 1862b). It consists in a network of nerve fibers and small ganglia situated between the longitudinal and circular muscle layers of the GI muscularis propria (Figure 14). Its main function is providing motor innervation to the two layers of smooth muscle cells, giving rise to the peristaltic movement necessary for the progression of bowel content.

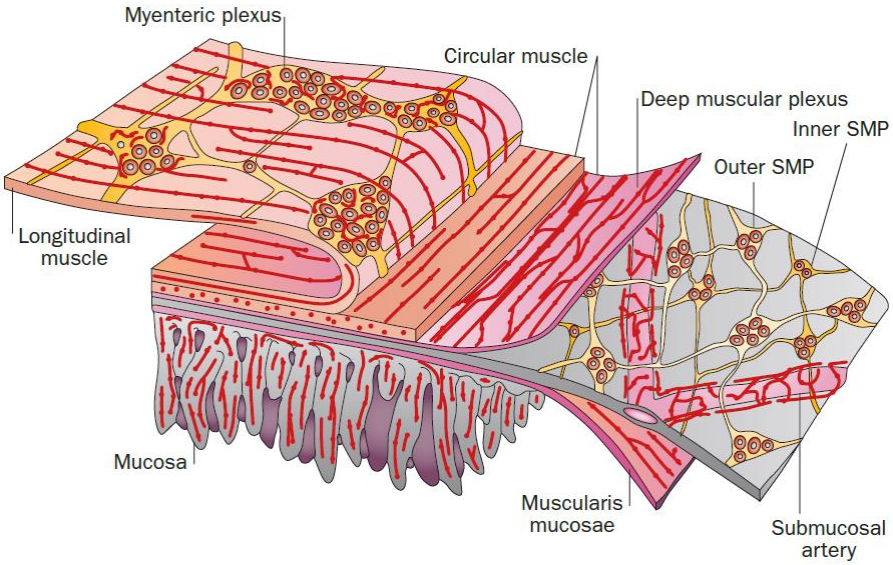

Figure 14. The organization of the ENS of human and medium-large mammals. The ENS is organized in two major ganglionated plexuses: the myenteric plexus, located between the longitudinal and circular muscle layers, and the submucosal plexus, located in the submucosa. Ganglia are formed of neurons and glial cells. The ganglia are sometimes referred to as the nodes of the plexus because they lie at the junctions of nerve strands, which in turn are called internodal or interganglionic strands, or sometimes interganglionic connectives. Nerve fiber bundles connect the ganglia and also form plexuses that innervate the longitudinal muscle, circular muscle, muscularis mucosae, intrinsic arteries and the mucosa. From Furness, 2012.

The myenteric plexus forms a continuous network around the circumference and along the GI tract, extending from the upper esophagus to the internal anal sphincter (Furness, 2006). The myenteric ganglia size, shape and orientation vary between animal species and from one segment of the intestine to another. A ganglionated plexus is also present within the submucosa layer of small and large intestine (Furness, 2006) (Figure 14). It was first described by Meissner (Meissner, 1857) and Billroth (Billroth, 1858). In general, the submucosal plexus has smaller ganglia and finer interganglionic strands compared to myenteric plexus (Henle, 1871). Submucosal plexus differs between species. Large mammals, like human and pig, have two layers of submucosal ganglia, and sometimes have an intermediate layer, displaying structural and functional differences between them (Timmermans et al., 2001). The outer plexus provides innervation to the circular and even the longitudinal musculature (Sanders and Smith 1986, Furness et al. 1990, Timmermans et al. 1994, 1997, Porter et al. 1999) as well as the mucosa. The inner plexus principally supplies the mucosa, innervating the muscularis mucosae smooth muscle and cells in the epithelial layer (enterocytes, Goblet cells, enteroendocrine cells, Paneth cells, microfold cells, cup cells, and tuft cells), respectively. It also has few neurons innervating the muscle (Porter et al. 1999, Timmermans et al. 2001). Small mammals, typified by the guinea-pig, display a single layer of submucosal ganglia containing secretomotor neurons but not motor neurons innervating the external muscle (Furness et al. 1984, 2003a). The ganglia of the submucosal plexus in small mammals most closely resemble those of the inner submucosal plexus of larger species (Furness, 2006). Nerve fibres from the submucosal plexus extend into the muscularis mucosae and the mucosa to innervate the muscularis mucosae smooth muscle and cells in the epithelial layer (enterocytes, Goblet cells, enteroendocrine cells, Paneth cells, microfold cells, cup cells, and tuft cells), respectively.

1.2.3.1.1.2 Gastrointestinal wall innervation

How the longitudinal muscle is innervated is determined by its thickness. In large animals, and in small animals where the muscle layer is thickened (e.g. where teniae coli occurs), a longitudinal muscle plexus, consisting in fine bundles of nerve fibers running parallel to the muscle, is present (Richardson, 1958). Where the muscle is less than about 10 muscle cells thick, the muscle layer is innervated by bundles of axons of the myenteric plexus that are lying against the inner surface of the muscle (Furness, 2006). The circular musculature is innervated throughout the thickness by fine nerve bundles running parallel to the length of muscle cells (Furness, 2006). The majority of nerve fibers derives from motor neurons with cell bodies in the myenteric ganglia, even if some axons come from the submucosal plexus. In large mammals, the number of fibers originating from the submucosal plexus is higher than in small ones. Fine nerve fibers bundles coming from submucosal plexus make

contact with the smooth muscle cells of muscularis mucosae as well (Furness, 2006). The mucosa is innervated by nerve bundles coming from the submucosal plexus and present throughout the lamina propria (Billroth, 1858). These fibers do not penetrate the intestinal epithelium, but they come close to the epithelial entero-endocrine cells and to lymphocytes aggregates as Peyer's patches, with which there is a functional interaction (Furness, 2006). Two types of nerve fiber bundles are associated with blood vessels in the GI tract. Paravascular nerve fibers follow the arteries, using them as a conduit to carry axons that innervate blood vessels as well as enteric ganglia, intestinal smooth muscle cells and the mucosa. The perivascular plexus consists in a network of fine nerve fiber bundles that surround arteries and arterioles and that contain both motor fibers and vascular primary afferent (sensory) nerve fibers (Furness, 2006).

1.2.3.1.2 The extrinsic innervation of the gastrointestinal tract

Connections between the GI tract and the CNS can be divided in vagal, spinal thoracolumbar and spinal lumbosacral (Furness et al., 2014) (Figure 15). Each of them contains afferent (sensory) and efferent (motor) innervation. The efferent pathways control or modify the activities of enteric neurons and consists of pre-enteric neurons ending within enteric ganglia. Pathway from CNS also contain neurons that directly make contact with effector tissues, such as striated muscle of the esophagus (vagal innervation), sphincters (sympathetic innervation) and intrinsic blood vessels (also sympathetic innervation). Studies have shown that the majority of visceral afferent fibers are thinly myelinated Aδ or unmyelinated C fibers that form unencapsulated "free" nerve endings in their target organs (Gebhart and Bielefeldt, 2016). Sensory endings of the gut have been recently divided into five categories based on their structure and location: intraganglionic laminar endings (IGLEs), mucosal endings, muscular-mucosal endings, intramuscular arrays (IMAs), and vascular endings (Brookes et al., 2013).

1.2.3.1.2.1 Vagal innervation

The vagus nerve is the most far-reaching nerve in the body: it provides sensory and motor innervation to the upper GI tract, meaning esophagus, stomach, proximal small intestine, liver, pancreas and less prominently in the distal small intestine, proximal colon and some pelvic structures (Cervero, 1994; Furness et al., 2014) (Figure 15). Notably, at least 80% of axons in the vagus nerve are afferent and have the cell bodies in the nodose (primarily) and the more rostral jugular ganglia, whereas the central terminals project principally to the nucleus of the solitary tract in the dorsal medulla (Gebhart and Bielefeldt, 2016). About 5% of vagal afferents terminate in the upper cervical spinal cord (C1-2) (Foreman, 1999). The main functions that are regulated by these fibers are appetite and satiety,

esophageal propulsion, gastric volume, contractile activity and acid secretion, contraction of the gallbladder and secretion of pancreatic enzymes (Furness et al., 2014). Moreover, the vagus nerve is involved the perception of aversive feelings such as bloating, nausea, apnea and unpleasantness associated with visceral pain (Gebhart and Bielefeldt, 2016). Three different types of vagal afferents are present in the GI tract, IGLEs, IMAs and mucosal varicose nerve endings (Furness et., 2014; Gebhart and Bielefeldt, 2016) (Figure 16). IGLEs are complex branching nerve endings that give rise to flat (laminar) expansions within myenteric ganglia (Furness et al., 2014).

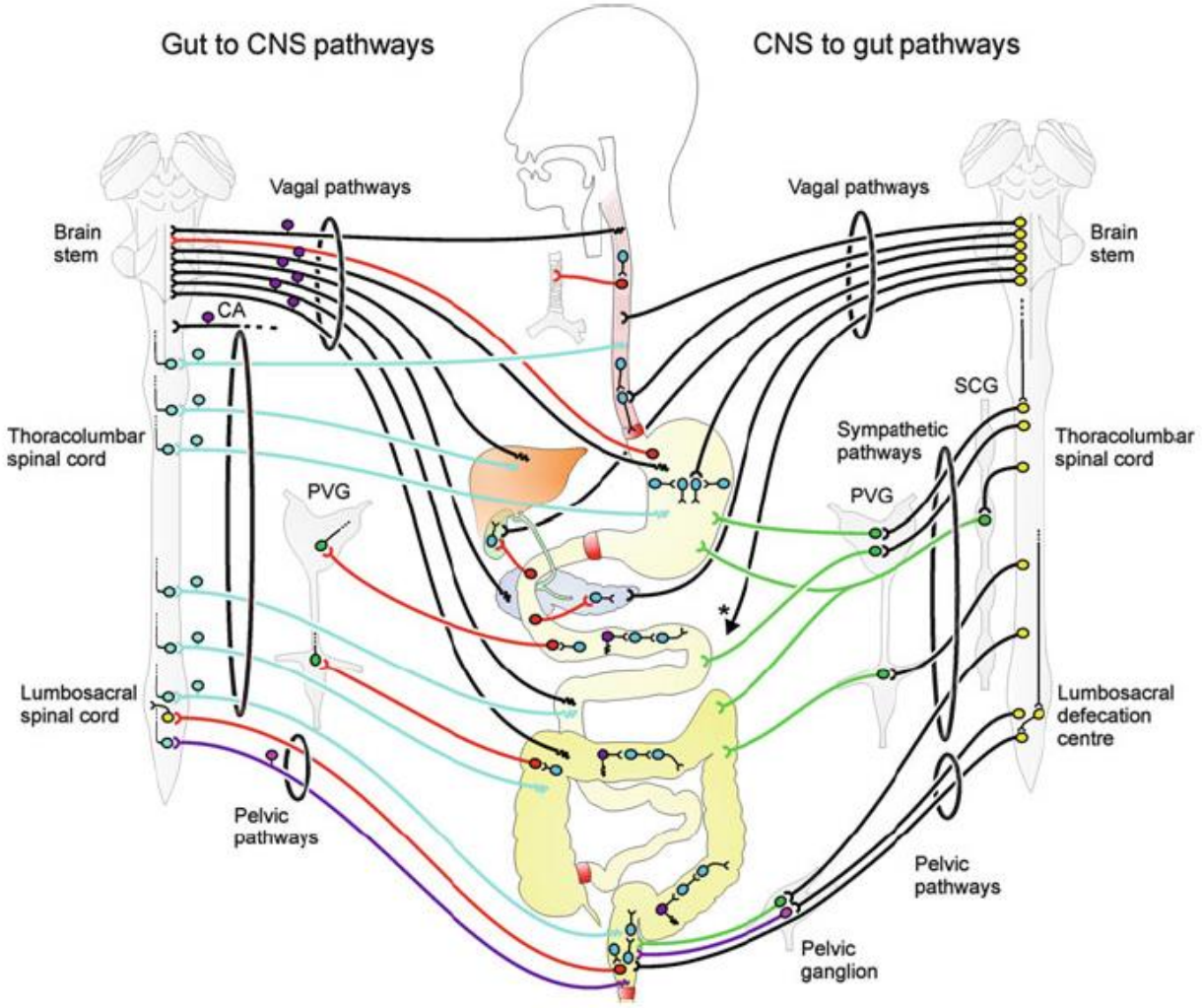

Figure 15. The innervation of the GI tract. The neural connections between the ENS, the CNS and sympathetic ganglia, and neural connections between the organs of GI tract are illustrated. Connections from the ENS to other organs and the CNS are shown at the *left*, and connections from the CNS to the gut are at the *right*. The small and large intestines contain full ENS reflex circuits (motor neurons and interneurons are displayed in *blue*, sensory neurons in *purple*). Pathways from the GI tract (*left*) project outwards, via intestinofugal neurons (*red*), to the CNS, sympathetic ganglia, gallbladder, pancreas and trachea. Some neurons in sympathetic prevertebral ganglia (PVG, *green*) receive both CNS and ENS inputs. Sensory information goes both to the ENS, via intrinsic primary afferent (sensory) neurons (*purple*) and to the CNS via extrinsic primary afferent neurons (EPANs) (*left*) that follow spinal and vagal nerve connections. Cervical afferents (CA) connect the esophagus to the cervical spinal cord. Pathways from the CNS reach the and GI effector tissues through vagal, sympathetic and pelvic pathways (*right*). Vagal medullary and pelvic spinal outflows include pre-enteric neurons (ending in enteric ganglia) and most gut-projecting sympathetic neurons with cell bodies in PVG are also pre-enteric neurons. SCG, sympathetic chain ganglia. From Furness et al., 2014.

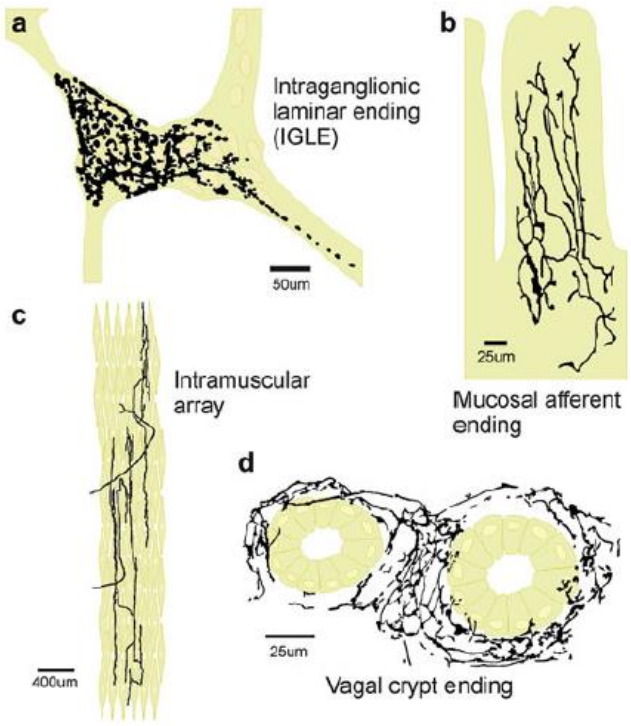

Figure 16. Sensory nerve endings in the GI tract. Different types of sensory endings exist in the intestine: (a) intraganglionic laminar endings (IGLEs); (b) mucosal varicose nerve endings supplying the villi; (c) intramuscular arrays (IMAs); (d) sensory endings around crypts in the small intestine. From Furness et al., 2014.

It has been found that fibers may branch into different shorter terminals within their target tissue, with each terminal forming an IGLE or clusters of IGLEs, meaning that visceral afferents may have multiple receptive fields (Berthoud et al., 2001; Page et al., 2002). Different studies have provided evidence that IGLEs are stretch receptors (Brookes et al., 2013; Zagorodnyuk et al., 2001) and that are primarily distributed in the proximal and very distal GI tract, suggesting a regulatory role in food intake and defecation, processes that are associated with conscious perception, but not pain (Gebhart and Bielefeldt, 2016). IMAs consist in afferent axons that branch within the GI muscular layers forming arrays of varicose fibers that run parallel to the muscles bundles (Berthoud and Powley, 1992). IMAs are thought to have a mechanoreceptive function as well, but in contrast to IGLEs, they are primarily found in proximal stomach and sphincteric structures whereas are uncommon in the intestines (Fox et al., 2000; Wang and Powley, 2000). Moreover, it has been shown that IMAs form synapse-like complexes with interstitial cells of Cajal (ICCs) and it has been hypothesized that these complexes may cooperatively work with smooth muscle to transduce specific stretch or muscle length information (Powley and Phillips, 2011). Since the contribution of vagal afferents to nociception is still controversial, it is reasonable to think that IGLEs and IMAs are involved in the perception of sensations such as fullness and bloating, but not of pain during gastric or intestinal distension (Gebhart and Bielefeldt, 2016). Three patterns of vagal mucosal afferent have been identified: gastric

mucosal afferent endings, afferents supplying villi (villus afferents) and intestinal crypts (crypt afferents) in small intestine (Powley et al., 2011). The terminals form varicose endings or circles in the villous, at crypts or around antral glands, suggesting a primary chemoreceptive role in luminal content and mucosal signals sensing (Gebhart and Bielefeldt, 2016). Many of these endings have been seen near enteroendocrine cells, suggesting a functional signalling between the two (Gautron et al., 2011). The vagal efferent pathways arise from the dorsal motor nucleus of the vagus and the nucleus ambiguous (Furness et al., 2014). Most of these neurons form synapses with neurons in enteric ganglia and thus are called "pre-enteric", whereas the others run directly to the striated muscle cells of the esophagus. The main functions of vagal innervation are to control esophageal propulsion, to relax the lower esophageal sphincter for swallowed food to pass, to increase gastric capacity, to facilitate antral contractions, to relax the pylorus, to increase gastric acid secretion, to contract the gallbladder and to promote pancreatic exocrine secretion. On the contrary, intestine is sparsely innervated by vagal fibers, with only small intestine showing the presence of few vagal efferents making contact with myenteric and submucosal ganglia (Holst et al., 1997).

1.2.3.1.2.2 Thoracolumbar innervation

The thoracolumbar spinal cord connects with the GI tract through spinal afferent neurons with cell bodies in DRG and through sympathetic efferent pathways (Furness et al., 2014) (Figure 15). As they pass through sympathetic prevertebral ganglia, the axons of spinal afferent neurons provide collaterals that form synapses with cell bodies of postganglionic neurons (Matthews and Cuello, 1982). Thoracolumbar afferent axons are almost all unmyelinated C-fibers. Spinal afferent endings are found around arterioles in the gut wall, in the muscle layer, myenteric ganglia, submucosal ganglia and lamina propria, whereas no axons were seen in the serosa (Spencer et al., 2014; Brookes et al., 2013; Green and Dockray, 1988; Gibbins et al., 1985). A high number of spinal afferents are immunoreactive for calcitonin gene-related peptide (CGRP), which is commonly taken to identify sensory axons (Zagorodnyuk et al., 2001, 2003, 2005). Moreover, they are usually positive for TRPV1 channel expression, which is associated with nociceptive afferents (Green and Dockray, 1988; Tan et al., 2008). Indeed, TRPV1 resulted involved in the response to distension and to acid in the lumen (Rong et al., 2004). Spinal pathway contains sympathetic efferent fibers as well (Furness et al., 2014). They have four primary targets: myenteric ganglia, submucosal ganglia, blood vessels and sphincter muscle. Sympathetic pathways have preganglionic and postganglionic (pre-enteric) neurons: the first ones have their cell bodies in the intermediolateral colums of spinal cord, whereas the second ones in the paravertebral and prevertebral ganglia. The cell bodies in paravertebral ganglia are mainly those involved in controlling the GI blood vessels (vasoconstrictor neurons), whereas there

are three classes of neurons in prevertebral ganglia: vasoconstrictor neurons, neurons controlling motility, and neurons controlling secretion (Furness, 2006). The vasoconstrictor neurons innervate the arteries directly and cause constriction, whereas neurons that influence motility do so in two ways. Firstly, they can inhibit both the excitatory effects of myenteric neurons on the stomach and intestine muscularis propria, thus slowing the passage of food contents in the gut lumen (Furness and Costa, 1974), and the secretomotor neuron activity of submucosal ganglia. Secondly, they can directly contract the sphincters of the GI tract, which, like the innervation of myenteric ganglia, inhibits transit of contents.

1.2.3.1.2.3 Pelvic innervation

Lombosacral spinal cord provides afferent and efferent innervation to distal colon and rectum via the pelvic nerves and sacral plexuses (Furness et al., 2014) (Figure 15). Pelvic nerves innervate distal gut in a similar way to vagus nerves provides innervation to proximal gut. However, unlike vagal afferents, pelvic ones include nociceptive fibers (Kyloh et al., 2011). The distension of the colon-rectum wall leads to the contraction of abdominal muscles in rats, response which has been seen to be a consequence of pain pathways stimulation (Ness and Gebhart, 1988). Indeed, this response was abolished when the pelvic (rectal) nerves were cut (Kyloh et al., 2011). Pelvic nerves carry afferent information from low threshold mechanosensors, which have been identified as IGLEs (Lynn et al., 2005). Rectal IGLEs respond to stretch over a wide range, including pain level (Zagorodnyuk et al., 2011). Mechanoreceptors are present in the mucosa as well, where they detect mild strokings of the mucosa, but not distension or contraction of the colon (Brierley et al., 2004). The efferent pathways in pelvic nerves provide innervation to enteric ganglia of the distal colon and rectum (Brookes et al., 2009). Cell bodies of pre-enteric neurons projecting to colon are in both the spinal cord and in pelvic ganglia (Olsson et al., 2006). For motility control, the innervation of enteric ganglia comes from the defecation centers that are in the lumbosacral spinal cord (Gonella et al., 1987). The pelvic pathways also carry fibers that cause vasodilation in the colon-rectum (Hulten, 1969).

1.2.3.2 Functionally defined enteric neurons

Enteric neurons can functionally be divided in three classes based on combinations of features (morphology, neurochemical properties, cell physiology, projections to targets and functional roles): 1) intrinsic primary afferent neurons (IPANs, or intrinsic sensory neurons), 2) interneurons and 3) motor neurons (Furness, 2006). IPANs detect the physical state of the organs (e.g. tension in the gut wall) as well as chemical features of the luminal contents (Furness et al., 2004). They react to these signals to trigger appropriate reflex control of functions including motility, secretion and blood flow.

IPANs connect with each other, with interneurons and directly with motor neurons. Interneurons connect with other interneurons and with motor neurons. Among motor neurons are muscle motor neurons, secretomotor neurons, secretomotor/vasodilator neurons, motor neurons to enteroendocrine cells, and an innervation of lymphoid follicles (Furness, 2006) (Figure 17).

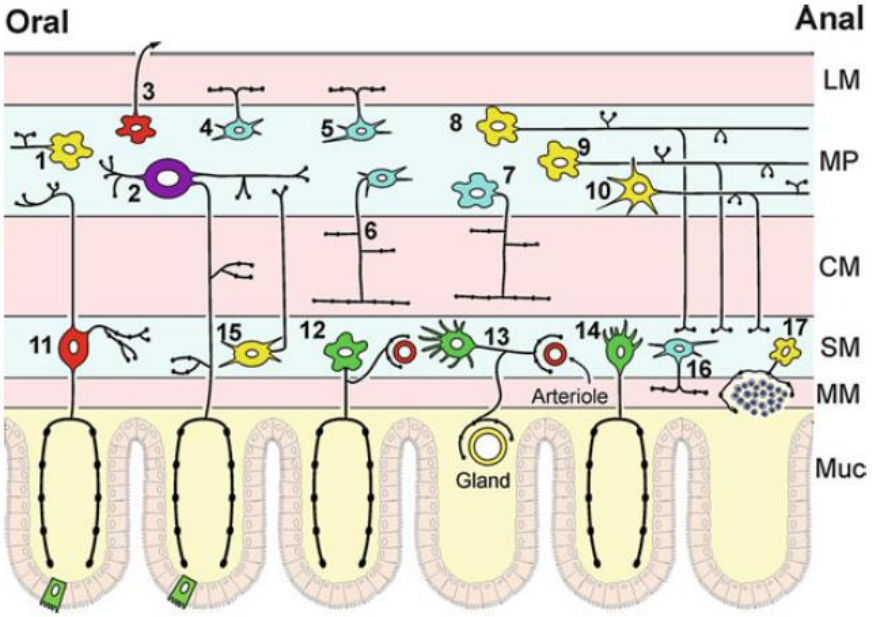

Figure 17. Neuron types in the ENS. The types of neurons in the small intestine, that have been defined by their functions, cell body morphologies, chemistries, key transmitters and projections to targets are shown. Neuron Types: Ascending interneurons (1); Myenteric intrinsic primary afferent neurons (IPANs) (2); Intestinofugal neurons (3); Excitatory longitudinal muscle motor neurons (4); Inhibitory longitudinal muscle motor neurons (5); Excitatory circular muscle motor neurons (6); Inhibitory circular muscle motor neurons (7); Descending interneurons (local reflex) (8); Descending interneurons (secretomotor and motility reflex) (9); Descending interneurons (migrating myoelectric complex) (10); Submucosal IPANs (11); Non-cholinergic secretomotor/ vasodilator neurons (12); Cholinergic secretomotor/vasodilator neuron (13); Cholinergic secretomotor (non-vasodilator) neurons (14); Uni-axonal neurons projecting to the myenteric plexus (15); motor neuron to the muscularis mucosa (16); innervation of Peyer's patches (17). Motor neurons to enteroendocrine cells are not illustrated. LM, longitudinal muscle, MP, myenteric plexus, CM, circular muscle, SM, submucosal plexus, Muc, mucosa. From Furness et al., 2014.

1.2.3.2.1 Intrinsic Primary Afferent Neurons

The state of the GI tract is detected by three types of cells: primary afferent neurons, entero-endocrine cells and immune cells (Furness et al., 1999). Primary afferent neurons associated with the gut can be divided in intrinsic and exstrinsic: IPANs present cell bodies, processes, and synaptic connections in the gut wall, whereas extrinsic primary afferent neurons (EPANs) have cell bodies in nodose and jugular ganglia (vagal afferents) or in DRGs (spinal afferents) (Figure 18). IPANs transduce and carry information regarding the chemical environment and physical state of their target tissues, conveying this information to integrative local reflexes that can modify the functional states of organs. Furthermore, signals are carried from the GI tract via extrinsic primary afferents to the CNS, which

trigger reflexes that act back on the gut. IPANs are able to respond to stimuli according to their intensities, durations, and patterns. Besides physiological stimuli IPANs can also function as nociceptors, thus triggering protective responses (via spinal pathways; Furness, 2006). In particular, IPANs are identified as large multi-axonal neurons (type II morphology) that are able to respond to changes in luminal chemistry, mechanical distortion of the mucosa and of their processes in the external musculature (Kirchgessner et al., 1992; Bertrand et al., 1997; Kunze et al., 1998; Furness et al., 1998).

1.2.3.2.2 Motor neurons

Muscle motor neurons are excitatory or inhibitory neurons that innervate the circular and longitudinal layers of muscularis propria and the muscularis mucosae. Contraction is mediated by neurotransmitters such as acetylcholine (Ach) and substance P (SP), whereas nitric oxide (NO), vasoactive intestinal peptide (VIP) and ATP-like transmitters release induce relaxation (Furness, 2006; Durnin et al., 2013).

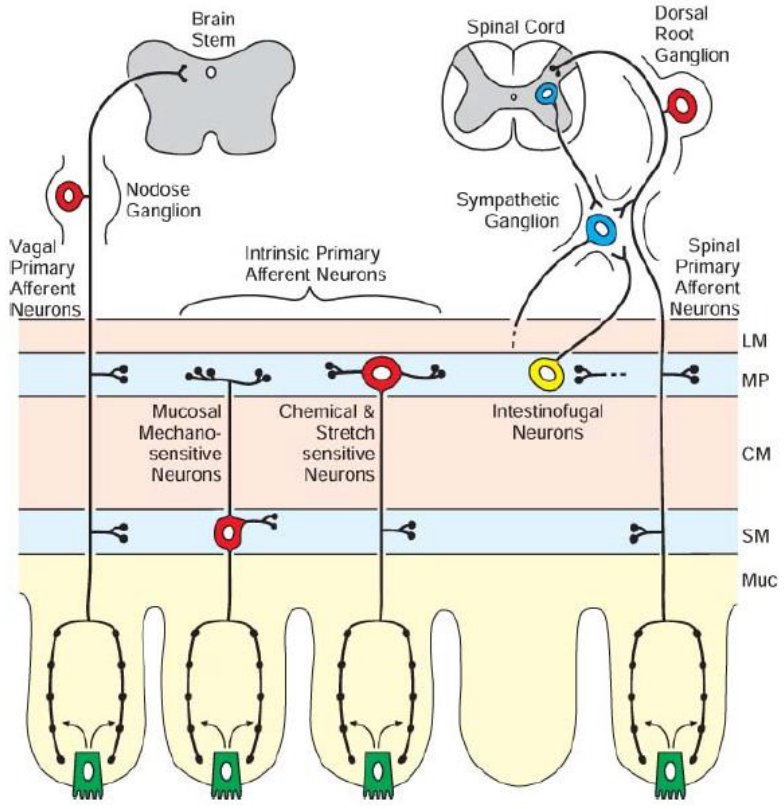

Figure 18. The afferent neurons of the digestive tract. Two classes of intrinsic primary afferent neuron (IPAN) have been identified: myenteric IPANs that respond to distortion of their processes in the external muscle layers and, via processes in the mucosa, to changes in luminal chemistry, and submucosal IPANs that detect mechanical distortion of the mucosa and luminal chemistry. EPANs have cell bodies in DRGs (spinal primary afferent neurons) and vagal (nodose and jugular) ganglia. Spinal primary afferent neurons supply collateral branches in prevertebral (sympathetic) ganglia and in the gut wall. Intestinofugal neurons are parts of the afferent limbs of entero-enteric reflex pathways. Nerve endings in the mucosa are activated by hormones, most prominently serotonin (5-HT), released from entero-endocrine cells (arrows). LM, longitudinal muscle; CM, circular muscle; MP, myenteric plexus; SM, submucosa; Muc, mucosa. Adapted From Furness, 2006.

The majority of muscle motor neurons innervating both circular and longitudinal layers have their cell bodies in myenteric ganglia. In large mammals a component of innervation comes from submucosal ganglia (Timmermans et al., 1997; Sanders and Smith, 1986; Furness et al., 1990; Timmermans et al., 2001). Innervation of muscularis mucosae derives from motor muscle neurons with cell bodies in the submucosal ganglia (Furness et al., 1990). Secretomotor and vasomotor neurons are responsible for the control of mucus secretion and local blood flow (Furness, 2000). Exocrine fluid secretion needs water supply and electrolytes from the blood, thus secretion and vasodilation are controlled together (Furness, 2006). Activation of mucosal motor neurons induces an active secretion of chloride ion across the intestinal mucosa followed by sodium and water secretion (Cooke et al., 1983; Keast, 1987). Two components of transmission to the mucosa have been identified: a cholinergic component and a non-cholinergic component (Cooke and Reddix, 1994; Keast et al., 1985). VIP both causes fluid secretion and increases blood flow (Schwartz et al., 1974; Banks et al., 2005), whereas Ach is both a stimulant of mucosal secretion and a vasodilator (Furness et al., 2014).

1.2.3.2.3 Interneurons

Interneurons are involved in the formation of local circuits. Within the myenteric plexus, the interneurons form ascending (oral direction of the signal) or descending (anal direction) neuronal chains with a much more complex chemical coding (Pompolo and Furness, 1993; Portbury et al., 1995; Young and Furness, 1995). The ascending interneurons appear to be involved in local motility reflexes, like two types of descending cholinergic neurons (nitric oxide synthases- (NOS) and serotonin- (5HT) containing neurons) (Gwynne and Bornstein, 2007). Another type of descending interneuron (Ach/somastatin (SOM) interneurons) might be involved in the passage of the migrating myoelectric complexes (MMC) along the intestine (Portbury et al., 1995).

1.2.3.3 Gatrointestinal pain: visceral nociception and hypersensitivity

Visceral sensory transduction is initiated by the stimulation of primary afferent fibers at their peripheral endings in the GI wall. Primary afferents transmit the evoked action potentials via vagal, spinal and pelvic pathways to neurons in the CNS (Brookes et al., 2013; Blackshaw et al., 2007; Bielefeldt et al., 2005). The stimulation within the physiological range unconsciously triggers localized reflex to coordinate sensory and motor function. In contrast, noxious stimulation activates a subpopulation of sensory fibers called nociceptors to generate nocifensive behavior in order to avoid potential tissue damage (Basbaum et al., 2009; Dubin and Patapoutian, 2010). These stimuli include hollow organ stretch/distension, traction on the mesentery, organ hypoxia/ischemia and chemical

stimuli (i.e. endogenous mediators of inflammatory processes) (Gebhart and Bielefeldt, 2016). The two main pathways responsible for carrying signal pain from the gut to the CNS are the thoracolumbar and lumbosacral ones, whereas vagal afferent fibers primarily transmit mechanical and chemical information (Furness et al., 2014). Three different classes of peripheral nociceptors are present in the gut: high threshold (mostly mechanical, which function in the noxious range), low threshold (intensity encoding, which function in the innocuous to noxious range) and silent nociceptors (which have a role in chronic visceral pain). Both unmyelinated (C-) and thinly myelinated (Aδ-) fibers are involved in nociception. C fibres are non-specific, high-threshold, and slowly adapting mechanoreceptors that encode tonic stimuli, whereas Aδ fibres are rapidly adapting mechanoreceptors that encode primarily phasic stimuli (Bueno et al., 1997; Cervero and Laird, 1999). It has been demonstrated that pathophysiological GI pain is both caused by a state of visceral hypersensitivity (VHS)/allodynia (pain response to a stimulus that is normally not painful) and hyperalgesia (increased pain response to a stimulus that is normally painful) (Giamberardino 1999). In hypersensitivity states, an alteration of both non-noxious and noxious stimuli processing is present at either peripheral or central (spinal) level. These alterations may correspond to a peripheral sensitization of primary afferents, mainly C fiber nociceptors, changes in endogenous pain-modulating systems, and/or recruitment of silent nociceptors with resulting activation of neurons at the spinal level. These alterations may be in part due to the upregulation of neuropeptides (e.g. SP, N-methyl-D-aspartate, and CGRP) (Bueno et al.1997; Cervero and Laird 1999; Mertz 2002). The ability of a nociceptor to sensitize is defined as an increase in response magnitude and decreased in response threshold (Gold and Gebhart, 2010). This is typically associated to a change in chemical features of the microenvironment at the site of afferent endings, generally resulting from tissue insult. In the gut, these insults range from ulceration and inflammation (e.g. IBD; Chron's disease (CD); etc.) to an apparent absence of pathophysiological causes (e.g. functional GI disorders, FGIDs). The mediators contributing to sensitization may be endogenous molecules released or synthesized at the site of insult, attracted there in response to insult, or translocated to the nociceptor membrane (e.g. receptor and ion channels). Insults may also cause post-translational modifications of key players as well as epigenetic changes over time (Gebhart and Bielefeldt, 2016).

1.2.3.3.1 Transient Receptor Potential channels: the role as molecular sensors

The peripheral nerve endings in the gut present many types of receptors and ion channels that allow the detection of chemical, mechanical, and thermal stimuli and the response to them. The set of molecular sensors that are best-characterized are the TRPs. TRP channels represent a large family of non-selective cation channels that were first identified as channels mediating brief excitatory events

in non-mammalian sensory systems (Blackshaw et al., 2010). They can be structurally divided in 6 subfamilies (Wu et al., 2010), among which 5 are involved in spice sensing, chemo-, thermo- and/or mechanosensation: vanilloid TRP (TRPV), melastatin TRP (TRPM), ankyrin TRP (TRPA), polycystin TRP (TRPP) and canonical or classical TRP (TRPC) (Holzer, 2011). The TRP channel subunits are made of 6 transmembrane domains with a pore between transmembrane domains 5 and 6 (Clapham et al., 2005; Wu et al., 2010). Four subunits form the functional channel, which can be open and close by conformational changes (Dhaka et al., 2006; Bandell et al., 2007). TRP channels are only weakly sensitive to depolarization but open in response to changes in temperature, binding of ligands or other alterations of the protein itself (Clapham et al., 2005; Matta and Ahern, 2007; Nilius et al., 2007; Wu et al., 2010). They have many distinct functions in the GI system, such as tasting food, sensing of chemicals and toxins produced by the GI microbiome or generated by tissue injury and inflammation, and perception of thermal and/or mechanical stimuli. Besides surveillance functions, they are also important for the control of membrane potential and excitability of neurons, epithelial cells, muscle cells and ICCs, play a role in Ca^{2+} and Mg^{2+} absorption, govern blood flow, pacemaker activity, motor activity, secretory processes and mucosal homeostasis, and impact on the development of GI cancer (Holzer et al., 2011).

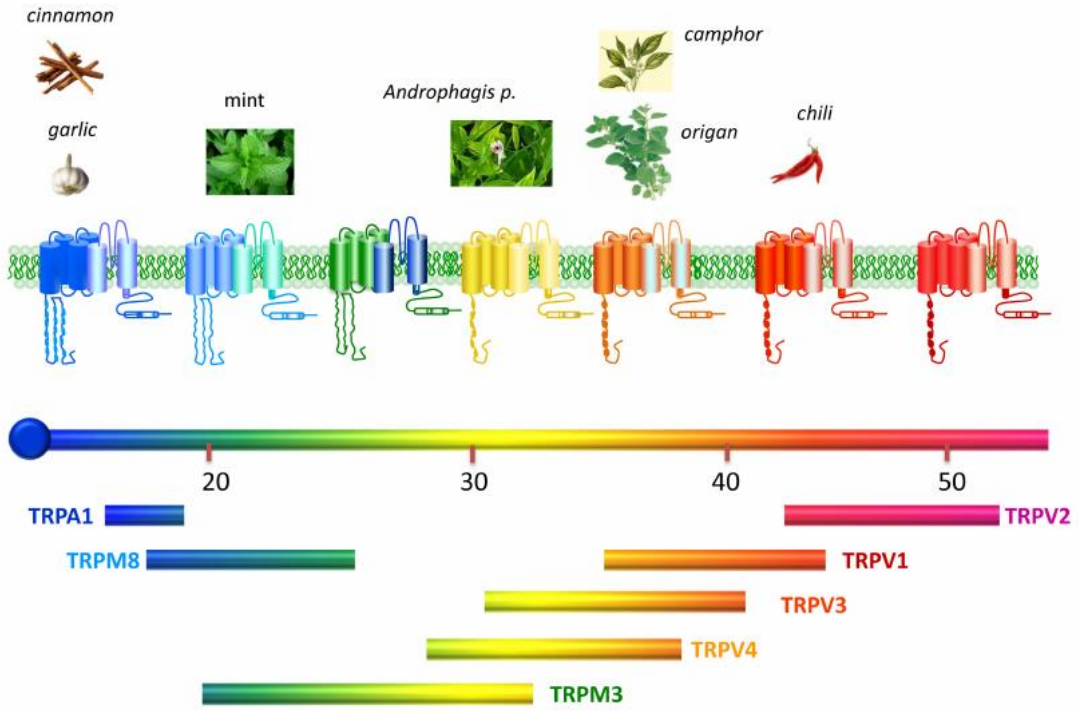

Figure 19. Thermotransient receptor potential (TRP) channels. Structurally thermoTRP are tetramers and each subunit contains six transmembrane domains (S1–S6), a hydrophobic pore loop linking transmembrane S5 and S6, and large cytoplasmic N- and C-terminals (NB not drawn to scale). All thermoTRPs have a variable number of ankyrin repeat domains in the N-terminus, except TRPM8 which has none and instead contains TRPM homology region. ThermoTRPs display distinct thermal thresholds from very noxious cold (TRPA1) to harmful hot (TRPV2). Each thermoTRP is also activated by specific natural or synthetic compounds, known to induce the relevant thermal and pain sensations in humans. From Ferrandiz-Huertas et al., 2014.

TRPs may have 3 different roles by operating as: 1) molecular sensors (detectors or primary transducers) of chemical and physical stimuli; 2) downstream or secondary transducers (or effectors) of cell activation mediated by G-protein-coupled receptors (GPCRs) or ion channel receptors; 3) ion transport channels responsible, e.g., for Ca^{2+} and Mg^{2+} homeostasis. TRP channels can translate the signals detected in two different ways, by realising neuropeptides from the endings of the TRP-expressing afferent fibers, which causes changes in local tissue function (Holzer, 1988; Maggi and Meli, 1988), and by transmission to the CNS resulting in autonomic reflex responses and sensation. Except for TRPA, the subfamilies consist of several members, each of which is activated by a variety of different stimuli (Figure 19). TRP channels are largely distributed in many tissues and cell types. A number of them appear to be universally expressed, whereas others exhibit more restricted expression patterns (Blackshaw et al., 2010). Beside the plasma membrane, TRP channels are also found in intracellular membranes where they are involved in the regulation of membrane trafficking, signal transduction, and vesicular homeostasis (Dong et al., 2010). Several clinical evidence show an altered TRP channel expression or function in FGIDs (Akbar et al., 2010; Akbar et al., 2008; Wouters et al., 2016). Moreover, preclinical models using TRP agonists and transgenic mouse models lacking TRP channels highlight the key role of TRPs in the development and maintenance of afferent hypersensitivity in the colon (Cenac et al., 2008; Van Den Wijngaard et al., 2009; Christianson et al., 2010; Holzer, 2011).

1.2.3.3.1.1 TRPV1

TRPV1 is the best characterized and most studied nociceptor in VHS. It is a voltage-gated outwardly rectifying cation channel activated by noxious heat (> 43°C), acidosis (pH < 6) (Tominaga et al. 1998), exogenous irritants such as vanilloid capsaicin (the pungent principle in hot peppers) (Caterina et al. 1997), allyl isothiocyanate (AITC, the pungent compound in mustard oil, horseradish and wasabi) (Everaerts et al. 2011), and a variety of endogenous lipid compounds, including anandamide (Gavva et al. 2008) and some lipoxygenase metabolites of arachidonic acids (Hwang et al. 2000). In the GI system, TRPV1 is expressed by both intrinsic and extrinsic sensory neurons as well as by epithelial and endocrine cells. In particular, it has been seen that in the rat, guinea-pig and murine gut the major sources of TRPV1 are spinal and vagal primary afferent fibers (Patterson et al., 2003; Ward et al., 2003; Holzer, 2004; Horie et al., 2004; Kadowaki et al., 2004; Robinson et al., 2004; Schicho et al., 2004; Banerjee et al., 2007; Ryu et al., 2010; Zhao et al., 2010). Both in DRG and nodose ganglia, only small and medium-sized neuronal cell bodies, which are known to give rise to C- and Aδ- fibers, express TRPV1 (Caterina et al., 1997; Guo et al., 1999; Michael and Priestley, 1999; Banerjee et al., 2007; Tan et al., 2008, 2009). Because of its pattern of expression, it has been

suggested that TRPV1 could play a crucial role in nociception (Ward et al., 2003; Brierley et al., 2005; Christianson et al., 2006). For example, it has been demonstrated that TRPV1 expression and/or deregulation is involved in VHS experienced by patients with different pathophysiological contexts, such as rectal hypersensitivity (Chan et al., 2003), IBD (Yiangou et al., 2001) and IBS (Akbar et al., 2008). For example, it has been seen that IBS patients with VHS identified by colorectal balloon distention experience more pain during rectal application of capsaicin compared with normosensitive patients and healthy individuals. Nevertheless, rectal TRPV1 mRNA and protein level of IBS patients was comparable to that of healthy individuals, suggesting that TRPV1 is sensitized rather than upregulated (van Wanrooij et al., 2014**)**. Moreover, the involvement of TRPV1 has also been demonstrated in various preclinical models of VHS. For example, mice deficient in TRPV1 failed to develop post-inflammatory VHS following acute colitis induced by dextran sulfate sodium (DSS) (Lapointe et al., 2015). It has been demonstrated that several inflammatory mediators and factors associated with hyperalgesia (e.g. bradykinin, 5-HT, neuronal growth factor, tryptase), but also mild acidosis, are able to sensitize TRPV1 and enhance the probability of channel gating by heat and capsaicin (Chuang et al., 2001; Ji et al., 2002; Amadesi et al., 2004; 2006; Sugiuar et al., 2004)

1.2.3.3.1.2 TRPV4

The fourth member of the TRP channels vanilloid subfamily is a Ca^{2+}-permeable cation channel activated by a variety of stimuli such as hypo-osmotic swelling (Liedtke et al., 2000; Strotmann et al., 2000**)**, strong acidosis (Suzuki et al., 2003), non-noxious warm temperatures (> 25°C) (Güler et al., 2002; Watanabe et al., 2002), mechanical distension (Suzuki et al., 2003a,b; Grant et al., 2007), shear stress (Gao et al., 2003), downstream metabolites of arachidonic acid (epoxyeicosatrienoic acids) (Cenac et al., 2015; Vriens et al., 2005; Watanabe et al., 2003) and phorbol esters (both protein kinase C-activating and non-activating phorbol esters) (Gao et al., 2003; Watanabe et al., 2002; Xu et al., 2003). In the GI tract of both human and mouse, TRPV4 is expressed by extrinsic sensory fibers innervating the outermost (serosal and mesenteric) layers (Brierley et al., 2008) as well as by a variety of non-neuronal cells such as epithelial and endothelial cells (Balemans et al., 2017), but is scarce in intramuscular or mucosal endings. It has also been demonstrated that TRPV4 expression is greater in the populations of DRG neurons innervating the colon, compared whole DRGs (Brierley et al., 2008). Recent evidence suggest TRPV4 has a role in visceral nociception. For example, it has been seen that the mechanosensory responses of serosal and mesenteric afferents in the colon were drastically decreased in TRPV4-deficient mice, whereas vagal and pelvic mucosal and muscular afferents showed no deficit (Brierley et al., 2008). Consistently, it has been demonstrated that TRPV4 activation by 4 a-phorbol 12,13-didecanoate causes visceral allodynia and hyperalgesia, and that this

channel is involved in visceral nociception in response to colorectal distention (Cenac et al., 2008). Moreover, it was also found that TRPV4 immunoreactivity is enriched in colon resections from IBD patients (Brierley et al., 2008). Also, TRPV4 mRNA is highly enriched in colonic biopsies obtained from patients with CD) and ulcerative colitis (UC), compared with healthy subjects (Fichna et al., 2012). Moreover, several evidence show that protease activated receptor 2 (PAR2) activation, which is implicated in the generation of VHS by mediators released from colonic biopsies of patients with IBS (Cenac et al., 2007; Buhner et al., 2009), increase the response on TRPV4 agonists in cultures of DRG neurons (Grant et al., 2007).

1.2.3.3.1.3 TRPA1

TRPA1 is activated by noxious cold (< 17°C), mechanical stimuli (Story et al., 2003) and by a variety of pungent compounds, such as such as cinnamaldehyde (in cinnamon) (Bandell et al., 2004), AITC (Jordt et al., 2004**)**, allicin (in garlic) (Bautista et al., 2005), menthol (Karashima et al., 2007), inflammatory fatty acids, prostaglandin metabolites, and hydrogen peroxide (Andersson et al., 2008; Materazzi et al., 2008). It has also been seen that TRPA1 acts as a sensor of bacterial lipopolysaccharides (Meseguer et al., 2014; Soldano et al., 2016). In mammals, TRPA1 is expressed by both intrinsic (vagal, splanchnic and pelvic pathways) and EPANs (Penuelas et al., 2007; Story et al., 2003). It was shown to be mainly expressed in afferents with mucosal and serosal/mesenteric mechanoreceptive fields (Brierley et al., 2009). In addition, also nonneuronal 5-hydroxytryptamine-releasing enterochromaffin cells (Nozawa et al., 2009), cholecystokinin-releasing endocrine cells (Qin et al., 2010), and intestinal epithelial cells (Kono et al., 2013) were found to express TRPA1. The majority of the literature on TRPA1 in VHS is based on preclinical studies. For example, a study demonstrated that intracolonic administration of a TRPA1 agonist increased the VMR in WT mice, whereas TRPA1-deficient mice did not show this effect, suggesting that TRPA1 plays a role in VHS (Brierley et al., 2009; Catteruzza et al., 2010). Interestingly, a recent study reported upregulation of TRPA1 mRNA expression in biopsies of active IBD patients but not in quiescent IBD patients, suggesting TRPA1 should be taken in consideration as a target for treating VHS (Kun et al., 2014).

1.2.3.3.1.4 TRPM8

TRPM8 is activated by cooling (< 28°C), menthol, and cooling compounds such as spearmint, eucalyptol, and icilin (TRPM8 agonist) (McKemy et al., 2002; Peier et al., 2002). Recent evidence suggests that TRPM8 is expressed by peripheral sensory neurons originating in nodose-petrosal ganglia and DRG and innervating visceral organs (McKemy et al., 2002; Harrington et al., 2011). For this reason, it has been suggested that it may be involved in the development of VHS (Balemans et

al., 2017). Preclinical models suggest that activation of TRPM8 results in a decreased visceral pain perception. For example, post-TNBS induced colonic mechano-hypersensitivity was significantly diminished by a mixture of the TRPM8 agonists (Adam et al., 2006). Moreover, different clinical trials showed IBS patients treated with enteric-coated peppermint oil present decreased abdominal pain (Cappello et al., 2007; Kline et al., 2001; Merat et al., 2010). Interestingly, one study showed that TRPM8 activation on colonic afferents leads to mechanical desensitization combined with decreased agonist-evoked responses to TRPA1 and TRPV1, suggesting that TRPM8 may couple to TRPV1 and TRPA1 to inhibit their downstream chemosensory and mechanosensory actions (Harrington et al., 2011). Nevertheless, it is noteworthy that not all studies confirm these antinociceptive evidence. For example, Hosoya and colleagues found an increased expression of TRPM8 in the distal colon mucosa of a 2,4,6-trinitrobenzene sulfonic acid (TNBS) and dextran sulfate sodium (DSS) mouse colitis model, and that treatment with the TRPM8 agonist WS-12 triggered increased visceral pain responses, compared with controls. Also, this was prevented by pretreatment with a TRPM8 antagonist (Hosoya et al., 2014). Therefore, it seems that TRPM8 is able to function in innocuous cool sensation, nociception, and analgesia. How TRPM8 may be able to carry out these different sensory modalities is still unclear and requires further investigation (Balemans et al., 2017).

1.2.3.3.2 Evaluation of visceral sensitivity

It's defined as "noxious" a stimulus that produces a potential or frank tissue damage (Ness and Gebhart, 1988). In animal testing, for any stimulus to be considered noxious in intensity, its application must trigger a nociceptive reflex or nocifensive behavior, such as a nociceptive withdrawal or pseudaffective response, passive or active avoidance of the stimulus, or other learned behavior. In the absence of evidence of a nocifensive behavioral response to the stimulus, assertion of the stimulus as noxious is uncertain (Gebhart and Bielefeldt, 2016). Cutaneous pain has always been easier to be studied, compared to visceral pain and there are two main reasons for this. Firstly, stimuli that activate cutaneous nociceptors are well known (cutting, crushing, pinch, heat) and, secondly, skin is readily accessible. On the contrary, organs are more difficult to reach and nociceptive stimuli adequate for causing visceral pain are really different and much more complicated to be reproduced. Visceral pain is known to be caused by insults such as ischemia (e.g. myocardium), inflammation (appendix), traction upon the mesentery and distension of hollow organs (Lewis, 1942; Ritchie, 1973; Ness and Gebhart, 1990). It is important to highlight that stimuli for studying visceral pain in animal models should match some criteria: 1) to mimic a natural stimulus, being related to human pathology and pain reports; 2) to be non-invasive; 3) to be controllable by the experimenter

(can be rapidly ended); 4) to generate quantifiable physiological and behavioural responses; 5) to be reproducible and 6) to be applicable to unanesthetized animals (Ness and Gebhart, 1988; Ness and Gebhart, 1990; Christianson and Gebhart, 2007). In the past, several noxious stimuli have been used by researchers, but none of them met all the above criteria. For example, electrical stimulation of isolated visceral nerves (splanchnic or pelvic nerve) is a reproducible and easily controlled stimulus but is neither a natural stimulus nor is organ specific. Moreover, it's not suitable as a stimulus to study abdominal pain in pathological conditions in which primary afferents are known to be altered. Ischemia is a commonly accepted noxious stimulus to cause visceral pain, especially in the case of diseased or recently traumatized tissue (e.g. after surgery), and it is known to produce pseudoaffective responses in animals. However, ischemic myocardium or infarcted bowel is often "silent" clinically, and reflex and neuronal responses to ischemia generally exhibit high variability both within and among preparations. Again, chemical stimuli (e.g. acetic acid) produce measurable physiologic responses, but lack reliability, specificity and reproducibility, are ethically questionable when used in awake, unanesthetized animals and are not controllable by the experimenter. On the contrary, a mechanical stimulus such as balloon distension of hollow organs reproduces a natural stimulus and produces vigorous, reliable and reproducible neuronal responses, thus fulfilling all criteria as adequate noxious visceral stimuli (Ness and Gebhart, 1988; Ness and Gebhart, 1990). Indeed, balloon distension of hollow organs has been widely used to study visceral nociception in many organs (gallbladder, esophagus, stomach, small bowel, colorectum, vagina, uterus, and urinary bladder) and animal models (rodents, cats, dogs and non-human primates) (Gebhart and Bielefeldt, 2016). The most characterized is CRD, which has the significant advantage that it can be performed in unanesthetized animals (Ness and Gebhart, 1988), whereas the distension of other organs may require anesthesia or sedation. Since late '80s, CRD has been extensively adopted to study visceral pain mechanisms and modulation in several animal models, such as rodents (Kamp et al., 2003; Coutinho et al., 2002; Ji and Traub, 2002), rabbit (Crawford et al., 1993), cat (Janig and Koltzenburg, 1991), dog (Cevese et al., 1992) and monkey (Al-Chaer et al., 1998). In CRD, a balloon is inserted into the discending colon via the anus, and balloon size, pressure and duration of balloon inflation are all under the control of the researcher (Ness and Gebhart, 1988). Noxious intensities of CRD produce many different measurable and quantifiable responses: increases in heart rate, respiration and blood pressure, and contraction of the abdominal musculature. CRD is based on the principle that balloon distension evokes a "guarding reflex" organized supraspinally that induces the contraction of the abdominal musculature. This response is called VMR and is intensity-dependent and temporally linked to stimulus onset and termination. The most reliable way to detect and quantify VMR is via electromyographic (EMG) electrodes, which are surgically inserted into the abdominal musculature

of the animal. EMG electrodes are typically placed in animals under anesthesia, and balloon is inserted under mild sedation. Animals are typically awake during CRD, although the model can be used also in sedated or mildly anesthetized animals (Ness and Gebhart, 1988). Another method to study, at behavioral level, the visceral sensitivity in response to CRD is measuring the AWR (Al-Chaer et al., 2000). This reflex consists in an involuntary motor reflex similar to the visceromotor reflex that involves a supraspinal loop and causes a visually detectable and quantifiable contraction of abdominal muscles. AWR is reproducible and dependent from the intensity of the stimulus and thus can be quantified through the assignment of a numerical semiquantitative score (Al-Chaer et al., 2000).

1.2.3.4 Enteric Glial Cells

Similarly to the CNS, the ENS is composed of neurons as well as glial cells, which form a complex network located in the GI wall, including pancreas and gall bladder (Komuro et al., 1982). The first observation of EGCs was reported by Dogiel in 1899 (Dogiel, 1899), then for the next 70 years, they were thought to be Schwann cells. In the early ‘70s, Gabella established that EGCs are a different type of glia, differing from those elsewhere in the peripheral nervous system (PNS), with an independent and distinctive identity (Gabella, 1972). In mammals, enteric neurons and glial cells are mostly organized in the myenteric and submucosal plexuses (Timmermans et al., 2001). EGCs are smaller than neurons and display several differently-shaped gliofilaments and processes. They can be found in direct contact with enteric neurons membranes, both in ganglia and nerve strands, and lack myelin sheaths (Gabella, 1972). EGCs number exceeds that of enteric neurons. For example, in the myenteric ganglia of guinea-pig ileum, EGCs were observed to be twice as abundant as neurons (Gabella, 1981). However, he EGC-to-neuron ratio differs between species as well as between the myenteric and submucosal plexus (Hoff et al., 2008). It has also been established that EGCs are more similar in structure and morphology to the astrocytes than to other glial-cell types of the PNS, such as Schwann cells (Gabella, 1981). Based on their location, EGCs can be divided in 4 morphologically different subclasses (Gulbransen and Sharkey, 2012; Boesmans et al., 2015). Type I EGCs are located within ganglia and have a star-shaped morphology, whereas interganglionic type II EGCs are more elongated. Mucosal and intramuscular EGCs have type III and IV morphology, respectively. Several markers can be used to identify EGCs. The transcription factor Sox10 (SRY-related HMG-box 10) (Hoff et al., 2008; Young et al., 2003), the glial fibrillary acidic protein (GFAP) (Jessen and Mirsky, 1980) and the S100 calcium-binding protein beta (S100β) (Ferri et al., 1982) are the most used (Neunlist et al., 2014; Coelho-Aguiar et al., 2015). Sox10 is expressed by enteric neuronal crest (NC) progenitors and thus is considered a general glial marker, whereas only distinct subpopulations of

EGCs display GFAP and/or S100β expression (Boesmans et al., 2015). Whether these distinct subpopulations of EGCs reflect developmentally programmed different cell types is still to be elucidated (Neunlist et al., 2014). Physiologically, EGCs play many roles. Increasing evidence show EGCs have an important role in homeostatis of ENS as well as of the whole GI system. Several studies demonstrate EGCs exert a neuroprotective action on enteric neurons in many different ways: by increasing neuronal survival and reducing oxidative stress-induced cell death (Abdo et al., 2010), secreting glial mediators with neuroprotective effects (Abdo et al., 2010; Anitha et al., 2006) as well as substrates for neuronal enzymes involved in neuromediator synthesis (Nagahama et al., 2001), regulating neuromediators expression (Aubé et al., 2006), regenerating enteric neurons (Joseph et al., 2011; Laranjeira et al., 2011) and participating in postnatal development of the ENS via expression of Toll-like receptor 2 (TLR2) (Brun et al., 2013). EGCs also have a role in the control of non-neuronal functions of the gut, such as in the regulation of GI motility and of intestinal epithelial barrier (IEB) homeostasis. As reviewed by Morales-Soto and Gulbransen (2019), several lines of evidence suggest that crosstalk between enteric glia and nociceptors contributes to mechanisms that drive visceral hypersensitivity, underlining a role for EGCs in pain perception in humans. Moreover, TRPV1 and TRPV4 pain-related ion channels have found to be expressed by EGCs and to have a role in glial maturation in the mouse (Yamamoto et al., 2016) and in inflammation in patients affected by colitis (D'Aldebert et al., 2011), respectively. Whether this expression may also contribute to activation/sensitization of visceral nociceptors is yet to be defined, even if some interesting results on peripheral GCs have shown that TRPV4 expression enhances purinergic signaling, possibly contributing to inflammatory pain (Rajasekhar et al., 2015). Indeed, several evidence show that EGCs dysfunction in vivo can lead to reduced gastric emptying, intestinal and colonic transit (Aubé et al., 2006; McClain et al., 2014; Nasser et al., 2006), and severe ablation of EGCs can induce a fulminant jejunoileitis, characterized by disruption of IEB integrity, in vivo (Bush et al., 1998; Cornet et al., 2001). A large body of evidence link EGCs alterations to many different pathophysiological conditions. In Parkinson's disease, the presence of enteric inflammation has been associated with glial dysregulation (Devos et al., 2013). In IBDs such as CD and UC, proliferation of EGCs has been found to be altered, as is the expression of GFAP and S100β (Coelho-Aguiar et al., 2015). EGC abnormalities have been displayed also in FGIDs such as slow transit constipation (STC)/colonic inertia and megacolon, two severe gut dysmotility disorders (Neunlist et al., 2014). Moreover, increase in GFAP signal in myenteric and submucosal plexuses was observed in a mouse model of mucopolysaccharidosis IIIB, suggesting enteric glial activation secondary to the lysosomal storage pathology (Fu et al., 2012).

1.3 Gastrointestinal symptoms of Fabry disease

GI symptoms are among the most common and earliest symptoms of FD (Van Wayjen, 1958; Hoffmann et al. 2007; Eng et al. 2007). Fabry Registry data indicate that non-specific GI problems are the initial presenting symptoms in about 23% of boys (median age 5 years) and in about 11% of girls (median age 9 years) (Ries et al., 2003; Hopkin et al., 2008). GI manifestations occur along the entire GI tract varying in intensity and frequency and include a wide range of symptoms, such as abdominal pain, diarrhoea, constipation, bloating, nausea and vomiting (Zar-Kessler et al., 2016). The most common and earliest complaint is abdominal pain, which affects up to one third of patients. They experience cramping mid-abdominal discomfort, which is frequently worsened by meals and increased stress, and severe and debilitating pain, commonly worsened by changes in diet and frequency of meals (Hoffmann et al. 2007). Occurring in 20% of patients, diarrhoea is the second most common GI symptom in FD. It is associated with significant urgency and frequency (up to 15 times a day), but not with blood or mucous in the stool, unlike other inflammatory GI disorders (Hoffmann et al. 2007). On the contrary, a subset of patients, mostly female, described debilitating constipation (Deegan et al. 2006), whereas another one experienced a cyclical pattern of alternate diarrhoea and constipation interspersed with period of normal bowel movements, generating complications for a correct diagnosis (Keshav et al. 2006). Sometimes patients experience also nausea, vomiting and early satiety, with significantly delayed gastric emptying (Argoff et al. 1998). Moreover, case reports showed some severe and localized disease manifestations such as cholelithiasis, achalasia, and autoimmune diseases, and rarely complications requiring interventions including jejuna diverticulosis, leading to perforation, pseudo obstruction, fistulas, and bowel ischemia (Politei et al. 2016). Prevalence of GI symptoms in FD is reported in Figure 20.

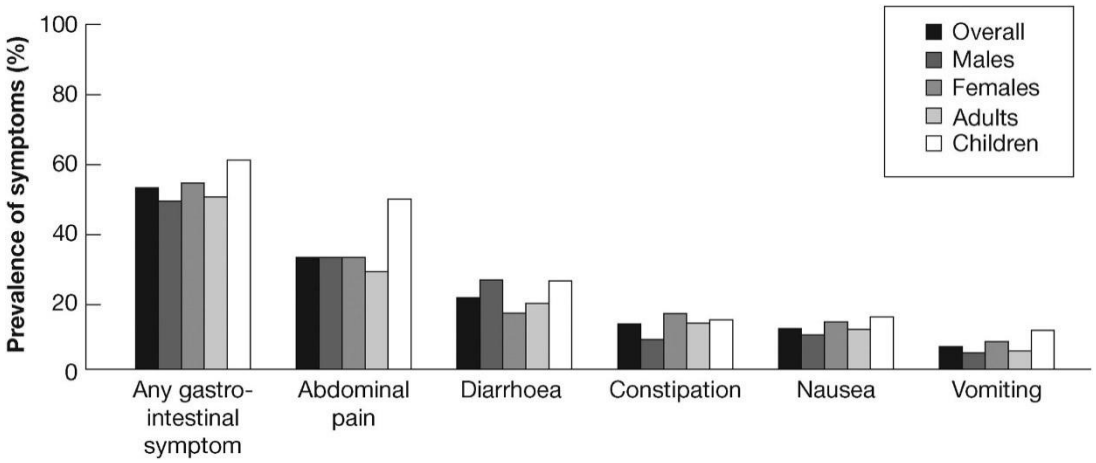

Figure 20. Prevalence of GI symptoms in FD. Reported prevalence of GI symptoms in 342 patients with FD: more than 50% of patients reported GI symptomatology. The most prevalent symptoms were abdominal pain and diarrhoea. From Hoffmann et al., 2007.

Weight loss due to malabsorption of nutrients is common among children (MacDermot et al., 2001; Buda et al., 2013). Generally, it occurs in boys, who are underweight and short for their age, whereas girls tend to have normal weight and height (MacDermot et al., 2001). GI manifestations have a great impact in patients' lives. It has been demonstrated that patients affected by FD commonly report a reduced health-related quality of life (HR-QoL) and depression (Müller, 2006; Hoffmann et al., 2007; Hopkin et al., 2008; Bolsover et al., 2014; Ali et al., 2018). A questionnaire for measuring the general health status of the population, the EuroQoL five-dimension (EQ-5D), has been developed. It provides a standardized tool to obtain a score ranging from -1 to 1 (Dolan, 1997; Hoffmann et al., 2007). In a cohort of adult FD patients, the mean EQ-5D baseline score resulted to be 0.63, compared to 0.72 of patients without GI symptoms ($p < 0.05$) (Hoffmann et al., 2007). Children with GI symptoms have also lower HR-QoL scores compared to healthy children (Hopkin et al., 2008; Wraith et al., 2008).

1.3.1 Correlation between non-specific gastrointestinal symptoms and Fabry disease

Since GI symptoms of FD are non-specific, especially those appearing early in life, and specific features of FD manifest in adulthood, many children, adolescents and adults are frequently misdiagnosed. When there is no evidence or suspicion of FD in the family, patients can carry other diagnoses including CD, celiac, or IBS, prior to receiving the correct diagnosis (Marchesoni et al., 2010). FD should be also considered as a possible cause of GI problems in patients who experience a long-term history of unexplained GI symptoms such as postprandial abdominal pain, non-inflammatory diarrhoea with frequent urgency, early satiety, gastroparesis, or chronic intestinal pseudo-obstruction (Zar-Kessler et al., 2016). Questionnaires created in order to identify non-specific GI symptoms may help differentiating FD from other common GI disorders. Patients with GI symptoms and undiagnosed FD often undergo various tests such as gastroscopy, colonoscopy, and barium meal without any abnormal results (MacDermot et al., 2001). If questionnaire results to provide a suspicion of FD, patients should be referred for confirmatory enzymatic and genotype testing. The Questionnaire on Paediatric GI Symptoms (Rome III criteria) is often used in order to specifically characterize GI symptoms and quickly identify FD-related symptoms (Pensabene et al., 2015). For this reason, the Gastrointestinal Symptom Rating Scale (Svedlund et al., 1988) has been modified with the inclusion of questions related to FD symptoms. In the Table 3, examples of these FD-related questions are shown.

• How many times (daily/weekly/monthly) do you feel pain in your abdomen?
• Do you suffer from diarrhoea alternating with constipation?
• Do you often feel nauseous or experience vomiting?
• Do you suffer from unexplained fever (i.e. not related to an infection)?
• Are you aware of intolerance to cold/heat?
• Do you have a reduced ability to sweat (particularly as a child)?
• Do you experience excessive burning pain in the extremities, especially in hands and feet? (Or did you experience this during your childhood/teenage years?)
• Have you had a recent eye (ophthalmic) examination? If yes, did your ophthalmologist mention some "ocular, in particular corneal," abnormality?
• Have any of your family members died early or unexpectedly?

Table 3. Examples of questions suitable for prompting consideration of Fabry disease in a patient with non-specific GI symptoms and no family history. From Hilz et al., 2018.

1.3.2 Pathophysiology of Fabry disease gastrointestinal symptoms

The pathophysiologic mechanisms by which FD causes these symptoms are poorly understood, even if it is known that these are the result of the accumulation of Gb3, which causes vascular dysfunction and malfunction of the ENS. Vascular abnormalities can be the reason of cell injury via both mechanical and signalling pathways: Gb3 accumulates in the endothelium and smooth muscle cells leading to vessel wall expansion (Namdar et al. 2012) and proliferation of the smooth muscle cell (Boutouyrie et al. 2002; Rombach et al. 2010). The result is the intraluminal thickening with subsequent decreased vessel flow, ultimately causing ischemia, infarction and eventual end-organ damage (Sheth et al. 1981). Muscle wall thickening areas associated with fibrotic areas adjoining the diverticula have also been described (Friedman et al. 1984). In particular, the formation of diverticula can be the result of long periods of dismotility, which cause intraluminal pressure areas with protrusion of intestinal mucosa. Autopsy and biopsy studies displayed myenteric and submucosal plexuses affected with inclusions, and histopathological analysis showed vacuolization of ganglion cells and surrounding axons with intracellular Gb3 accumulation (Politei et al. 2016). Indeed, neurologic involvement has been demonstrated to be extremely important in GI manifestations of FD. The ANS neuropathy is the effect of both neuronal Gb3 accumulation and vascular occlusion of peripheral nerve vasa vasorum, which leads to neuronal ischemia and dysregulation (Hilz et al. 2002). The DRG have the finest associated blood vessels and so these are particularly susceptible to injury from vascular modifications (Keshav et al. 2006). In addition, some results show preferential

disruption in the small, thin, unmyelinated nerve fibres associated with peripheral pain perception and the ENS (Dutsch et al. 2002). Moreover, it has also been reported that the typical Gb3 lysosomal inclusions are present also in intestinal smooth muscle cells and pericytes (Flynn et al. 1972; Deniz et al. 2011). Although clear clinical signs of GI problems have not been reported yet in α-Gal A KO mice, Bangari and colleagues found several alterations in the GI tract of these mice. In mouse cross sections of the ileum and colon, high-resolution light microscopy (HRLM) and transmission electron microscopy (TEM) revealed lysosomal storage inclusions in a few smooth muscle cells of the intestinal wall. Moreover, several neurons in the myenteric and submucosal plexuses were considerably enlarged and vacuolated, and both HRLM and TEM showed membrane-bound lysosomal inclusions within enlarged myenteric plexus ganglion cells and smooth muscle cells of KO mice. Gb3 levels in samples of ileum and colon from α-Gal A KO and control mice were determined by mass spectrometric analysis: significantly elevated Gb3 levels were found in small intestine of α-Gal A KO mice, compared with small intestine of control mice. Finally, IF staining with anti-CD77 antibody confirmed the molecular specificity of the storage inclusions. Hence, these findings indicate the potential utility of α-Gal A KO mice as a model for investigating FD neuropathy and enteropathy (Bangari et al. 2015). Although accumulation and ischemia are the leading causes of disease manifestations, recent studies suppose that Gb3 deposition may also be the cause of alterations in invariant natural killer T cells (Pereira et al. 2013), leading to an amplified inflammatory response. Moreover, in a mouse model, it was shown that Gb3 accumulation generates interference with the NO pathways inducing a prothrombotic environment (Park, et al. 2009; Kang et al. 2014). These alterations can be translated in the clinical GI symptoms of FD. For example, it is postulated that abdominal pain is due to inadequate blood flow to the GI tract. Furthermore, small-fibre neuropathy, like peripheral neuropathy-causing acroparesthesias, probably contributes to the abdominal pain. The diarrhoea is hypothesised to be due to a combination of processes: ANS abnormalities, Gb3 accumulation within the villi (Zar-Kessler et al. 2016) and bacterial overgrowth due to the neuropathic-reduced peristalsis (i.e. Helicobacter Pylori) (Franceschi et al. 2015). The bacterial overgrowth may also predispose to malabsorption and diverticula formation. Finally, the upper GI symptoms may be due to substrate accumulation causing neuronal dysfunction (O'Brien et al. 1982). It is noteworthy that Di Martino and colleagues evaluated the inter-variability of GI symptoms recurrence in 49 FD patients: they used a pharmacogenomics approach to explore genetic factors potentially involved in clinical manifestations in FD. They performed, by using the DMET Plus platform, a profiling of 1936 common and complex functional variants (Single Nucleotide Polymorphism (SNPs), insertions, duplications, deletions) across 231 genes encoding for drug-metabolizing enzymes and drug transport proteins, and identified nine SNPs potentially associated

with GI symptoms. However, the effects of these variants on the pathogenesis of FD remain to be studied (Di Martino et al. 2016). Many studies explain that introduction of ERT can improve patients' overall health status, including GI symptoms (Hoffmann et al. 2007; Schiffmann et al. 2014). These results are promising as indicate that some GI manifestations may be reversible, in at least a subset of patients. Thus, as it is known that Gb3 deposition begins in utero, there is significant emphasis on early initiation of ERT. With earlier and correct diagnosis of the GI symptoms of FD, patients may be able to initiate an appropriate treatment, thus improving their quality of life (Zar-Kessler et al. 2016).

2 AIM

FD is a rare, progressive, multi-organ, X-linked inherited, metabolic storage disorder characterized by a deficient or absent activity of the lysosomal enzyme α-Gal A. This deficiency causes a progressive accumulation of GSLs, primarily Gb3, in several cell types, such as endothelial, renal, cardiac and neuronal cells, triggering a wide range of systemic alterations including peripheral fiber damage, stroke, and renal and cardiac dysfunctions (Desnick et al., 2001; Germain, 2010). In the classical phenotype of FD, the earliest presenting symptoms in childhood are typically neuropathic pain, mainly burning paroxysmal hand and foot pains (acroparesthesias), and GI problems, which can severely influence the quality of life (Schiffmann and Scott, 2002; Zar-Kessler et al., 2016). Pain can manifest as episodic crisis with pain attacks originating in the extremities that can last for several days or even weeks, or chronic pain, characterized by burning and tingling paresthesia. Indeed, several studies have shown that almost all male and about half to three quarters of female Fabry patients show diagnostic features compatible with small fiber neuropathy (SFN), a peripheral neuropathy affecting the thinly myelinated Aδ fibers, which transmit mechanical pain sensitivity to pinprick stimuli, and the unmyelinated C fibers, which transmit warm sensation and pain sensitivity to heat. In particular, Fabry patients display reduced intra-epidermal nerve fiber density (IENFD) and impaired mechanical and thermal perception (Politei et al., 2016; Biegstraaten et al., 2012). The pathophysiological mechanisms underpinning these alterations are still poorly understood. It has been hypothesized that Gb3 deposits in DRG neurons may cause neuronal damage leading to reduction of IENFD (Kahn, 1973) as well as alteration of cellular excitability (Üçeyler et al., 2011; Tuttolomondo et al., 2013). Moreover, Gb3 could lead to chronic nerve ischemia by accumulating within endothelial cells of blood vessels supplying nerve fibers (Gayathri et al., 2008). Another possible hypothesis is that the increase in the number of small regenerating unmyelinated fibers (Tomé et al., 1977) may generate hyperexcitability and spontaneous firing of sprouting unmyelinated neurites arising from nociceptive axons (Politei et al., 2016). Finally, as seen in mice by Choi and colleagues (2015), exogenous Gb3 and lyso-Gb3 may contribute to activate sensory fibers inducing mechanical allodynia. In the context of neuropathy, it has been recently demonstrated that the α-Gal A (-/0) hemizygous male mice, the murine model of FD (Ohshima et al., 1997), share many symptoms with FD patients and presents structural and molecular alterations in peripheral neuronal terminations as well as in DRGs neurons. In particular, it has been shown that this murine model of FD presents a decreased IENFD, altered molecular and functional expression of pain-related ion channels: a constant cold hypoalgesia, and a heat hyperalgesia in young age which turns into hypoalgesia with aging (Lakoma et al., 2014 and 2016; Üçeyler et al., 2016; Namer et al., 2017; Hoffman et al., 2018).

GI symptoms of FD occur at various levels along the entire GI tract, with variable intensity and frequency and include abdominal pain, bloating, diarrhoea, constipation, nausea, vomit and early satiety (Zar-Kessler et al., 2016). Unfortunately, many of these symptoms are non-specific, thus patients with FD are frequently misdiagnosed. It is believed that these symptoms are the result of the accumulation of Gb3, which may cause vascular dysfunction and malfunction of the ANS, the responsible of gut mobility. It has been demonstrated that the ANS neuropathy is the effect of both neuronal Gb3 accumulation and vascular occlusion of peripheral nerve vasa vasorum, which leads to neuronal ischemia and dysregulation (Hilz, 2002). Indeed, in a murine model of the disease, sections of the ileum and colon show lysosomal storage inclusions in smooth muscle cells of the intestinal wall and several neurons in the myenteric and submucosal plexuses appear considerably enlarged and vacuolated (Bangari et al., 2015). However, despite these evidences, the exact mechanisms of pain perception and the structural/functional modifications of the GI system in the FD are still poorly understood. To investigate the pathophysiological mechanisms of GI symptoms, we carry out the first morphological and molecular characterization of the colon of the α-Gal A (-/0) mouse, by evaluating the macroscopic and microscopic damage, the myenteric plexus ganglia area and neuronal density, the Gb3 deposits and the density of fibers innervating the colonic mucosa (Masotti et al., 2019). In addition, we assessed for the first time the presence of visceral pain in the α-Gal A (-/0) mouse by studying the VMR and AWR in response to CRD. Moreover, immunofluorescence (IF) protocols to stain pain-related ion channels in the colonic wall of both α-Gal A (-/0) and α-Gal A (+/0) were optimized and the pattern of expression was evaluated by molecular and cellular techniques. Nevertheless, further studies are required to assess the presence of differences in terms of molecular and functional expression. In fact, we thought that the electrophysiological characterization of enteric neurons and glia could have been useful to gain further insight into visceral pain perception mechanisms in α-Gal A (-/0) mice. For this purpose, we optimized the protocols to obtain three different types of primary culture from mouse intestine: a mixed culture containing both enteric neurons and glia, a co-culture system with EGCs which allow to obtain an enriched culture of enteric neurons and finally, an enriched culture of EGCs.

3 MATERIALS AND METHODS

3.1 Animals and maintenance

Heterozygous female mice for α-Gal A gene deletion (+/-), JAX strain B6;129-Gla$^{tm/1Kul}$/J and WT male α-Gal A (+/0), same JAX strain B6;129-Gla$^{tm/1Kul}$/J were purchased from Charles River Laboratories Italia s.r.l. (stock number 003535; Jackson Laboratory; Bar Harbor; ME, USA). Briefly, this strain is cryopreserved as sperm from hemizygous mutant males. As the α-Gal A gene is located on the X chromosome, when the cryo-recovered strain is created by in vitro fertilization (IVF), using oocytes from B6;129 SF1/J females, all the resulting females are heterozygotes and all the males wild type. Thus, all the recovered mice belong to the same mixed genetic background. The heterozygous female α-Gal A (+/-) mice and α-Gal A (+/0) male mice were crossed to give the F1 generation, thus obtaining females α-Gal A (+/-), females α-Gal A (+/+), male α-Gal A (+/0) and KO males α-Gal A (-/0). To obtain the F2 generation, we further crossed females α-Gal A (+/-) with males α-Gal A (-/0), generating females α-Gal A (+/-) and (-/-), not used in this study, and males α-Gal A (-/0) and α-Gal A (+/0). Therefore, in each experiment here presented, we used α-Gal A (-/0) male mice compared to α-Gal A (+/0) male littermates as controls (Masotti et al., 2019). Both α-Gal A (+/-) and (-/0), mice were housed in groups of 6 in individually ventilated cages (Tecniplast, Italy) with water and food *ad libitum* in controlled environmental conditions: lights on from 7.00 am to 7.00 pm, 22 ± 2°C temperature and 65% humidity. Once reached sexual maturity (21-28 days), males and females were separated. For all the experiments 6 groups of animals were used, based on genotype and age: 8- to 10 week-old, 16- to 20 week-old and 12 month-old α-Gal A (-/0) and α-Gal A (+/0). Because of male greater severity, we decided to focus our study only on α-Gal A (-/0) male mice. All efforts were made to minimize animal suffering and the number of animals used was kept to a minimum by the experimental design. All the procedures followed in this work were in compliance with the European Community Council Directive of November 24, 1986 (86/609/EEC) and were approved by the Ethical committee of the University of Bologna (prot. N.43.IX/9).

3.2 Genotyping

In order to check mice genotype, meaning the presence/absence of GLA gene, we performed the genotyping of the murine colony (Masotti et al., 2019). Genomic DNA was extracted from the last part (1-3 mm) of mice tails. Biopsies were achieved by using sterile scissors. Every mouse was monitored to ensure the blood flow stop. Samples were put into Eppendorf tubes containing 50µL of Lysis buffer (25 mM NaOH, 0.2 mM Na_2 -EDTA; pH 12.4) and placed in the termociclator for 45 minutes at 95°C. The reaction was blocked by adding 50µL of Neutralization buffer (40 mM TRIS-

HCl; pH 5.4) to each tube. The extracted DNA was added to polymerase chain reaction (PCR) mix, shown in Table 4.

	Final concentration	Volume per sample (µL)
10X Reaction buffer	1X	2
25 mM $MgCl_2$ Solution	2 mM	1.6
10 mM dNTP mix	0.2 mM	0.4
20 µM WT1 forward	1 µM	2
20 µM WT2 reverse	1 µM	2
20 µM Fabry mut.	1 µM	2
5 U/µL Taq Polymerase	0.02U/µL	0.08
H_2O ultrapure		7.92
DNA template /H_2O in the control		2
Total volume		20

Table 4. Master mix composition per sample. 10X PCR Buffer without $MgCl_2$ (SigmaMillipore, Burlington, Massachusetts, USA); 25 mM $MgCl_2$ Solution, Magnesium chloride (PCR Reagent, Sigma); 10 mM dNTP, deoxynucleotide Mix (PCR Reagent, Sigma); 5 units/µl Taq Polymerase from Thermus aquaticus; WT1 forward, forward WT primer MW:6176.0 µg/µmole (Invitrogen, Carlsbad, California, USA); WT2 reverse, reverse WT primer MW:6045.0 µg/µmole (Invitrogen); Fabry mut., mutant Fabry reverse primer MW:6159.0 µg/µmole (Invitrogen).

WT forward and reverse primers were $oIMR_{5947}$ (5'-AGGTCCACAGCAAAGGATTG-3') and $oIMR_{5948}$ (5'-GCAAGTTGCCCTCTGACTTC-3'), respectively. The amplification products were two 295 bp-long bands in α-GalA (+/+) females and one band in α-GalA (+/0) males. The mutant reverse primer $oIMR_{7415}$ (5'-GCCAGAGGCCACTTGTGTAG-3') gave two 202 bp-long bands in α-GalA (-/-) females and one band in α-GalA (-/0) males. The PCR amplification program is shown in Table 5.

Program	Cycles	Time	Temperature
Starting denaturation	1	3'	94°C
Denaturation	35	30''	94°C
Annealing		1'	64°C
Elongation		1'	72°C
Final elongation	1	2'	72°C

Table 5. PCR amplification program.

Electrophoresis was performed using a 1.8% agarose gel (100V, 45 min). Briefly, agarose (1.8 g) was dissolved in TAE 1X buffer (100 ml, 40 mM Tris-acetate, 1 mM EDTA) and ethidium bromide (EtBr, 0.5 μg/ml) was added to the gel for U.V. light revelation (λ 254 nm). Before electrophoresis, the 10X loading dye buffer (0.9% SDS, 50% glycerol, 0.05% bromophenol blue, Takara) was added to DNA samples. Samples were then loaded into the wells along with an appropriate volume of DNA size marker (MassRuler DNA Ladder Mix ready-to-use, Thermo Fisher Scientific, Waltham, Massachusetts, USA). The gel was exposed to U.V. trans illuminator for DNA bands visualization.

3.3 Tissue collection and sample preparation

Mice were anesthetized using Halothane and euthanized by cervical dislocation (Masotti et al., 2019). Ventral incision was made using scissors and forceps. The intestine was cut after the stomach and before the distal colon and removed with a clamp. The GI lumen was washed with phosphate-buffered saline (PBS 10 mM, pH 7.4) to remove intestinal contents. Short portions (approximately 1cm) of proximal/middle colon (Figure 21) were cut and fixed in 4% paraformaldehyde (PFA, diluted in PBS) overnight at 4°C. The samples were washed with PBS (3x5 min, room temperature (RT), agitation) and stored in PBS with 0.1% sodium azide until use (short-term storage). Subsequently, samples were prepared for histomorfological and molecular evaluation. The mesentery was removed at the stereomicroscope Nikon SMZ645 (Nikon, Tokyo, Japan) by using a Sylgard dish and a sterile scalpel. Samples were further cut into pieces about 3-4 mm-long and cryoprotected in PBS with 30% sucrose and 0.05% sodium azide (overnight, 4°C, agitation). Once sank to the well bottom, the tissue was embedded in Tissue Tek® O.C.T.™ Compound (O.C.T.= Optimal Cutting Temperature, Killik, Bio Optica, Milan, Italy) and sectioned with a cryostat Leica CM1850 (Leica biosystem, Wetzlar, Germany) (Figure 22).

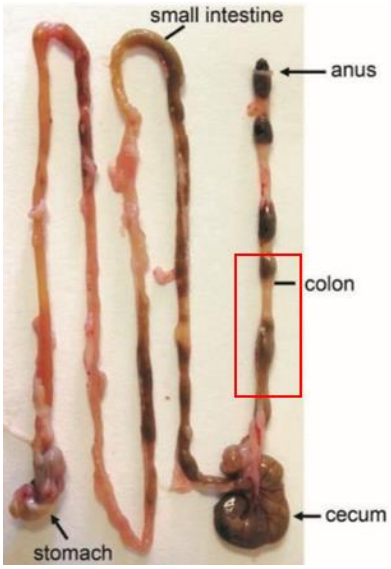

Figure 21. Anatomical structure of mouse GI tract. Proximal/middle colon is highlighted by the *red box*.

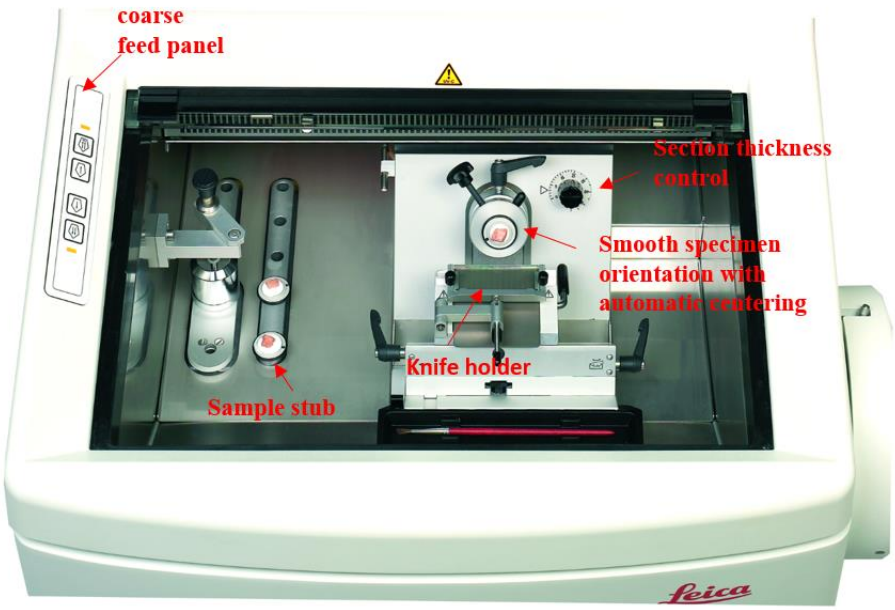

Figure 22. Main components of the Leica CM1850 cryostat. From Leica biosystem website.

Before inclusion, samples were put into a small box for a few minutes at RT to acclimate to O.C.T. Cylinder-shaped supports made of parafilm were fixed on the cryostat stubs and pre-cooled to the temperature recommended by the manufacturer for the GI specimens (-20/-22 °C). Cylinders were filled with O.C.T and the pre-acclimatized samples were transferred into them, perpendicularly to the stubs, in order to get longitudinal sections. After solidification, the frozen samples were left in the cryostat chamber for 20-30 minutes to acclimate O.C.T. to the cutting temperature. Before cutting, parafilm cylinder was removed using tweezers and the stub was put on the chuck to hold it. Ten µm-thick cross sections of colon were cut and collected on polylysine-coated slides (Superfrost UltraPlus®, Thermo Fisher Scientific) to perform hematoxylin and eosin (H&E) staining and immunohistochemical (IHC) analysis. Slides were let dry for 30 minutes and stored at -20°C. Fifty µm-thick cross free-floating sections of colon were cut and stored at 4°C in PBS/sodium azide (0.05%) in order to perform IF analysis.

3.4 Macroscopic damage assessment of mice colon

Macroscopic damage was evaluated (Masotti et al., 2019) by applying the following standardized criteria (Wallace et al., 1990): adherence of colon with abdominal organs (0 = not present; 1 = mild; 2 = major) and feces consistency (0 = formed; 1 = loose; 2 = liquid). In addition, hyperemia, swelling, ulcers, ulcers associated with inflamed tissue and necrosis were evaluated and scored 0-5, respectively.

3.5 Histomorphological analysis of mice colon

3.5.1 Hematoxylin and Eosin staining

Colon 10-μm-thick transverse frozen sections were stained with H&E for the microscopic damage assessment (Masotti et al., 2019). Slides were let air dry for 5-10 minutes at RT, rehydrated in PBS (5 min, RT) and then stained in Harris Haematoxylin (1.5 min, RT) (Bio-Optica). Slides were cleared 3 times in ultrapure water of Type-1 (Milli-Q) (1 min each) and dipped in a basic solution of 0.3% NH_4OH diluted in Milli-Q (5 sec). Slides were washed twice in Milli-Q (1 min, RT), stained in Eosin-Y (1.5 min, RT) (Bio-Optica) and cleared 3 times. Finally, slides were dried, mounted with Fluoromount-G mounting medium (Sigma-Aldrich) and sealed with nail polish.

3.5.2 Immunohistochemical analysis

IHC was performed on 10μm-thick transverse frozen colon sections in order to carry out the histomorphometric evaluation of myenteric plexus ganglia (Masotti et al., 2019). Slides were defrosted for 10 minutes at RT and rehydrated in PBS for 10 minutes. Endogenous peroxidase activity was quenched by the incubation with 0.3% hydrogen peroxide (H_2O_2) diluted in methanol for 30 minutes at RT. Slides were then washed in PBS for 10 minutes, dried and incubated for 1 hour with an appropriate volume of protein block solution (5% bovine serum albumin (BSA), Sigma-Aldrich, 0.1% Triton X-100, Sigma-Aldrich) diluted in PBS in order to block non-specific binding sites. The incubation was performed directly on slides by using a super PAP pen (Liquid blocker mini). Subsequently, slides were dried and incubated overnight at 4°C in humid chamber with the rabbit anti-pan neuronal marker protein gene product 9.5 (PGP9.5) primary antibody (dilution 1:800, Abcam, Cambridge, UK) diluted in PBS with 5% BSA and 0.1% Triton X-100. The morning after, slides were brought to RT for 10 minutes, quickly dived into a solution of 0.01% Triton X-100 diluted in PBS, washed in PBS for 10 minutes and then incubated with the donkey anti-rabbit IgG secondary antibody conjugated with the horseradish peroxidase (HRP) (1:1000; Santa Cruz, Inc, Dallas, Texas, USA) diluted in PBS with 5% BSA (30 min, RT). Slides were dived again into the 0.01% Triton X-100 solution, washed in PBS for 10 minutes and incubated for 2.5 minutes at RT with the 3,3-diaminobenzidine tetrahydrochloride (DAB) solution: DAB (0.1 mg/ml, Sigma-Aldrich), PBS, distilled water and 0.015% H_2O_2. Slides were washed in distilled water (1min) and counterstained with Harrys haematoxylin (1.5 min, RT) for nuclei visualization. After 3 washes (3x1 min), slides were dried, mounted with Glycerol (Sigma-Aldrich) and air-dried overnight. The specificity of the signal was assured by incubation with only secondary antibody (no signal detected).

3.5.3 Immunofluorescence analysis

Gb3, PGP9.5 and neurofilament light polypeptide (NF-L) were detected by IF in order to evaluate Gb3 accumulation, neuronal fiber density and the specificity of PGP9.5 as a neuronal marker, respectively (Masotti et al., 2019). Staining were carried out on 50μm-thick transverse free-floating sections of mice colon. Sections were processed in separated chambers for each mouse, using the same conditions for all the samples. Sections were put into 48-multi well plates (2 sections per well) using a Pasteur pipette and washed with PBS (5 min, RT, gentle agitation) in order to remove the O.C.T. Gentle agitation was used for all the steps. Sections were blocked with 5% BSA diluted in PBS with 0.5% Triton X-100 (1 h, RT). Samples were then incubated in humid chamber with primary antibodies diluted in PBS, 1% BSA, 0.5% Triton X-100 (overnight, 4°C). PGP9.5 and Type IV Collagen double staining was performed at RT. After washing (PBS, 4x20 min, RT), sections were incubated with secondary antibodies in humid chamber (2 h, RT). From now on, all the steps were carried out in the dark. Sections were finally incubated with 4′,6-diaminobenzidine-2-phenylindole (DAPI, Sigma-Aldrich) for 10 minutes at RT, washed (4x10 min) and mounted with Fluoromount-G mounting medium (Sigma-Aldrich). Sections were transferred on polylysine-coated slides (Superfrost UltraPlus®, Thermo Fisher Scientific) by using a Pasteur pipette and mounted with Fluoromount-G mounting medium (Sigma-Aldrich). Experimental and negative control samples (without primary Ab) were processed in parallel in different reaction chambers. The specificity of each immunofluorescent signal was assured by incubation with only secondary antibody and no signal was detected. The fluorescent signal of negative control samples was taken as threshold to detect the specific signal. The following antibodies were used: rabbit anti-PGP9.5 (1:1000; Abcam), goat anti-type IV Collagen (1:200; Southern Biotech, Melbourne, Vic., Australia), rat anti-Gb3 (1:100; Abcam), goat anti-NF-L (1:250, Santa Cruz), Cy3 donkey anti-rabbit (1:400; Jackson ImmunoResearch, Laboratories lnc., West Grove, Pennsylvania, USA), Cy2 donkey anti-goat (1:400; Jackson ImmunoResearch), Cy3 donkey anti-rat (1:400; Jackson ImmunoResearch) and Cy2 donkey anti-rabbit (1:400, Jackson ImmunoResearch). PGP9.5 and TRPV1, TRPV4, TRPA1 or TRPM8 double IF staining were carried out as previously described by using primary antibodies from the same host species (rabbit). For this purpose, we used monovalent Fab Fragments of affinity-purified secondary antibodies to achieve both labelling and the effective blocking of the first primary antibody, in order to prevent overlapping detection of antigens. Samples were incubated (overnight, RT) with the primary antibody rabbit anti-TRPV1 (1:200, Alomone, Jerusalem, Israel) or anti-TRPV4 (1:300, Abcam) or anti-TRPA1 (1:400, Novus Biologicals, Centennial, Colorado, USA) or anti-TRPM8 (1:50, Santa Cruz). Sections were washed and incubated (2 h, RT) with an excess of Cy3-conjungated

Fab fragments donkey anti-rabbit secondary antibody (1:100, Jackson ImmunoResearch). The samples were washed and incubated (overnight, RT) with the second primary antibody, the rabbit anti-PGP9.5 (1:1000, Abcam). After washing, sections were incubated (2 h, RT) with the Cy2-donkey anti rabbit secondary antibody (1:400, Jackson ImmunoResearch). Sections were finally stained with DAPI.

3.6 Data acquisition and evaluation

3.6.1 Microscopic damage assessment

The histomorphometric analysis was carried out on the H&E-stained slides (n = 3 per group, 4 sections per sample), which were scanned by using a digital microscope at 10X magnification (Coolscope Nikon) (Masotti et al., 2019). Microscopic damage was assessed by evaluating the following parameters (Erben et al., 2014): presence of inflammatory infiltrates, abnormal crypt architecture, and/or presence of crypt abscesses, goblet cells loss, epithelial changes, and thickening of the muscle layer. The evaluation of GI wall thickness was carried out by analysing the H&E-stained sections at the light microscope Nikon Eclipse 90i (Nikon), a fully motorized upright microscope equipped with a high-sensitivity monochrome camera (CoolSNAP HQ2) and a colour camera (Nikon DS-2Mv). NIS-Elements imaging software was used to perform the quantification. We measured the thickness of the GI muscularis propria, meaning both longitudinal and circular layer and the myenteric plexus in between, by drawing a line in opposite points of the circumference, only where the tissue was intact (Figure 23).

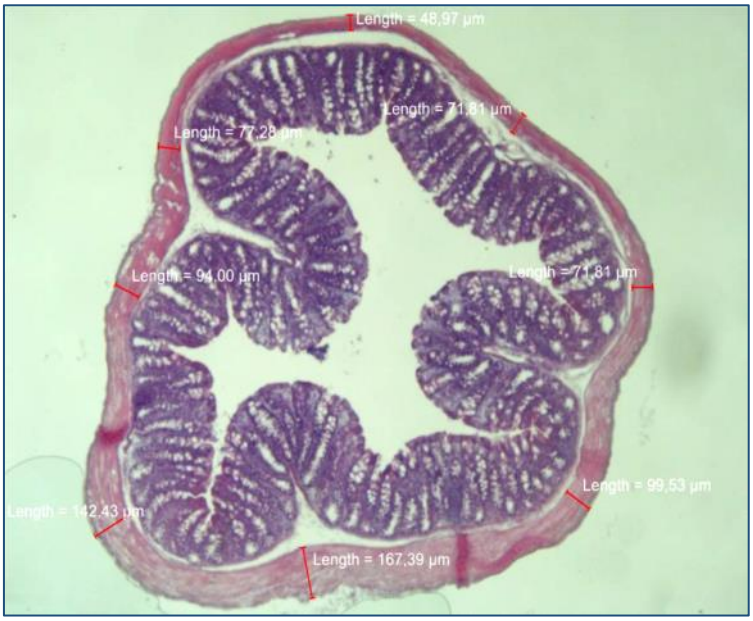

Figure 23. Representative image of the muscular thickness evaluation. The muscular layer thickness was carried out on the H&E-stained sections and measured by using light microscopy (Nikon Eclipse 90i) and the NIS-Elements imaging software. At 4X magnification, four to eight measures in opposite points were taken for each section only where the tissue was intact, and 4-8 sections for each sample were analyzed (n = 5 per group).

3.6.2 Evaluation of myenteric plexus area and nuclear density

Quantitative evaluation of myenteric plexus area and nuclear density were carried out on DAB-stained sections (n = 4 per group, 1-6 sections per sample), and representative images were taken by using the Nikon Eclipse 90i light microscope and the NIS-Elements imaging software (Masotti et al., 2019). Intact PGP9.5 immunoreactive ganglia present in 7 photomicrographies taken at 20X magnification were measured and counted as previously described by Ippolito and colleagues (Ippolito et al., 2009). The fields were recorded starting in a random point of the section. We analysed 7 fields because this is the lowest number of intact fields that we could obtain in all the samples in our hands. In this way we normalized the cells count. The perimeter of intact ganglia was drawn manually by using the "*annotation and measurement*" tool and the area of each ganglion was measured. The PGP9.5-positive cells within these ganglia were counted in order to study the cell density.

3.6.3 Evaluation of Gb3 accumulation and PGP9.5-Gb3 colocalization

The IF analysis to quantitatively assess the Gb3 deposits was carried out on the images of Gb3- and Type IV collagen-stained sections by using ImageJ software (NIH, Bethesda, Maryland, USA) (n = 3 per group, 1 section per sample) (Masotti et al., 2019). Representative images were taken as single confocal sections at 40X magnification and separately for each channel. The *region of interest* (ROI) tool was used to selectively analyze the red pixels within specific areas. *Freehand selection* and *ROI Manager* tools were used to draw the perimeter of ROIs (muscular and muscularis mucosa layers, and mucosa) and to measure the selected areas, respectively. On the red channel, the threshold value (*Image_Adjust_Threshold*) was set and each of these selections was saved. Every image was then processed by using *Find Maxima* Tool (setting the same threshold value) in order to count Gb3 deposits, in terms of red spots. The evaluation of PGP9.5-Gb3 colocalization was carried out, as already described (Lakoma et al., 2014) on images captured with a Nikon D-Eclipse C1 inverted laser scanning confocal microscope and processed by ImageJ software (n = 3 per group, 1 section per sample). The images were taken as stacks of 35-50 μm every 0.5 μm, at 40X magnification and separately for each channel. As PGP9.5-Cy2 signal was higher, due to a major antibody penetrance, the sections to be acquired were chosen based on Gb3-Cy3 signal. Before colocalization analysis, the background was removed from the images. These stacks were proceeded to analyze the colocalization by using the *adaptive threshold* plugin. Each stack was processed using the same value of threshold for each cyanine (Cy2 and Cy3 separately).

3.6.4 Evaluation of mucosal nerve fiber density

Mucosal nerve fiber density (NFD) identified by PGP 9.5-positive staining was calculated per linear millimeter of muscularis mucosae (n = 5 per group, 1-6 sections per sample) (Masotti et al., 2019). In order to identify the muscularis mucosae, we employed Type IV collagen as a marker of muscular layer, muscularis mucosae, and lamina propria. Fluorescent images of PGP9.5 and Type IV collagen-stained sections of colon were captured on a Nikon D-Eclipse C1 inverted laser scanning confocal microscope. In particular, they were taken separately for each channel as 35- to 50-μm-thick stacks every 0.5 μm, at 40X magnification, and analyzed using ImageJ software. By selecting *Z project* tool and choosing *Max intensity* option, we obtained z-stack reconstruction. The line along the muscularis mucosae was drawn by using the *segmented line* tool. The ROIs was added to the *ROI Manager* and measured. Only non-scattered neuronal and non-swelled fibers crossing the horizontal band of muscularis mucosae were counted.

3.6.5 Analysis of PGP9.5/NF-L colocalization

Fluorescent images of PGP9.5 and NF-L staining were taken on a Nikon D-Eclipse C1 inverted laser scanning confocal microscope, as 35-50 thick stacks every 0.5μm, at 40X magnification, and separately for each channel. Only images of myenteric plexus ganglia were captured. ImageJ was used for the image analysis. By selecting *Z project* tool and choosing *Max intensity* option, we obtained z-stack reconstruction. Channels were merged in order to evaluate PGP9.5 and NF-L co-localization. Finally, the z-stack 3-D reconstruction with laser confocal imaging was performed.

3.7 Determination of serum cytokine levels

Blood samples (~200 μL) were collected from 8- to 10 week-old, 16- to 20 week-old and 12 month-old α-Gal A (-/0) and α-Gal A (+/0) mice as described (Tuck et al., 2009). Serum was collected and stored at -80°C until analysis. Cytokine levels were determined using a multiplexed mouse bead immunoassay kit (Bio-Rad, Hercules, California, USA) (n = 6 per group) (Masotti et al., 2019). The six-plex assays (Interleukins IL-1β, IL-6, IL-10, IL-17A, Interferon γ IFNγ, and tumor necrosis factor α TNFα) were performed in 96-well plates following the manufacturer's instructions. Microsphere magnetic beads coated with monoclonal antibodies against the different cytokines were added to the wells. After 30 minutes of incubation, the wells were washed and biotinylated secondary antibodies were added. After 30 minutes of incubation at RT, beads were washed and incubated for 10 minutes with streptavidin conjugated to the fluorescent protein phycoerythrin (PE) (streptavidin-PE). After washing, the beads (a minimum of 100 per cytokine) were analyzed in the Bio-Plex 200 instrument (Bio-Rad). Sample concentrations were estimated with a standard curve using a fifth-order

polynomial equation and expressed as pg/mL after adjusting for the dilution factor (Bio-Plex Manager software 5.0, Bio-Rad). The sensitivities of the assay were 3.14 pg/mL (IL-1β), 1.34 pg/mL (IL-6), 1.38 pg/mL (IL-10), 2.38 pg/mL (IL-17), 1.38 pg/mL (IFNγ), and 2.73 pg/mL (TNFα). Samples below detection limit of the assay were recorded as zero. The intra-assay CV was <14%.

3.8 Assessment of colon sensitivity by colorectal distension

3.8.1 Evaluation of the VisceroMotor Response and intraluminal pressure

The protocol that we performed for the assessment of colon sensitivity by CRD and VMR evaluation was first developed in the rat (Ness and Gebhart, 1988) and then adapted to the mouse (Christianson and Gebhart, 2007). Twelve month-old α-Gal A (-/0) and α-Gal A (+/0) mice (n = 5 per group) were anesthetized by using Isoflurane (2%; Ecuphar) and two EMG electrode wires (Teflon-coated stainless steel wire, diameter: 0.6 mm, length: 12-15 cm; Cooner wire, Chatsworth, California, USA) were sutured into the external oblique muscle of the abdomen and externalised at the back of the neck level (Figure 24). In order to allow full recovery after surgery, we waited for one week before performing CRD. Mice were housed individually to avoid tangling of the electrode wires between mice and to prevent cage mates from damaging the wire leads. The state of health of mice was checked every day and wounds were re-sutured if needed following anaesthesia. In order to perform CRD and VMR evaluation, mice were anesthetized using Isoflurane (2%; Ecuphar, Milan, Italy). The two electrode wire leads were connected to the system for EMG recordings and a 2 cm long balloon made of lubed up latex (Figure 25a) was inserted trans-anally into the descending colon of mice (Figure 25c). The balloon was previously assembled to an embolectomy catheter connected to a syringe and to a pressure sensor (Disposable Blood Pressure (BP) Transducer, ADInstruments, Dunedin, New Zealand) (Figure 25b). The distention was applied by filling the balloon with different volumes of water (50, 100, 200 and 300 µL) by using the syringe. EMG signal was evaluated during the 30 seconds before and during the balloon distension, whereas the intraluminal colonic pressure only at the moment of distension, by using LabChart 8 software (ADInstruments) (Figure 26). The balloon was deflated at the end of each distension. We waited 5 minutes between each measurement. The whole protocol was carried out keeping the mouse on a heating pad (~ 37°C). The EMG signal was recorded, amplified, filtered (Animal Bio Amp and Bridge Amp, ADInstruments) and digitalised (PowerLab 4/35, ADIinstruments). Finally, the digital signal was analysed and quantified by using LabChart 8 software (ADInstruments). The software automatically calculates the area under the curve (AUC), expressed as mV/s, of both the periods of time, with AUC before distension representing the basal. VMR is derived by firstly subtracting the basal AUC from the AUC during distension and

secondly by diving the result by the basal AUC and multiplying the ratio by 100. The result represents the percentage of increase from the basal.

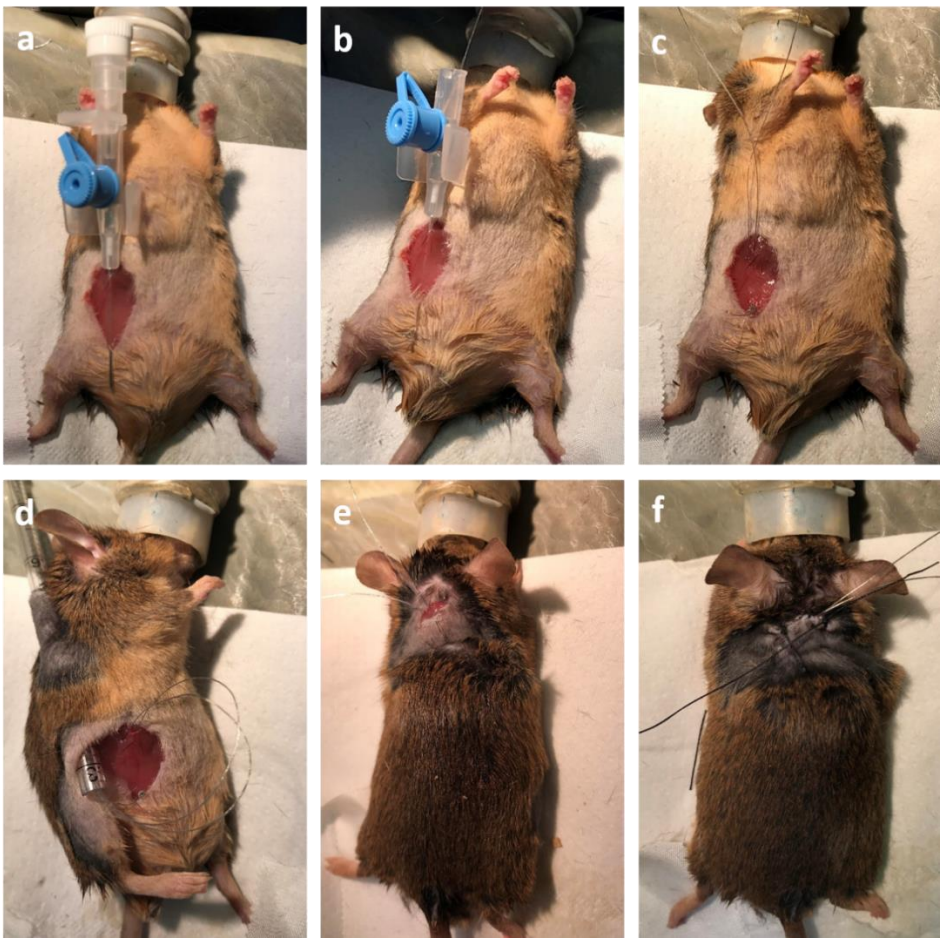

Figure 24: Illustration of the method for implanting electrode wires into the abdominal muscles for EMG recordings. One at a time, mice were anesthetized by using Isoflurane (2%) and the hair in the lower right abdominal area and at the back of the neck was removed with a shaver. By using a sterile scalpel, a 1 cm incision was made in the skin in the lower right abdomen and the skin around the incision was separated from the musculature by using small sterile scissors. The two sterile electrode wires were knotted in the terminal part and the Teflon coating was removed from the 0.3-0.5 cm near the knot by using a scalpel blade. A 25-G sterile needle was inserted in a caudal direction into the abdominal musculature (*panel a*) and one electrode wire was thread through it so that the uncoated segment was completely inserted into the musculature (*panel b*). The needle was removed and the step was repeated to place the second electrode wire in parallel position (*panel c*). In order to make the electrode wires emerge at the back of the neck level, a 1 mL serological pipet was passed subcutaneously (caudal to cranial) until the back of the neck, where a 1 cm incision was made in the skin by using sterile forceps (*panel d*). The two EMG electrode wires were then inserted into the pipet and externalised (*panel d* and *e*). The pipet was removed and 3-0 Prolene and silk (Ethicon, Somerville, New Jersey, USA) were used to stitch the abdomen and the back of the neck, respectively (*panel f*). Each electrode wire was secured separately to the superficial musculature of the neck, separating the wires to exit individually. The exteriorised electrode wire leads were trimmed to 2-3 cm in length. Wounds were kept wet with sterile saline solution (0.9% NaCl) during operation and they were disinfected with Betadine once sutured. The whole operation was carried out keeping the mouse on a heating pad (~ 37°C).

3.8.2 Evaluation of the Abdominal Withdrawal Reflex

Behavioral response after CRD was evaluated through the assessment of AWR in awake animals (the same used for VMR evaluation), as described on rats by Al-Chaer and colleagues (Al-Chaer et al., 2000).

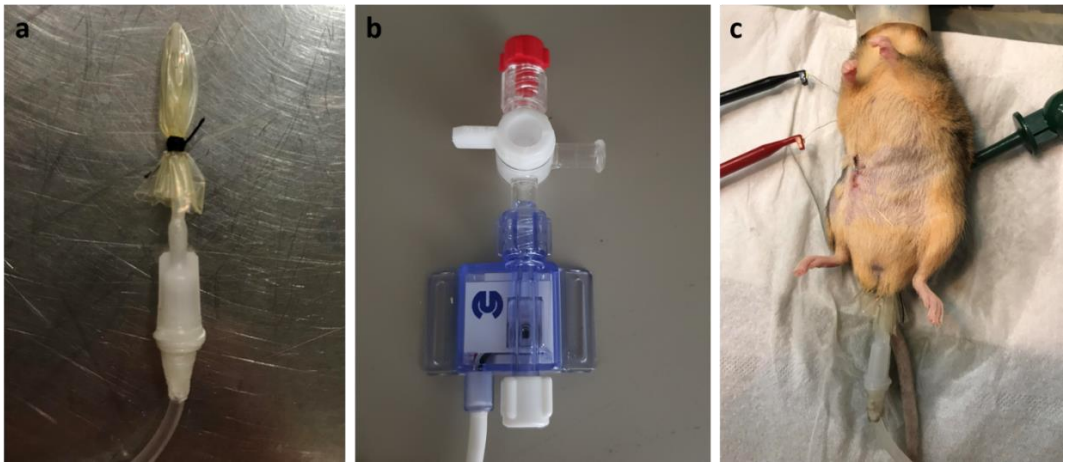

Figure 25: Images of the lubed up latex balloon, the embolectomy catheter connected to the intraluminal pressure sensor and EMG electrodes used for CRD and VMR evaluation. (A) The image shows the balloon used to induce CRD. Balloons were prepared by stretching a square (3 x 3 cm) of thin lubed up latex over an embolectomy catheter, generating a cylinder 2 cm long and 1 cm in diameter. Balloons were tied with 6-0 silk 15 mm from the tip of the tubing and 20 mm from the closed end of the balloon (5 mm allowance for inflation). (B) The image displays the embolectomy catheter connected to the pressure sensor (Disposable Blood Pressure (BP) Transducer, ADInstruments) needed for intraluminal colonic pressure recordings. (C) The image shows the balloon insertion and EMG electrodes connection (Cooner wire). One at a time, mice were anesthetized by using Isoflurane (2%) and the distal colon was cleaned with warm saline solution instilled by using a syringe. The terminal part (0.3-0.5 cm) of the two electrode wire leads were stripped from Teflon coating by using a scalpel blade and connected to the system for EMG recordings via two connection wires (in *black* and *red*). The ground wire (in *green*) was leaned on the mouse side. The balloon was then inserted trans-anally into the descending colon of mice until the silk tie was 5 mm inside the rectum (total insertion distance, 25 mm).

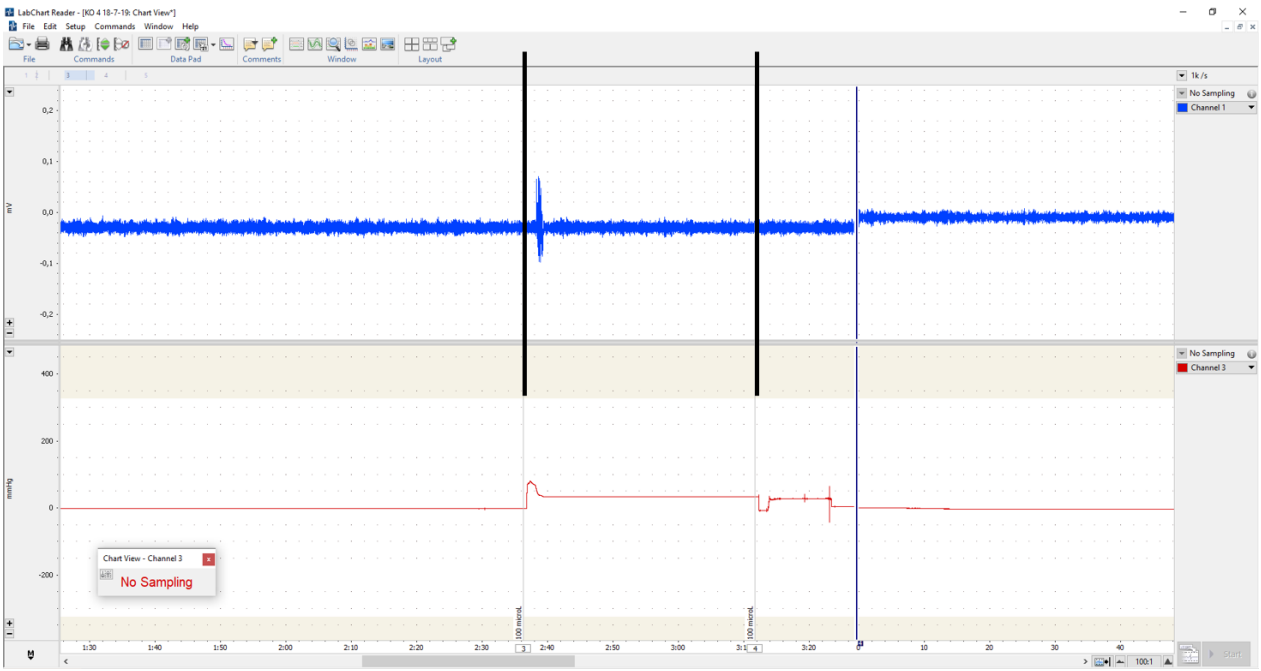

Figure 26. EMG signal and intraluminal pressure recordings. The figure shows an example of the recordings of EMG signal, expressed as mV (*blue line*), and intraluminal colonic pressure, expressed as mmHg (*red line*), for VMR evaluation by CRD. The starting and ending points of balloon distension (example with 100 µL) are indicated by the first and second vertical *black lines*, respectively. EMG signal was evaluated during the 30 seconds before (*to the left of first vertical black line*) and during (*in between the two vertical black lines*) the balloon distension, whereas the intraluminal colonic pressure only at the moment of distension (*pick*), by using LabChart 8 software (ADInstruments). The software automatically calculates the area under the curve (AUC), expressed as mV/s, of both the periods of time, with AUC before distension representing the basal. VMR is derived by firstly subtracting the basal AUC from the AUC during distension and secondly by diving the result by the basal AUC and multiplying the ratio by 100. The result represents the percentage of increase from the basal.

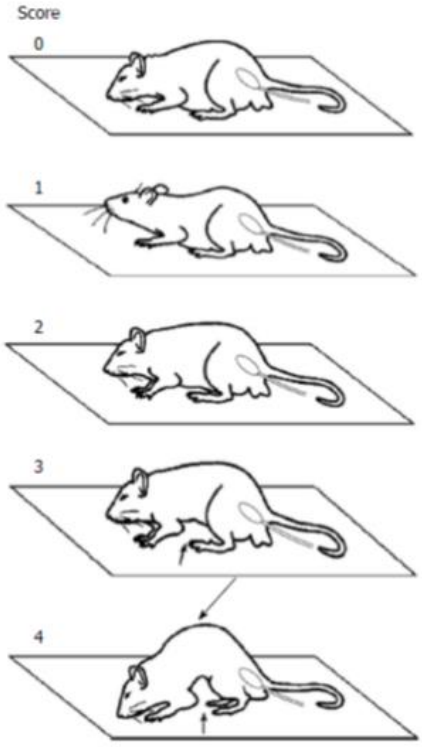

Figure 27: AWR scores. (0) No behavioral response; (1) The mouse becomes immobile during the CRD and occasionally clinches the head at the onset of the stimulus; (2) A mild contraction in the abdominal muscles is observed, but the mouse does not lift its abdomen off the platform (arrows indicate the contraction observed in the abdomen and over the flank); (3) A strong contraction of the abdominal muscles is observed and the mouse lifts its abdomen off the platform (*arrow*); (4) A severe contraction of the abdominal muscles is manifested by body arching and the mouse lifts its pelvic structures off the platform (*arrows*). From Chen et al. 2014.

AWR evaluation was carried out after EMG recordings, after making sure the mice were wide-awake before performing the evaluation (~ 20/30 minutes after the awakening from anaesthesia). Before awakening, the distention balloons were secured by using Parafilm to the mice's tail. Measurement of the AWR consisted of visual observation of the animal response to graded CRD (50, 100, 200 and 300 µL) and assignment of an AWR score (Figure 27): 0, no behavioral response to CRD; 1, brief head movement followed by immobility; 2, contraction of abdominal muscles; 3, lifting of abdomen; 4, body arching and lifting of pelvic structures. We waited ~ 2-3 minutes between one measurement and the other.

3.9 Statistical analysis

Homogeneity of variances was checked by using Levene's test and analysis of variance was carried out by using unpaired Student's *t* test with Statistica 10 software (StatSoft, Tulsa, Oklahoma, USA). Two-way ANOVA followed by Bonferroni's post hoc test was performed to assess differences in PGP9.5-positive cell density within ganglia. OriginLab (OriginLab corporation, Northampton, Massachusetts, USA) software was used to perform one-way ANOVA followed by Bonferroni's post

hoc test in order to evaluate VMR, AWR and intraluminal pressure responses. *P*-values of <0.05 (*), $P < 0.01$ (**), and $P < 0.001$ (***) were chosen as indicating significance. The "n" value indicates the number of mice used in every analysis presented, except in primary cultures experiments, where it indicates the times the experiment was repeated.

3.10 Primary cultures of enteric nervous system cells

3.10.1 Animals and maintenance

C57BL/6 mice were purchased from Janvier Labs (Janvier Labs, Le Genest-Saint-Isle, France). Mice were housed in groups of 6 in individually ventilated cages with water and food *ad libitum* in controlled environmental conditions: lights on from 7.00 am to 7.00 pm, 22 ± 2°C temperature and 65% humidity. Once reached sexual maturity (21-28 days), males and females were separated. All efforts were made to minimize both animal suffering and the number of animals used. Researchers were accredited by the French National Veterinary Agency and the experiments were carried out in accordance with the institutional guidelines of the French Ethical Committee.

3.10.2 Primary cell cultures of Enteric Nervous System from mouse embryos

3.10.2.1 Mice breeding and embryos collection

In order to obtain primary cultures of ENS cells from mouse embryos intestine, we based on a protocol developed in the rat (Chevalier et al., 2008), and based on the work of Gomes and colleagues we decided to use mouse embryos starting from embryonic day (E13) (Gomes et al., 2009). For each experiment, one male mouse was mated with one female in order to obtain embryos at E13 or E14. Females were checked for the vaginal plug (E0) the following morning. When pregnant, they were anesthetized using Isoflurane and sacrificed by cervical dislocation on E13 or E14. Ventral incision was made and the gravid uterus with conceptuses were removed and put into a petri dish full of Hank's Balanced Salt Solution (HBSS; Sigma) with 50 U/mL Penicillin and Streptomycin (PS; Invitrogen).

3.10.2.2 Dissection of embryos intestines

Embryos were released by cutting the uterus wall, removing the placenta and transecting the umbilical cord. Subsequently, they were transferred into a Sylgard dish full of HBSS/PS and fastened with pins at the neck and lower abdomen level, positioning them face upwards. At the dissecting microscope, the abdominal walls of embryos were gently opened using forceps and the GI tracts from the stomach to the colon were collected and put into a petri dish full of HBSS/PS. The stomach, the pancreas and the mesentery were gently removed in this order by using forceps. Intestines were then pooled together into an Eppendorf tube with 800 µL of HBSS/PS.

3.10.2.3 Mechanical dissociation and enzymatic digestion of embryos intestines

Intestines were transferred into a petri dish and chopped using a scalpel. Tissue fragments were collected into a falcon tube by using 10 mL of 3 g/L glucose serum-free medium (DMEM/F-12, HEPES (Thermo Fisher Scientific/Gibco) with 2mM L-Glutamine (L-Glu; Invitrogen) and 50 U/mL PS (Invitrogen), and digested with 0.1% Trypsin (Sigma) at 37°C for 15 minutes. Trypsin reaction was stopped by adding 20 mL of 3 g/L glucose complete medium (DMEM/F-12, HEPES; Gibco) containing 10% heat-inactivated fetal bovine serum (FBS), 2 mM L-Glu (Invitrogen) and 50 U/mL PS (Invitrogen) (37°C, 5 min). Tissue fragments were treated with 0.01% DNase I (Sigma) at 37°C for 10 minutes and, after a vigorous resuspension with a 10 mL pipette, cells were centrifuged (750 rpm, 10 min) and resuspended in an appropriate volume of 3 g/L glucose complete medium (DMEM/F-12, HEPES; Gibco).

3.10.2.4 Cell plating and maintenance

Cells were finally counted and plated at a density of 456 000 cells per well into a 24-well plate (Corning, Corning, New York, USA), previously coated with 0.5% Gelatin (Sigma) diluted in sterile PBS. Coating was done by leaving the gelatin into the wells for at least 20 minutes at 37°C and quickly washing the wells for 3 times with sterile PBS just before cell seeding. After 20 hours, the medium was replaced by 0.9 g/L glucose serum-free medium (DMEM, no glucose + Ham's F 12 Nutrient mix, 1:1; Gibco) with 1% N-2 neuronal supplement (Invitrogen), 2 mM L-Glu (Invitrogen) and 50 U/mL PS (Invitrogen). Cells were cultured (5% CO_2, 37°C) until fixation replacing the half of the medium every other day. Cells were kept until day in vitro (DIV) 9.

3.10.3 Primary cell cultures of enteric neurons from mouse embryos

3.10.3.1 Plating of embryonic enteric glial cells derived from rat

In order to obtain primary cultures of enteric neurons from mouse embryos intestine, we based on a protocol developed in the rat (Le Berre-Scoul et al., 2017). EGCs were previously obtained in Dott. Neunlist laboratory as described by Van Landeghem and colleagues (Van Landeghem et al. 2011). Briefly, glial cells were derived from ENS cultures obtained from intestines of E15 rat embryos. Glial cells were maintained (5% CO_2, 37°C) as a cell line in 4.5 g/L glucose complete medium (DMEM, high glucose; Gibco) containing 10% FBS, 2 mM L-Glu (Invitrogen) and 50 U/mL PS (Invitrogen). Three days before embryo dissection, in order to constitute the 50% confluent glial feeder layer, cells were counted and plated into a 24-well plate, at a density of 15 000 cells per well. Three hours before neuronal culture, the medium was replaced by the serum-free Neurobasal medium (Gibco) with the

addition of the supplement B-27 (1%; Gibco), which increases neuronal survival and maturation. Two mM L-Glu (Invitrogen) and 50 U/mL PS (Invitrogen) were also added to the medium.

3.10.3.2 Coating of coverslips

Coverslips (10 mm of diameter) were sterilised with 70% Ethanol for 1 hour. Once dried, 3 dots of hot sterile paraffin (pre-heated at 200°C) were made on one side of each coverslip. Coverslips were coated on the side of the dots with poly-L-lysine (1 mg/mL; Sigma) diluted in borate buffer (0.1 M, pH 8.5) (overnight, RT), or with Type I collagen (0.04 mg/mL; Corning) diluted in acetic acid buffer (20 mM) (overnight, 4°C), or with a mix of the two solutions (overnight, RT) or with 0.5% Gelatin (Sigma) (20 min, 37°C). The poly-L-lysine solution was filtrated before use. Coverslips coated with poly-L-lysine were washed twice with sterile water, whereas the others were washed 3 times with sterile PBS. Coverslips were put into a 24-well plate (1 per well) with the paraffin dots pointing up, and conditioned, inside the incubator (5% CO_2, 37°C), by 4.5 g/L glucose complete medium (DMEM, high glucose; Gibco) until the day of dissection. On the contrary, coverslips coated with Gelatin were prepared the same day of cell seeding and were quickly washed for 3 times with sterile PBS just before plating the cells.

3.10.3.3 Cell plating and maintenance

ENS cells suspension was obtained as described before (paragraphs 3.10.2.1 - 3.10.2.3). Cells were counted and plated into the 24-well plate containing the coated coverslips at a concentration of 350000 cells per coverslip. In order to let the cells to attach, the plate was left into the incubator for 3 hours (5% CO_2, 37°C). The coverslips were then inverted into the wells of the 24-well plate with the 50% confluent glial feeder layer, so that ENS and glial cells were turned towards each other. After 24 hours into the incubator (5% CO_2, 37°C), cytosine arabinoside (AraC, 5 µM; Calbiochem, San Diego, California, United States) was added in order to hinder the growth of rapidly dividing cells such as glial cells and myofibroblasts. Cells were cultured (5% CO_2, 37°C) until fixation replacing the half of the medium every 4 days. Cells were kept until DIV9.

3.10.4 Enteric Glial Cell cultures derived from adult mouse

3.10.4.1 Coating of plates

In order to obtain EGCs cultures from adult mice intestine, we based on a protocol previously developed by Soret and colleagues (Soret et al., 2013). A 24-well plate was firstly coated with Poly-L-Lysine (20 min, RT) and secondly with Laminin (1h, RT; Thermo Fisher Scientific). Both were diluted in sterile water at a concentration of 10 µg/mL and 50 µg/mL, respectively. Poly-L-Lysine

was discarded and the plate was left to air dry overnight at RT, whereas after discarding Laminin an appropriate volume of medium was added in order to condition the wells. Two media were used: the 4.5 g/L glucose complete medium (DMEM, high glucose; Gibco) containing 10% FBS, 2 mM L-Glu (Invitrogen) and 50 U/mL PS (Invitrogen), or the 3 g/L glucose complete medium (DMEM/F-12, HEPES; Gibco) containing 10% FBS, 2 mM L-Glu (Invitrogen), 50 U/mL PS (Invitrogen), 0.1 g/100mL sodium bicarbonate ($NaHCO_3$), 2% distilled water, 0.025% Amphotericin B and 0.2% Gentamycine.

3.10.4.2 Intestine collection

Adult mice were anesthetized using Isoflurane and sacrificed by cervical dislocation. Ventral incision was made using scissors and forceps. The intestine was cut after the stomach and before the anus and placed into a 50 mL Falcon tube full of cold (4°C) Krebs solution (0.187 g/L monosodium phosphate, 6.84 g/L sodium chloride, 0.35 g/L potassium chloride, 2.1 g/L sodium bicarbonate, 1.98 g/L glucose, 0.368 g/L calcium chloride dihydrate, 0.244 g/L magnesium chloride hexahydrate).

3.10.4.3 Dissection

The GI lumen was washed with cold Krebs solution by using a syringe and a tip to remove all the content. Short portions (approximately 1cm) of jejunum and ileum were cut and put into a petri dish placed on ice, entirely covered by cold Krebs solution. The pieces of intestine, one at a time, were placed on the tip and dried with a tissue. After removing the mesentery by using forceps and scissors, the longitudinal muscle/myenteric plexus (LM/MP) layer was collected starting by using forceps with fine tip and put into a new petri dish with cold Krebs solution (to be replaced every 15 minutes).

3.10.4.4 Mechanical dissociation and enzymatic digestion

In order to dissociate myenteric plexus ganglia from the longitudinal muscular layer, the tissue was transferred into a gentleMACS C tube (Miltenyi Biotech, Bergisch Gladbach, Germany) containing 12.5 µg/mL Liberase Thermolysin High (TH; Roche, Basel, Switzerland) in 5 mL of warm 3 g/L glucose complete medium (DMEM/F-12, HEPES; Gibco) with 10% FBS, 2 mM L-Glu (Invitrogen), 50 U/mL PS (Invitrogen), 0.1 g/100mL sodium bicarbonate ($NaHCO_3$), 2% distilled water, 0.025% Amphotericin B and 0.2% Gentamycine. The tissue derived from different mice was processed into different tubes (~ 150 mg of tissue per sample). Tubes were put into the gentleMACS Dissociator (Miltenyi Biotech) for 1 minute (program “mbrain 03.01”), then gently rotated on the MACSmix Tube Rotator (Miltenyi Biotech) at 37°C for 20 minutes, and finally put again into the gentleMACS Dissociator (Miltenyi Biotech) for 1 minute (program “mbrain 03.01”). After adding 10 mL of warm

3 g/L glucose complete medium (DMEM/F-12, HEPES; Gibco) containing 10% FBS, 2 mM L-Glu (Invitrogen), 50 U/mL PS (Invitrogen), 0.1 g/100mL sodium bicarbonate ($NaHCO_3$), 2% distilled water, 0.025% Amphotericin B and 0.2% Gentamycine, tubes were inverted twice and centrifuged at 1500 rpm for 5 minutes. The supernatant was discarded and the tissue was resuspended in 10 mL of the 4.5 g/L glucose complete medium (DMEM, high glucose; Gibco) containing 10% FBS, 2 mM L-Glu (Invitrogen) and 50 U/mL PS (Invitrogen), or the 3 g/L glucose complete medium (DMEM/F-12, HEPES; Gibco) containing 10% FBS, 2 mM L-Glu (Invitrogen), 50 U/mL PS (Invitrogen), 0.1 g/100mL sodium bicarbonate ($NaHCO_3$), 2% distilled water, 0.025% Amphotericin B and 0.2% Gentamycine.

3.10.4.5 Ganglia collection and glial cell expansion

The suspension was transferred into a 10 cm culture dish. At the dissection microscope, ganglia were collected by using a 200 µL tip and put into the coated 24-well plate (50 ganglia per well). Ganglia are simply recognizable since they have a rod-like appearance and are really bright, whereas smooth muscle cells have a cloud-like appearance and are less bright compared to ganglia. Only the ganglia that were fully dissociated from smooth muscle cells were picked up. The plate was then put into the incubator (5% CO_2, 37°C) until ganglia attached to the bottom (~72 hours). The medium was then fully replaced with the 4.5 g/L glucose complete medium (DMEM, high glucose; Gibco) containing 10% FBS, 2 mM L-Glu (Invitrogen) and 50 U/mL PS (Invitrogen). EGCs were cultured (5% CO_2, 37°C) until fixation replacing the medium twice a week: half-replacing it the first time, and fully replacing it the second time (after 1 wash with warm PBS). Once reached the 80% of confluence, EGCs were passed: after removing smooth muscle cells with a tip, cells were washed twice with warm PBS, trypsinized and plated into a new plate with the 4.5 g/L glucose complete medium (DMEM, high glucose; Gibco) containing 10% FBS, 2 mM L-Glu (Invitrogen) and 50 U/mL PS (Invitrogen). In order to expand the culture, when 80% confluent, EGCs were sequentially passed in plate/flask of increasing size. Two different-sized plates were used for p1: the 12- and the 6-well plate. Cells were kept until p8.

3.10.5 Immunofluorescence staining

ENS, neuronal and glial cultures were fixed in 4% PFA (Sigma-Aldrich) (15 min, RT), washed 3 times with PBS and stored at 4°C in PBS containing 0.1% NaN_3 (Sigma-Aldrich) (PBS/ NaN_3) until IF staining. Cells were permeabilised with Triton 0.25% diluted in PBS/ NaN_3 (5 min, RT) and non-specific sites were blocked with 10% BSA (Sigma-Aldrich) diluted in PBS (30 min, RT). Cells were incubated with primary antibodies (4°C, overnight), washed 3 times with PBS (10 min, RT),

incubated with secondary antibodies (1.5h, RT) and washed again twice (5 min, RT). Cultures were stained with DAPI (1:5000; Sigma-Aldrich) for 5 minutes at RT and washed (2x5 min, RT). All the steps were carried out with gentle agitation. ENS and glial cells were stored at 4°C in PBS/ NaN_3, whereas the coverslips with neuronal cultures were mounted by using the ProLong Gold Antifade Mountant (Invitrogen) and stored at RT in the dark. The following primary and secondary antibodies were used: mouse anti-human neuronal protein HuC/HuD (1:500; Molecular Probes, Eugene, Oregon, USA), rabbit anti-beta III Tubulin (Tuj-1) (1:500; Abcam), rabbit anti-GFAP (1:500; Agilent/Dako, Santa Clara, California, USA), goat anti-Sox10 (1:500; Santa Cruz), mouse anti-PGP9.5 (1:250; Thermo Fisher scientific), Cy3-donkey anti-mouse (1:500; Jackson ImmunoResearch), Cy3-donkey anti-rabbit (1:500; Jackson ImmunoResearch), FluoProbes 488-donkey anti-rabbit (1:200; Interchim, Montlucon, France), AF488-donkey anti-mouse (1:500; Molecular Probes), Cy5-donkey anti-goat (1:500; Jackson ImmunoResearch).

3.10.6 Data acquisition

Representative images of cultures were taken by using the following microscopes: Axio Zoom.V16 fluorescence zoom microscope (Carl Zeiss, Oberkochen, Germany) and IX50 Inverted Fluorescence Phase Contrast Microscope (Olympus, Shinjuku, Tokyo, Japan) equipped with the high-resolution digital camera DP71 (Olympus).

4 RESULTS

4.1 Genotyping of α-Gal A (+/0) and α-Gal A (-/0) mice

The experiments were conducted on the α-Gal A (-/0) male mice JAX strain B6;129-Glatm/1Kul/J (stock number 003535), which were compared with the α-Gal A (+/0) male mice counterpart, same JAX strain B6;129-Glatm/1Kul/J. We focused the study only on male mice, due to the fact that the greater severity of the disease occurs in male patients. We analysed six groups of animals, based on age and genotype: 8- to 10-week-old α-Gal A (+/0) and α-Gal A (-/0), 16- to 20-week-old α-Gal A (+/0) and α-Gal A (-/0) and 12-month-old α-Gal A (+/0) and α-Gal A (-/0) mice. In order to check mice genotype, meaning the presence/absence of GLA gene, we periodically performed the genotyping of the murine colony. The electrophoresis gel of the DNA isolated from mice tails and amplified by PCR shows bands of 295 bp and 202 bp for α-Gal A (+/0) and α-Gal A (-/0) hemizygous male mice, respectively (Figure 28).

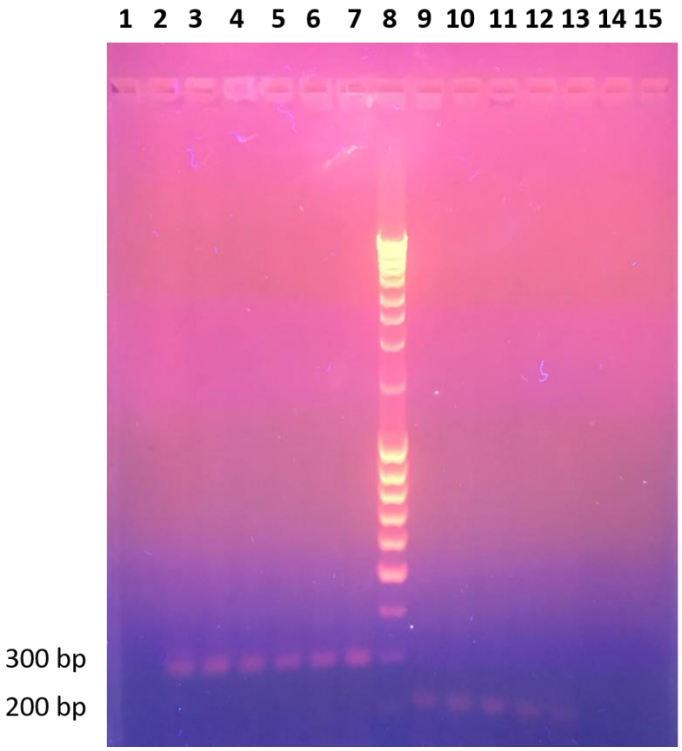

Figure 28. Representative image of DNA genotyping of α-Gal A (+/0) and α-Gal A (-/0). The DNA of 11 different animals was separated (*lanes 2-7* and *9-13*) along with the DNA ladder marker (*lane 8*) by electrophoresis and visualised by UV trans illumination. As expected, the DNA of α-Gal A (+/0) mice, separated in *lanes 2-7*, gave 295 bp-long bands, whereas the DNA of α-Gal A (-/0) mice, separated in *lanes 9-13*, gave 202 bp-long band. Lanes 1 and 15 were left empty and the blank (mix w/o DNA) was loaded in lane 14.

4.2 Macroscopic and microscopic damage assessment in α-Gal A (-/0) mice colon

We first investigate the anatomical and morphological structure of the GI wall in the FD mouse model, compared to controls. Macroscopic damage evaluation did not detect any manifest sign of inflammation, ulcer or necrotizing tissue (Masotti et al., 2019). Moreover, there was no difference in feces consistency between α-Gal A (+/0) and α-Gal A (-/0) mice. Subsequently, we focused on microscopic damage (Masotti et al., 2019).

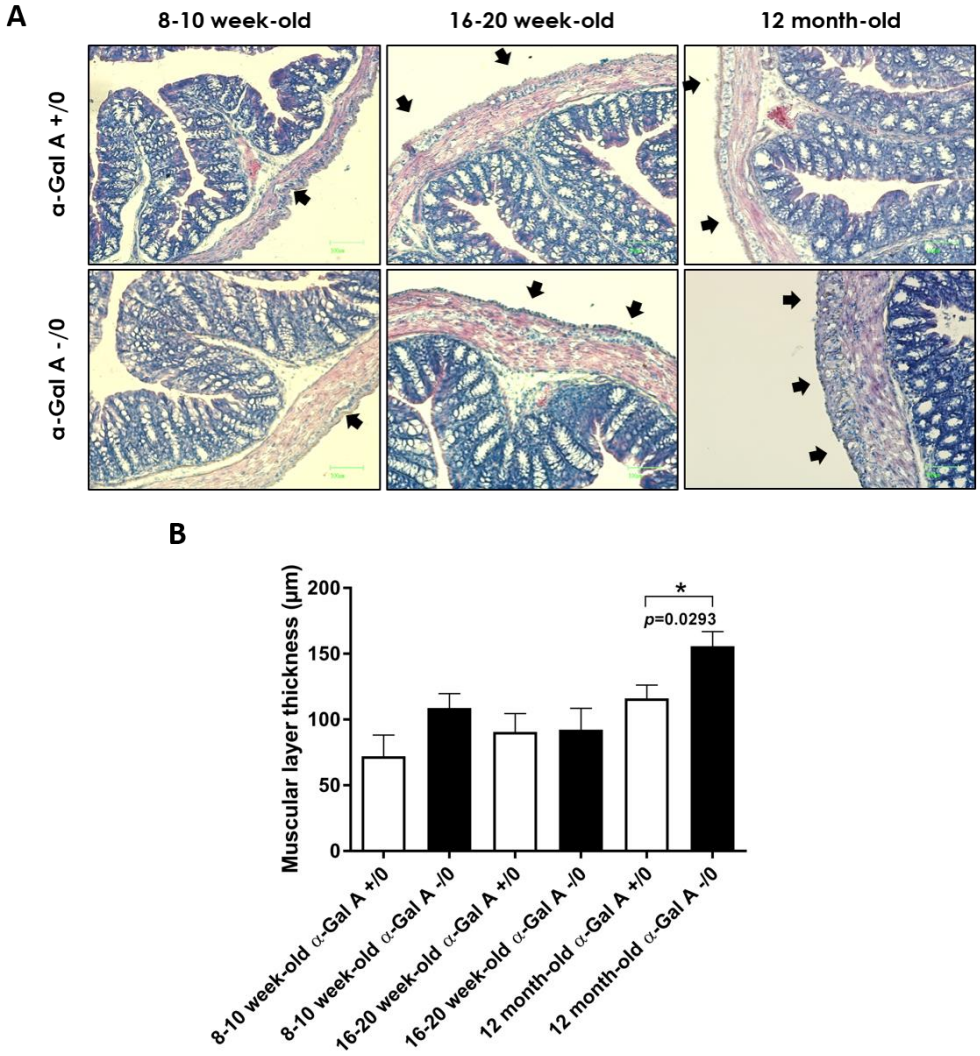

Figure 29. Representative images of H&E-stained colon sections of α-Gal A +/0 and −/0 mice and statistical analysis of muscular layer thickness. Ten-µm-thick transverse frozen sections of 8- to 10-week-old, 16- to 20-week-old, and 12-month-old α-Gal A +/0 and α-Gal −/0 male mice colon were stained with H&E for the histomorphological evaluation (n = 3, four sections per sample). Representative images were taken at 10X magnification at digital microscope (Coolscope Nikon, Amsterdam, NL, USA) (A). *Black arrows* indicate the muscular layer and the myenteric plexus ganglia. Scale bar: 100 µm. The muscular layer thickness was measured by using light microscopy (Nikon Eclipse 90i, Amsterdam, NL, USA) and the NIS-Elements imaging software. Four to eight measures in opposite points were taken for each section, and 4-8 sections for each sample were analyzed (n = 5 per group; the sample whose muscular thickness measure was the farthest from the mean value of the distribution was excluded). In (B), the graph shows the GI wall thickness measures, expressed in µm (*y-axis*), of 8- to 10-week-old, 16- to 20-week-old, and 12-month-old α-Gal A +/0 and α-Gal −/0 male mice (*x-axis*). Homogeneity of variances was checked by using Levene's test and analysis of variance was carried out by using unpaired Student's t test with Statistica 10 software. P-values of <0.05 (*), P < 0.01 (**), and P < 0.001 (***) were chosen as indicating significance. Columns represent mean ± SEM.

In order to analyse the GI tract histomorphology of the FD model, we carried out a H&E staining on transverse frozen colon sections to evaluate the phenotypic differences between α-Gal A (+/0) and α-Gal A (-/0) mice at the three different ages. Since GI symptoms of FD can be confused with others IBD symptoms and there are no standard parameters for a histomorphological evaluation of FD patients GI tract, we relied on a number of criteria used to assess colonic inflammation in different murine models of IBD (Erben et al., 2014): 1) evaluation of inflammatory cell infiltrates, 2) epithelial changes (such as Goblet cell loss and hyperplasia, visible as crypt elongation), 3) muscular layer thickening and 4) mucosal architecture alterations (ulceration, tissue granulation, irregular crypts, crypt loss, villous blunting). The representative images of the histopathological evaluation are shown in Figure 29 (Masotti et al., 2019). The analysis showed that the α-Gal A (-/0) cross sections of mouse colon do not present inflammatory cell infiltrates such as neutrophils, eosinophils, monocytes, plasma cells and lymphocytes at mucosal level, and display a normal epithelium with an intact villous architecture, similarly to the corresponding controls at each age studied. However, histomorphological analysis of circular and longitudinal colon muscular layers revealed a trend toward an increase in thickness in α-Gal A −/0 compared to α-Gal A +/0 mice (Figure 29A, black arrows). Therefore, in order to quantitatively evaluate the muscular layer thickness of the colon, we performed a manual measurement on the H&E-stained colon sections by using the NIS-Elements imaging software. The results display that 12-month-old α-Gal A −/0 mice showed a higher increase ($P = 0.0293$, [*]), compared to the 8- to 10-week-old ($P = 0.0966$) and 16- to 20-week-old α-Gal A −/0 mice ($P = 0.9425$; Figure 29B). Interestingly, an age-related increase in the muscular thickness within groups was observed, both in α-Gal A +/0 and α-Gal A −/0 mice.

4.3 Determination of serum cytokine levels in α-Gal A (-/0) mice

In order to gain more information on the cytokine profile of the α-Gal A (-/0) genotype compared to α-Gal A (+/0), we subsequently quantified the serum concentrations of IL-1β, IL-6, IL-10, IL-17A, IFNγ, and TNFα cytokines. There was no significant difference between serum samples derived by α-Gal A (−/0) and α-Gal A (+/0) genotypes at all ages analyzed, although an increasing trend was detected in the oldest group (data not shown) (Masotti et al., 2019).

4.4 Evaluation of myenteric plexus area and nuclear density in α-Gal A (-/0) mice colon

In order to determine whether the observed thickening of the muscular layer was due to an increased size of muscular or neuronal component, we next evaluated the area of myenteric plexus ganglia using the pan-neuronal marker PGP9.5 (Figure 30A) (Masotti et al., 2019).

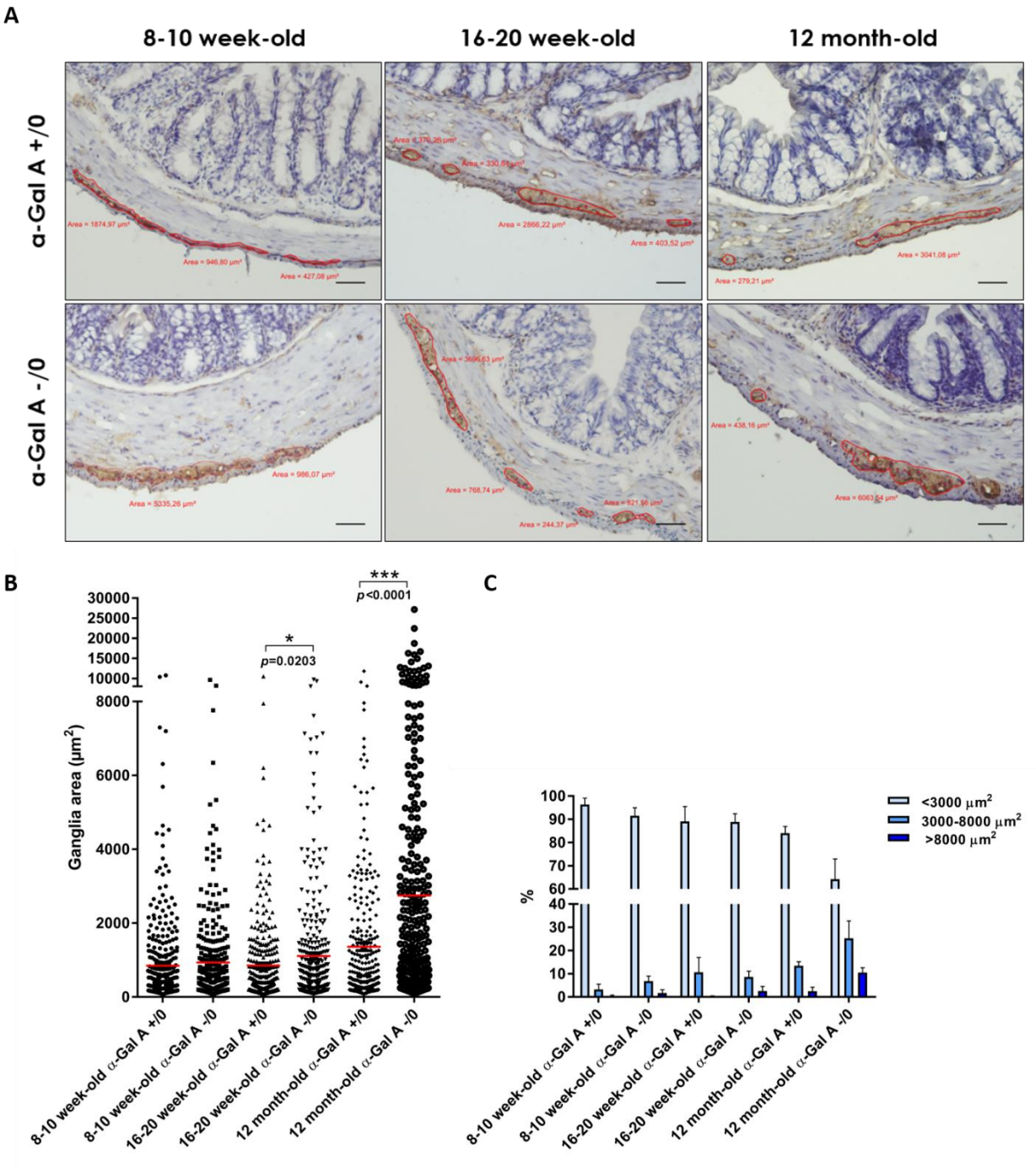

Figure 30. Representative images and statistical analysis of the myenteric plexus ganglia area in α-Gal A +/0 and −/0 mice. Myenteric plexus ganglia were detected as PGP9.5 immunoreactive ganglionic neuropil by IHC on 10-μm-thick transverse cryo-sections of 8- to 10-wk-old, 16- to 20-wk-old, and 12-mo-old α-Gal A +/0 and −/0 mice colon (n = 4, 1-6 sections per sample). Sections were counterstained with hematoxylin to stain nuclei. In panel A, representative images of myenteric plexus ganglia taken at 20X magnification at fluorescence microscope Nikon Eclipse 90i are shown. The area of intact ganglia was drawn and measured by using the NIS-Elements imaging software (*red lines and values*). PGP9.5-positive cells were marked (*red crosses*) in order to be counted. Neurons are characterized by brown perikaryon, dark red nuclei, and blue nucleoli. Glial cells are non-immunoreactive for PGP9.5 and can be recognized by their small blue nuclei. Scale bar: 50 μm. In panel B, the dispersion of the ganglia area (*y-axis*) in the six experimental groups (*x-axis*) is displayed. Each symbol represents a ganglion. Homogeneity of variances was checked by using Levene's test and analysis of variance was carried out by using unpaired Student's t test with Statistica 10 software. P-values of <0.05 (*), P < 0.01 (**), and P < 0.001 (***) were chosen as indicating significance. Horizontal bars (*red lines*) represent the mean value. In panel C, the distribution on a percentage basis of the myenteric plexus ganglia areas in α-Gal A +/0 and −/0 mice is shown. The graph is obtained by dividing the analyzed ganglia into three subgroups (<3000 μm2, 3000-8000 μm2, and >8000 μm2), according to the ganglia distribution in the scatter plot (panel B).

The histomorphometric analysis showed an increased trend of ganglion mean area comparing either 8- to 10-week-old (P = 0.3952) or 16- to 20 (P = 0.0203 [*])-week-old α-Gal A −/0 to α-Gal A +/0 mice. This increase was more pronounced in the 12-month-old α-Gal A −/0 mice compared to control age (P < 0.0001 [***]). The same age-related increase was also present irrespectively of mice genotype (Figure 30B) (Masotti et al., 2019). Next, we analyzed the ganglia population of each group upon their dimension considering increasing size ranges (<3000 μm^2, 3000-8000 μm^2, and >8000 μm^2; Figure 30C) (Masotti et al., 2019). In line with the previous analysis, 12-month-old α-Gal A −/0 mice clearly presented larger ganglia. Moreover, an age-dependent increase in number of the largest ganglia (>3000 μm^2) was also detected in all ages. Notably, the 12-month-old α-Gal A −/0 mice displayed 25% and 11% of ganglia with an area in the range of 3000-8000 μm^2 and larger than 8000 μm^2, respectively, compared to 14% and 3% of the corresponding controls (Figure 30C). This observation can in part explain the muscular thickening and is consistent with hypertrophy due to Gb3 deposition and/or hyperplasia. In order to determine whether the large-sized ganglia contain a higher number of neurons (hyperplastic) or neurons with an expanded cytoplasm (hypertrophic), we carried out a quantitative analysis of nuclei density within ganglia, expressed as number of PGP9.5-positive neurons per ganglion (as shown in the red perimeter of the Figure 30A). We performed a linear regression analysis in order to obtain the slope values of the lines, used as indicator of neuronal density (Figure 31) (Masotti et al., 2019). The analysis did not reveal any difference between α-Gal A −/0 and +/0 mice, at none of the three ages. In particular, in Figure 31A, it is shown that line slopes are the same when comparing α-Gal A −/0 mice to their respective controls and statistical analysis did not reveal differences between genotypes as well (Figure 31B). Nevertheless, neuronal density of 12-month-old α-Gal A −/0 mice resulted lower when compared to both 8- to 10-week-old α-Gal A −/0 (P = 0.0183, [*]) and α-Gal A +/0 mice (P = 0.0096, [**]; Figure 31B), suggesting that both age and genotype may affect neuronal density of myenteric plexus ganglia by inducing a hypertrophic state.

4.5 Evaluation of PGP9.5 and NF-L co-localization

In order to demonstrate the specificity of PGP9.5 as a neuronal marker, we carried out an IF analysis on 50 μm-thick free-floating sections of colon of 12 months α-Gal A (+/0) and α-Gal A (-/0) mice by using the anti-PGP9.5 and the anti-NF-L primary antibodies. The results show how PGP9.5 and NF-L staining co-localize in myenteric plexus ganglia, providing evidence of the specificity of PGP9.5 as a neuronal marker (Figure 32).

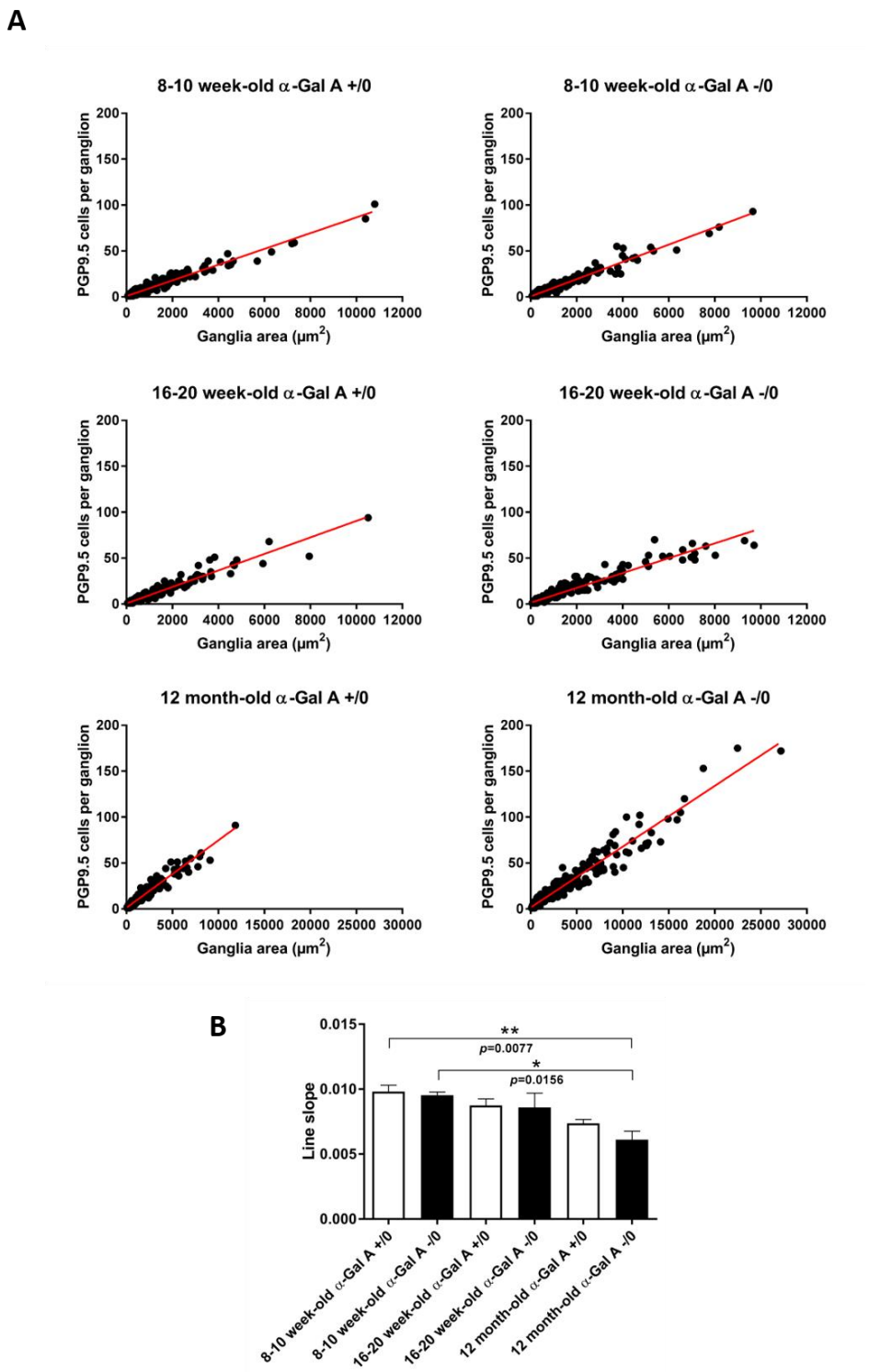

Figure 31. Statistical analysis of PGP9.5 cells in myenteric plexus ganglia of α-Gal A +/0 and −/0 mice. The number of PGP9.5-positive cells per ganglion was evaluated on the same images used for ganglia area analysis (n = 4, 1-6 sections per sample). In panel A, the scatter plots were obtained by plotting the number of PGP9.5-positive cells per ganglion (*y-axis*) on the basis of their area expressed in μm² *(x-axis*). The comparison between 8- to 10-wk-old, 16- to 20-wk-old, and 12-mo-old α-Gal A +/0 (left) and α-Gal A −/0 (right) mice is displayed. Symbols represent ganglia. Each graph was obtained by plotting together the data of all the mice analyzed. A linear regression analysis was performed in order to obtain the slope values of the lines ("m" value of line equation) that were used as indicator of neuronal density (*red lines*). In panel B, the histogram shows the statistical analysis of line slopes (*y-axis*) in the six experimental groups (*x-axis*). Columns represent the mean ± SEM. Homogeneity of variances was checked by using Levene's test with Statistica 10 software and analysis of variance was carried out by performing a two-way ANOVA followed by Bonferroni's post hoc test for statistical significance. P-values of <0.05 (*), P < 0.01 (**), and P < 0.001 (***) were chosen as indicating significance.

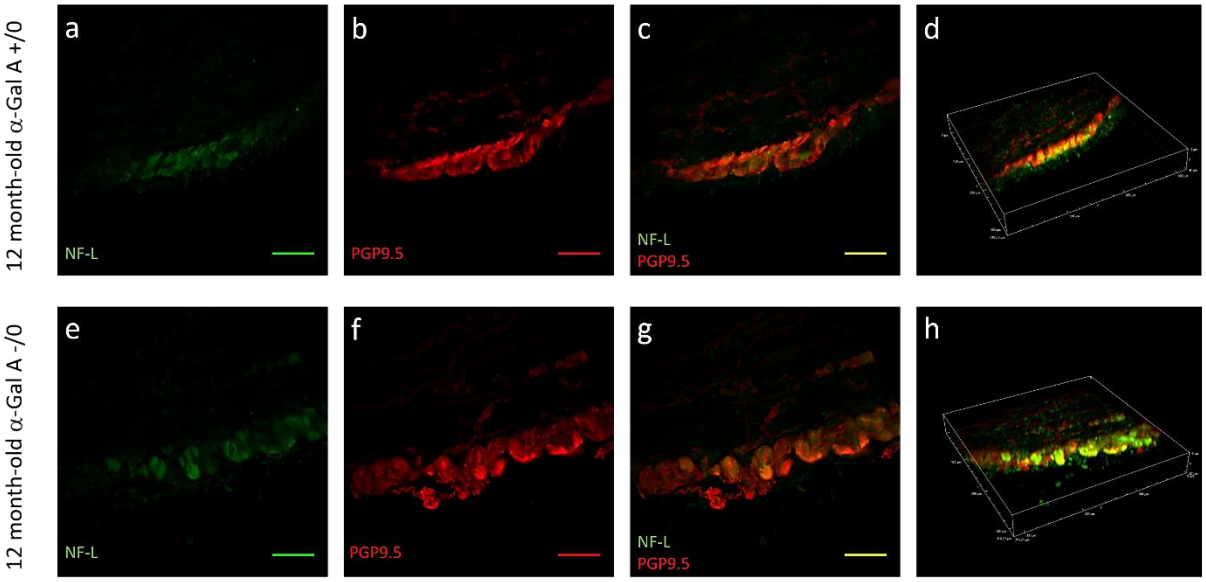

Figure 32. Representative images of the colocalization of NF-L and PGP9.5 staining on colon sections of α-Gal A (+/0) and (-/0) mice. The staining was carried out on 50µm-thick transverse free-floating sections of 12-month-old α-Gal A (+/0) (*a, b, c, d*) and α-Gal A (-/0) (*e, f, g, h*) mice colon. Representative images of the ganglia of the myenteric plexus are shown. The images were captured on a Nikon D-Eclipse C1 inverted laser scanning confocal microscope at 40X magnification and analysed by Image J (NIH, http://rsb.info.nih.gov/ij/). Scale bar: 50µm. The images of NF-L (*green; a, e*) and PGP9.5 (*red; b, f*) stacks are shown on the *left*. On the *right*, the images *c* and *g* show the merge of the two channels, and the images *d* and *h* show the z-stacks 3D reconstruction.

4.6 Evaluation of Gb3 deposits in α-Gal A (-/0) mice colon

In light of the previous results, we next localized Gb3 deposits across the wall of the colon in α-Gal A -/0 and +/0 mice. Gb3 immunostaining showed a similar positive staining in the mucosa layer of both α-Gal A -/0 and α-Gal A +/0 colon sections (Figure 33, inset green arrows) (Masotti et al., 2019). In contrast, submucosal and muscular Gb3 storage was widely present only in α-Gal A -/0 mice, whereas in the α-Gal A +/0 mice colon, Gb3 signal was barely detectable. Interestingly, the Gb3 deposition differences between α-Gal A -/0 and α-Gal A +/0 mentioned above are maintained for all the ages in the analyzed groups (Figure 33). To gain further insight on the localization of Gb3 deposits, we carried out a double IF staining of Gb3 and PGP9.5 to evaluate colocalization. As shown in Figure 34, we confirmed that Gb3 inclusions are markedly abundant in submucosal and myenteric plexuses in α-Gal A −/0 compared α-Gal A +/0 (Masotti et al., 2019).

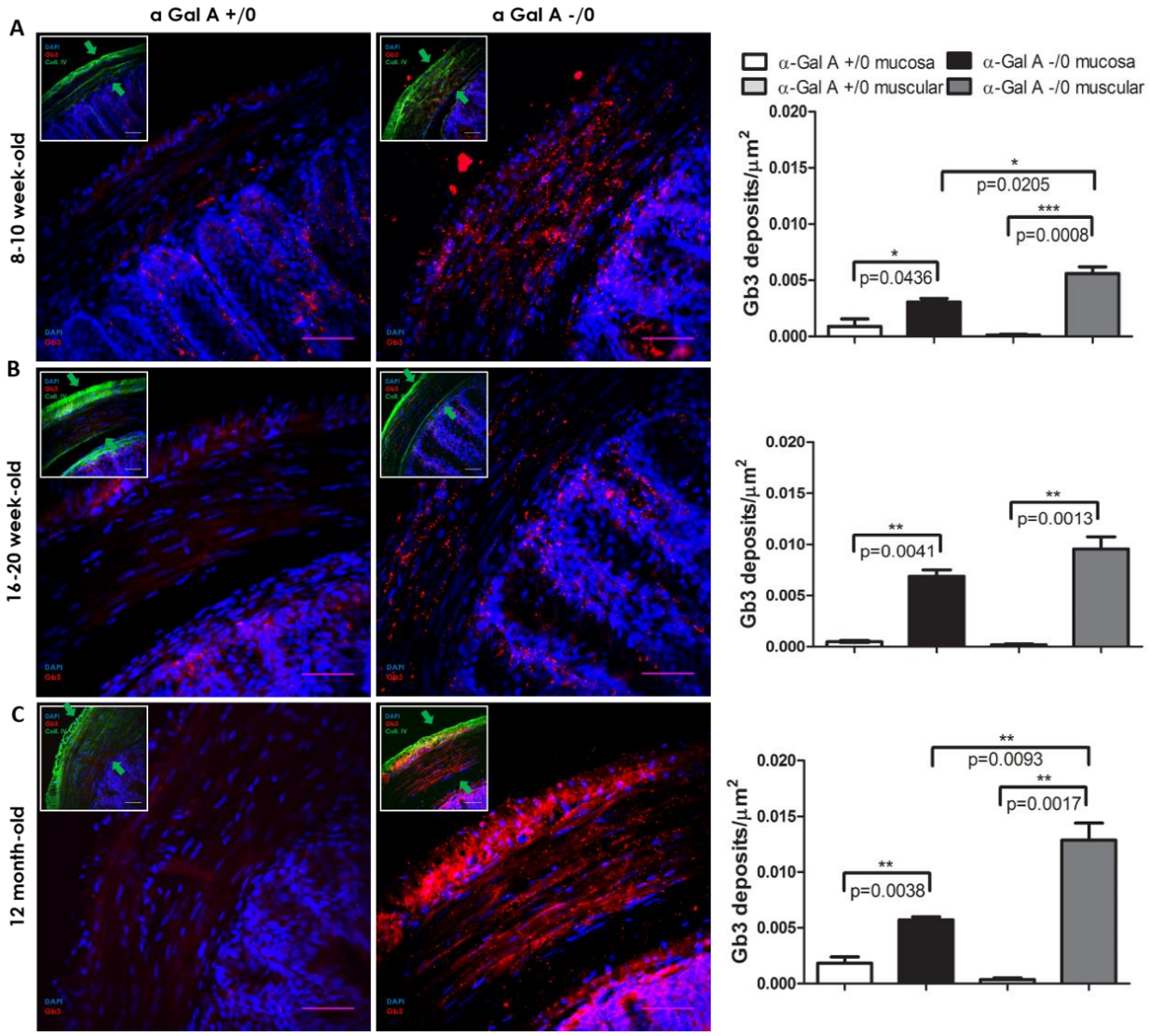

Figure 33. Representative images of Gb3 staining on colon sections of α-Gal A (-/0) and (+/0) mice. Gb3 (*red*) and type IV collagen (*green*) were detected by IF in 50µm-thick transverse cryo-sections of 8- to 10 week-old (A), 16- to 20 week-old (B), and 12 month-old (C) α-Gal A (-/0) and α-Gal A (+/0) male mice colon to stain Gb3 deposits and the wall muscular layer, muscularis mucosae and lamina propria, respectively. Nuclei were stained with DAPI (*blue*). Fluorescent images were captured on a Nikon D-Eclipse C1 inverted laser scanning confocal microscope. Representative images of the muscular layer (*green arrows*) were taken as single confocal sections at 40X magnification and separately for each channel. The EZ-C1 3.90 Free Viewer and Image J (NIH, http://rsb.info.nih.gov/ij/) software were used for image analysis. Scale bar: 50µm. In the *right panel* of each figure, the Gb3 quantification is expressed as Gb3 spots per square micrometer, the mucosa and muscular layers is shown. Homogeneity of variances was checked by using Levene's test and analysis of variance was carried out by using unpaired Student's t test with Statistica 10 software. P-values of <0.05 (*), P < 0.01 (**), and P < 0.001 (***) were chosen as indicating significance.

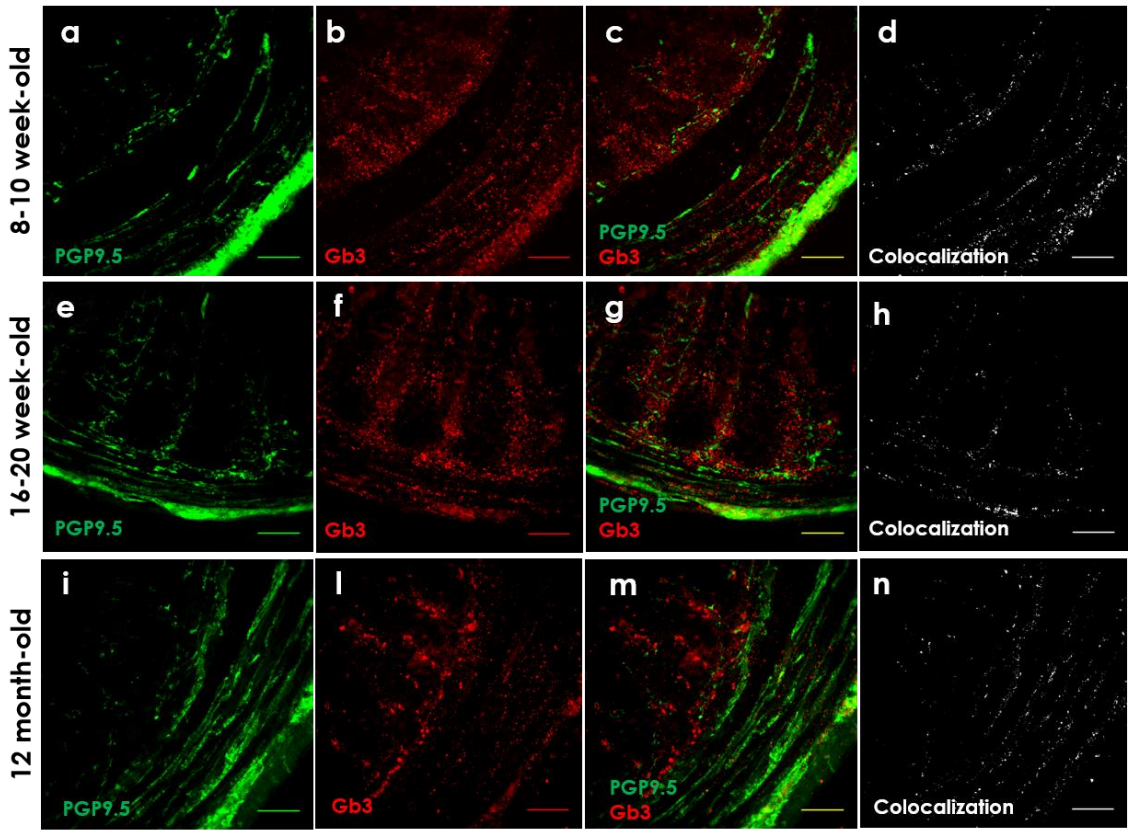

Figure 34. Representative images of the colocalization of Gb3 and PGP9.5 staining on colon sections of α-Gal A (-/0) mice. The staining was carried out on 50µm-thick transverse floating sections of 8- to 10 week-old (*a, b, c, d*), 16- to 20 week-old (*e, f, g, h*), and 12 month-old (*i, l, m, n*) of α-Gal A (+/0) and α-Gal A (-/0) mice colon (n = 3, one section per sample). Only the muscular layer of α-Gal A (-/0) mice is shown because the muscular layer of α-Gal A (+/0) mice is negative. The images were captured on a Nikon D-Eclipse C1 inverted laser scanning confocal microscope at 40X magnification and analysed by Image J (NIH, http://rsb.info.nih.gov/ij/). Scale bar: 50µm. On the *left* the images of PGP9.5 (*green*; *a, e, i*), and Gb3 (*red*; *b, f, l*) stacks are shown. The images *c, g, m* show the merge of the two channels. On the *right*, the panels *d, h, n* the merge images were modified with the function "make binary" (*black* and *white*) to better visualize the colocalization between Gb3 and PGP9.5.

4.7 Evaluation of mucosal nerve fiber density in α-Gal A (-/0) mice colon

Next, we investigated NFD entering the colonic mucosa through IF analysis of PGP9.5-positive nerve fibers on transverse floating sections of all ages α-Gal A -/0 and α-Gal A +/0 male mice colon. IF analysis revealed that PGP9.5-positive fibers were either morphologically different, such as fragmented, scattered, or swelled (Figure 35A-C) (Masotti et al., 2019) and present in lower abundance in α-Gal A −/0 mice regardless the age, compared to α-Gal A (+/0) mice. Alpha-Gal A (-/0) mice showed a decreased NFD of the mucosal innervation in all group ages, which was statistically significant both in the youngest (P = 0.0162, [*]) and oldest group (P = 0.0114, [*]). Moreover, 16- to 20-week-old mice showed an akin result although not statistically significant (P = 0.067; Figure 36) (Masotti et al., 2019).

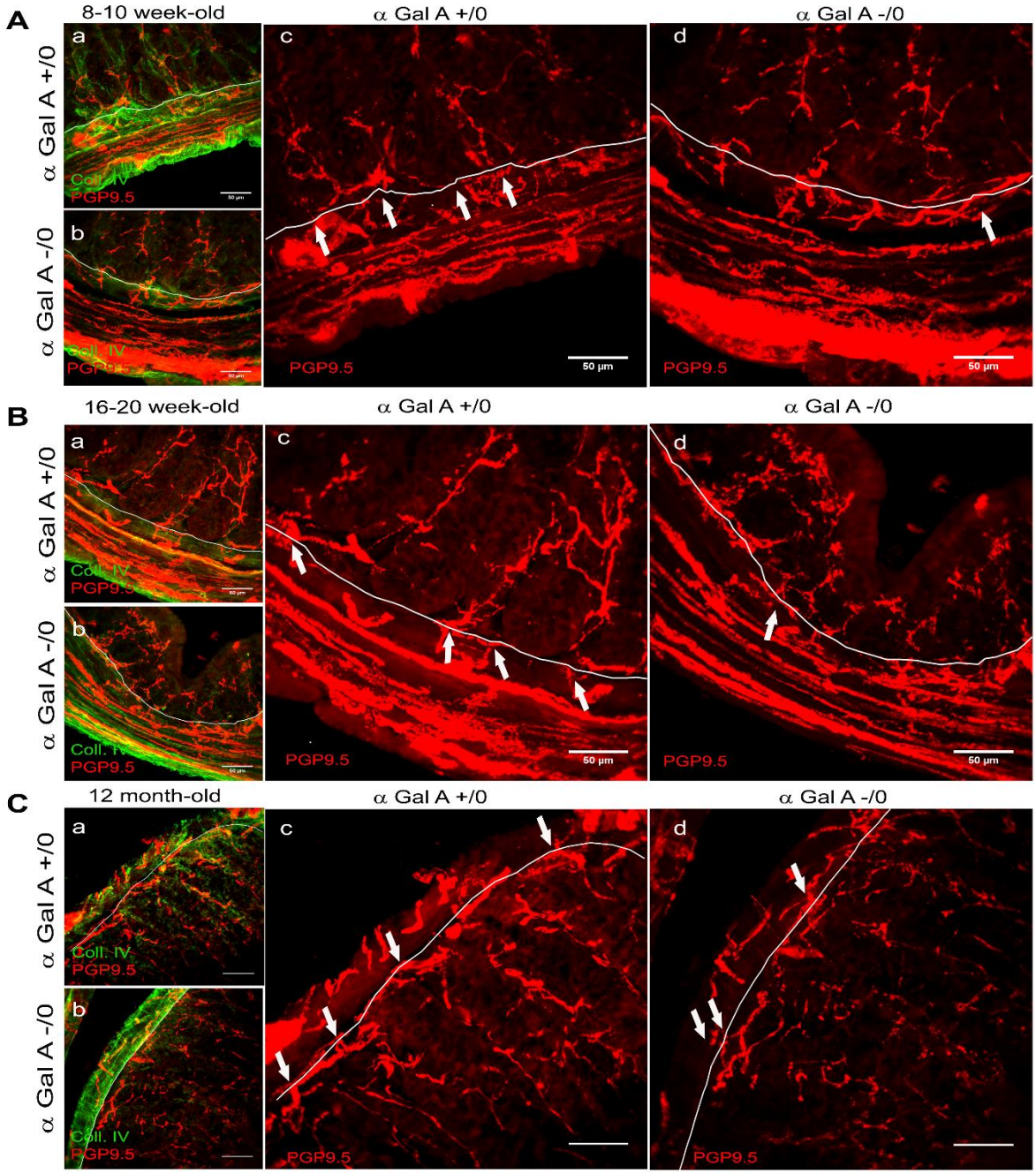

Figure 35. Representative images of PGP9.5 staining and nerve fiber count of α-Gal A (-/0) and (+/0) mice. PGP9.5 (*red*) and type IV collagen (*green*) were detected by IF in 50µm-thick transverse cryo-sections of 8-10 week-old (*A*), 16-20 week-old (*B*) and 12 month-old (*C*) α-Gal A (+/0) (*a, c*) and α-Gal A (-/0) (*b, d*) male mice colon to stain nerve fibers and muscular layer, muscularis mucosae and lamina propria, respectively (n = 5, 1-6 sections per sample). Fluorescent images were captured on a Nikon D-Eclipse C1 inverted laser scanning confocal microscope. Representative images of nerve fibers in the muscular layer and mucosa were taken as stacks of 35-50 µm every 0.5 µm, at 40X magnification and separately for each channel. Image J (NIH, http://rsb.info.nih.gov/ij/) software was used for image analysis: on the maximum intensity projection of green channel the mark-up of the muscularis mucosae inner side (toward the lumen; *white lines*) was done and, on the maximum intensity projection of red channel, non-scattered mucosal nerve fibers marked with PGP9.5 crossing the line (*white arrows*) were counted. The density of the nerve fibers entering the enteric mucosa was calculated per linear millimetre of muscularis mucosae. Scale bar: 50µm.

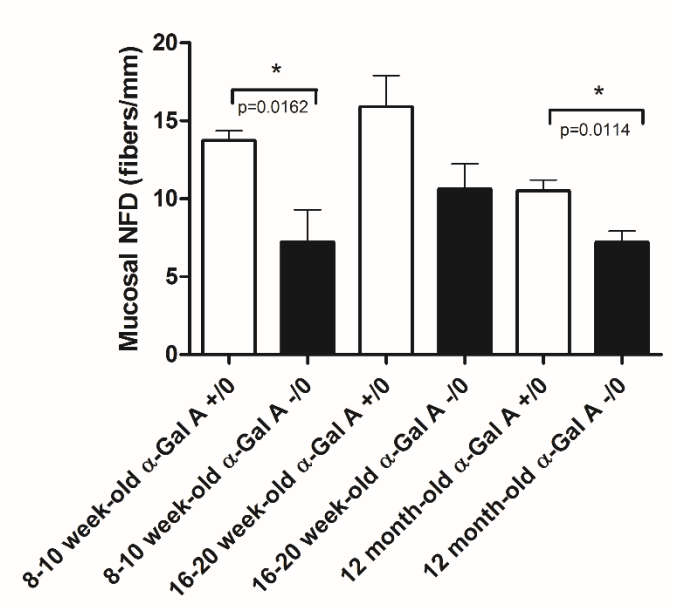

Figure 36. Statistical analysis of mucosal NFD in α-Gal A (+/0) and (-/0) mice. Nerve fibers were detected as PGP9.5 + cells by IF in 50µm-thick transverse frozen sections of 8- to 10 week-old, 16- to 20 week-old, and 12 month-old α-Gal A (+/0) and (-/0) mice colon (n = 5, 1-6 sections per sample were analysed per group; the sample whose mucosal NFD measure was the farthest from the mean value of the distribution was excluded). The histogram shows the mucosal NFD (*y-axis*), expressed as number of PGP9.5 positive cells per linear millimeter of muscularis mucosae in the six groups analyzed (*x-axis*). Columns represent mean ±SEM. Homogeneity of variances was checked by using Levene's test and analysis of variance was carried out by using unpaired Student's t test with Statistica 10 software. P-values of < 0.05 (*), p < 0.01 (**) and p < 0.001 (***) were chosen as indicating significance.

4.8 Assessment of colon sensitivity of α-Gal A (-/0) mice by colorectal distension

In order to assess differences in visceral sensitivity between 12-month-old α-Gal A (+/0) and α-Gal A (-/0) mice, we evaluated VMR, intraluminal pressure and AWR by CRD. Results of VMR evaluation show that, EMG recordings of α -Gal A +/0 mice did not display any increase from the basal following CRD, at none of the distension volumes, as demonstrated by VMR values (Figure 37, grey symbols). On the contrary, a significantly higher VMR was detected in α-Gal A (-/0) mice. In particular, compared to α-Gal A (+/0), they displayed greater VMR values following CRD induced by the higher volumes injected (100 µL, *P* = 0,01694 [*]; 200 µL, *P* = 0,01149 [*]; 300 µL, *P* = 6,39718 E^{-7} [***]) (Figure 37, black symbols). On the contrary, no difference was detected with the lowest volume (50 µL). VMR seemed to be volume-dependent in α-Gal A (-/0), since VMR values to 300 µL distension resulted higher, compared to those obtained in response to 100 µL distension (Figure 37, black symbols). However, despite the higher volume, α-Gal A (-/0) mice responded with a lower VMR at the distension with 200 µL, compared to the distension with 100 µL. We hypothesized that this could be due the fact that we analyzed only 5 mice per group and thus these data are to be considered as preliminary. Intraluminal pressure analysis displayed a volume-dependent increase both in α-Gal A (+/0) and α-Gal A (-/0) mice, but did not show any differences between the

two, except for the distension with 200 µL that revealed a higher intraluminal pressure value in α-Gal A (-/0) mice (P = 0.0145 [*]) (Figure 38).

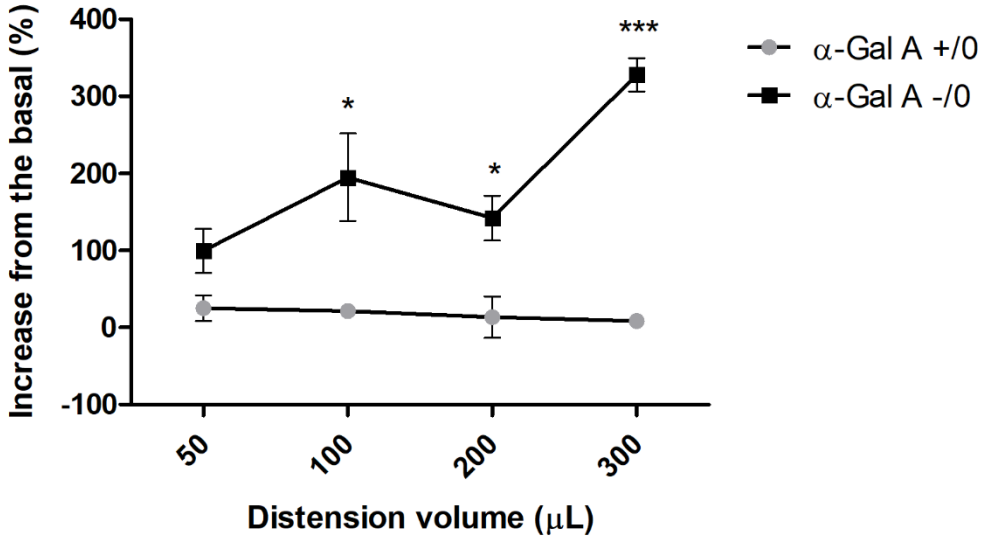

Figure 37. Assessment of VMR to CRD in 12-month-old α-Gal A (+/0) and α-Gal A (-/0) mice. The graph shows the statistical analysis of the assessment of VMR (*y axis*), expressed as percentage of increase from the basal, to CRD induced by different volumes of water (*x axis*), in anesthetized α-Gal A (+/0) (*grey*) and α-Gal A (-/0) (*black*) mice (n = 5 per group). Each symbol represents mean ± SEM. Origin software was used to perform one-way ANOVA for statistical significance between α-Gal A +/0 and −/0 mice. P-values of <0.05 (*), P < 0.01 (**), and P < 0.001 (***) were chosen as indicating significance.

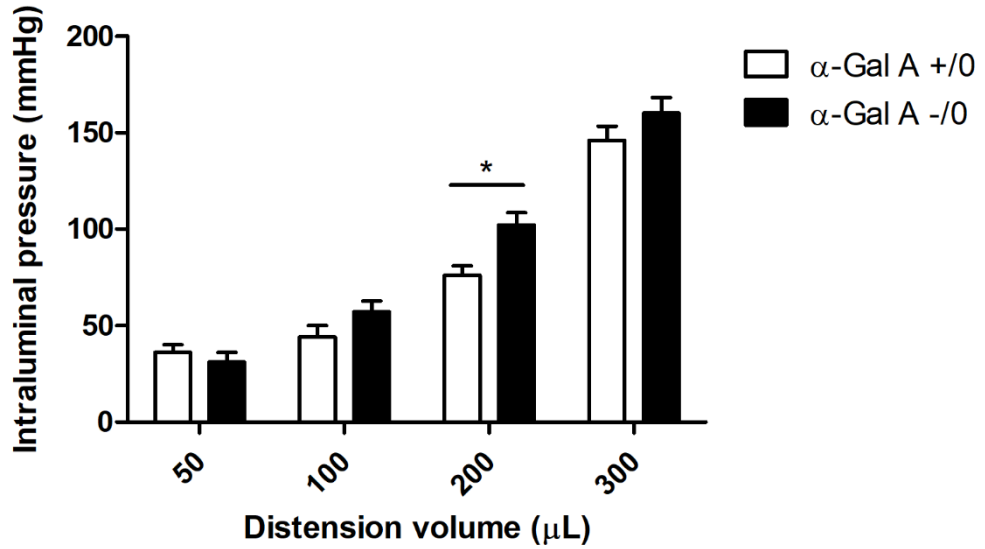

Figure 38. Assessment of intraluminal pressure in response to CRD in 12-month-old α-Gal A (+/0) and α-Gal A (-/0) mice. The graph shows the statistical analysis of the assessment of intraluminal pressure (*y axis*), expressed as mmHg, in response to CRD induced by different volumes of water (*x axis*), in anesthetized α-Gal A (+/0) (*grey*) and α-Gal A (-/0) (*black*) mice (n = 5 per group). Each column represents mean ± SEM. Origin software was used to perform one-way ANOVA for statistical significance between α-Gal A (+/0) and (−/0) mice. P-values of <0.05 (*), P < 0.01 (**), and P < 0.001 (***) were chosen as indicating significance.

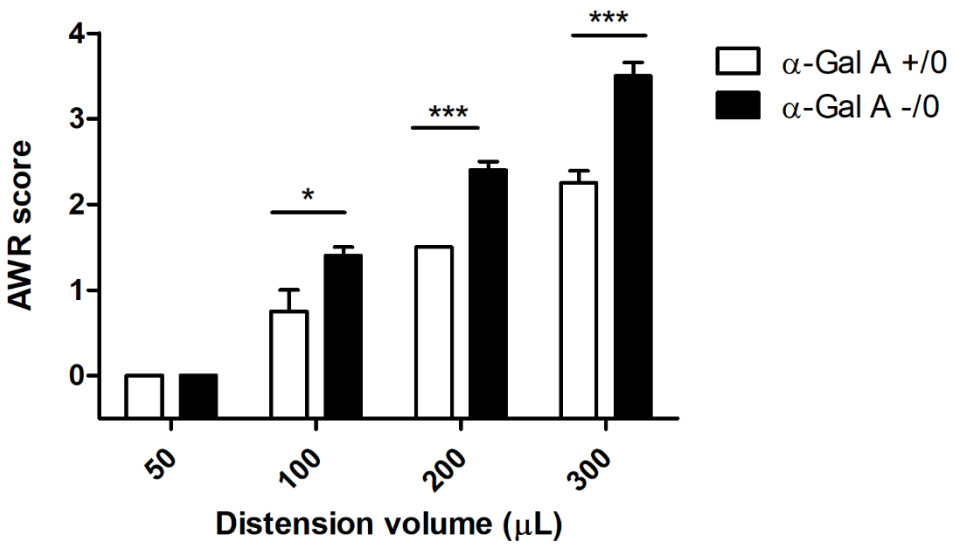

Figure 39. Assessment of AWR in response to CRD in 12-month-old α-Gal A (+/0) and α-Gal A (-/0) mice. The graph shows the statistical analysis of the assessment of AWR (*y axis*), expressed as AWR score (1-4), in response to CRD induced by different volumes of water (*x axis*), in unanesthetized α-Gal A (+/0) (*grey*) and α-Gal A (-/0) (*black*) mice (n = 5 per group). Each column represents mean ± SEM. Origin software was used to perform one-way ANOVA for statistical significance between α-Gal A (+/0) and (−/0) mice. P-values of <0.05 (*), P < 0.01 (**), and P < 0.001 (***) were chosen as indicating significance.

AWR assessment revealed a volume-dependent increase of responses in both α-Gal A (+/0) and α-Gal A (-/0) mice (Figure 39). Similarly to VMR evaluation, α-Gal A (-/0) mice displayed higher AWR score at all the volumes injected (100 µL, *P* = P=0,0339 [*]; 200 µL, *P* = P=7,93725 E^{-5} [***]; 300 µL, *P* = 7,40884 E^{-4} [***]), except with the lowest volume that did not induce any response in both α-Gal A (+/0) and α-Gal A (-/0) mice. All together these results suggest that 12-month-old α-Gal A (-/0) mice present visceral hyperalgesia, as shown by VMR and AWR evaluations, but that their intraluminal pressure is comparable to that of controls.

4.9 Evaluation of TRPV1, TRPV4, TRPA1 and TRPM8 expression in α-Gal A (-/0) and α-Gal A (+/0) mice colon: optimization of IF protocols

In order to assess the presence of alterations in the expression of pain-related ion channels in the colon of α-Gal A +/0 and -/0 mice, we optimized the IF protocols to stain TRPV1, TRPV4, TRPA1 and TRPM8 in 50-µm-thick transverse cryo-sections of α-Gal A +/0 and -/0 mice colon. Ion channels expression was assessed only in 12-month-old mice but not in 8- to 10- and 16- to 20-week-old mice, since the aim of the experiment was the optimization of IF protocols. TRPV1 immunoreactivity was detected at level of nerve fibers in the myenteric plexus ganglia and in the muscularis propria, both in circular and longitudinal muscular layer (Figure 40, white arrows), whereas TRPV4, TRPA1 and TRPM8 immunoreactivity was found in neuronal cell bodies of both the myenteric and submucosal plexus ganglia (Figure 41-43, white arrows). The pattern of expression of TRPV1, TRPV4, TRPA1 and TRPM8 was the same for both α-Gal A +/0 and -/0 mice (Figure 40-43).

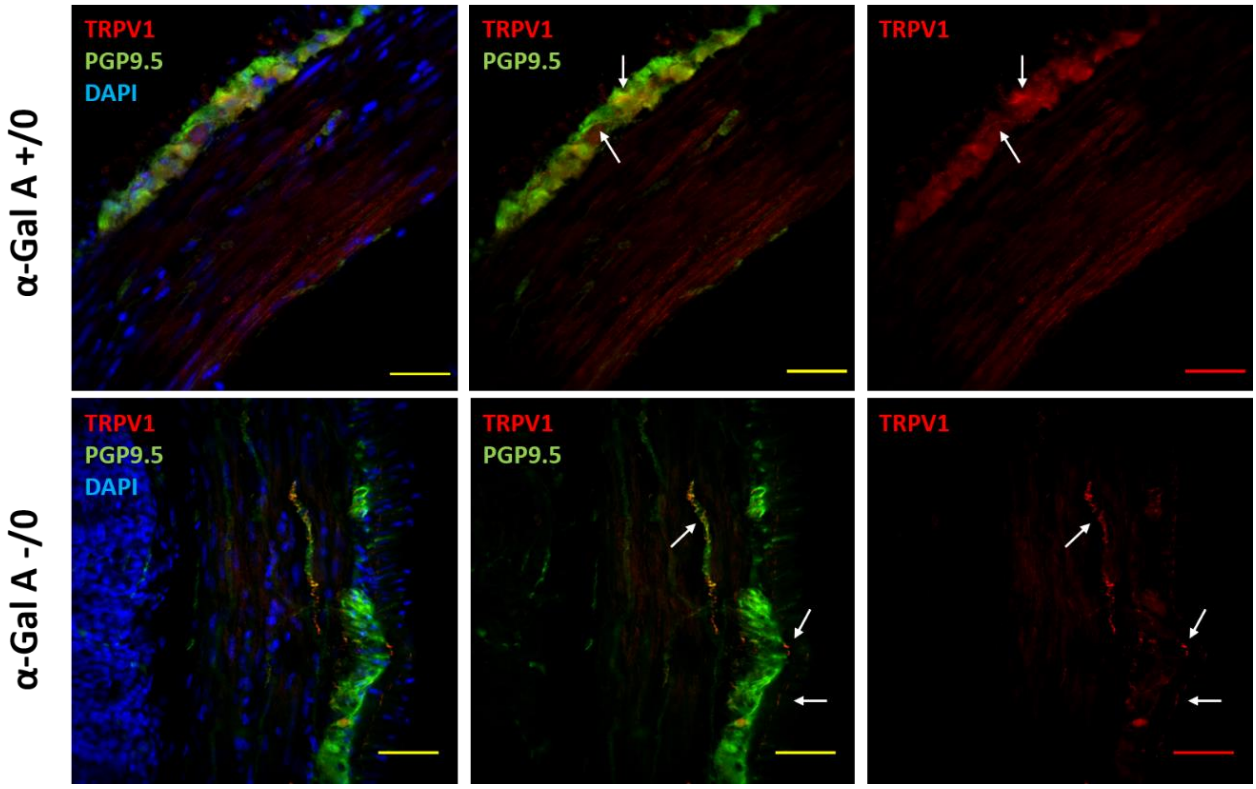

Figure 40. Representative images of TRPV1 staining in α-Gal A (-/0) and (+/0) mice colon. TRPV1 (*red*) and PGP9.5 (*green*) were detected by IF in 50µm-thick transverse cryo-sections of 12-month-old α-Gal A (+/0) and α-Gal A (-/0) male mice colon in order to stain TRPV1 and neurons, respectively. The figure displays representative images of TRPV1 immunoreactivity (*white arrows*) in the muscular layer of colon. Fluorescent images were captured on a Nikon D-Eclipse C1 inverted laser scanning confocal microscope at 40X magnification. Image J (NIH, http://rsb.info.nih.gov/ij/) software was used to modify images. Scale bar: 50µm.

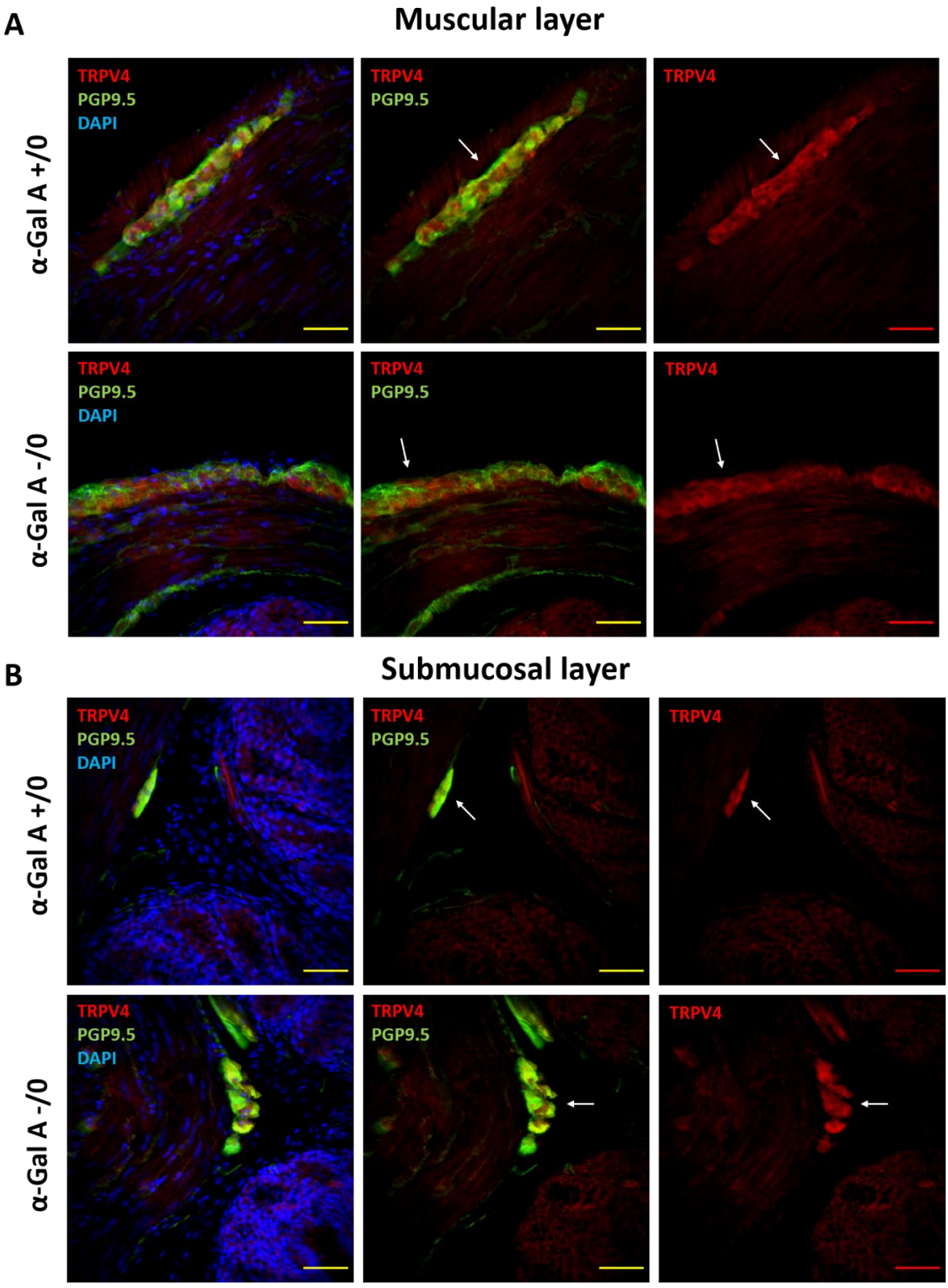

Figure 41. Representative images of TRPV4 staining in α-Gal A (-/0) and (+/0) mice colon. TRPV4 (*red*) and PGP9.5 (*green*) were detected by IF in 50µm-thick transverse cryo-sections of 12-month-old α-Gal A (+/0) and α-Gal A (-/0) male mice colon in order to stain TRPV4 and neurons, respectively. The figure displays representative images of TRPV4 immunoreactivity (*white arrows*) in the muscular (*upper panels*) and submucosal (*lower panels*) layer of colon. Fluorescent images were captured on a Nikon D-Eclipse C1 inverted laser scanning confocal microscope at 40X magnification. Image J (NIH, http://rsb.info.nih.gov/ij/) software was used to modify images. Scale bar: 50µm.

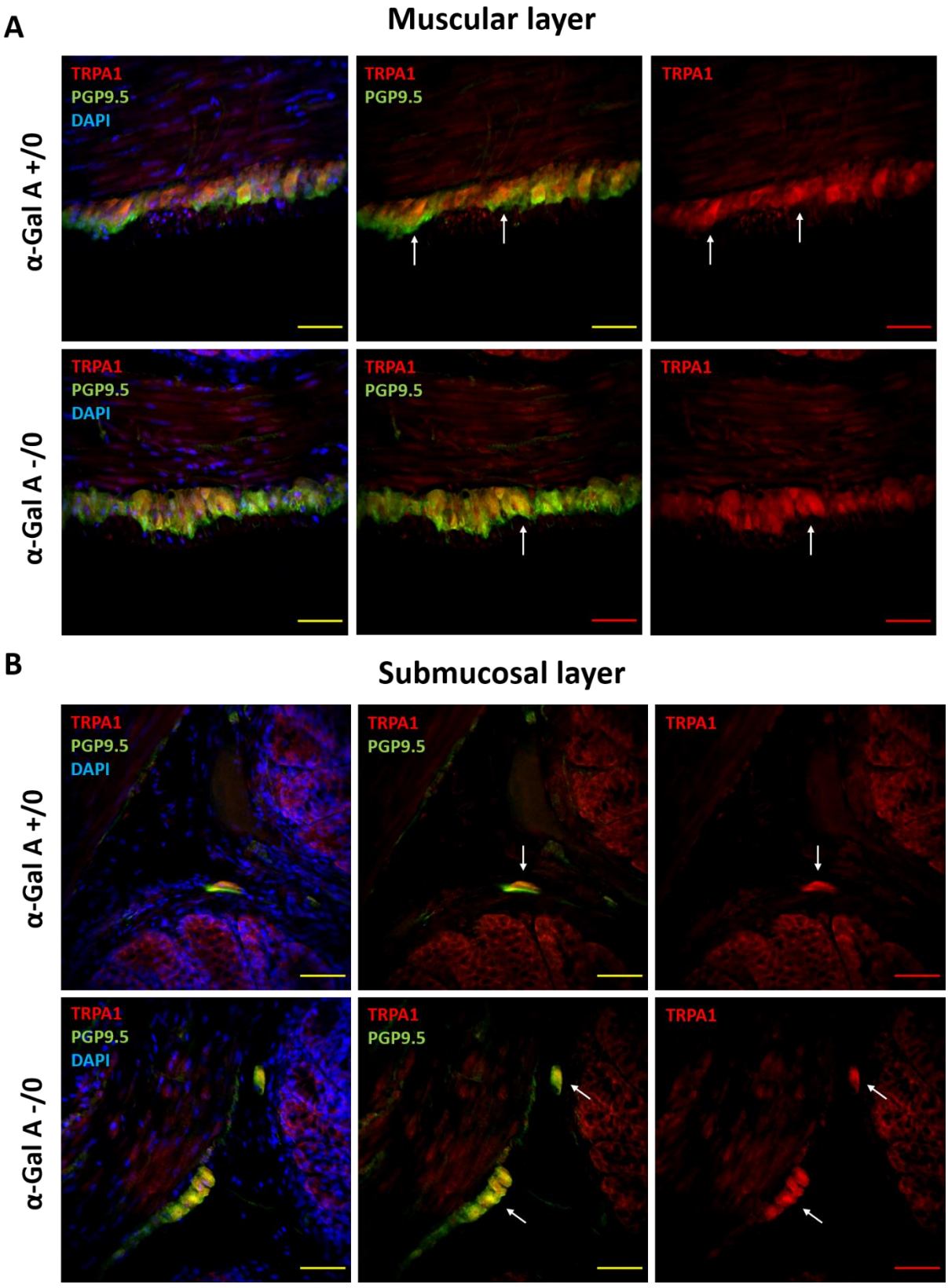

Figure 42. Representative images of TRPA1 staining in α-Gal A (-/0) and (+/0) mice colon. TRPA1 (*red*) and PGP9.5 (*green*) were detected by IF in 50µm-thick transverse cryo-sections of 12-month-old α-Gal A (+/0) and α-Gal A (-/0) male mice colon in order to stain TRPA1 and neurons, respectively. The figure displays representative images of TRPA1 immunoreactivity (*white arrows*) in the muscular (*upper panels*) and submucosal (*lower panels*) layer of colon. Fluorescent images were captured on a Nikon D-Eclipse C1 inverted laser scanning confocal microscope at 40X magnification. Image J (NIH, http://rsb.info.nih.gov/ij/) software was used to modify images. Scale bar: 50µm.

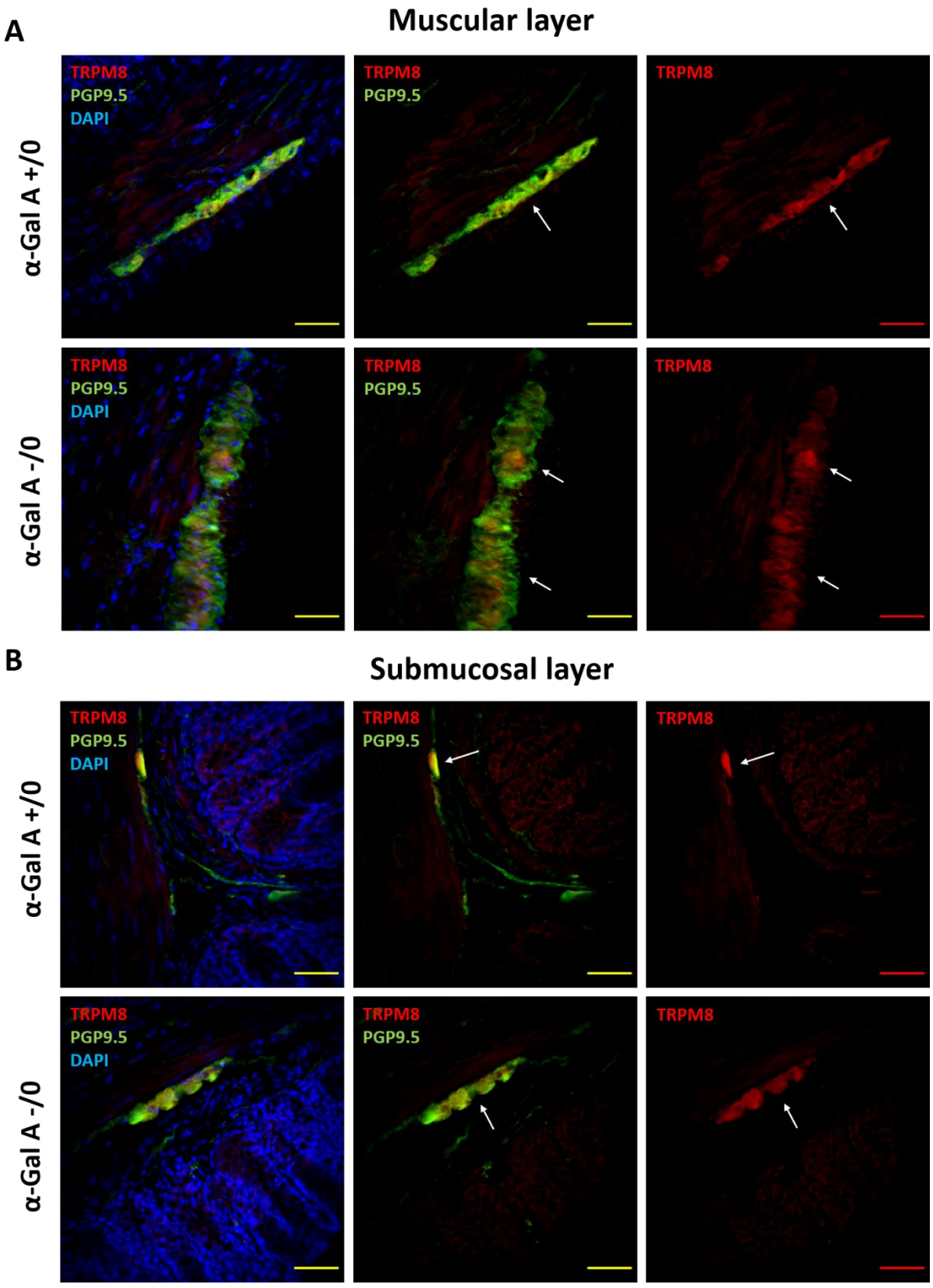

Figure 43. Representative images of TRPM8 staining in α-Gal A (-/0) and (+/0) mice colon. TRPM8 (*red*) and PGP9.5 (*green*) were detected by IF in 50µm-thick transverse cryo-sections of 12-month-old α-Gal A (+/0) and α-Gal A (-/0) male mice colon in order to stain TRPM8 and neurons, respectively. The figure displays representative images of TRPM8 immunoreactivity (*white arrows*) in the muscular (*upper panels*) and submucosal (*lower panels*) layer of colon. Fluorescent images were captured on a Nikon D-Eclipse C1 inverted laser scanning confocal microscope at 40X magnification. Image J (NIH, http://rsb.info.nih.gov/ij/) software was used to modify images. Scale bar: 50µm.

4.10 Primary cultures of enteric nervous system cells: optimization of protocols

4.10.1 Primary cell cultures of Enteric Nervous System from E14 mouse embryos intestine

In order to obtain primary cultures of ENS cells, intestines of E13 embryos were dissected and digested both mechanically and enzymatically as previously described (n = 2) (Chevalier et al., 2008; Gomes et al., 2009). By DIV4, the dissociated cells derived by embryos intestines formed a monolayer of myofibroblasts, in which ganglion-like structures became visible at the phase contrast microscope (*not shown*). Figure 44 shows representative images of ENS cultures fixed at DIV8 and stained for the neuronal RNA binding proteins HuC/HuD, the major constituent of neuronal microtubules Tuj1 and the glia intermediate filament protein GFAP. Hu and Tuj1 were chosen as markers of neuronal cell bodies and processes (both dendrites and axons), respectively, and GFAP as a marker of glial cells. IF staining confirmed the presence of ganglion-like structures, meaning groups of at least two neuronal cell bodies, which contain glial cells as well (Figure 44A, D and G).

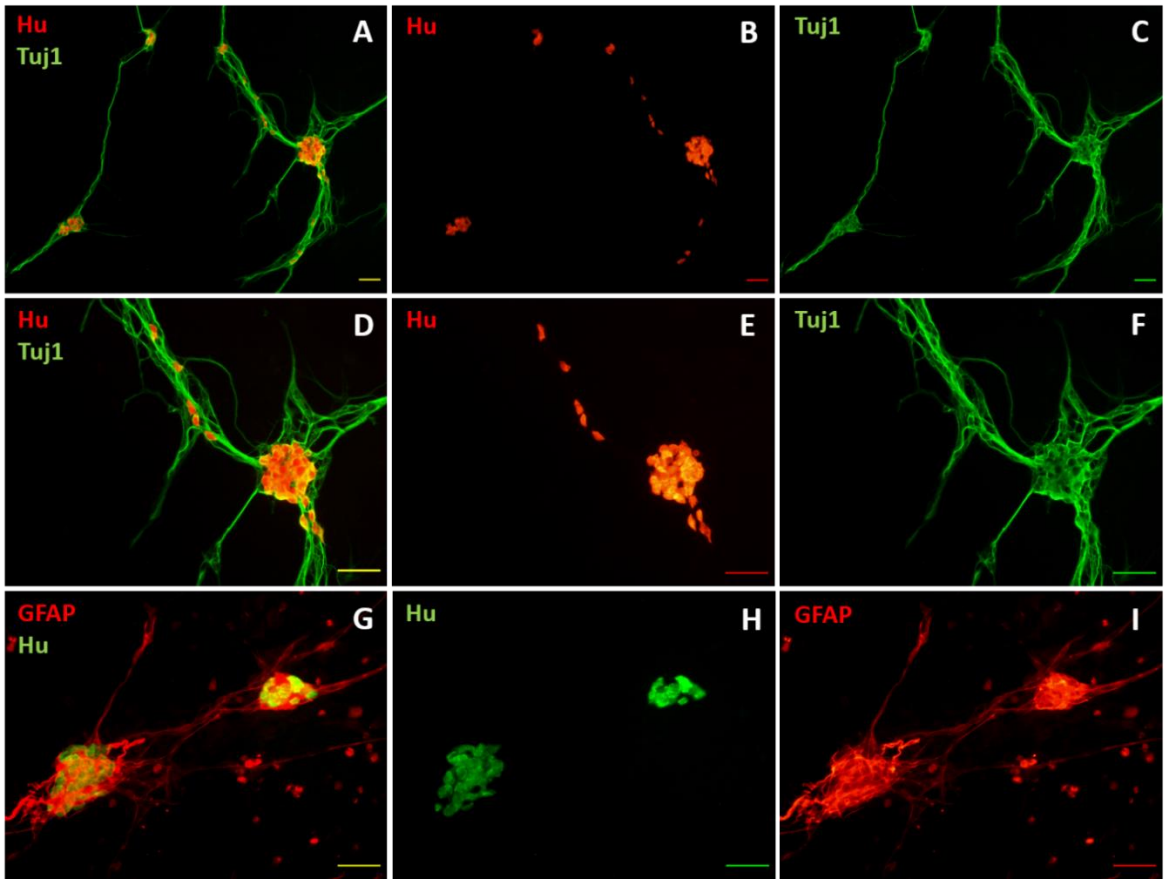

Figure 44. Representative images of ENS primary cultures derived by E13 embryos intestines. The figure shows representative pictures of ENS primary cultures derived by E13 embryos intestines fixed at DIV8 and stained for Hu (*A*, *B*, *D*, *E*, *G*, *H*), Tuj1 (*A*, *C*, *D*, *F*) and GFAP (*G* and *I*), in order to label neuronal cell bodies, neuronal cell processes (both dendrites and axons) and glial cells, respectively. A field of the picture shown in the upper panels (*A*-*C*) is displayed at a higher magnification in the middle panels (*D*-*F*). Images were captured on the IX50 Inverted Fluorescence Phase Contrast Microscope (Olympus) equipped with the high-resolution digital camera DP71 (Olympus) and modified by using ImageJ (NIH, http://rsb.info.nih.gov/ij/). Scale bar: 50 µm.

The images show that neurons and glia grew in close proximity and that both of them formed strands that connect different ganglion-like structures. Nevertheless, the mean number of cells obtained from the dissociation of E13 embryos intestines of one pregnant female was around 2 million cells, which is too low to set up molecular/cellular biology experiments, considering that the maximum number of wells that can be obtained with this amount of cells is 4 (456 000 cells per well). Therefore, we decided to use embryos at E14 (n = 3). ENS cultures derived by E14 embryos intestines grew and developed properly, giving rise to the characteristic ganglion-like structures containing both neuronal and glial cells that interconnect by means of interganglionic fiber strands (Figure 45A, B and C).

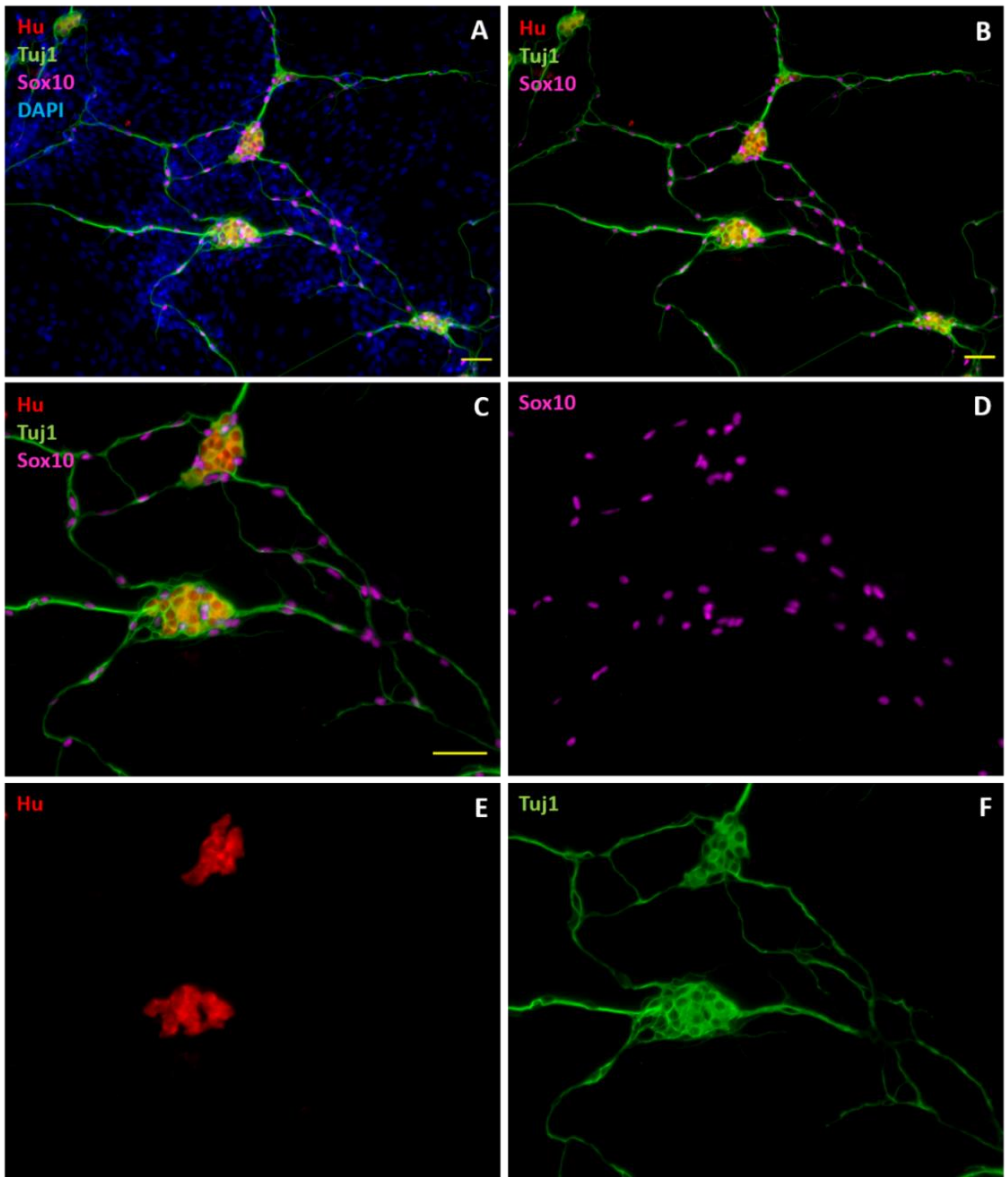

Figure 45. Representative images of ENS primary cultures derived by E14 embryos intestines. The figure shows representative pictures of ENS primary cultures derived by E14 embryos intestines fixed at DIV9 and stained for Hu (*red*), Tuj1 (*green*) and Sox10 (*magenta*), in order to label neuronal cell bodies, neuronal cell processes (both dendrites and axons) and glial cell bodies, respectively. Cell nuclei were stained with DAPI (*blue*). A field of the picture shown in the upper panels (*A, B*) is displayed at a higher magnification in the middle (*C, D*) and lower panels (*E, F*). Images were captured on the Axio Zoom.V16 fluorescence zoom microscope (Zeiss) and modified by using ImageJ (NIH, http://rsb.info.nih.gov/ij/). Scale bar: 50 µm.

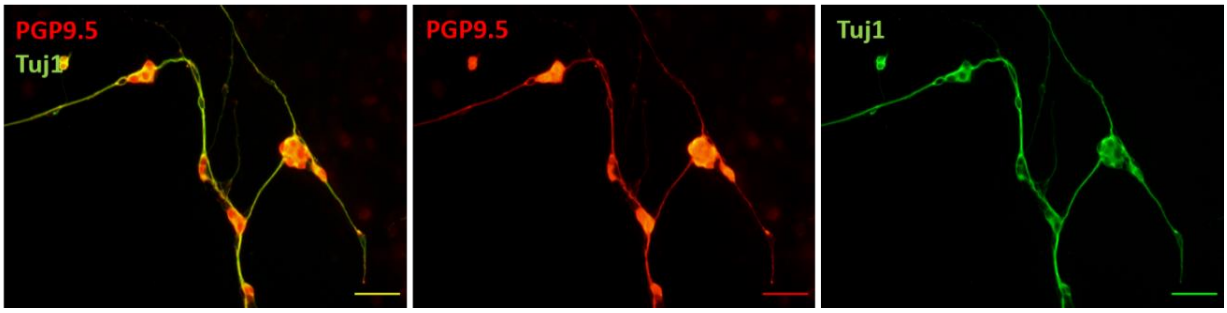

Figure 46. Comparison between PGP9.5 and Tuj1 staining patterns in ENS primary cultures derived by mouse embryos. The figure shows PGP9.5 (*red*) and Tuj1 (*green*) staining in ENS primary cultures derived by E13 embryos intestines fixed at DIV8. Images were captured on the IX50 Inverted Fluorescence Phase Contrast Microscope (Olympus) equipped with the high-resolution digital camera DP71 (Olympus) and modified by using ImageJ (NIH, http://rsb.info.nih.gov/ij/). Scale bar: 50 µm.

Glial cell bodies were identified by Sox10 immunoreactivity (Figure 45A-D). Since we did not have an anti-alpha-smooth muscle actin (α-SMA) primary antibody that worked on mouse cultures, we could not specifically label the layer of myofibroblasts underneath the ganglion-like structures. However, since they have a characteristic spindle-shape and big nuclei, they were well recognizable at the phase-contrast microscope (*not shown*) and DAPI staining allowed us to label them, even if in a non-specifically way (Figure 45A). The mean number of cells obtained from the dissociation of E14 embryos intestines of one pregnant female was around 4 million cells, which is the double of the number obtained with E13 embryos (9 wells vs. 4 wells, respectively), suggesting E14 is the best option. Since in our previous work (Masotti et al., 2019) we used PGP9.5 as a pan neuronal marker, it was decided to double stain ENS cultures for PGP9.5 and Tuj1, in order to compare to two staining patterns. As Figure 46 shows, the two staining are completely overlapping, except for neuronal bodies that are labelled only by the anti-PGP9.5 antibody.

4.10.2 Primary cell cultures of enteric neurons from E14 mouse embryos intestine

In order to obtain pure primary cultures of enteric neurons, intestines of E14 embryos were dissected and digested both mechanically and enzymatically. Based on the work of Le berre-scoul and colleagues, we decided to coat the coverslips for the growth of neurons with poly-L-lysine (n = 4) (Le berre-scoul et al., 2017). The results show that neurons developed properly, forming ganglion-like structures connected through interganglionic strands, as shown by Hu and Tuj1 staining (Figure 47). The number of myofibroblasts decreased as the culture grew from DIV5 to DIV9, as displayed by DAPI, but so did the number of ganglion-like structures, as shown by Hu staining (Figure 47). This was found to be due to a detachment of the neuronal mesh from coverslips, suggesting that poly-L-lysine is not appropriate as coating for mouse primary cultures of enteric neurons from embryos intestines. For this reason, we tried to coat the coverslips with Type I collagen (n = 3). Although the

neuronal mesh developed properly and the number of ganglia remained high even at DIV9, the myofibroblasts did not die, demonstrating that Type I collagen is not a suitable coating either to obtain an enriched neuronal culture (Figure 48). Therefore, we decided to coat the coverslips with two other types of solutions, a mix 1:1 of poly-L-lysine and Type I collagen (n = 1) and Gelatin (n = 1). Gelatin coating not only caused neuronal culture detachment (Figure 49), similarly to poly-L-lysine coating (Figure 47), but also promoted the growth of myofibroblasts, whose number remained high (DIV9) (Figure 49), similarly to Type I collagen coating (Figure 48). On the contrary, the mixture 1:1 of poly-L-lysine and Type I collagen showed several advantages: the neuronal mesh developed properly, it did not detach and the number of myofibroblasts remained relatively low (Figure 49). Together these findings suggest the mixture 1:1 of poly-L-lysine and Type I collagen is the best option for coating the coverslips in order to obtain an enriched neuronal culture from mouse embryos. We simultaneously checked whether glial cells were present in the culture, and as shown by Figure 50, they were not detected.

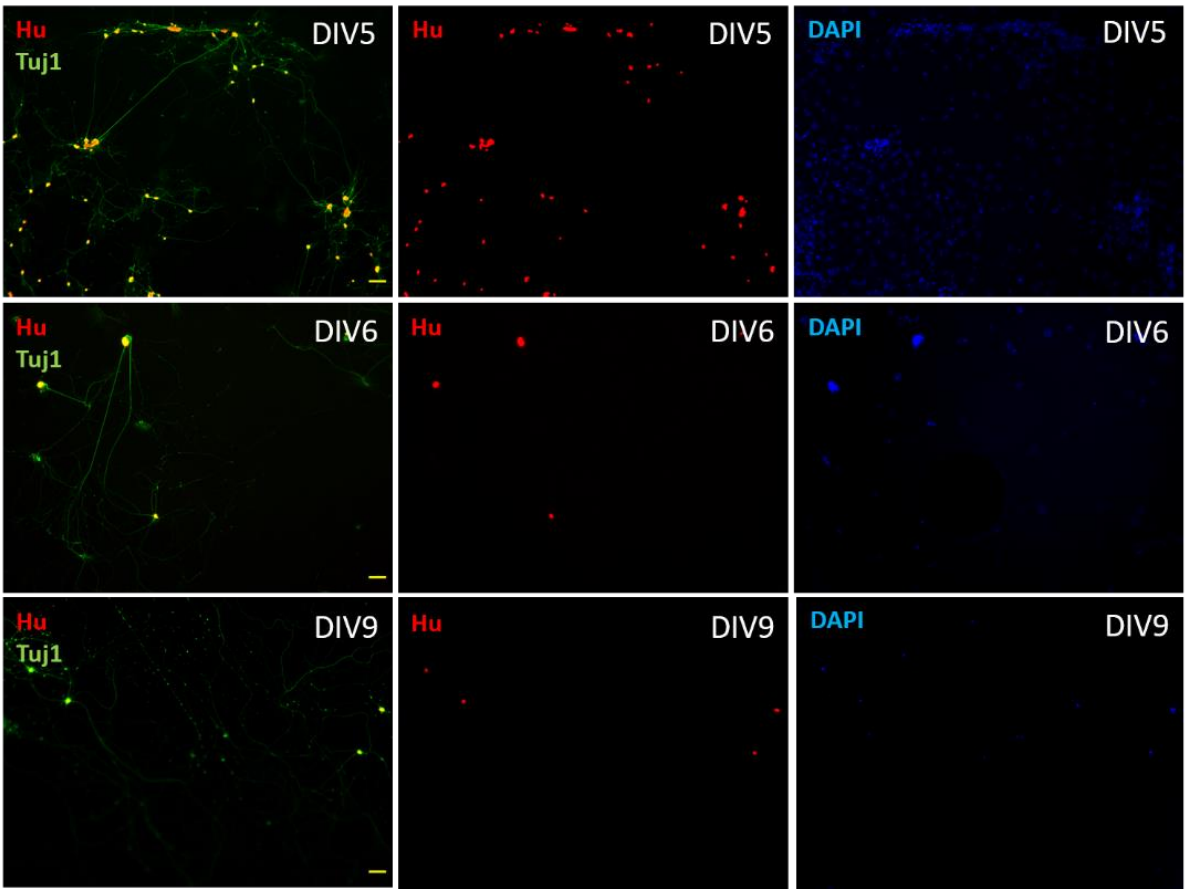

Figure 47. Representative images of enteric neurons primary cultures derived by E14 embryos intestines plated on poly-L-lysine-coated coverslips. The figure shows representative pictures of enteric neurons primary cultures derived by E14 embryos intestines plated on poly-L-lysine-coated coverslips, fixed at DIV5, 6 and 9 and stained for Hu (*red*) and Tuj1 (*green*), in order to label neuronal cell bodies and neuronal cell processes (both dendrites and axons), respectively. Cell nuclei were stained with DAPI (*blue*). Images were captured on the Axio Zoom.V16 fluorescence zoom microscope (Zeiss) and modified by using ImageJ (NIH, http://rsb.info.nih.gov/ij/). Scale bar: 200 and 100 µm (*middle panels*).

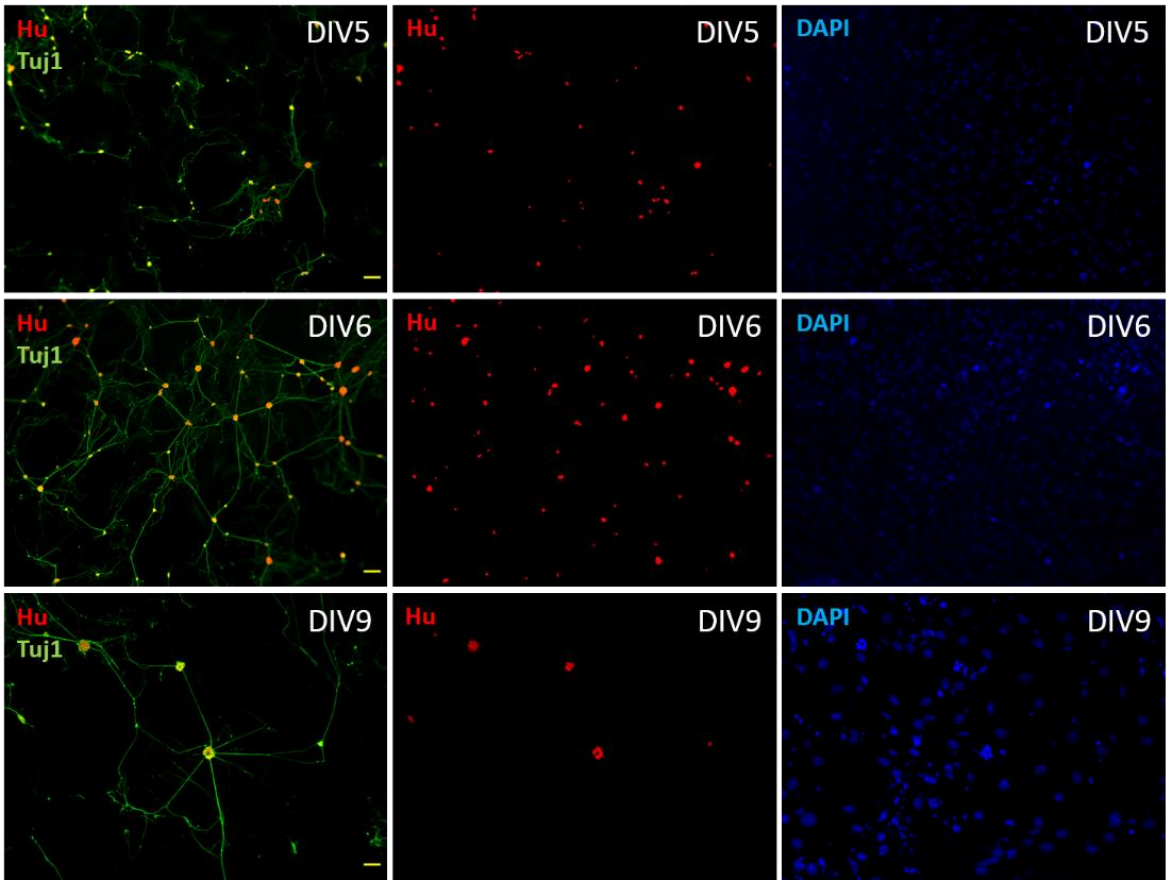

Figure 48. Representative images of enteric neurons primary cultures derived by E14 embryos intestines plated on Type I collagen-coated coverslips. The figure shows representative pictures of enteric neurons primary cultures derived by E14 embryos intestines plated on Type I collagen-coated coverslips, fixed at DIV5, 6 and 9 and stained for Hu (*red*) and Tuj1 (*green*), in order to label neuronal cell bodies and neuronal cell processes (both dendrites and axons), respectively. Cell nuclei were stained with DAPI (*blue*). Images were captured on the Axio Zoom.V16 fluorescence zoom microscope (Zeiss) and modified by using ImageJ (NIH, http://rsb.info.nih.gov/ij/). Scale bar: 200 and 100 µm (*lower panels*).

4.10.3 Enteric Glia Cells cultures from adult mouse intestine

In order to obtain cultures of enteric EGCs, the LM/MP layer was dissected from intestines of adult mice and digested both mechanically and enzymatically. Once ganglia were dissected and seeded in wells coated with both poly-L-lysine and Laminin, they were supposed to attach to the bottom, and glial cells to grow. However, only a few ganglia resulted attached to the bottom of the wells at DIV3 (n = 4) and indeed glial cells were too few to survive and grow. We thought this could be due the plating medium, the 3 g/L glucose complete medium (DMEM/F-12, HEPES; Gibco) containing 10% FBS, 2 mM L-Glu (Invitrogen), 50 U/mL PS (Invitrogen), 0.1 g/100mL sodium bicarbonate ($NaHCO_3$), 2% distilled water, 0.025% Amphotericin B and 0.2% Gentamycine, a medium generally used for organotypic cultures ("organotypic medium"). Therefore, in order to improve the adhesion, we tested two different plating conditions by seeding the ganglia or in the medium used to culture glial cells ("glial medium"), the 4.5 g/L glucose complete medium (DMEM, high glucose; Gibco)

containing 10% FBS, 2 mM L-Glu (Invitrogen) and 50 U/mL PS (Invitrogen) (n = 2), or in a mix 1:1 of organotypic and glial medium (n= 2). The mix 1:1 of glial and organotypic medium promoted ganglia attachment and glial cell growth, resulting to be the best condition for plating ganglia. We also noticed that glial cells cultures expansion must be gradual, otherwise cells die, meaning that they should be expanded as follows: 24-well plate (p0), 12-well plate (p1), 6-well plate (p2), T25 flask (p3), T75 flask (p4).

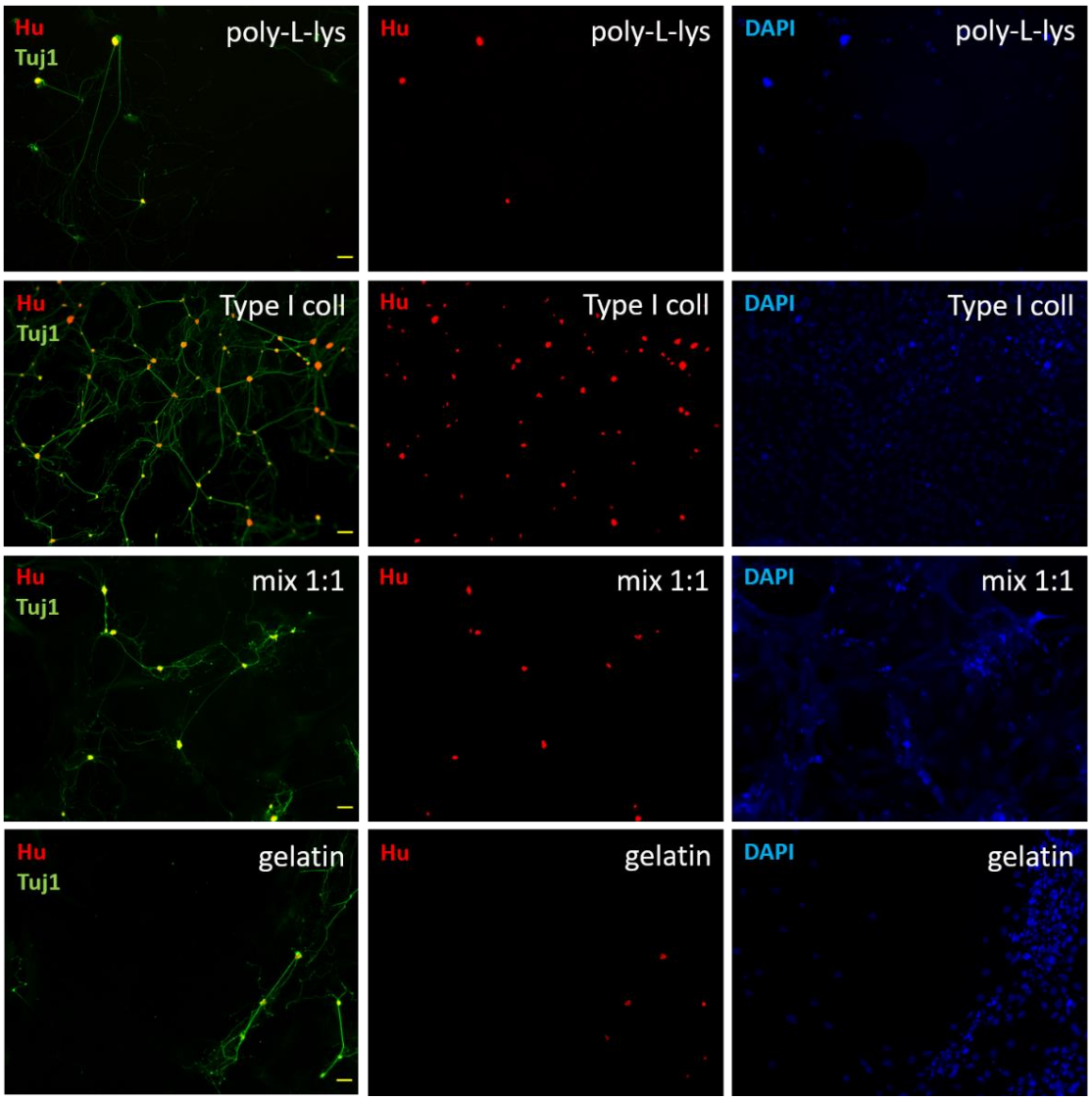

Figure 49. Representative images of enteric neurons primary cultures derived by E14 embryos intestines plated on coverslips coated with poly-L-lysine, Type I collagen, a mix 1:1 of poly-L-lysine and Type I collagen, and gelatin. The figure shows representative pictures of enteric neurons primary cultures derived by E14 embryos intestines plated on coverslips coated with poly-L-lysine, Type I collagen, a mix 1:1 of poly-L-lysine and Type I collagen, and gelatin. Cultures were fixed at DIV6 (*poly-L-lysine-, Type I collagen- and mix 1:1-coated coverslips*) and 9 (*gelatin-coated coverslips*) and stained for Hu (*red*) and Tuj1 (*green*), in order to label neuronal cell bodies and neuronal cell processes (both dendrites and axons), respectively. Cell nuclei were stained with DAPI (*blue*). Images were captured on the Axio Zoom.V16 fluorescence zoom microscope (Zeiss) and modified by using ImageJ (NIH, http://rsb.info.nih.gov/ij/). Scale bar: 200 and 100 µm (*upper panels*).

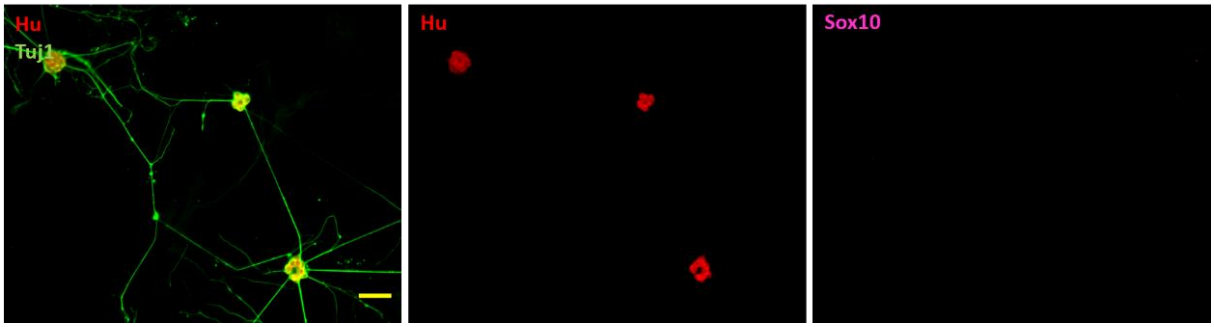

Figure 50. Representative images of enteric neurons primary cultures derived by E14 embryos intestines stained for Sox10. The figure shows representative pictures of enteric neurons primary cultures derived by E14 embryos intestines plated on Type I collagen-coated coverslips, fixed at DIV9 and stained for Hu (*red*), Tuj1 (*green*) and Sox10 in order to label neuronal cell bodies, neuronal cell processes (both dendrites and axons) and glial cell bodies respectively. Cell nuclei were stained with DAPI (*blue*). Images were captured on the Axio Zoom.V16 fluorescence zoom microscope (Zeiss) and modified by using ImageJ (NIH, http://rsb.info.nih.gov/ij/). Scale bar: 100 µm.

5 DISCUSSION

GI symptoms are among the earliest and most frequent symptoms of FD, affecting the half of adults (49.8%) and up to 60% of children (60.8%) (Hoffmann et al., 2007). Registry data from the Fabry Outcome Survey show that abdominal pain is the most common GI complaint, being experienced by up to one third of patients (Hoffmann et al., 2007). They describe colic with severe debilitating burning pain in the mid and lower abdomen, superficial skin tenderness, bloating and cramping, as well as mid-abdominal discomfort that generally is worsened by meals, stress, changes in diet and meal plans (MacDermot et al., 2001; Zar-Kessler et al., 2016). It has been hypothesized that the pathophysiological mechanisms accounting for GI symptoms of FD are mainly three: dysfunction of the ANS responsible for gut motility, vasculopathy affecting GI circulation, and tissue inflammation related to Gb3 accumulation (Zar-Kessler et al., 2016, Politei et al., 2017). However, the pathophysiology of these symptoms is complex and multifactorial and the exact mechanisms of pain perception and the structural/functional modifications occurring in the GI wall are still poorly understood. The α-Gal A (-/0) mouse, the murine model of FD (Ohshima et al., 1997), has already given proof to be a useful and reliable model to study neuropathic pain (Lakoma et al., 2014 and 2016; Üçeyler et al., 2016; Namer et al., 2017; Hoffman et al., 2018). Moreover, lysosomal storage inclusions have been found in smooth muscle cells of small and large intestine muscularis propria as well as in enlarged and vacuolated neurons of both myenteric and submucosal plexus, suggesting that the α-Gal A (-/0) mouse could be a good model also for investigating FD neuropathy (Bangari et al., 2015).

Here we aim at understanding the molecular mechanisms underpinning the GI symptoms of FD. For this purpose, we used the α-Gal A (-/0) male mouse to characterize anatomical, morphological and molecular features of the colon tract (Masotti et al., 2019). Furthermore, we propose to describe the presence of visceral pain in the α-Gal A (-/0) mouse by studying the VMR and AWR in response to CRD. Firstly, we decided to evaluate the macroscopic and microscopic damage of colonic wall. In this context, it is important to mention that some GI symptoms experienced by FD patients mirror those of others IBDs (Hilz et al., 2018). For this reason, since we were not able to find any standard parameter for the histomorphological evaluation of colon in Fabry patients, we relied on criteria used to assess colonic inflammation in different mouse and rat models of IBD (Wallace and Keenan, 1990; Erben et al., 2014). Notably, we did not detect any difference between α-Gal A -/0 and α-Gal A +/0 model based on macroscopic damage parameters. In addition, cross sections of α-Gal A -/0 mouse colon did not present any remarkable sign of inflammatory infiltrate at mucosal level and displayed a normal epithelium with intact villous architecture compared to

controls (Figure 29). These findings are consistent with the result of colonoscopies and skin histological analysis of Fabry patients, which normally do not show any sign of mucosal damage or inflammation (O'Brien et al., 1975; Jack et al., 1991) as well as with patients reports that do not indicate mucous or blood in the stool (MacDermot et al., 2001; Keshav, 2006). Interestingly, the analysis of microscopic damage of the colonic wall displayed an increasing trend of the thickness of the muscular layer in α-Gal A -/0 mice colon, but not in α-Gal A +/0 controls, culminating at the age of 12 months (Figures 30). This result is in line with reports of patients presenting a thickening of the intestinal muscular layer and Gb3 deposits in smooth muscle cells (Friedman et al., 1984). This unusual thickening in α-Gal A -/0 mice may indeed derive by the presence of Gb3 deposits in smooth muscle and neuronal cells or, alternatively, might indicate tissue hypertrophy or hyperplasia. It has been indeed demonstrated that Gb3 accumulates both in the endothelium and smooth muscle cells leading to vessel wall expansion (Namdar et al., 2012), as well as to alteration of cellular signaling pathway inducing extra cellular matrix proliferation of the smooth muscle cell, ultimately leading to hypertrophy, myopathy, and vascular remodeling (Boutouyrie et al., 2002; Rombach et al., 2010). Therefore, the combination of these processes could lead to intestinal muscular layer thickening and decreased blood flow, causing ischemic episodes and tissue damage (Sheth and Swick, 1980; Sheth et al., 1981; Valbuena et al., 2012). The microscopic damage assessment revealed also an increasing trend of the size of the myenteric ganglia (Figure 29). In this scenario, myenteric plexus ganglia are pivotal structures for the regulation of gut motility, and, within the ENS, they are proposed as a target system to explain a variety of colonic motor dysfunction, ranging from inflammatory disease to functional disturbances (De Giorgio et al., 2007; Di Nardo et al., 2008; Furness, 2000). In FD patients, Gb3 is known to accumulate in both myenteric and submucosal plexus ganglia and this accumulation is believed to be the cause of gut dysmotility, gastroparesis and visceral pain (O'Brien et al., 1982; Buda et al., 2013; Politei et al., 2016; Zar-Kessler et al., 2016; Hilz et al., 2018). Upon this basis, we performed a histomorphological evaluation of myenteric ganglia through the analysis of the immunoreactivity of colon sections to the pan-neuronal marker PGP9.5 (Figure 30A, red areas). To demonstrate the specificity of PGP9.5 as a neuronal marker, we double stained colon sections of α-Gal A (+/0) and α-Gal A (-/0) mice for both PGP9.5 and NF-L. We have performed the double staining because the NF-L marker belongs to the family of the intermediate filament protein family and is a major component of neuronal cytoskeletons (Cavaliere et al., 2007). The 3D reconstruction of myenteric plexus ganglia showed that PGP9.5 and NF-L staining co-localized (Figure 32), providing evidence of the specificity of PGP9.5 as a neuronal marker. In the analysis of myenteric plexus ganglia area, we observed an age-dependent increase in the ganglia mean area (Figure 30A, B). Furthermore, among the population of the ganglia observed, we detected a higher number of large-

sized ganglia, which was age-related and more pronounced in the 12-month α-Gal A -/0 compared to α-Gal A +/0 (Figure 30C). In light of this finding, we analyzed the ganglia cellular density in terms of number of neurons per ganglion in order to define this morphological change associated with hypertrophic or a hyperplastic condition. We decided to plot the number of PGP9.5-positive cells per ganglion on the basis of their area, expressed in μm^2, and to perform a linear regression analysis in order to obtain the slope values of the lines, which were used as indicator of neuronal density. Interestingly, the analysis did not show any difference between α-Gal A -/0 and +/0 mice, at none of the three ages studied (Figure 31A, B), but neuronal density of 12-month-old α-Gal A -/0 mice resulted lower when compared to both α-Gal A -/0 (P = 0.0183, [*]) and α-Gal A +/0 mice (P = 0.0096, [**]; Figure 31B). These results demonstrate that both age and genotype may affect neuronal density of myenteric plexus ganglia by inducing hypertrophy. This finding is in line with previous analysis and suggests that age-correlated Gb3 accumulation is the main cause of the size increase in the ganglia of the myenteric plexus ganglia. Following the histomorphological evaluation results, we next observed the localization of Gb3 deposits in cross sections of the colon wall from α-Gal A -/0 mice by IF and confocal imaging. Gb3 immunoreactivity showed a uniform distribution in the mucosa of both α-Gal A +/0 and α-Gal A -/0 mice at all ages (Figure 33). In contrast, double staining of Gb3 and PGP9.5 confirmed that Gb3 inclusions are markedly more present in submucosal and myenteric plexuses (Figure 34), consistently with both the increased muscular thickness (Figure 29) and the enlarged area of myenteric plexus ganglia (Figure 30) of α-Gal A -/0 mice compared to α-Gal A +/0 controls. Considering the decreased cells density in myenteric plexus ganglia among the age of the α-Gal A -/0 compared to α-Gal A +/0 (Figure 31), Gb3 deposits could represent the main cause of the increased ganglion area observed. These findings are in line with the clinical evaluation of FD patients whose histological descriptions of the GI tract display vacuolization of ganglion cells and surrounding axons with intracellular Gb3 deposits (Flynn et al., 1972; O'Brien et al., 1982; Jack et al., 1991; Sheth et al., 1981; Friedman et al., 1984; Jardine et al., 1994; Deniz et al., 2011; Hilz et al., 2018). The GSLs accumulation in intestinal myenteric ganglia is believed to cause a decrease of peristaltic movements and focal spastic contractions, leading to lack of coordination of the myogenic activity and intestinal dismotility (Flynn et al., 1972; Bryan et al., 1977; Cable et al., 1982; O'Brien et al., 1982). Dismotility, in turn, may lead to intestinal stasis, bacterial overgrowth and diarrhea (O'Brien et al., 1982; Jack et al., 1991; Buda et al., 2013; Zar-Kessler et al., 2016). In addition, it can increase intraluminal pressure with subsequent formation of diverticula in both small and large intestine (Sheth et al., 1981; O'Brien et al., 1982; Jack et al., 1991; Politei et al., 2016). Colonic dysmotility may also lead to the pseudo-obstruction syndrome, which simulates intestinal necrosis (Politei et al., 2016). Recently, chronic intestinal pseudo-obstruction was indeed reported in a patient group as a result of

substrate deposition at both autonomic ganglia and smooth muscle cell level (Politei et al., 2017; Hilz et al., 2018). Thus, a morphological change in enteric ganglia, together with the intestinal smooth muscle cell Gb3 storage, may play a paramount role in intestinal dysfunctions experienced by FD patients. Moreover, these alterations could trigger secondary pathological processes reflecting a tissue response (e.g. hypertrophy, impaired sensory perception). Gb3 deposition in myenteric ganglion cells has been associated with visceral pain (O'Brien et al., 1982; Buda et al., 2013; Politei et al., 2016; Zar-Kessler et al., 2016; Hilz et al., 2018). It has been demonstrated that Gb3 accumulation leads to an impaired cellular function, such as limited contractility of muscular cells and to an altered expression of ion channels in DRG neurons (Gadoth and Sandbank, 1983; Burlina et al., 2011; Choi et al., 2015; Lakomá et al., 2016; Kummer et al., 2018). These alterations are likely to be the cause of the impaired pain, mechanical and thermal perception (Rodrigues et al., 2009; Lakomá et al., 2014; Namer et al., 2017; Kummer et al., 2018). It has to be underlined that our study did not specify whether vascular occlusion, a potential pathogenetic mechanism of FD occurring in cerebral and different additional tissues in human FD, may contribute to the alterations detected in the colon innervation. Although colon vessels appeared open at our general histomorphological evaluation, a focused study using a specific marker of endothelium vessels is needed to assess the patency of colon vessels and whether vascular occlusion may contribute to the abnormalities of colon innervation we found in FD mice. Therefore, even if the underlying pathophysiology has not been investigated, it is reasonable to hypothesize an involvement of myenteric plexus and smooth muscle cells in the onset of the GI symptoms of FD. Also, we previously reported that the expression of the pan neuronal marker PGP9.5 showed a significant decreased and scattered pattern of neuronal endings in the frontal skin paw of α-Gal A -/0 mice, in comparison with their α-Gal A +/0 littermates (Lakomá et al., 2016). This result mirrors the decrease in neuronal terminations marked by PGP9.5 in skin biopsies of human patients with SFN (Donadio et al., 2013; Liguori et al., 2017). Based on these findings, we next studied the density of nerve fibers entering the colonic mucosa, through IF analysis of PGP9.5-positive nerve fibers on transverse floating sections of 8- to 10-week-old, 16- to 20-week-old, and 12-month-old α-Gal A +/0 and α-Gal A −/0 male mice colon. α-Gal A -/0 mice of all the age groups showed an important decrease in PGP9.5-positive innervation entering the mucosa, compared to α-Gal A +/0 controls (Figure 36). Moreover, in α-Gal A -/0 male mice colon, we found morphological alterations such as nerve fibers fragmentations, scattering, and swelling (Figures 36). These findings confirm the previous observation in the mice frontal paws and epidermis of dorsal skin of the KO model (Lakomá et al., 2014) and human skin biopsies of Fabry patients (Sheth et al., 1981; Dütsch et al., 2002; Donadio et al., 2012). Besides endocrine messages released from entero-endocrine cells in the mucosal epithelium and immune messages carried by circulating lymphocytes activated by

antigens presented to them from the lumen, signals from GI mucosa are also conveyed by neurons whose receptive endings are in the lamina propria and beneath the mucosal epithelium. Some of these afferent neurons have cell bodies in enteric ganglia (IPANs and intestinofugal neurons) whereas others have them in extrinsic ganglia (EPANs), and together convey chemical and mucosa-related mechanical stimuli (Furness, 2006). Therefore, it is reasonable to think that GSLs accumulation-related damage to small caliber, thinly myelinated or unmyelinated sensory fibers of the colonic mucosa is likely to contribute to abdominal pain and dysmotility (Hilz et al., 2018). Finally, in order to gain more information on the cytokine profile of the α-Gal A (−/0) genotype, we quantified the serum concentrations of IL-1β, IL-6, IL-10, IL-17A, IFNγ, and TNFα cytokines. We did not find any significant difference between serum samples derived by α-Gal A (−/0) and α-Gal A (+/0) mice at all ages analyzed. On the contrary, different studies have shown an implication of the immune response in FD, as reviewed by Rozenfeld and Feriozzi (Rozenfeld and Feriozzi, 2017). For example, one study demonstrated that cultured PBMCs from Fabry patients present a higher proinflammatory cytokine expression and production (TNF-α and IL-1β) and provided direct evidence of Gb3 having a proinflammatory role, likely mediated by TLR4 (De Francesco et al., 2013). In FD, it has been demonstrated that also lyso-Gb3 can be recognized by TLR4 and trigger Notch1 signaling, in turn activating the nuclear factor kappa B (NF-κB) pathway, resulting in the production of pro-inflammatory cytokines and giving rise to systemic and local inflammatory responses (Anders et al., 2004; Sanchez-Niño et al., 2015). Similarly, another study displayed that the pro-inflammatory cytokines IL-6 and TNF-α are increased in Fabry patients (Biancini et al., 2012).

Given these results, we thought that besides the histomorphological differences, the murine model of FD could display also functional alterations, such as visceral pain perception. Evaluation of VMR to CRD is a technique that is widely used for assessing changes in visceral sensitivity in animals that either have a genetic mutation or have been treated intracolonically or otherwise to model bowel disorders (Christianson and Gebhart, 2007). In this context, it has been demonstrated that mice lacking TRPV1 or acid sensing ion channel 3 (ASIC3) ion channels display significantly reduced VMRs during CRD, compared to controls (Jones et al., 2005). Conversely, mice or rats treated intracolonically with substances inducing experimental bowel disorders have significantly greater VMRs than do vehicle-treated animals (Sengupta et al., 1999; Tobin et al., 2004; Jones et al., 2007). Another method commonly used for studying visceral sensitivity in rodent models of bowel disorders, which takes in consideration also the conscious level of pain perception, is AWR evaluation (Al-Chaer et al., 2000; Chen et al., 2014). We decided to evaluate for the first time the visceral sensitivity in the α-Gal A (-/0) mouse by studying both VMR and AWR to CRD in 12-month old mice. Interestingly, we found that α-Gal A (-/0) mice, compared to controls, display greater VMR values to

CRD induced by the higher volumes injected in the balloon (100, 200 and 300 µL), and that this increase in VMR seems to be volume-dependent (Figure 37). Similarly, α-Gal A (-/0) mice obtained higher AWR score at all the volumes injected, except with the lowest volume that did not induce any response in both α-Gal A (+/0) and α-Gal A (-/0) mice (Figure 39). Again, we saw that the increase of response was volume-dependent. Together these results suggest that 12-month-old α-Gal A (-/0) mice present visceral hyperalgesia. These findings likely mirror the severe abdominal pain experience by Fabry patients (Hoffmann et al., 2007) and provides additional proof that the α-Gal A (-/0) male mouse is a reliable model to study pain in FD. Moreover, we evaluated intraluminal pressure at the moment of CRD. Our analysis displays a volume-dependent increase of intraluminal pressure values both in α-Gal A (+/0) and α-Gal A (-/0) mice, but no differences between the two, except for the distension with 200 µL that revealed a higher intraluminal pressure value in α-Gal A (-/0) mice (Figure 38). Therefore, in general, our murine model does not seem to display differences in terms of intraluminal pressure compared to controls. In contrast, several case study have demonstrated that Fabry patients display high intraluminal pressure secondary to dysmotility and leading to diverticula formation in the duodenum, jejunum, and colon (Sheth et al., 1981; O'Brien et al., 1982; Jack et al., 1991; Politei et al., 2016), with severe and potentially fatal consequences (Hilz et al., 2018). It has been hypothesized that the formation of diverticula may be caused by long periods of dysmotility, which may induce high intraluminal pressure areas with protrusion of intestinal mucosa. Moreover, hypoflux in small intestinal vessels secondary to luminal stenosis may contribute to the weakening of these smooth muscle fibers exposed to irregular contractions (Kusama et al., 1993). It is reasonable to think that the 12-month-old α-Gal A (-/0) mice do not display this particular pathological situation that, since Gb3 accumulation is progressive, maybe could be only found in older mice. However, it is important to take in consideration that we analyzed only 5 mice per group and thus these data are to be considered as preliminary. Indeed, further studies will be performed on 8- to 10-week-old, 16- to 20-week-old and 12-month-old mice, considering a higher number of animals per group (n = 10). Moreover, as previously described by Laird and colleagues (2001), in order to evaluate the involvement of different pain-related ion channels (for instance TRPV1) in the visceral hyperalgesia shown by α-Gal A (-/0) mice, we would like to study the behavioral responses of animals to chemical stimulation of the colon (for instance by using capsaicin).

Given the histomorphological and functional abnormalities we detected in α-Gal A (-/0) mice colon, we thought to assess the presence of alterations in the expression of pain-related ion channels. A broad range of ion channels and receptors are involved in visceral pain perception, such as ATP ion-gated channels, voltage-gated sodium (Na_v) and calcium (Ca_v) channels, protease-activated receptors (PAR2), TRPs, as well as serotonin, cannabinoids and cholecystokinin receptors (Arcela de

Carvalho Rocha et al., 2014; Beyder and Farrugia, 2016; Fuentes and Christianson, 2016; Erickson et al., 2018). TRPs are among the most characterized (Blackshaw et al., 2010; Boesmans et al., 2011; Holzer, 2011; Balemans et al., 2017; Beckers et al., 2017). For this purpose, we optimized the IF protocols to stain TRPV1, TRPV4, TRPA1 and TRPM8 in 50-µm-thick transverse cryo-sections of α-Gal A (+/0) and (-/0) mice colon. Ion channels expression was assessed only in 12-month-old mice but not in 8- to 10- and 16- to 20-week-old mice, since the aim of the experiment was the optimization of IF protocols. Fabry patients often experience heat intolerance (Germain, 2010) as well as abdominal pain that is worsened by meals containing hot or spicy food (Clarke, 2007), therefore we thought that TRPV1 could be involved in visceral pain perception in FD. Evidence proving TRPV1 involvement in FD neuropathic pain are several. For example, we previously demonstrated that TRPV1 overexpression in epidermal neuronal fibers of forepaws and DRG neurons correlated with heat hyperalgesia in young α-Gal A (-/0) male mice (Lakomá et al., 2014 and 2016). Similarly, it has been demonstrated that an increased neuronal TRPV1 protein immunoreactivity in DRG neurons (Hofmann et al., 2018) correlates with heat hypersensitivity in naïve young α-Gal A (-/0) mice and may turn to heat hyposensitivity with aging (Üçeyleret al., 2016) due to stress-induced degeneration of peripheral afferents. However, it was also shown that challenging the neurons with capsaicin still induced heat hyperalgesia in old mice and that this effect was caused by TRPV1 overexpression in the nerve fibers left and not by its dysfunction (Hofmann et al., 2018). Our staining of colon sections demonstrates that TRPV1 is expressed by nerve fibers in the myenteric plexus ganglia and in the muscularis propria, both in circular and longitudinal muscular layer, of both α-Gal A (+/0) and (-/0) mice (Figure 40). This staining is consistent with studies where TRPV1 immunoreactivity was found in nerve fibers, but not cell bodies, distributed in the myenteric plexus ganglia and both the longitudinal and circular muscular layer (Ward et al., 2003; Matsumoto et al., 2009 and 2011). This distribution is consistent with the expression of TRPV1 by both extrinsic and intrinsic afferent endings (Blackshaw et al., 2010; Holzer, 2011; Balemans et al., 2017). To our knowledge, TRPV4 has never been associated to FD. However, TRPV4 is expressed by the extrinsic sensory fibers innervating the outermost (serosal and mesenteric) layers of intestine and is clearly involved in the response to noxious distension pressures (Brierley et al., 2008; Holzer, 2011; Balemans et al., 2017). Moreover, it has been associated to visceral nociception (Brierley et al., 2008), hyperalgesia (Cenac et al., 2008) and bowel disorders such as IBD (Brierley et al., 2008), UC and CD (Fichna et al., 2012). For these reasons, we decided to assess its expression in the colon of α-Gal A +/0 and -/0 mice. We found TRPV4 immunoreactivity in neuronal cell bodies of both the myenteric and submucosal plexus ganglia of both α-Gal A +/0 and -/0 mice (Figure 41), expression pattern which is line with the literature (Fichna et al., 2015). In the next step, we decided to evaluate the expression of TRPA1 ion

channel that responds to AITC, the pungent compound in mustard oil, horseradish and wasabi, to noxious cold (<17°C) and to mechanical stimuli (Balemans et al., 2017). It is important to mention that, TRPA1 channel is highly expressed by extrinsic primary afferent nerves as well as by intrinsic enteric neurons (Holzer, 2011; Balemans et al., 2017) and it has been associated to VHS (Brierley et al., 2009; Catteruzza et al., 2010). Intriguingly, it was demonstrated to be involved in mechanical hypersensitivity in a rat model of FD (Miller et al., 2018). We found TRPA1 immunoreactivity in neuronal cell bodies of both the myenteric and submucosal plexus ganglia of both α-Gal A +/0 and -/0 mice (Figure 42). This pattern of expression correlates with what found in other studies (Kun et al., 2014). Finally, we decided to assess TRPM8 expression, which is activated by low temperatures and cooling compounds (Balemans et al., 2017). This ion channel is expressed by peripheral sensory neurons of visceral organs (Balemans et al., 2017) and the decrease of its protein level in the epidermis of frontal paws of α-Gal A -/0 mice was found to correlate with a decreased sensibility to cold stimuli in FD male mice (Lakomá et al., 2014). We found TRPM8 immunoreactivity in neuronal cell bodies of both the myenteric and submucosal plexus ganglia of both α-Gal A +/0 and -/0 mice (Figure 43). On the contrary, in the literature, TRPM8 immunoreactivity has been reported in nerve fibers, and not in cell bodies, present in the mucosa, subumucosal and muscle layers (Harrington et al., 2011; Hosoya et al., 2014). Moreover, in other studies, TRPV1, TRPV4 and TRPA1 immunoreactivities were found to be present also in other structures of the colonic mucosa, which resulted negative in our IF analysis. For example, TRPV1 is reported to be expressed also in nerve fibers present in the mucosa and submucosa as well as in endocrine and epithelial cells of colonic mucosa (Ward et al., 2003; Matsumoto et al., 2009 and 2011). TRPV4 was reported to be expressed also by intestinal epithelial cells (Balemans et al., 2017), and similarly, TRPA1 expression was found in epithelial and enterochromaffin cells (Kun et al., 2014; Balemans et al., 2017). We hypothesized that the different mice genetic backgrounds, different antibodies used and the fact the we so far analyzed only one α-Gal A +/0 animal and one α-Gal A -/0 animal with 4 sections per mouse, could explain these discrepancies in terms of staining patterns. We will carry out further studies to both evaluate TRPV1, TRPV4, TRPA1 and TRPM8 pattern of expression and assess the presence of differences between α-Gal A +/0 and α-Gal A -/0 mice in terms of molecular and functional expression, at all the three ages studied (8- to 10-week-old, 16- to 20-week-old and 12-month-old mice), in a higher number of animals and section per sample. Moreover, we are also interested in studying the Na_V 1.7, Na_V 1.8 and Na_V 1.9 channels, since this family of ion channels is essential in sensory neurons for the initial transduction of sensory stimuli (included pain), the electrogenesis of the action potential and neurotransmitter release from sensory neuron terminals (Bennett et al., 2019). Indeed, several members of this family are involved in many functional GI disorders (Beyder and Farrugia, 2016;

Erickson et al., 2018) and, moreover, their expression and functionality were found to be altered in different murine models of FD (Lakomá et al., 2014; Namer et al., 2017; Hofmann et al., 2018).

Finally, we thought that the electrophysiological characterization of enteric neurons and glia could have been useful to gain further insight into visceral pain perception mechanisms in α-Gal A (-/0) mice. For this purpose, we optimized the protocols for obtaining three different types of primary culture from mouse intestine. We developed the procedures on the basis of a protocols previously developed in the rat (Chevalier et al., 2008; Le berre-scoul et al., 2017) and in the mouse (Soret et al., 2013) in the Dr. Neunlist's laboratory, where I carried out my period abroad for the PhD program. The first type of primary culture we developed is a mixed culture derived from E14 embryos intestines containing both enteric neurons and glia and thus called "ENS primary culture". As reported by different groups, by DIV4, the dissociated cells form a monolayer of myofibroblasts, in which ganglion-like structures become visible at the phase contrast microscope (Chevalier et al., 2008; Gomes et al., 2009). In the following days, the cultures grow and develop properly, giving rise to the characteristic "ganglia" containing both neuronal and glial cells, which interconnect by means of interganglionic fiber strands (Chevalier et al., 2008; Gomes et al., 2009) (Figure 45). This type of culture has been demonstrated to be a useful and powerful tool to characterize enteric neurons and glia and study their development and molecular communication mechanisms. For example, cultures can be characterized for different markers in order to assess the morphology of cells (e.g. Hu, Tuj1, PGP9.5, microtubule-associated protein 2 (MAP2), GFAP, Sox10, S100β, αSMA), the chemical coding of neurons (e.g. choline acetyltransferase (ChAT), NOS, VIP) and the formation of synaptic contacts (Synapthophysin) (Chevalier et al., 2008; Gomes et al., 2009). Moreover, cell cultures can be treated with drugs or supplements and, in turn, analyzed at cellular/molecular and functional level (Gomes et al., 2009; Chevalier et al., 2008). The second type of primary culture we developed is a co-culture system with rat embryonic EGCs which allow to obtain an enriched culture of enteric neurons. In this protocol, the two cell types are first prepared separately, and are combined only once the neurons have attached to the coverslips. Operating with this procedure, the neurons and the glia grow in close proximity but remain separated by a narrow gap provided by the paraffin dots stuck on the glass coverslip (Le berre-scoul et al., 2017). In the cultures we obtained from mouse E14 embryos, neuronal mesh grows and develops properly, giving rise to the characteristic ganglion-like structures that contain only neurons and that interconnect by means of interganglionic fiber strands (Figure 49 and 50). Although it does not allow the totally abolishment of myofibroblasts growth as poly-L-lysine does in rat cultures (Le berre-scoul et al., 2017), we found that the mixture 1:1 of poly-L-lysine and Type I collagen is the best tested option in terms of coating of coverslips, allowing neuronal cells to develop without detaching from coverslips (Figure 49). The best advantage of this type of culture is

that it allows to have enteric neurons separated from glia and, therefore, it can be used to study the roles exerted by EGCs on neurons, such as the formation of the axonal arborization and of synaptic connections between enteric neurons (Le berre-scoul et al., 2017). Moreover, it could be used to functionally characterize enteric neurons by patch clamp technique and to collect them in order to analyze them by quantitative PCR and western blot. The last primary culture we obtained is an enriched culture of EGCs from adult mouse intestine. We found that a mix 1:1 of "organotypic" and "glial" medium was the best plating condition for ganglia adhesion and glial cell growth. This plating condition was tested twice (n = 2) and we could assess glial cell growth and expansion (p0) (*not shown*). Usually, a low percentage of myofibroblasts is also present in the culture, therefore staining with glial and muscular markers is usually done from p1 on, in order to allow cell culture to expand before characterization (Soret et al., 2013). Unfortunately, we were not able to stain EGCs and characterize them because when cells were passed from the 24-well plate (p0) to the 6-well plate (p1), they died (n = 2). We hypothesized this could be due to the fact that cell density was too low in the 6-well plate to allow cells to survive and expand, and that passing the cells in a 12-well plate at p1 could be a better option. This type of culture can be used to morphologically, molecularly and functionally characterize the mouse EGCs (Soret et al., 2013).

Overall in this work, we observed histomorhological and molecular alterations that are likely to be part of the pathophysiological causes at the basis of gut motor dysfunctions experienced by FD patients (Masotti et al., 2019). Taken together with the functional analysis of visceral sensitivity, the results demonstrate that the α-Gal A (−/0) male mouse represents a reliable model for translational studies on visceral pain and GI symptoms in FD. Moreover, we have provided the optimization of useful protocols for the molecular and functional analysis of α-Gal A (−/0) mice ENS cells. Therefore, together with further studies, this work could help identify new therapeutic targets for the treatment of visceral pain in FD.

6 REFERENCES

Abdo H, Derkinderen P, Gomes P, Chevalier J, Aubert P, Masson D, et al. Enteric glial cells protect neurons from oxidative stress in part via reduced glutathione. FASEB J. 2010 Apr;24(4):1082–94.

Abe A, Gregory S, Lee L, Killen PD, Brady RO, Kulkarni A, et al. Reduction of globotriaosylceramide in Fabry disease mice by substrate deprivation. J Clin Invest. 2000 Jun;105(11):1563–71.

Adam B, Liebregts T, Best J, Bechmann L, Lackner C, Neumann J, et al. A combination of peppermint oil and caraway oil attenuates the post-inflammatory visceral hyperalgesia in a rat model. Scand J Gastroenterol. 2006 Feb;41(2):155–60.

Adlercreutz D, Weadge JT, Petersen BO, Duus JØ, Dovichi NJ, Palcic MM. Enzymatic synthesis of Gb3 and iGb3 ceramides. Carbohydr Res. 2010 Jul 2;345(10):1384–8.

Akbar A, Yiangou Y, Facer P, Brydon WG, Walters JRF, Anand P, et al. Expression of the TRPV1 receptor differs in quiescent inflammatory bowel disease with or without abdominal pain. Gut. 2010 Jun;59(6):767–74.

Akbar A, Yiangou Y, Facer P, Walters JRF, Anand P, Ghosh S. Increased capsaicin receptor TRPV1-expressing sensory fibres in irritable bowel syndrome and their correlation with abdominal pain. Gut. 2008 Jul;57(7):923–9.

Al-Chaer ED, Feng Y, Willis WD. A role for the dorsal column in nociceptive visceral input into the thalamus of primates. J Neurophysiol. 1998 Jun;79(6):3143–50.

Al-Chaer ED, Kawasaki M, Pasricha PJ. A new model of chronic visceral hypersensitivity in adult rats induced by colon irritation during postnatal development. Gastroenterology. 2000 Nov;119(5):1276–85.

Ali N, Gillespie S, Laney D. Treatment of Depression in Adults with Fabry Disease. JIMD Rep. 2018;38:13–21.

Amadesi S, Nie J, Vergnolle N, Cottrell GS, Grady EF, Trevisani M, et al. Protease-activated receptor 2 sensitizes the capsaicin receptor transient receptor potential vanilloid receptor 1 to induce hyperalgesia. J Neurosci. 2004 May 5;24(18):4300–12.

Anders H-J, Banas B, Schlöndorff D. Signaling danger: toll-like receptors and their potential roles in kidney disease. J Am Soc Nephrol. 2004 Apr;15(4):854–67.

Anderson W. A Case of "Angeio-Keratoma."*. British Journal of Dermatology. 1898;10(4):113–7.

Andersson DA, Gentry C, Moss S, Bevan S. Transient receptor potential A1 is a sensory receptor for multiple products of oxidative stress. J Neurosci. 2008 Mar 5;28(10):2485–94.

Animal and the Partner, Knock-out mouse [internet]. [cited 2019 Oct 13]. Available from: https://animals-partner.blogspot.com/2015/05/knockout-mouse-knockout-animals.html.

Anitha M, Gondha C, Sutliff R, Parsadanian A, Mwangi S, Sitaraman SV, et al. GDNF rescues hyperglycemia-induced diabetic enteric neuropathy through activation of the PI3K/Akt pathway. J Clin Invest. 2006 Feb;116(2):344–56.

Argoff CE, Barton NW, Brady RO, Ziessman HA. Gastrointestinal symptoms and delayed gastric emptying in Fabry's disease: response to metoclopramide. Nucl Med Commun. 1998 Sep;19(9):887–91.

Askari H, Kaneski CR, Semino-Mora C, Desai P, Ang A, Kleiner DE, et al. Cellular and tissue localization of globotriaosylceramide in Fabry disease. Virchows Arch. 2007 Oct;451(4):823–34.

Aubé A-C, Cabarrocas J, Bauer J, Philippe D, Aubert P, Doulay F, et al. Changes in enteric neurone phenotype and intestinal functions in a transgenic mouse model of enteric glia disruption. Gut. 2006 May;55(5):630–7.

Auerbach L (1862a) Ueber einen Plexus gangliosus myogastricus. Jahres-Bericht. Abh. Schlesischen. Gesells. Vaterland. Cult. 39: 103‑104.

Auerbach L (1862b) Ueber einen Plexus myentericus, einen bisher unbekannten ganglio-nervosen Apparat im Darmkanal der Wirbelthiere. Verlag von E. Morgenstern, Breslau.

Auray-Blais C, Cyr D, Ntwari A, West ML, Cox-Brinkman J, Bichet DG, et al. Urinary globotriaosylceramide excretion correlates with the genotype in children and adults with Fabry disease. Mol Genet Metab. 2008 Mar;93(3):331–40.

Balemans D, Boeckxstaens GE, Talavera K, Wouters MM. Transient receptor potential ion channel function in sensory transduction and cellular signaling cascades underlying visceral hypersensitivity. Am J Physiol Gastrointest Liver Physiol. 2017 Jun 1;312(6):G635–48.

Bandell M, Macpherson LJ, Patapoutian A. From chills to chilis: mechanisms for thermosensation and chemesthesis via thermoTRPs. Curr Opin Neurobiol. 2007 Aug;17(4):490–7.

Bandell M, Story GM, Hwang SW, Viswanath V, Eid SR, Petrus MJ, et al. Noxious cold ion channel TRPA1 is activated by pungent compounds and bradykinin. Neuron. 2004 Mar 25;41(6):849–57.

Banerjee B, Medda BK, Lazarova Z, Bansal N, Shaker R, Sengupta JN. Effect of reflux-induced inflammation on transient receptor potential vanilloid one (TRPV1) expression in primary sensory neurons innervating the oesophagus of rats. Neurogastroenterol Motil. 2007 Aug;19(8):681–91.

Bangari DS, Ashe KM, Desnick RJ, Maloney C, Lydon J, Piepenhagen P, et al. α-Galactosidase A knockout mice: progressive organ pathology resembles the type 2 later-onset phenotype of Fabry disease. Am J Pathol. 2015 Mar;185(3):651–65.

Banks MR, Farthing MJG, Robberecht P, Burleigh DE. Antisecretory actions of a novel vasoactive intestinal polypeptide (VIP) antagonist in human and rat small intestine. Br J Pharmacol. 2005 Apr;144(7):994–1001.

Basbaum AI, Bautista DM, Scherrer G, Julius D. Cellular and molecular mechanisms of pain. Cell. 2009 Oct 16;139(2):267–84.

Bautista DM, Movahed P, Hinman A, Axelsson HE, Sterner O, Högestätt ED, et al. Pungent products from garlic activate the sensory ion channel TRPA1. Proc Natl Acad Sci USA. 2005 Aug 23;102(34):12248–52.

Bayliss WM, Starling EH. The movements and innervation of the small intestine. J Physiol. 1899 May 11;24(2):99–143.

Beckers AB, Weerts ZZRM, Helyes Z, Masclee AAM, Keszthelyi D. Review article: transient receptor potential channels as possible therapeutic targets in irritable bowel syndrome. Aliment Pharmacol Ther. 2017 Nov;46(10):938-952.

Bekri S. Importance of glycosylation in enzyme replacement therapy. In: Mehta A, Beck M, Sunder-Plassmann G, editors. Fabry Disease: Perspectives from 5 Years of FOS [Internet]. Oxford: Oxford PharmaGenesis; 2006 [cited 2019 Oct 15]. Available from: http://www.ncbi.nlm.nih.gov/books/NBK11598/

Benjamin ER, Flanagan JJ, Schilling A, Chang HH, Agarwal L, Katz E, et al. The pharmacological chaperone 1-deoxygalactonojirimycin increases alpha-galactosidase A levels in Fabry patient cell lines. J Inherit Metab Dis. 2009 Jun;32(3):424–40.

Bennett DL, Clark AJ, Huang J, Waxman SG, Dib-Hajj SD. The Role of Voltage-Gated Sodium Channels in Pain Signaling. Physiol Rev. 2019 Jan 99: 1079–1151.

Berthoud HR, Lynn PA, Blackshaw LA. Vagal and spinal mechanosensors in the rat stomach and colon have multiple receptive fields. Am J Physiol Regul Integr Comp Physiol. 2001 May;280(5):R1371-1381.

Berthoud HR, Powley TL. Vagal afferent innervation of the rat fundic stomach: morphological characterization of the gastric tension receptor. J Comp Neurol. 1992 May 8;319(2):261–76.

Bertrand PP, Kunze WA, Bornstein JC, Furness JB, Smith ML. Analysis of the responses of myenteric neurons in the small intestine to chemical stimulation of the mucosa. Am J Physiol. 1997 Aug;273(2 Pt 1):G422-435.

Beyder A and Farrugia G. Ion channelopathies in functional GI disorders. Am J Physiol Gastrointest Liver Physiol. 2016 Oct 1;311(4):G581-G586.

Biancini GB, Vanzin CS, Rodrigues DB, Deon M, Ribas GS, Barschak AG, et al. Globotriaosylceramide is correlated with oxidative stress and inflammation in Fabry patients treated with enzyme replacement therapy. Biochim Biophys Acta. 2012 Feb;1822(2):226–32.

Biegstraaten M, Hollak CEM, Bakkers M, Faber CG, Aerts JMFG, van Schaik IN. Small fiber neuropathy in Fabry disease. Mol Genet Metab. 2012 Jun;106(2):135–41.

Bielefeldt K, Christianson JA, Davis BM. Basic and clinical aspects of visceral sensation: transmission in the CNS. Neurogastroenterol Motil. 2005 Aug;17(4):488–99.

Billroth T (1858) Einige Beobachtungen uber das ausgedehnte Vorkommen von Nervenanastomosen im Tractus Intestinalis. Arch. Anat. Physiol. Leipzig 148‑158.

Bishop DF, Desnick RJ. Affinity purification of alpha-galactosidase A from human spleen, placenta, and plasma with elimination of pyrogen contamination. Properties of the purified splenic enzyme compared to other forms. J Biol Chem. 1981 Feb 10;256(3):1307–16.

Bishop DF, Kornreich R, Desnick RJ. Structural organization of the human alpha-galactosidase A gene: further evidence for the absence of a 3’ untranslated region. Proc Natl Acad Sci U S A. 1988 Jun;85(11):3903–7.

Blackshaw LA, Brierley SM, Hughes PA. TRP channels: new targets for visceral pain. Gut. 2010 Jan;59(1):126–35.

Blackshaw LA, Brookes SJH, Grundy D, Schemann M. Sensory transmission in the gastrointestinal tract. Neurogastroenterol Motil. 2007 Jan;19(1 Suppl):1–19.

Boesmans W, Lasrado R, Vanden Berghe P, Pachnis V. Heterogeneity and phenotypic plasticity of glial cells in the mammalian enteric nervous system. Glia. 2015 Feb;63(2):229–41.

Boesmans W, Owsianik G, Tack J, Voets T, Vanden Berghe P. TRP channels in neurogastroenterology: opportunities for therapeutic intervention. Br J Pharmacol. 2011 Jan;162(1):18-37.

Bokhari SRA, Zulfiqar H, Hariz A. Fabry Disease. In: StatPearls [Internet]. Treasure Island (FL): StatPearls Publishing; 2019 [cited 2019 Oct 15]. Available from: http://www.ncbi.nlm.nih.gov/books/NBK435996/

Bolsover FE, Murphy E, Cipolotti L, Werring DJ, Lachmann RH. Cognitive dysfunction and depression in Fabry disease: a systematic review. J Inherit Metab Dis. 2014 Mar;37(2):177–87.

Boutouyrie P, Laurent S, Laloux B, Lidove O, Grunfeld JP, Germain DP. Arterial remodelling in Fabry disease. Acta Paediatr Suppl. 2002;91(439):62–6.

Brady RO, Gal AE, Bradley RM, Martensson E, Warshaw AL, Laster L. Enzymatic Defect in Fabry's Disease. New England Journal of Medicine. 1967 May 25;276(21):1163–7.

Brierley SM, Carter R, Jones W, Xu L, Robinson DR, Hicks GA, et al. Differential chemosensory function and receptor expression of splanchnic and pelvic colonic afferents in mice. J Physiol (Lond). 2005 Aug 15;567(Pt 1):267–81.

Brierley SM, Hughes PA, Page AJ, Kwan KY, Martin CM, O'Donnell TA, et al. The ion channel TRPA1 is required for normal mechanosensation and is modulated by algesic stimuli. Gastroenterology. 2009 Dec;137(6):2084-2095.e3.

Brierley SM, Jones RCW, Gebhart GF, Blackshaw LA. Splanchnic and pelvic mechanosensory afferents signal different qualities of colonic stimuli in mice. Gastroenterology. 2004 Jul;127(1):166–78.

Brierley SM, Page AJ, Hughes PA, Adam B, Liebregts T, Cooper NJ, et al. Selective role for TRPV4 ion channels in visceral sensory pathways. Gastroenterology. 2008 Jun;134(7):2059–69.

Brogden G, Shammas H, Maalouf K, Naim SL, Wetzel G, Amiri M, et al. Case study on the pathophysiology of Fabry disease: abnormalities of cellular membranes can be reversed by substrate reduction in vitro. Biosci Rep. 2017 30;37(2).

Brookes SJ, Dinning PG, Gladman MA. Neuroanatomy and physiology of colorectal function and defaecation: from basic science to human clinical studies. Neurogastroenterol Motil. 2009 Dec;21 Suppl 2:9–19.

Brookes SJH, Spencer NJ, Costa M, Zagorodnyuk VP. Extrinsic primary afferent signalling in the gut. Nat Rev Gastroenterol Hepatol. 2013 May;10(5):286–96.

Brun P, Giron MC, Qesari M, Porzionato A, Caputi V, Zoppellaro C, et al. Toll-like receptor 2 regulates intestinal inflammation by controlling integrity of the enteric nervous system. Gastroenterology. 2013 Dec;145(6):1323–33.

Bruni S, Loschi L, Incerti C, Gabrielli O, Coppa GV. Update on treatment of lysosomal storage diseases. Acta Myol. 2007 Jul;26(1):87–92.

Bryan A, Knauft RF, Burns WA. Small bowel perforation in Fabry's disease. Ann Intern Med. 1977 Mar;86(3):315–6.

Buda P, Książyk J, Tylki-Szymanska A. Gastroenterological complications of Anderson-Fabry disease. Curr Pharm Des. 2013;19(33):6009–13.

Bueno L, Fioramonti J, Delvaux M, Frexinos J. Mediators and pharmacology of visceral sensitivity: from basic to clinical investigations. Gastroenterology. 1997 May;112(5):1714–43.

Buhner S, Li Q, Vignali S, Barbara G, De Giorgio R, Stanghellini V, et al. Activation of human enteric neurons by supernatants of colonic biopsy specimens from patients with irritable bowel syndrome. Gastroenterology. 2009 Oct;137(4):1425–34.

Burlina AP, Sims KB, Politei JM, Bennett GJ, Baron R, Sommer C, et al. Early diagnosis of peripheral nervous system involvement in Fabry disease and treatment of neuropathic pain: the report of an expert panel. BMC Neurol. 2011 May 27;11:61.

Burlina A, Politei J. The Central Nervous System Involvement in Fabry Disease: A Review. Journal of Inborn Errors of Metabolism & Screening 2016, Volume 4: 1–7.

Bush TG, Savidge TC, Freeman TC, Cox HJ, Campbell EA, Mucke L, et al. Fulminant jejuno-ileitis following ablation of enteric glia in adult transgenic mice. Cell. 1998 Apr 17;93(2):189–201.

Cable WJ, Kolodny EH, Adams RD. Fabry disease: impaired autonomic function. Neurology. 1982 May;32(5):498–502.

Cappello G, Spezzaferro M, Grossi L, Manzoli L, Marzio L. Peppermint oil (Mintoil) in the treatment of irritable bowel syndrome: a prospective double blind placebo-controlled randomized trial. Dig Liver Dis. 2007 Jun;39(6):530–6.

Cardone M. Prospects for gene therapy in inherited neurodegenerative diseases. Curr Opin Neurol. 2007 Apr;20(2):151–8.

Caterina MJ, Schumacher MA, Tominaga M, Rosen TA, Levine JD, Julius D. The capsaicin receptor: a heat-activated ion channel in the pain pathway. Nature. 1997 Oct 23;389(6653):816–24.

Cattaruzza F, Spreadbury I, Miranda-Morales M, Grady EF, Vanner S, Bunnett NW. Transient receptor potential ankyrin-1 has a major role in mediating visceral pain in mice. Am J Physiol Gastrointest Liver Physiol. 2010 Jan;298(1):G81-91.

Cavaliere F, Amadio S, Dinkel K, Reymann KG, Volonté C. P2 receptor antagonist trinitrophenyl-adenosine-triphosphate protects hippocampus from oxygen and glucose deprivation cell death. J Pharmacol Exp Ther. 2007 Oct;323(1):70–7.

Cenac N, Altier C, Chapman K, Liedtke W, Zamponi G, Vergnolle N. Transient receptor potential vanilloid-4 has a major role in visceral hypersensitivity symptoms. Gastroenterology. 2008 Sep;135(3):937–46, 946.e1-2.

Cenac N, Andrews CN, Holzhausen M, Chapman K, Cottrell G, Andrade-Gordon P, et al. Role for protease activity in visceral pain in irritable bowel syndrome. J Clin Invest. 2007 Mar;117(3):636–

47.

Cenac N, Bautzova T, Le Faouder P, Veldhuis NA, Poole DP, Rolland C, et al. Quantification and Potential Functions of Endogenous Agonists of Transient Receptor Potential Channels in Patients With Irritable Bowel Syndrome. Gastroenterology. 2015 Aug;149(2):433-444.e7.

Cervero F, Laird JM. Visceral pain. Lancet. 1999 Jun 19;353(9170):2145–8.

Cervero F. Sensory innervation of the viscera: peripheral basis of visceral pain. Physiol Rev. 1994 Jan;74(1):95–138.

Cevese A, Mary DA, Poltronieri R, Schena F, Vacca G. Haemodynamic effects of distension of the descending colon in anaesthetized dogs. J Physiol (Lond). 1992 Feb;447:409–23.

Chan CLH, Facer P, Davis JB, Smith GD, Egerton J, Bountra C, et al. Sensory fibres expressing capsaicin receptor TRPV1 in patients with rectal hypersensitivity and faecal urgency. Lancet. 2003 Feb 1;361(9355):385–91.

Charrow J. A 14-year-old boy with pain in hands and feet. Pediatr Ann. 2009 Apr;38(4):190, 192.

Chen Y, Lin C, Tang Y, Chen A-Q, Liu C-Y, Lu D-L. ZD 7288, an HCN channel blocker, attenuates chronic visceral pain in irritable bowel syndrome-like rats. World J Gastroenterol. 2014 Feb 28;20(8):2091–7.

Chevalier J, Derkinderen P, Gomes P, Thinard R, Naveilhan P, Vanden Berghe P, et al. Activity-dependent regulation of tyrosine hydroxylase expression in the enteric nervous system. J Physiol. 2008 Apr 1;586(Pt 7):1963–75.

Chitkara DK, Rawat DJ, Talley NJ. The epidemiology of childhood recurrent abdominal pain in Western countries: a systematic review. Am J Gastroenterol. 2005 Aug;100(8):1868–75.

Choi L, Vernon J, Kopach O, Minett MS, Mills K, Clayton PT, et al. The Fabry disease-associated lipid Lyso-Gb3 enhances voltage-gated calcium currents in sensory neurons and causes pain. Neurosci Lett. 2015 May 6;594:163–8.

Christianson JA, Bielefeldt K, Malin SA, Davis BM. Neonatal colon insult alters growth factor expression and TRPA1 responses in adult mice. Pain. 2010 Nov;151(2):540–9.

Christianson JA, Gebhart GF. Assessment of colon sensitivity by luminal distension in mice. Nat Protoc. 2007;2(10):2624–31.

Christianson JA, McIlwrath SL, Koerber HR, Davis BM. Transient receptor potential vanilloid 1-immunopositive neurons in the mouse are more prevalent within colon afferents compared to skin and muscle afferents. Neuroscience. 2006 Jun 19;140(1):247–57.

Chuang HH, Prescott ED, Kong H, Shields S, Jordt SE, Basbaum AI, et al. Bradykinin and nerve growth factor release the capsaicin receptor from PtdIns(4,5)P2-mediated inhibition. Nature. 2001 Jun 21;411(6840):957–62.

Clapham DE, Julius D, Montell C, Schultz G. International Union of Pharmacology. XLIX. Nomenclature and structure-function relationships of transient receptor potential channels. Pharmacol Rev. 2005 Dec;57(4):427–50.

Clarke JTR. Narrative review: Fabry disease. Ann Intern Med. 2007 Mar 20;146(6):425–33.

Clevers HC, Bevins CL. Paneth cells: maestros of the small intestinal crypts. Annu Rev Physiol. 2013;75:289–311.

Coelho-Aguiar J de M, Bon-Frauches AC, Gomes ALT, Veríssimo CP, Aguiar DP, Matias D, et al. The enteric glia: identity and functions. Glia. 2015 Jun;63(6):921–35.

Cole AL, Lee PJ, Hughes DA, Deegan PB, Waldek S, Lachmann RH. Depression in adults with Fabry disease: a common and under-diagnosed problem. J Inherit Metab Dis. 2007 Nov;30(6):943–51.

Colloca L, Ludman T, Bouhassira D, Baron R, Dickenson AH, Yarnitsky D, Freeman R, Truini A, Attal N, Finnerup NB, Eccleston C, Kalso E, Bennett DL, Dworkin RH, Raja SN. Neuropathic pain. Nat Rev Dis Primers. 2017 Feb 16;3:17002.

Cooke HJ, Reddix RA (1994) Neural regulation of intestinal electrolyte transport. In: Johnson LR (ed) Physiology of the gastrointestinal tract, 3rd edn. Raven Press, New York, pp 2083–2132.

Cooke HJ, Shonnard K, Wood JD. Effects of neuronal stimulation on mucosal transport in guinea pig ileum. Am J Physiol. 1983 Aug;245(2):G290-296.

Cornet A, Savidge TC, Cabarrocas J, Deng WL, Colombel JF, Lassmann H, et al. Enterocolitis induced by autoimmune targeting of enteric glial cells: a possible mechanism in Crohn's disease? Proc Natl Acad Sci USA. 2001 Nov 6;98(23):13306–11.

Coutinho SV, Plotsky PM, Sablad M, Miller JC, Zhou H, Bayati AI, et al. Neonatal maternal separation alters stress-induced responses to viscerosomatic nociceptive stimuli in rat. Am J Physiol Gastrointest Liver Physiol. 2002 Feb;282(2):G307-316.

Crawford ME, Jensen FM, Toftdahl DB, Madsen JB. Direct spinal effect of intrathecal and extradural midazolam on visceral noxious stimulation in rabbits. Br J Anaesth. 1993 Jun;70(6):642–6.

Cremonini F, Talley NJ. Irritable bowel syndrome: epidemiology, natural history, health care seeking and emerging risk factors. Gastroenterol Clin North Am. 2005 Jun;34(2):189–204.

D'Aldebert E, Cenac N, Rousset P, Martin L, Rolland C, Chapman K, Selves J, Alric L, Vinel JP, Vergnolle N. Transient receptor potential vanilloid 4 activated inflammatory signals by intestinal epithelial cells and colitis in mice. Gastroenterology. 2011 Jan;140(1):275-85.

D'Angelo G, Capasso S, Sticco L, Russo D. Glycosphingolipids: synthesis and functions. FEBS J. 2013 Dec;280(24):6338–53.

de Carvalho Rocha HA, Dantas BP, Rolim TL, Costa BA, de Medeiros AC. Main ion channels and receptors associated with visceral hypersensitivity in irritable bowel syndrome. Ann Gastroenterol. 2014;27(3):200-206.

De Francesco PN, Mucci JM, Ceci R, Fossati CA, Rozenfeld PA. Fabry disease peripheral blood immune cells release inflammatory cytokines: role of globotriaosylceramide. Mol Genet Metab. 2013 May;109(1):93–9.

De Giorgio R, Barbara G, Furness JB, Tonini M. Novel therapeutic targets for enteric nervous system disorders. Trends Pharmacol Sci. 2007 Sep;28(9):473–81.

Deegan PB, Baehner AF, Barba Romero M-A, Hughes DA, Kampmann C, Beck M, et al. Natural history of Fabry disease in females in the Fabry Outcome Survey. J Med Genet. 2006 Apr;43(4):347–52.

Delobel A, Roy S, Touboul D, Gaudin K, Germain DP, Baillet A, et al. Atmospheric pressure photoionization coupled to porous graphitic carbon liquid chromatography for the analysis of globotriaosylceramides. Application to Fabry disease. J Mass Spectrom. 2006 Jan;41(1):50–8.

Deniz K, Yurci A, Yağbasan A, Tekelioğlu F, Gürsoy S, Güven K. Colonic involvement in Fabry disease. Int J Surg Pathol. 2011 Dec;19(6):777–8.

Desnick RJ, Allen KY, Desnick SJ, Raman MK, Bernlohr RW, Krivit W. Fabry's disease: enzymatic diagnosis of hemizygotes and heterozygotes. Alpha-galactosidase activities in plasma, serum, urine, and leukocytes. J Lab Clin Med. 1973 Feb;81(2):157–71.

Desnick RJ, Brady RO. Fabry disease in childhood. J Pediatr. 2004 May;144(5 Suppl):S20-26.

Desnick RJ, Ioannou Y, Eng CM. a-Galactosidase A deficiency: Fabry disease. The metabolic and molecular bases of inherited disease. 2001 Jan 1;

Desnick RJ, Schuchman EH. Enzyme replacement therapy for lysosomal diseases: lessons from 20 years of experience and remaining challenges. Annu Rev Genomics Hum Genet. 2012;13:307–35.

Desnick RJ, Wasserstein MP, Banikazemi M. Fabry disease (alpha-galactosidase A deficiency): renal involvement and enzyme replacement therapy. Contrib Nephrol. 2001;(136):174–92.

Desnick RJ. Prenatal diagnosis of Fabry disease. Prenat Diagn. 2007 Aug;27(8):693–4.

Devos D, Lebouvier T, Lardeux B, Biraud M, Rouaud T, Pouclet H, et al. Colonic inflammation in Parkinson's disease. Neurobiol Dis. 2013 Feb;50:42–8.

Dhaka A, Viswanath V, Patapoutian A. Trp ion channels and temperature sensation. Annu Rev Neurosci. 2006;29:135–61.

Di Martino MT, Scionti F, Sestito S, Nicoletti A, Arbitrio M, Hiram Guzzi P, et al. Genetic variants associated with gastrointestinal symptoms in Fabry disease. Oncotarget. 2016 Dec 27;7(52):85895–904.

Di Nardo G, Blandizzi C, Volta U, Colucci R, Stanghellini V, Barbara G, et al. Review article: molecular, pathological and therapeutic features of human enteric neuropathies. Aliment Pharmacol Ther. 2008 Jul;28(1):25–42.

Dobrovolny R, Dvorakova L, Ledvinova J, Magage S, Bultas J, Lubanda JC, et al. Relationship between X-inactivation and clinical involvement in Fabry heterozygotes. Eleven novel mutations in the alpha-galactosidase A gene in the Czech and Slovak population. J Mol Med. 2005 Aug;83(8):647–54.

Dobyns WB, Filauro A, Tomson BN, Chan AS, Ho AW, Ting NT, et al. Inheritance of most X-linked traits is not dominant or recessive, just X-linked. Am J Med Genet A. 2004 Aug 30;129A(2):136–43.

Dogiel AS. Über den Bau der Ganglien in den Gefl echten des Darmes und der Gallenblase des Menschen und der Säugetiere. Arch Anat Physiol Leipzig Anat Abt Jg 1899:130–158.

Dolan P. Modeling valuations for EuroQol health states. Med Care. 1997 Nov;35(11):1095–108.

Donadio V, Incensi A, Cortelli P, Giannoccaro MP, Jaber MA, Baruzzi A, et al. Skin sympathetic fiber α-synuclein deposits: a potential biomarker for pure autonomic failure. Neurology. 2013 Feb 19;80(8):725–32.

Donadio V, Incensi A, Giannoccaro MP, Cortelli P, Di Stasi V, Pizza F, et al. Peripheral autonomic neuropathy: diagnostic contribution of skin biopsy. J Neuropathol Exp Neurol. 2012 Nov;71(11):1000–8.

Dong X-P, Wang X, Xu H. TRP channels of intracellular membranes. J Neurochem. 2010 Apr;113(2):313–28.

Dubin AE, Patapoutian A. Nociceptors: the sensors of the pain pathway. J Clin Invest. 2010 Nov;120(11):3760–72.

Durnin L, Sanders KM, Mutafova-Yambolieva VN. Differential release of β-NAD+ and ATP upon activation of enteric motor neurons in primate and murine colons. Neurogastroenterol Motil. 2013 Mar;25(3):e194–204.

Dütsch M, Marthol H, Stemper B, Brys M, Haendl T, Hilz MJ. Small fiber dysfunction predominates in Fabry neuropathy. J Clin Neurophysiol. 2002 Dec;19(6):575–86.

Duve C. Exploring cells with a centrifuge. Science. 1975 Jul 18;189(4198):186–94.

Elleder M, Bradová V, Smíd F, Buděsínský M, Harzer K, Kustermann-Kuhn B, et al. Cardiocyte storage and hypertrophy as a sole manifestation of Fabry's disease. Report on a case simulating hypertrophic non-obstructive cardiomyopathy. Virchows Arch A Pathol Anat Histopathol. 1990;417(5):449–55.

Eng CM, Fletcher J, Wilcox WR, Waldek S, Scott CR, Sillence DO, et al. Fabry disease: baseline medical characteristics of a cohort of 1765 males and females in the Fabry Registry. J Inherit Metab Dis. 2007 Apr;30(2):184–92.

Eng CM, Germain DP, Banikazemi M, Warnock DG, Wanner C, Hopkin RJ, et al. Fabry disease: guidelines for the evaluation and management of multi-organ system involvement. Genet Med. 2006 Sep;8(9):539–48.

Erben U, Loddenkemper C, Doerfel K, Spieckermann S, Haller D, Heimesaat MM, et al. A guide to histomorphological evaluation of intestinal inflammation in mouse models. Int J Clin Exp Pathol. 2014;7(8):4557–76.

Erickson A, Deiteren A, Harrington AM, Garcia-Caraballo S, Castro J, Caldwell A, Grundy L, Brierley SM. Voltage-gated sodium channels: (NaV)igating the field to determine their contribution to visceral nociception. J Physiol. 2018 Mar 1;596(5):785-807.

Everaerts W, Gees M, Alpizar YA, Farre R, Leten C, Apetrei A, et al. The capsaicin receptor TRPV1 is a crucial mediator of the noxious effects of mustard oil. Curr Biol. 2011 Feb 22;21(4):316–21.

Fabry disease news, 2019 [Internet]. AVR-RD-01 Phase 2 Trial in Fabry Disease Soon to Open in United States [cited 2019 Oct 16]. Available from: https://fabrydiseasenews.com/2019/05/15/avr-rd-01-phase-2-trial-in-fabry-disease-soon-opening-in-the-us/.

Fabry J. Ein Beitrag zur Kenntniss der Purpura haemorrhagica nodularis (Purpura papulosa haemorrhagica Hebrae). Arch f Dermat. 1898 Dec 1;43(1):187–200.

Fan JQ, Ishii S, Asano N, Suzuki Y. Accelerated transport and maturation of lysosomal alpha-galactosidase A in Fabry lymphoblasts by an enzyme inhibitor. Nat Med. 1999 Jan;5(1):112–5.

Feriozzi S, Schwarting A, Sunder-Plassmann G, West M, Cybulla M, International Fabry Outcome Survey Investigators. Agalsidase alfa slows the decline in renal function in patients with Fabry disease. Am J Nephrol. 2009;29(5):353–61.

Ferrandiz-Huertas C, Mathivanan S, Wolf CJ, Devesa I, Ferrer-Montiel A. Trafficking of ThermoTRP Channels. Membranes (Basel). 2014 Aug 19;4(3):525–64.

Ferri GL, Probert L, Cocchia D, Michetti F, Marangos PJ, Polak JM. Evidence for the presence of S-100 protein in the glial component of the human enteric nervous system. Nature. 1982 Jun 3;297(5865):409–10.

Fichna J, Mokrowiecka A, Cygankiewicz AI, Zakrzewski PK, Małecka-Panas E, Janecka A, et al. Transient receptor potential vanilloid 4 blockade protects against experimental colitis in mice: a new strategy for inflammatory bowel diseases treatment? Neurogastroenterol Motil. 2012 Nov;24(11):e557-560.

Fichna J, Poole DP, Veldhuis N, MacEachern SJ, Saur D, Zakrzewski PK, et al. Transient receptor potential vanilloid 4 inhibits mouse colonic motility by activating NO-dependent enteric neurotransmission. J Mol Med. 2015 Dec;93(12):1297–309.

Flynn DM, Lake BD, Boothby CB, Young EP. Gut lesions in Fabry's disease without a rash. Arch Dis Child. 1972 Feb;47(251):26–33.

Foreman RD. Mechanisms of cardiac pain. Annu Rev Physiol. 1999;61:143–67.

Fox EA, Phillips RJ, Martinson FA, Baronowsky EA, Powley TL. Vagal afferent innervation of smooth muscle in the stomach and duodenum of the mouse: morphology and topography. J Comp Neurol. 2000 Dec 18;428(3):558–76.

Franceschi F, Zampetti A, Gigante G, Gasbarrini A. Helicobacter pylori and small intestinal bacterial overgrowth affect gastrointestinal symptoms in Fabry's disease. Dig Liver Dis. 2015 Jul;47(7):618–9.

Frankel AE, Kreitman RJ, Sausville EA. Targeted Toxins. Clin Cancer Res. 2000 Feb 1;6(2):326–34.

Friedman LS, Kirkham SE, Thistlethwaite JR, Platika D, Kolodny EH, Schuffler MD. Jejunal diverticulosis with perforation as a complication of Fabry's disease. Gastroenterology. 1984 Mar;86(3):558–63.

Fu H, Bartz JD, Jr RLS, McCarty DM. Peripheral Nervous System Neuropathology and Progressive Sensory Impairments in a Mouse Model of Mucopolysaccharidosis IIIB. PLOS ONE. 2012 Sep 25;7(9):e45992.

Fuentes IM and Christianson JA. Ion channels, ion channel receptors, and visceral hypersensitivity in irritable bowel syndrome. Neurogastroenterol Motil. 2016 Nov;28(11):1613-1618.

Furness JB, Alex G, Clark MJ, Lal VV (2003a) Morphologies and projections of defined classes of neurons in the submucosa of the guinea-pig small intestine. Anat. Rec. 272A: 475‑483.

Furness JB, Callaghan BP, Rivera LR, Cho H-J. The enteric nervous system and gastrointestinal innervation: integrated local and central control. Adv Exp Med Biol. 2014;817:39–71.

Furness JB, Costa M, Keast JR. Choline acetyltransferase- and peptide immunoreactivity of submucous neurons in the small intestine of the guinea-pig. Cell Tissue Res. 1984;237(2):329–36.

Furness JB, Costa M. The adrenergic innervation of the gastrointestinal tract. Ergeb Physiol. 1974;69(0):2–51.

Furness JB, Jones C, Nurgali K, Clerc N. Intrinsic primary afferent neurons and nerve circuits within the intestine. Prog Neurobiol. 2004 Feb;72(2):143–64.

Furness JB, Kunze WA, Bertrand PP, Clerc N, Bornstein JC. Intrinsic primary afferent neurons of the intestine. Prog Neurobiol. 1998 Jan;54(1):1–18.

Furness JB, Kunze WA, Clerc N. Nutrient tasting and signaling mechanisms in the gut. II. The intestine as a sensory organ: neural, endocrine, and immune responses. Am J Physiol. 1999;277(5):G922-928.

Furness JB, Lloyd KC, Sternini C, Walsh JH. Projections of substance P, vasoactive intestinal peptide and tyrosine hydroxylase immunoreactive nerve fibres in the canine intestine, with special reference to the innervation of the circular muscle. Arch Histol Cytol. 1990 May;53(2):129–40.

Furness JB. The enteric nervous system and neurogastroenterology. Nat Rev Gastroenterol Hepatol. 2012 Mar 6;9(5):286–94.

Furness JB. The Enteric Nervous System. Oxford: Blackwell 2006.

Furness JB. Types of neurons in the enteric nervous system. J Auton Nerv Syst. 2000 Jul 3;81(1–3):87–96.

Gabella G. Fine structure of the myenteric plexus in the guinea-pig ileum. J Anat. 1972 Jan;111(Pt 1):69–97.

Gabella G. Ultrastructure of the nerve plexuses of the mammalian intestine: the enteric glial cells. Neuroscience. 1981;6(3):425–36.

Gadoth N, Sandbank U. Involvement of dorsal root ganglia in Fabry's disease. J Med Genet. 1983 Aug;20(4):309–12.

Gal A, Hughes DA, Winchester B. Toward a consensus in the laboratory diagnostics of Fabry disease - recommendations of a European expert group. J Inherit Metab Dis. 2011 Apr;34(2):509–14.

Gal A. Molecular Genetics of Fabry Disease and Genotype–Phenotype Correlation. In: Elstein D, Altarescu G, Beck M, editors. Fabry Disease [Internet]. Dordrecht: Springer Netherlands; 2010 [cited 2019 Oct 16]. p. 3–19. Available from: https://doi.org/10.1007/978-90-481-9033-1_1.

Gao X, Wu L, O'Neil RG. Temperature-modulated diversity of TRPV4 channel gating: activation by physical stresses and phorbol ester derivatives through protein kinase C-dependent and -independent pathways. J Biol Chem. 2003 Jul 18;278(29):27129–37.

Garman SC, Garboczi DN. The Molecular Defect Leading to Fabry Disease: Structure of Human α-Galactosidase. Journal of Molecular Biology. 2004 Mar 19;337(2):319–35.

Garman SC. Structure-function relationships in alpha-galactosidase A. Acta Paediatr. 2007 Apr;96(455):6–16.

Gautron L, Sakata I, Udit S, Zigman JM, Wood JN, Elmquist JK. Genetic tracing of Nav1.8-expressing vagal afferents in the mouse. J Comp Neurol. 2011 Oct 15;519(15):3085–101.

Gavva NR, Treanor JJS, Garami A, Fang L, Surapaneni S, Akrami A, et al. Pharmacological blockade of the vanilloid receptor TRPV1 elicits marked hyperthermia in humans. Pain. 2008 May;136(1–2):202–10.

Gayathri N, Yasha TC, Kanjalkar M, Agarwal S, Sagar BKC, Santosh V, et al. Fabry's disease: An ultrastructural study of nerve biopsy. Ann Indian Acad Neurol. 2008 Jul;11(3):182–4.

Gebhart GF, Bielefeldt K. Physiology of Visceral Pain. Compr Physiol. 2016 15;6(4):1609–33.

Germain DP, Fan J-Q. Pharmacological chaperone therapy by active-site-specific chaperones in Fabry disease: in vitro and preclinical studies. Int J Clin Pharmacol Ther. 2009;47 Suppl 1:S111-117.

Germain DP, Hughes DA, Nicholls K, Bichet DG, Giugliani R, Wilcox WR, et al. Treatment of Fabry's Disease with the Pharmacologic Chaperone Migalastat. N Engl J Med. 2016 Aug 11;375(6):545–55.

Germain DP, Waldek S, Banikazemi M, Bushinsky DA, Charrow J, Desnick RJ, et al. Sustained, long-term renal stabilization after 54 months of agalsidase beta therapy in patients with Fabry disease. J Am Soc Nephrol. 2007 May;18(5):1547–57.

Germain DP. [Fabry's disease (alpha-galactosidase-A deficiency): physiopathology, clinical signs, and genetic aspects]. J Soc Biol. 2002;196(2):161–73.

Germain DP. Fabry disease. Orphanet J Rare Dis. 2010 Nov 22;5:30.

Ghosh P, Dahms NM, Kornfeld S. Mannose 6-phosphate receptors: new twists in the tale. Nat Rev Mol Cell Biol. 2003 Mar;4(3):202–12.

Giamberardino MA. Recent and forgotten aspects of visceral pain. Eur J Pain. 1999 Jun;3(2):77–92.

Gibbins IL, Furness JB, Costa M, MacIntyre I, Hillyard CJ, Girgis S. Co-localization of calcitonin gene-related peptide-like immunoreactivity with substance P in cutaneous, vascular and visceral sensory neurons of guinea pigs. Neurosci Lett. 1985 Jun 12;57(2):125–30.

Gold MS, Gebhart GF. Nociceptor sensitization in pain pathogenesis. Nat Med. 2010 Nov;16(11):1248–57.

Gomes P, Chevalier J, Boesmans W, Roosen L, van den Abbeel V, Neunlist M, et al. ATP-dependent paracrine communication between enteric neurons and glia in a primary cell culture derived from embryonic mice. Neurogastroenterol Motil. 2009 Aug;21(8):870-e62.

Gonella J, Bouvier M, Blanquet F. Extrinsic nervous control of motility of small and large intestines and related sphincters. Physiol Rev. 1987 Jul;67(3):902–61.

Grant AD, Cottrell GS, Amadesi S, Trevisani M, Nicoletti P, Materazzi S, et al. Protease-activated receptor 2 sensitizes the transient receptor potential vanilloid 4 ion channel to cause mechanical hyperalgesia in mice. J Physiol (Lond). 2007 Feb 1;578(Pt 3):715–33.

Green T, Dockray GJ. Characterization of the peptidergic afferent innervation of the stomach in the rat, mouse and guinea-pig. Neuroscience. 1988 Apr;25(1):181–93.

Gubler MC, Lenoir G, Grünfeld JP, Ulmann A, Droz D, Habib R. Early renal changes in hemizygous and heterozygous patients with Fabry's disease. Kidney Int. 1978 Mar;13(3):223–35.

Gulbransen BD, Sharkey KA. Novel functional roles for enteric glia in the gastrointestinal tract. Nat Rev Gastroenterol Hepatol. 2012 Nov;9(11):625–32.

Güler AD, Lee H, Iida T, Shimizu I, Tominaga M, Caterina M. Heat-evoked activation of the ion channel, TRPV4. J Neurosci. 2002 Aug 1;22(15):6408–14.

Guo A, Vulchanova L, Wang J, Li X, Elde R. Immunocytochemical localization of the vanilloid receptor 1 (VR1): relationship to neuropeptides, the P2X3 purinoceptor and IB4 binding sites. Eur J Neurosci. 1999 Mar;11(3):946–58.

Gupta SN, Ries M, Murray GJ, Quirk JM, Brady RO, Lidicker JR, et al. Skin-impedance in Fabry Disease: a prospective, controlled, non-randomized clinical study. BMC Neurol. 2008 Nov 6;8:41.

Gwynne RM, Bornstein JC. Synaptic transmission at functionally identified synapses in the enteric nervous system: roles for both ionotropic and metabotropic receptors. Curr Neuropharmacol. 2007 Mar;5(1):1–17.

Hakomori S. Structure and function of glycosphingolipids and sphingolipids: recollections and future trends. Biochim Biophys Acta. 2008 Mar;1780(3):325–46.

Hakomori S. Tumor-associated carbohydrate antigens defining tumor malignancy: basis for development of anti-cancer vaccines. Adv Exp Med Biol. 2001;491:369–402.

Happle R. X-chromosome inactivation: role in skin disease expression. Acta Paediatr Suppl. 2006 Apr;95(451):16–23.

Harrington AM, Hughes PA, Martin CM, Yang J, Castro J, Isaacs NJ, et al. A novel role for TRPM8 in visceral afferent function. Pain. 2011 Jul;152(7):1459–68.

Heare T, Alp NJ, Priestman DA, Kulkarni AB, Qasba P, Butters TD, et al. Severe endothelial dysfunction in the aorta of a mouse model of Fabry disease; partial prevention by N-butyldeoxynojirimycin treatment. J Inherit Metab Dis. 2007 Feb;30(1):79–87.

Henle J (1871) Handbuch der systematischen Anatomie des Menschen. Band III., Abt. 2. Nervenlehre. Vieweg und Sohn, Braunschweig.

Hilz MJ, Arbustini E, Dagna L, Gasbarrini A, Goizet C, Lacombe D, et al. Non-specific gastrointestinal features: Could it be Fabry disease? Digestive and Liver Disease. 2018 May 1;50(5):429–37.

Hilz MJ, Stemper B, Kolodny EH. Lower limb cold exposure induces pain and prolonged small fiber dysfunction in Fabry patients. Pain. 2000 Feb;84(2–3):361–5.

Hilz MJ, Brys M, Marthol H, Stemper B, Dütsch M. Enzyme replacement therapy improves function of C-, Adelta-, and Abeta-nerve fibers in Fabry neuropathy. Neurology 2004;62:1066–1072.

Hilz MJ. Evaluation of peripheral and autonomic nerve function in Fabry disease. Acta Paediatr Suppl. 2002;91(439):38–42.

Hoff S, Zeller F, von Weyhern CWH, Wegner M, Schemann M, Michel K, et al. Quantitative assessment of glial cells in the human and guinea pig enteric nervous system with an anti-Sox8/9/10 antibody. J Comp Neurol. 2008 Aug 1;509(4):356–71.

Hoffmann B, Beck M, Sunder-Plassmann G, Borsini W, Ricci R, Mehta A, et al. Nature and prevalence of pain in Fabry disease and its response to enzyme replacement therapy--a retrospective analysis from the Fabry Outcome Survey. Clin J Pain. 2007 Aug;23(6):535–42.

Hoffmann B, Schwarz M, Mehta A, Keshav S, Fabry Outcome Survey European Investigators. Gastrointestinal symptoms in 342 patients with Fabry disease: prevalence and response to enzyme replacement therapy. Clin Gastroenterol Hepatol. 2007 Dec;5(12):1447–53.

Hofmann L, Hose D, Grießhammer A, Blum R, Döring F, Dib-Hajj S, et al. Characterization of small fiber pathology in a mouse model of Fabry disease. Elife. 2018 17;7.

Holst MC, Kelly JB, Powley TL. Vagal preganglionic projections to the enteric nervous system characterized with Phaseolus vulgaris-leucoagglutinin. J Comp Neurol. 1997 Apr 28;381(1):81–100.

Holzer P. Local effector functions of capsaicin-sensitive sensory nerve endings: involvement of tachykinins, calcitonin gene-related peptide and other neuropeptides. Neuroscience. 1988 Mar;24(3):739–68.

Holzer P. Transient receptor potential (TRP) channels as drug targets for diseases of the digestive system. Pharmacol Ther. 2011 Jul;131(1):142–70.

Holzer P. TRPV1 and the gut: from a tasty receptor for a painful vanilloid to a key player in hyperalgesia. Eur J Pharmacol. 2004 Oct 1;500(1–3):231–41.

Hopkin RJ, Bissler J, Banikazemi M, Clarke L, Eng CM, Germain DP, et al. Characterization of Fabry disease in 352 pediatric patients in the Fabry Registry. Pediatr Res. 2008 Nov;64(5):550–5.

Hopkin RJ, Jefferies JL, Laney DA, Lawson VH, Mauer M, Taylor MR, et al. The management and treatment of children with Fabry disease: A United States-based perspective. Mol Genet Metab. 2016 Feb;117(2):104–13.

Hopkins PV, Campbell C, Klug T, Rogers S, Raburn-Miller J, Kiesling J. Lysosomal storage disorder screening implementation: findings from the first six months of full population pilot testing in Missouri. J Pediatr. 2015 Jan;166(1):172–7.

Horie S, Yamamoto H, Michael GJ, Uchida M, Belai A, Watanabe K, et al. Protective role of vanilloid receptor type 1 in HCl-induced gastric mucosal lesions in rats. Scand J Gastroenterol. 2004 Apr;39(4):303–12.

Hosoya T, Matsumoto K, Tashima K, Nakamura H, Fujino H, Murayama T, et al. TRPM8 has a key role in experimental colitis-induced visceral hyperalgesia in mice. Neurogastroenterol Motil. 2014 Aug;26(8):1112–21.

Hozumi I, Nishizawa M, Ariga T, Miyatake T. Biochemical and clinical analysis of accumulated glycolipids in symptomatic heterozygotes of angiokeratoma corporis diffusum (Fabry's disease) in comparison with hemizygotes. J Lipid Res. 1990 Feb;31(2):335–40.

Hughes DA, Elliott PM, Shah J, Zuckerman J, Coghlan G, Brookes J, et al. Effects of enzyme replacement therapy on the cardiomyopathy of Anderson-Fabry disease: a randomised, double-blind, placebo-controlled clinical trial of agalsidase alfa. Heart. 2008 Feb;94(2):153–8.

Hulten L (1969) Reflex control of colonic motility and blood flow. Acta Physiol Scand 335 (Suppl):77–93.

Human Gene Mutation Database (HGMD) at the Institute of Medical Genetics in Cardiff, Public database, GLA gene, 2017 [Internet]. [cited 2019 Oct 15]. Available from: https://www.google.com/search?client=firefox-b-d&q=Human+Gene+Mutation+Database+%28HGMD%29.

Hwang SW, Cho H, Kwak J, Lee SY, Kang CJ, Jung J, et al. Direct activation of capsaicin receptors by products of lipoxygenases: endogenous capsaicin-like substances. Proc Natl Acad Sci USA. 2000 May 23;97(11):6155–60.

Hwu W-L, Chien Y-H, Lee N-C, Chiang S-C, Dobrovolny R, Huang A-C, et al. Newborn screening for Fabry disease in Taiwan reveals a high incidence of the later-onset GLA mutation c.936+919G>A (IVS4+919G>A). Hum Mutat. 2009 Oct;30(10):1397–405.

Hyams JS, Davis P, Sylvester FA, Zeiter DK, Justinich CJ, Lerer T. Dyspepsia in children and adolescents: a prospective study. J Pediatr Gastroenterol Nutr. 2000 Apr;30(4):413–8.

Ichikawa S, Nakajo N, Sakiyama H, Hirabayashi Y. A mouse B16 melanoma mutant deficient in glycolipids. Proc Natl Acad Sci USA. 1994 Mar 29;91(7):2703–7.

ImageJ, NIH, Bethesda, Maryland, USA. Available at: http://rsb.info.nih.gov/ij/.

Ioannou YA, Bishop DF, Desnick RJ. Overexpression of human alpha-galactosidase A results in its intracellular aggregation, crystallization in lysosomes, and selective secretion. J Cell Biol. 1992 Dec;119(5):1137–50.

Ioannou YA, Zeidner KM, Grace ME, Desnick RJ. Human alpha-galactosidase A: glycosylation site 3 is essential for enzyme solubility. Biochem J. 1998 Jun 15;332(Pt 3):789–97.

Ippolito C, Segnani C, De Giorgio R, Blandizzi C, Mattii L, Castagna M, et al. Quantitative evaluation of myenteric ganglion cells in normal human left colon: implications for histopathological analysis. Cell Tissue Res. 2009 May;336(2):191–201.

Ishii S, Chang H-H, Kawasaki K, Yasuda K, Wu H-L, Garman SC, et al. Mutant α-galactosidase A enzymes identified in Fabry disease patients with residual enzyme activity: biochemical characterization and restoration of normal intracellular processing by 1-deoxygalactonojirimycin. Biochem J. 2007 Sep 1;406(Pt 2):285–95.

Jack CI, Morris AI, Nasmyth DG, Carroll N. Colonic involvement in Fabry's disease. Postgrad Med J. 1991 Jun;67(788):584–5.

Jänig W, Koltzenburg M. Receptive properties of sacral primary afferent neurons supplying the colon. J Neurophysiol. 1991 May;65(5):1067–77.

Jardine DL, Fitzpatrick MA, Troughton WD, Tie AB. Small bowel ischaemia in Fabry's disease. J Gastroenterol Hepatol. 1994 Apr;9(2):201–4.

Jessen KR, Mirsky R. Glial cells in the enteric nervous system contain glial fibrillary acidic protein. Nature. 1980 Aug 14;286(5774):736–7.

Ji R-R, Samad TA, Jin S-X, Schmoll R, Woolf CJ. p38 MAPK activation by NGF in primary sensory neurons after inflammation increases TRPV1 levels and maintains heat hyperalgesia. Neuron. 2002 Sep 26;36(1):57–68.

Ji Y, Traub RJ. Differential effects of spinal CNQX on two populations of dorsal horn neurons responding to colorectal distension in the rat. Pain. 2002 Sep;99(1–2):217–22.

Johansson D, Kosovac E, Moharer J, Ljuslinder I, Brännström T, Johansson A, et al. Expression of verotoxin-1 receptor Gb3 in breast cancer tissue and verotoxin-1 signal transduction to apoptosis. BMC Cancer. 2009 Feb 26;9:67.

Jones RCW, Otsuka E, Wagstrom E, Jensen CS, Price MP, Gebhart GF. Short-term sensitization of colon mechanoreceptors is associated with long-term hypersensitivity to colon distention in the mouse. Gastroenterology. 2007 Jul;133(1):184–94.

Jones RCW, Xu L, Gebhart GF. The mechanosensitivity of mouse colon afferent fibers and their sensitization by inflammatory mediators require transient receptor potential vanilloid 1 and acid-sensing ion channel 3. J Neurosci. 2005 Nov 23;25(47):10981–9.

Jordt S-E, Bautista DM, Chuang H-H, McKemy DD, Zygmunt PM, Högestätt ED, et al. Mustard oils and cannabinoids excite sensory nerve fibres through the TRP channel ANKTM1. Nature. 2004 Jan 15;427(6971):260–5.

Joseph NM, He S, Quintana E, Kim Y-G, Núñez G, Morrison SJ. Enteric glia are multipotent in culture but primarily form glia in the adult rodent gut. J Clin Invest. 2011 Sep;121(9):3398–411.

Kadowaki M, Kuramoto H, Takaki M. Combined determination with functional and morphological studies of origin of nerve fibers expressing transient receptor potential vanilloid 1 in the myenteric plexus of the rat jejunum. Auton Neurosci. 2004 Nov 30;116(1–2):11–8.

Kahn P. Anderson-Fabry disease: a histopathological study of three cases with observations on the mechanism of production of pain. J Neurol Neurosurg Psychiatry. 1973 Dec;36(6):1053–62.

Kamp EH, Jones RCW, Tillman SR, Gebhart GF. Quantitative assessment and characterization of visceral nociception and hyperalgesia in mice. Am J Physiol Gastrointest Liver Physiol. 2003 Mar;284(3):G434-444.

Kampmann C, Wiethoff CM, Whybra C, Baehner FA, Mengel E, Beck M. Cardiac manifestations of Anderson-Fabry disease in children and adolescents. Acta Paediatr. 2008 Apr;97(4):463–9.

Kang JJ, Shu L, Park JL, Shayman JA, Bodary PF. Endothelial nitric oxide synthase uncoupling and microvascular dysfunction in the mesentery of mice deficient in α-galactosidase A. Am J Physiol Gastrointest Liver Physiol. 2014 Jan;306(2):G140-146.

Kang JL, Rajpert-De Meyts E, Wiels J, Skakkebaek NE. Expression of the glycolipid globotriaosylceramide (Gb3) in testicular carcinoma in situ. Virchows Arch. 1995;426(4):369–74.

Kang WH, Chun SI, Lee S. Generalized anhidrosis associated with Fabry's disease. J Am Acad Dermatol. 1987 Nov;17(5 Pt 2):883–7.

Karashima Y, Damann N, Prenen J, Talavera K, Segal A, Voets T, et al. Bimodal action of menthol on the transient receptor potential channel TRPA1. J Neurosci. 2007 Sep 12;27(37):9874–84.

Keast JR, Furness JB, Costa M. Investigations of nerve populations influencing ion transport that can be stimulated electrically, by serotonin and by a nicotinic agonist. Naunyn Schmiedebergs Arch Pharmacol. 1985 Nov;331(2–3):260–6.

Keast JR. Mucosal innervation and control of water and ion transport in the intestine. Rev Physiol Biochem Pharmacol. 1987;109:1–59.

Keshav S. Gastrointestinal manifestations of Fabry disease. In: Mehta A, Beck M, Sunder-Plassmann G, editors. Fabry Disease: Perspectives from 5 Years of FOS [Internet]. Oxford: Oxford PharmaGenesis; 2006 [cited 2019 Oct 16]. Available from: http://www.ncbi.nlm.nih.gov/books/NBK11570/

Khanna R, Soska R, Lun Y, Feng J, Frascella M, Young B, et al. The pharmacological chaperone 1-deoxygalactonojirimycin reduces tissue globotriaosylceramide levels in a mouse model of Fabry disease. Mol Ther. 2010 Jan;18(1):23–33.

Kint JA. The Enzyme Defect in Fabry's Disease. Nature. 1970 Sep;227(5263):1173–1173.

Kirchgessner AL, Tamir H, Gershon MD. Identification and stimulation by serotonin of intrinsic sensory neurons of the submucosal plexus of the guinea pig gut: activity-induced expression of Fos immunoreactivity. J Neurosci. 1992 Jan;12(1):235–48.

Kline RM, Kline JJ, Di Palma J null, Barbero GJ. Enteric-coated, pH-dependent peppermint oil capsules for the treatment of irritable bowel syndrome in children. J Pediatr. 2001 Jan;138(1):125–8.

Komuro T, Bałuk P, Burnstock G. An ultrastructural study of neurons and non-neuronal cells in the myenteric plexus of the rabbit colon. Neuroscience. 1982 Jul;7(7):1797–806.

Kono T, Kaneko A, Omiya Y, Ohbuchi K, Ohno N, Yamamoto M. Epithelial transient receptor potential ankyrin 1 (TRPA1)-dependent adrenomedullin upregulates blood flow in rat small intestine. Am J Physiol Gastrointest Liver Physiol. 2013 Feb 15;304(4):G428-436.

Kornreich R, Bishop DF, Desnick RJ. Alpha-galactosidase A gene rearrangements causing Fabry disease. Identification of short direct repeats at breakpoints in an Alu-rich gene. J Biol Chem. 1990 May 6;265(16):9319–26.

Kovbasnjuk O, Mourtazina R, Baibakov B, Wang T, Elowsky C, Choti MA, et al. The glycosphingolipid globotriaosylceramide in the metastatic transformation of colon cancer. Proc Natl Acad Sci USA. 2005 Dec 27;102(52):19087–92.

Kummer KK, Kalpachidou T, Kress M, Langeslag M. Signatures of Altered Gene Expression in Dorsal Root Ganglia of a Fabry Disease Mouse Model. Front Mol Neurosci. 2017;10:449.

Kun J, Szitter I, Kemény A, Perkecz A, Kereskai L, Pohóczky K, et al. Upregulation of the transient receptor potential ankyrin 1 ion channel in the inflamed human and mouse colon and its protective roles. PLoS ONE. 2014;9(9):e108164.

Kunze WA, Furness JB, Bertrand PP, Bornstein JC. Intracellular recording from myenteric neurons of the guinea-pig ileum that respond to stretch. J Physiol (Lond). 1998 Feb 1;506 (Pt 3):827–42.

Kusama M, Kimura K, Koyanagi Y, Tsuchida A, Yoshimatsu A, Ebinara Y. [A case report of atypical Fabry's disease with colon cancer]. Nihon Geka Gakkai Zasshi. 1993 Jul;94(7):755–7.

Kyloh M, Nicholas S, Zagorodnyuk VP, Brookes SJ, Spencer NJ. Identification of the visceral pain pathway activated by noxious colorectal distension in mice. Front Neurosci. 2011;5:16.

Laird JM, Martinez-Caro L, Garcia-Nicas E, Cervero F. A new model of visceral pain and referred hyperalgesia in the mouse. Pain. 2001 Jun;92(3):335-42.

Lakomá J, Rimondini R, Donadio V, Liguori R, Caprini M (2014). Pain Related Channels Are Differentially Expressed in Neuronal and Non-Neuronal Cells of Glabrous Skin of Fabry Knockout Male Mice. PLoS ONE 9(10): e108641.

Lakomá J, Rimondini R, Ferrer Montiel A, Donadio V, Liguori R, Caprini M. Increased expression of Trpv1 in peripheral terminals mediates thermal nociception in Fabry disease mouse model. Mol Pain. 2016;12.

Lapointe TK, Basso L, Iftinca MC, Flynn R, Chapman K, Dietrich G, et al. TRPV1 sensitization mediates postinflammatory visceral pain following acute colitis. Am J Physiol Gastrointest Liver Physiol. 2015 Jul 15;309(2):G87-99.

Laranjeira C, Sandgren K, Kessaris N, Richardson W, Potocnik A, Vanden Berghe P, et al. Glial cells in the mouse enteric nervous system can undergo neurogenesis in response to injury. J Clin Invest. 2011 Sep;121(9):3412–24.

Le Berre-Scoul C, Chevalier J, Oleynikova E, Cossais F, Talon S, Neunlist M, et al. A novel enteric neuron–glia coculture system reveals the role of glia in neuronal development. J Physiol. 2017 Jan 15;595(2):583–98.

Lee K, Jin X, Zhang K, Copertino L, Andrews L, Baker-Malcolm J, et al. A biochemical and pharmacological comparison of enzyme replacement therapies for the glycolipid storage disorder Fabry disease. Glycobiology. 2003 Apr 1;13(4):305–13.

Leica biosystem, CM1850 UV Cryostat [internet]. [cited 2019 Oct 18]. Available from: https://www.leicabiosystems.com/histology-equipment/cryostats/products/leica-cm1850-uv/.

Lemansky P, Bishop DF, Desnick RJ, Hasilik A, von Figura K. Synthesis and processing of alpha-galactosidase A in human fibroblasts. Evidence for different mutations in Fabry disease. J Biol Chem. 1987 Feb 15;262(5):2062–5.

Lewis T. Pain. New York: The Macmillan Press, 1942.

Liedtke W, Choe Y, Martí-Renom MA, Bell AM, Denis CS, Sali A, et al. Vanilloid receptor-related osmotically activated channel (VR-OAC), a candidate vertebrate osmoreceptor. Cell. 2000 Oct 27;103(3):525–35.

Liguori R, Incensi A, de Pasqua S, Mignani R, Fileccia E, Santostefano M, et al. Skin globotriaosylceramide 3 deposits are specific to Fabry disease with classical mutations and associated with small fibre neuropathy. PLoS ONE. 2017;12(7):e0180581.

Liguori R, Di Stasi V, Bugiardini E, et al. Small fiber neuropathy in female patients with Fabry disease. Muscle Nerve 2010;41:409–412.

Lin H-Y, Chong K-W, Hsu J-H, Yu H-C, Shih C-C, Huang C-H, et al. High incidence of the cardiac variant of Fabry disease revealed by newborn screening in the Taiwan Chinese population. Circ Cardiovasc Genet. 2009 Oct;2(5):450–6.

Linthorst GE, Vedder AC, Aerts JMFG, Hollak CEM. Screening for Fabry disease using whole blood spots fails to identify one-third of female carriers. Clin Chim Acta. 2005 Mar;353(1–2):201–3.

Lynn P, Zagorodnyuk V, Hennig G, Costa M, Brookes S. Mechanical activation of rectal intraganglionic laminar endings in the guinea pig distal gut. J Physiol (Lond). 2005 Apr 15;564(Pt 2):589–601.

Lyon MF. Gene action in the X-chromosome of the mouse (Mus musculus L.). Nature. 1961 Apr 22;190:372–3.

MacDermot KD, Holmes A, Miners AH. Anderson-Fabry disease: clinical manifestations and impact of disease in a cohort of 98 hemizygous males. J Med Genet. 2001 Nov;38(11):750–60.

Maggi CA, Meli A. The sensory-efferent function of capsaicin-sensitive sensory neurons. Gen Pharmacol. 1988;19(1):1–43.

Mangeney M, Lingwood CA, Taga S, Caillou B, Tursz T, Wiels J. Apoptosis induced in Burkitt's lymphoma cells via Gb3/CD77, a glycolipid antigen. Cancer Res. 1993 Nov 1;53(21):5314–9.

Mangeney M, Richard Y, Coulaud D, Tursz T, Wiels J. CD77: an antigen of germinal center B cells entering apoptosis. European Journal of Immunology. 1991;21(5):1131–40.

Marchesoni CL, Roa N, Pardal AM, Neumann P, Cáceres G, Martínez P, et al. Misdiagnosis in Fabry disease. J Pediatr. 2010 May;156(5):828–31.

Markham A. Migalastat: First Global Approval. Drugs. 2016 Jul;76(11):1147–52.

Masotti M, Delprete C, Dothel G, Donadio V, Rimondini R, Politei JM, et al. Altered globotriaosylceramide accumulation and mucosal neuronal fiber density in the colon of the Fabry disease mouse model. Neurogastroenterology & Motility. 2019;31(3):e13529.

Materazzi S, Nassini R, Andrè E, Campi B, Amadesi S, Trevisani M, et al. Cox-dependent fatty acid metabolites cause pain through activation of the irritant receptor TRPA1. Proc Natl Acad Sci USA. 2008 Aug 19;105(33):12045–50.

Matsumoto K, Hosoya T, Tashima K, Namiki T, Murayama T, Horie S. Distribution of transient receptor potential vanilloid 1 channel-expressing nerve fibers in mouse rectal and colonic enteric nervous system: relationship to peptidergic and nitrergic neurons. Neuroscience. 2011 Jan 13;172:518–34.

Matsumoto K, Kurosawa E, Terui H, Hosoya T, Tashima K, Murayama T, et al. Localization of TRPV1 and contractile effect of capsaicin in mouse large intestine: high abundance and sensitivity in rectum and distal colon. Am J Physiol Gastrointest Liver Physiol. 2009 Aug;297(2):G348-360.

Matta JA, Ahern GP. Voltage is a partial activator of rat thermosensitive TRP channels. J Physiol (Lond). 2007 Dec 1;585(Pt 2):469–82.

Matthews MR, Cuello AC. Substance P-immunoreactive peripheral branches of sensory neurons innervate guinea pig sympathetic neurons. Proc Natl Acad Sci USA. 1982 Mar;79(5):1668–72.

McClain J, Grubišić V, Fried D, Gomez-Suarez RA, Leinninger GM, Sévigny J, et al. Ca2+ responses in enteric glia are mediated by connexin-43 hemichannels and modulate colonic transit in mice. Gastroenterology. 2014 Feb;146(2):497-507.e1.

McKemy DD, Neuhausser WM, Julius D. Identification of a cold receptor reveals a general role for TRP channels in thermosensation. Nature. 2002 Mar 7;416(6876):52–8.

Mechtler TP, Stary S, Metz TF, De Jesús VR, Greber-Platzer S, Pollak A, et al. Neonatal screening for lysosomal storage disorders: feasibility and incidence from a nationwide study in Austria. Lancet. 2012 Jan 28;379(9813):335–41.

Meissner G (1857) Uber die Nerven der Darmwand. Z. Ration. Med. N. F. 8: 364‑366.

Merat S, Khalili S, Mostajabi P, Ghorbani A, Ansari R, Malekzadeh R. The effect of enteric-coated, delayed-release peppermint oil on irritable bowel syndrome. Dig Dis Sci. 2010 May;55(5):1385–90.

Merrill AH. Sphingolipid and glycosphingolipid metabolic pathways in the era of sphingolipidomics. Chem Rev. 2011 Oct 12;111(10):6387–422.

Mertz KD, Weisheit G, Schilling K, Lüers GH. Electroporation of primary neural cultures: a simple method for directed gene transfer in vitro. Histochem Cell Biol. 2002 Dec;118(6):501–6.

Meseguer V, Alpizar YA, Luis E, Tajada S, Denlinger B, Fajardo O, et al. TRPA1 channels mediate acute neurogenic inflammation and pain produced by bacterial endotoxins. Nat Commun. 2014;5:3125.

Michael GJ, Priestley JV. Differential expression of the mRNA for the vanilloid receptor subtype 1 in cells of the adult rat dorsal root and nodose ganglia and its downregulation by axotomy. J Neurosci. 1999 Mar 1;19(5):1844–54.

Miller JJ, Aoki K, Moehring F, Murphy CA, O'Hara CL, Tiemeyer M, et al. Neuropathic pain in a Fabry disease rat model. JCI Insight. 2018 22;3(6).

Möhrenschlager M, Braun-Falco M, Ring J, Abeck D. Fabry disease: recognition and management of cutaneous manifestations. Am J Clin Dermatol. 2003;4(3):189–96.

Morales-Soto W, Gulbransen BD. Enteric Glia: A New Player in Abdominal Pain. Cell Mol Gastroenterol Hepatol. 2019;7(2):433-445.

Morrone A, Cavicchi C, Bardelli T, Antuzzi D, Parini R, Di Rocco M, et al. Fabry disease: molecular studies in Italian patients and X inactivation analysis in manifesting carriers. J Med Genet. 2003 Aug;40(8):e103.

Müller MJ. Neuropsychiatric and psychosocial aspects of Fabry disease. In: Mehta A, Beck M, Sunder-Plassmann G, editors. Fabry Disease: Perspectives from 5 Years of FOS [Internet]. Oxford: Oxford PharmaGenesis; 2006 [cited 2019 Oct 16]. Available from: http://www.ncbi.nlm.nih.gov/books/NBK11618/

Nagahama M, Semba R, Tsuzuki M, Aoki E. L-arginine immunoreactive enteric glial cells in the enteric nervous system of rat ileum. Biol Signals Recept. 2001 Oct;10(5):336–40.

Nagao Y, Nakashima H, Fukuhara Y, Shimmoto M, Oshima A, Ikari Y, et al. Hypertrophic cardiomyopathy in late-onset variant of Fabry disease with high residual activity of alpha-galactosidase A. Clin Genet. 1991 Mar;39(3):233–7.

Nakao S, Kodama C, Takenaka T, Tanaka A, Yasumoto Y, Yoshida A, et al. Fabry disease: detection of undiagnosed hemodialysis patients and identification of a "renal variant" phenotype. Kidney Int. 2003 Sep;64(3):801–7.

Nakao S, Takenaka T, Maeda M, Kodama C, Tanaka A, Tahara M, et al. An atypical variant of Fabry's disease in men with left ventricular hypertrophy. N Engl J Med. 1995 Aug 3;333(5):288–93.

Naleschinski D, Arning K, Baron R. Fabry disease--pain doctors have to find the missing ones. Pain. 2009 Sep;145(1–2):10–1.

Namdar M, Gebhard C, Studiger R, Shi Y, Mocharla P, Schmied C, et al. Globotriaosylsphingosine accumulation and not alpha-galactosidase-A deficiency causes endothelial dysfunction in Fabry disease. PLoS ONE. 2012;7(4):e36373.

Namer B, Ørstavik K, Schmidt R, Mair N, Kleggetveit IP, Zeidler M, et al. Changes in Ionic Conductance Signature of Nociceptive Neurons Underlying Fabry Disease Phenotype. Front Neurol. 2017;8:335.

Nasser Y, Fernandez E, Keenan CM, Ho W, Oland LD, Tibbles LA, et al. Role of enteric glia in intestinal physiology: effects of the gliotoxin fluorocitrate on motor and secretory function. Am J Physiol Gastrointest Liver Physiol. 2006 Nov;291(5):G912-927.

National Institute of Health (NIH), Genetics home reference, GLA gene, 2019 [Internet]. [cited 2019 Oct 14]. Available from: https://ghr.nlm.nih.gov/gene/GLA.

NCT03454893 - Open-Label, Study Of Efficacy and Safety Of AVR-RD-01 for Treatment -Naive Subjects With Classic Fabry Disease - Full Text View - ClinicalTrials.gov [Internet]. [cited 2019 Oct 16]. Available from: https://clinicaltrials.gov/ct2/show/NCT03454893.

Ness TJ, Gebhart GF. Colorectal distension as a noxious visceral stimulus: physiologic and pharmacologic characterization of pseudaffective reflexes in the rat. Brain Res. 1988 May 31;450(1–2):153–69.

Ness TJ, Gebhart GF. Visceral pain: a review of experimental studies. Pain. 1990 May;41(2):167–234.

Neunlist M, Rolli-Derkinderen M, Latorre R, Van Landeghem L, Coron E, Derkinderen P, et al. Enteric glial cells: recent developments and future directions. Gastroenterology. 2014 Dec;147(6):1230–7.

Nguyen TLA, Vieira-Silva S, Liston A, Raes J. How informative is the mouse for human gut microbiota research? Dis Model Mech. 2015 Jan;8(1):1–16.

NIH, ClinicalTrials.gov, Interventional Studies Fabry disease, 2019 [Internet]. [cited 2019 Oct 16]. Available from: https://clinicaltrials.gov/ct2/results?cond=Fabry+Disease&Search=Apply&age_v=&gndr=&type=Intr&rslt=.

Nilius B, Owsianik G, Voets T, Peters JA. Transient receptor potential cation channels in disease.

Physiol Rev. 2007 Jan;87(1):165–217.

Nozawa K, Kawabata-Shoda E, Doihara H, Kojima R, Okada H, Mochizuki S, et al. TRPA1 regulates gastrointestinal motility through serotonin release from enterochromaffin cells. Proc Natl Acad Sci USA. 2009 Mar 3;106(9):3408–13.

O'Brien BD, Shnitka TK, McDougall R, Walker K, Costopoulos L, Lentle B, et al. Pathophysiologic and ultrastructural basis for intestinal symptoms in Fabry's disease. Gastroenterology. 1982 May;82(5 Pt 1):957–62.

O'Brien JS, Bernett J, Veath ML, Paa D. Lysosomal Storage Disorders: Diagnosis by Ultrastructural Examination of Skin Biopsy Specimens. Arch Neurol. 1975 Sep 1;32(9):592–9.

Ohshima T, Murray GJ, Swaim WD, Longenecker G, Quirk JM, Cardarelli CO, et al. alpha-Galactosidase A deficient mice: a model of Fabry disease. Proc Natl Acad Sci USA. 1997 Mar 18;94(6):2540–4.

Ohshima T, Ward JM, Huh CG, Longenecker G, Veeranna null, Pant HC, et al. Targeted disruption of the cyclin-dependent kinase 5 gene results in abnormal corticogenesis, neuronal pathology and perinatal death. Proc Natl Acad Sci USA. 1996 Oct 1;93(20):11173–8.

Olsson C, Chen BN, Jones S, Chataway TK, Costa M, Brookes SJH. Comparison of extrinsic efferent innervation of guinea pig distal colon and rectum. J Comp Neurol. 2006 Jun 20;496(6):787–801.

Orteu CH, Jansen T, Lidove O, Jaussaud R, Hughes DA, Pintos-Morell G, et al. Fabry disease and the skin: data from FOS, the Fabry outcome survey. Br J Dermatol. 2007 Aug;157(2):331–7.

Ortiz A, Germain DP, Desnick RJ, Politei J, Mauer M, Burlina A, et al. Fabry disease revisited: Management and treatment recommendations for adult patients. Mol Genet Metab. 2018;123(4):416–27.

Pabst O, Herbrand H, Worbs T, Friedrichsen M, Yan S, Hoffmann MW, et al. Cryptopatches and isolated lymphoid follicles: dynamic lymphoid tissues dispensable for the generation of intraepithelial lymphocytes. Eur J Immunol. 2005 Jan;35(1):98–107.

Page AJ, Martin CM, Blackshaw LA. Vagal mechanoreceptors and chemoreceptors in mouse stomach and esophagus. J Neurophysiol. 2002 Apr;87(4):2095–103.

Parenti G, Andria G, Valenzano KJ. Pharmacological Chaperone Therapy: Preclinical Development, Clinical Translation, and Prospects for the Treatment of Lysosomal Storage Disorders. Mol Ther. 2015 Jul;23(7):1138–48.

Parenti G, Pignata C, Vajro P, Salerno M. New strategies for the treatment of lysosomal storage diseases (review). Int J Mol Med. 2013 Jan;31(1):11–20.

Park JL, Shu L, Shayman JA. Differential involvement of COX1 and COX2 in the vasculopathy associated with the alpha-galactosidase A-knockout mouse. Am J Physiol Heart Circ Physiol. 2009 Apr;296(4):H1133-1140.

Pathway medicine, gastrointestinal medicine, GI tract histology [Internet]. [cited 2019 Oct 16]. Available from: http://www.pathwaymedicine.org/gi-tract-histology.

Patterson LM, Zheng H, Ward SM, Berthoud H-R. Vanilloid receptor (VR1) expression in vagal

afferent neurons innervating the gastrointestinal tract. Cell Tissue Res. 2003 Mar;311(3):277–87.

Peier AM, Moqrich A, Hergarden AC, Reeve AJ, Andersson DA, Story GM, Earley TJ, Dragoni I, McIntyre P, Bevan S, Patapoutian A. A TRP channel that senses cold stimuli and menthol. *Cell* 108:705–715, 2002.

Penati R, Fumagalli F, Calbi V, Bernardo ME, Aiuti A. Gene therapy for lysosomal storage disorders: recent advances for metachromatic leukodystrophy and mucopolysaccaridosis I. J Inherit Metab Dis. 2017;40(4):543–54.

Pensabene L, Sestito S, Nicoletti A, Graziano F, Strisciuglio P, Concolino D. Gastrointestinal Symptoms of Patients with Fabry Disease. Gastroenterol Res Pract. 2016;2016:9712831.

Penuelas A, Tashima K, Tsuchiya S, Matsumoto K, Nakamura T, Horie S, et al. Contractile effect of TRPA1 receptor agonists in the isolated mouse intestine. Eur J Pharmacol. 2007 Dec 8;576(1–3):143–50.

Pereira CS, Azevedo O, Maia ML, Dias AF, Sa-Miranda C, Macedo MF. Invariant natural killer T cells are phenotypically and functionally altered in Fabry disease. Mol Genet Metab. 2013 Apr;108(4):241–8.

Politei J, Durand C, Schenone AB, Torres A, Mukdsi J, Thurberg BL. Chronic intestinal pseudo-obstruction. Did you search for lysosomal storage diseases? Mol Genet Metab Rep. 2017 Jun;11:8–11.

Politei J, Thurberg BL, Wallace E, Warnock D, Serebrinsky G, Durand C, et al. Gastrointestinal involvement in Fabry disease. So important, yet often neglected. Clin Genet. 2016 Jan;89(1):5–9.

Politei JM, Durand C, Schenone AB. Small Fiber Neuropathy in Fabry Disease: a Review of Pathophysiology and Treatment. Journal of Inborn Errors of Metabolism and Screening. 2016 Jan 1;4:2326409816661351.

Pompolo S, Furness JB. Origins of synaptic inputs to calretinin immunoreactive neurons in the guinea-pig small intestine. J Neurocytol. 1993 Jul;22(7):531–46.

Portbury AL, Pompolo S, Furness JB, Stebbing MJ, Kunze WA, Bornstein JC, et al. Cholinergic, somatostatin-immunoreactive interneurons in the guinea pig intestine: morphology, ultrastructure, connections and projections. J Anat. 1995 Oct;187 (Pt 2):303–21.

Porter AJ, Wattchow DA, Brookes SJ, Costa M. Projections of nitric oxide synthase and vasoactive intestinal polypeptide-reactive submucosal neurons in the human colon. J Gastroenterol Hepatol. 1999 Dec;14(12):1180–7.

Powley TL, Phillips RJ. Vagal intramuscular array afferents form complexes with interstitial cells of Cajal in gastrointestinal smooth muscle: analogues of muscle spindle organs? Neuroscience. 2011 Jul 14;186:188–200.

Powley TL, Spaulding RA, Haglof SA. Vagal afferent innervation of the proximal gastrointestinal tract mucosa: chemoreceptor and mechanoreceptor architecture. J Comp Neurol. 2011 Mar 1;519(4):644–60.

Qin H, Luo J, Qi S, Xu H, Sung JJY, Bian Z. Visceral hypersensitivity induced by activation of transient receptor potential vanilloid type 1 is mediated through the serotonin pathway in rat colon.

Eur J Pharmacol. 2010 Nov 25;647(1–3):75–83.

Rajasekhar P, Poole DP, Liedtke W, Bunnett NW, Veldhuis NA. P2Y1 Receptor Activation of the TRPV4 Ion Channel Enhances Purinergic Signaling in Satellite Glial Cells. J Biol Chem. 2015 Nov 27;290(48):29051-62.

Ramaswami U, Najafian B, Schieppati A, Mauer M, Bichet DG. Assessment of renal pathology and dysfunction in children with Fabry disease. Clin J Am Soc Nephrol. 2010 Feb;5(2):365–70.

Ramaswami U, Whybra C, Parini R, Pintos-Morell G, Mehta A, Sunder-Plassmann G, et al. Clinical manifestations of Fabry disease in children: data from the Fabry Outcome Survey. Acta Paediatr. 2006 Jan;95(1):86–92.

Richardson KC. Electronmicroscopic observations on Auerbach's plexus in the rabbit, with special reference to the problem of smooth muscle innervation. Am J Anat. 1958 Jul;103(1):99–135.

Ries M, Gupta S, Moore DF, Sachdev V, Quirk JM, Murray GJ, et al. Pediatric Fabry disease. Pediatrics. 2005 Mar;115(3):e344-355.

Ries M, Ramaswami U, Parini R, Lindblad B, Whybra C, Willers I, et al. The early clinical phenotype of Fabry disease: a study on 35 European children and adolescents. Eur J Pediatr. 2003 Nov;162(11):767–72.

Ritchie J. Pain from distension of the pelvic colon by inflating a balloon in the irritable colon syndrome. Gut. 1973 Feb;14(2):125–32.

Robinson DR, McNaughton PA, Evans ML, Hicks GA. Characterization of the primary spinal afferent innervation of the mouse colon using retrograde labelling. Neurogastroenterol Motil. 2004 Feb;16(1):113–24.

Rodrigues LG, Ferraz MJ, Rodrigues D, Pais-Vieira M, Lima D, Brady RO, et al. Neurophysiological, behavioral and morphological abnormalities in the Fabry knockout mice. Neurobiol Dis. 2009 Jan;33(1):48–56.

Rombach SM, Twickler TB, Aerts JMFG, Linthorst GE, Wijburg FA, Hollak CEM. Vasculopathy in patients with Fabry disease: current controversies and research directions. Mol Genet Metab. 2010 Feb;99(2):99–108.

Rong W, Hillsley K, Davis JB, Hicks G, Winchester WJ, Grundy D. Jejunal afferent nerve sensitivity in wild-type and TRPV1 knockout mice. J Physiol (Lond). 2004 Nov 1;560(Pt 3):867–81.

Rozenfeld P, Feriozzi S. Contribution of inflammatory pathways to Fabry disease pathogenesis. Mol Genet Metab. 2017;122(3):19–27.

Rozenfeld PA. Fabry disease: treatment and diagnosis. IUBMB Life. 2009 Nov;61(11):1043–50.

Ryu V, Gallaher Z, Czaja K. Plasticity of nodose ganglion neurons after capsaicin- and vagotomy-induced nerve damage in adult rats. Neuroscience. 2010 Jun 2;167(4):1227–38.

Sakuraba H, Murata-Ohsawa M, Kawashima I, Tajima Y, Kotani M, Ohshima T, et al. Comparison of the effects of agalsidase alfa and agalsidase beta on cultured human Fabry fibroblasts and Fabry mice. J Hum Genet. 2006;51(3):180–8.

Sanchez-Niño MD, Carpio D, Sanz AB, Ruiz-Ortega M, Mezzano S, Ortiz A. Lyso-Gb3 activates Notch1 in human podocytes. Hum Mol Genet. 2015 Oct 15;24(20):5720–32.

Sanders KM, Smith TK. Motoneurones of the submucous plexus regulate electrical activity of the circular muscle of canine proximal colon. J Physiol (Lond). 1986 Nov;380:293–310.

Sands MS, Davidson BL. Gene therapy for lysosomal storage diseases. Mol Ther. 2006 May;13(5):839–49.

Savidge TC, Newman P, Pothoulakis C, Ruhl A, Neunlist M, Bourreille A, et al. Enteric glia regulate intestinal barrier function and inflammation via release of S-nitrosoglutathione. Gastroenterology. 2007 Apr;132(4):1344–58.

Schicho R, Florian W, Liebmann I, Holzer P, Lippe IT. Increased expression of TRPV1 receptor in dorsal root ganglia by acid insult of the rat gastric mucosa. Eur J Neurosci. 2004 Apr;19(7):1811–8.

Schiffmann R, Pastores GM, Lien Y-HH, Castaneda V, Chang P, Martin R, et al. Agalsidase alfa in pediatric patients with Fabry disease: a 6.5-year open-label follow-up study. Orphanet J Rare Dis. 2014 Nov 26;9:169.

Schiffmann R, Scott LJC. Pathophysiology and assessment of neuropathic pain in Fabry disease. Acta Paediatrica. 2002;91(s439):48–52.

Schwartz CJ, Kimberg DV, Sheerin HE, Field M, Said SI. Vasoactive intestinal peptide stimulation of adenylate cyclase and active electrolyte secretion in intestinal mucosa. J Clin Invest. 1974 Sep;54(3):536–44.

Scudamore, C.L. A Practical Guide to the Histology of the Mouse. Chapter 3, Gastrointestinal system. 43-62, 2014.

Sengupta JN, Snider A, Su X, Gebhart GF. Effects of kappa opioids in the inflamed rat colon. Pain. 1999 Feb;79(2–3):175–85.

Sessa A, Meroni M, Battini G, Maglio A, Brambilla PL, Bertella M, et al. Renal pathological changes in Fabry disease. J Inherit Metab Dis. 2001;24 Suppl 2:66–70; discussion 65.

Shabbeer J, Robinson M, Desnick RJ. Detection of alpha-galactosidase a mutations causing Fabry disease by denaturing high performance liquid chromatography. Hum Mutat. 2005 Mar;25(3):299-305.

Shelley ED, Shelley WB, Kurczynski TW. Painful fingers, heat intolerance, and telangiectases of the ear: easily ignored childhood signs of Fabry disease. Pediatr Dermatol. 1995 Sep;12(3):215–9.

Sheth KJ, Good TA, Murphy JV. Heterozygote detection in Fabry disease utilizing multiple enzyme activities. Am J Med Genet. 1981;10(2):141–6.

Sheth KJ, Swick HM. Peripheral nerve conduction in Fabry disease. Ann Neurol. 1980 Apr;7(4):319–23.

Sheth KJ, Werlin SL, Freeman ME, Hodach AE. Gastrointestinal structure and function in Fabry's disease. Am J Gastroenterol. 1981 Sep;76(3):246–51.

Simmons, D. (2008) The use of animal models in studying genetic disease: transgenesis and induced

mutation. Nature Education 1(1):70

Sodi A, Ioannidis AS, Mehta A, Davey C, Beck M, Pitz S. Ocular manifestations of Fabry's disease: data from the Fabry Outcome Survey. Br J Ophthalmol. 2007 Feb;91(2):210–4.

Soldano A, Alpizar YA, Boonen B, Franco L, López-Requena A, Liu G, et al. Gustatory-mediated avoidance of bacterial lipopolysaccharides via TRPA1 activation in Drosophila. Elife. 2016 14;5.

Soret R, Coquenlorge S, Cossais F, Meurette G, Rolli-Derkinderen M, Neunlist M. Characterization of human, mouse, and rat cultures of enteric glial cells and their effect on intestinal epithelial cells. Neurogastroenterol Motil. 2013 Nov;25(11):e755-764.

Spada M, Pagliardini S, Yasuda M, Tukel T, Thiagarajan G, Sakuraba H, et al. High Incidence of Later-Onset Fabry Disease Revealed by Newborn Screening. Am J Hum Genet. 2006 Jul;79(1):31–40.

Spencer NJ, Kyloh M, Duffield M. Identification of different types of spinal afferent nerve endings that encode noxious and innocuous stimuli in the large intestine using a novel anterograde tracing technique. PLoS ONE. 2014;9(11):e112466.

Stenson et al. (2017) The Human Gene Mutation Database: towards a comprehensive repository of inherited mutation data for medical research, genetic diagnosis and next-generation sequencing studies. Hum Genet 136:665-677.

Story GM, Peier AM, Reeve AJ, Eid SR, Mosbacher J, Hricik TR, et al. ANKTM1, a TRP-like channel expressed in nociceptive neurons, is activated by cold temperatures. Cell. 2003 Mar 21;112(6):819–29.

Strotmann R, Harteneck C, Nunnenmacher K, Schultz G, Plant TD. OTRPC4, a nonselective cation channel that confers sensitivity to extracellular osmolarity. Nat Cell Biol. 2000 Oct;2(10):695–702.

Sugiuar T, Bielefeldt K, Gebhart GF. TRPV1 function in mouse colon sensory neurons is enhanced by metabotropic 5-hydroxytryptamine receptor activation. J Neurosci. 2004 Oct 27;24(43):9521–30.

Suzuki M, Mizuno A, Kodaira K, Imai M. Impaired pressure sensation in mice lacking TRPV4. J Biol Chem. 2003 Jun 20;278(25):22664–8.

Suzuki M, Watanabe Y, Oyama Y, Mizuno A, Kusano E, Hirao A, et al. Localization of mechanosensitive channel TRPV4 in mouse skin. Neurosci Lett. 2003 Dec 26;353(3):189–92.

Svedlund J, Sjödin I, Dotevall G. GSRS--a clinical rating scale for gastrointestinal symptoms in patients with irritable bowel syndrome and peptic ulcer disease. Dig Dis Sci. 1988 Feb;33(2):129–34.

Taga S, Carlier K, Mishal Z, Capoulade C, Mangeney M, Lécluse Y, et al. Intracellular signaling events in CD77-mediated apoptosis of Burkitt's lymphoma cells. Blood. 1997 Oct 1;90(7):2757–67.

Tan LL, Bornstein JC, Anderson CR. Distinct chemical classes of medium-sized transient receptor potential channel vanilloid 1-immunoreactive dorsal root ganglion neurons innervate the adult mouse jejunum and colon. Neuroscience. 2008 Oct 2;156(2):334–43.

Tan LL, Bornstein JC, Anderson CR. Neurochemical and morphological phenotypes of vagal afferent neurons innervating the adult mouse jejunum. Neurogastroenterol Motil. 2009 Sep;21(9):994–1001.

Tielemans MM, Jaspers Focks J, van Rossum LGM, Eikendal T, Jansen JBMJ, Laheij RJF, et al. Gastrointestinal symptoms are still prevalent and negatively impact health-related quality of life: a large cross-sectional population based study in The Netherlands. PLoS ONE. 2013;8(7):e69876.

Timmermans JP, Adriaensen D, Cornelissen W, Scheuermann DW. Structural organization and neuropeptide distribution in the mammalian enteric nervous system, with special attention to those components involved in mucosal reflexes. Comp Biochem Physiol A Physiol. 1997 Oct;118(2):331–40.

Timmermans JP, Barbiers M, Scheuermann DW, Stach W, Adriaensen D, Mayer B, et al. Distribution pattern, neurochemical features and projections of nitrergic neurons in the pig small intestine. Ann Anat. 1994 Dec;176(6):515–25.

Timmermans JP, Hens J, Adriaensen D. Outer submucous plexus: an intrinsic nerve network involved in both secretory and motility processes in the intestine of large mammals and humans. Anat Rec. 2001 01;262(1):71–8.

Tobin JM, Delbridge LMD, Di Nicolantonio R, Bhathal P. Development of colorectal sensitization is associated with increased eosinophils and mast cells in dextran sulfate sodium-treated rats. Dig Dis Sci. 2004 Aug;49(7–8):1302–10.

Tokuda Y, Takahashi O, Ohde S, Shakudo M, Yanai H, Shimbo T, et al. Gastrointestinal symptoms in a Japanese population: a health diary study. World J Gastroenterol. 2007 Jan 28;13(4):572–8.

Tomé FM, Fardeau M, Lenoir G. Ultrastructure of muscle and sensory nerve in Fabry's disease. Acta Neuropathol. 1977 Jun 15;38(3):187–94.

Tominaga M, Caterina MJ, Malmberg AB, Rosen TA, Gilbert H, Skinner K, et al. The cloned capsaicin receptor integrates multiple pain-producing stimuli. Neuron. 1998 Sep;21(3):531–43.

Tøndel C, Bostad L, Hirth A, Svarstad E. Renal biopsy findings in children and adolescents with Fabry disease and minimal albuminuria. Am J Kidney Dis. 2008 May;51(5):767–76.

Tøndel C, Bostad L, Larsen KK, Hirth A, Vikse BE, Houge G, et al. Agalsidase benefits renal histology in young patients with Fabry disease. J Am Soc Nephrol. 2013 Jan;24(1):137–48.

Touboul D, Roy S, Germain DP, Chaminade P, Brunelle A, Laprévote O. MALDI-TOF and cluster-TOF-SIMS imaging of Fabry disease biomarkers. International Journal of Mass Spectrometry. 2007 Feb 1;260(2):158–65.

Toumi F, Neunlist M, Cassagnau E, Parois S, Laboisse CL, Galmiche J-P, et al. Human submucosal neurones regulate intestinal epithelial cell proliferation: evidence from a novel co-culture model. Neurogastroenterol Motil. 2003 Jun;15(3):239–42.

Treuting, P.M., and S.M. Dintzis. '12 - Lower Gastrointestinal Tract'. Comparative Anatomy and Histology, 177–92, 2012.

Tuck MK, Chan DW, Chia D, Godwin AK, Grizzle WE, Krueger KE, et al. Standard Operating Procedures for Serum and Plasma Collection: Early Detection Research Network Consensus Statement Standard Operating Procedure Integration Working Group. J Proteome Res. 2009 Jan;8(1):113–7.

Tuttolomondo A, Pecoraro R, Simonetta I, Miceli S, Pinto A, Licata G. Anderson-Fabry disease: a

multiorgan disease. Curr Pharm Des. 2013;19(33):5974–96.

Üçeyler N, Biko L, Hose D, Hofmann L, Sommer C. Comprehensive and differential long-term characterization of the alpha-galactosidase A deficient mouse model of Fabry disease focusing on the sensory system and pain development. Mol Pain. 2016;12.

Üçeyler N, Ganendiran S, Kramer D, Sommer C. Characterization of pain in Fabry disease. Clin J Pain 2014;30:915–920.

Üçeyler N, Kahn AK, Kramer D, et al. Impaired small fiber conduction in patients with Fabry disease: A neurophysiological case-control study. BMC Neurol 2013;13:47.

Üçeyler N, He L, Schönfeld D, Kahn A-K, Reiners K, Hilz MJ, et al. Small fibers in Fabry disease: baseline and follow-up data under enzyme replacement therapy. Journal of the Peripheral Nervous System. 2011;16(4):304–14.

Valbuena C, Leitão D, Carneiro F, Oliveira JP. Immunohistochemical diagnosis of Fabry nephropathy and localisation of globotriaosylceramide deposits in paraffin-embedded kidney tissue sections. Virchows Arch. 2012 Feb;460(2):211–21.

van den Wijngaard RM, Klooker TK, Welting O, Stanisor OI, Wouters MM, van der Coelen D, et al. Essential role for TRPV1 in stress-induced (mast cell-dependent) colonic hypersensitivity in maternally separated rats. Neurogastroenterol Motil. 2009 Oct;21(10):1107-e94.

Van Landeghem L, Chevalier J, Mahé MM, Wedel T, Urvil P, Derkinderen P, et al. Enteric glia promote intestinal mucosal healing via activation of focal adhesion kinase and release of proEGF. Am J Physiol Gastrointest Liver Physiol. 2011 Jun;300(6):G976–87.

van Wanrooij SJM, Wouters MM, Van Oudenhove L, Vanbrabant W, Mondelaers S, Kollmann P, et al. Sensitivity testing in irritable bowel syndrome with rectal capsaicin stimulations: role of TRPV1 upregulation and sensitization in visceral hypersensitivity? Am J Gastroenterol. 2014 Jan;109(1):99–109.

Van Wayjen RG. [Enterocolitis as a symptom of angiokeratoma corporis diffusum (Ruiter-Pompen-Wyers-Kühnau thesaurismosis)]. Ned Tijdschr Geneeskd. 1958 Sep 27;102(39):1941–3.

Vedder AC, Linthorst GE, Houge G, Groener JEM, Ormel EE, Bouma BJ, et al. Treatment of Fabry disease: outcome of a comparative trial with agalsidase alfa or beta at a dose of 0.2 mg/kg. PLoS ONE. 2007 Jul 11;2(7):e598.

von Scheidt W, Eng CM, Fitzmaurice TF, Erdmann E, Hübner G, Olsen EG, et al. An atypical variant of Fabry's disease with manifestations confined to the myocardium. N Engl J Med. 1991 Feb 7;324(6):395–9.

Vriens J, Owsianik G, Fisslthaler B, Suzuki M, Janssens A, Voets T, et al. Modulation of the Ca2 permeable cation channel TRPV4 by cytochrome P450 epoxygenases in vascular endothelium. Circ Res. 2005 Oct 28;97(9):908–15.

Wallace JL, Keenan CM. An orally active inhibitor of leukotriene synthesis accelerates healing in a rat model of colitis. Am J Physiol. 1990 Apr;258(4 Pt 1):G527-534.

Wang FB, Powley TL. Topographic inventories of vagal afferents in gastrointestinal muscle. J Comp Neurol. 2000 Jun 5;421(3):302–24.

Wanner C, Arad M, Baron R, Burlina A, Elliott PM, Feldt-Rasmussen U, et al. European expert consensus statement on therapeutic goals in Fabry disease. Mol Genet Metab. 2018;124(3):189–203.

Ward SM, Bayguinov J, Won K-J, Grundy D, Berthoud HR. Distribution of the vanilloid receptor (VR1) in the gastrointestinal tract. J Comp Neurol. 2003 Oct 6;465(1):121–35.

Watanabe H, Davis JB, Smart D, Jerman JC, Smith GD, Hayes P, et al. Activation of TRPV4 channels (hVRL-2/mTRP12) by phorbol derivatives. J Biol Chem. 2002 Apr 19;277(16):13569–77.

Watanabe H, Vriens J, Prenen J, Droogmans G, Voets T, Nilius B. Anandamide and arachidonic acid use epoxyeicosatrienoic acids to activate TRPV4 channels. Nature. 2003 Jul 24;424(6947):434–8.

Watanabe H, Vriens J, Suh SH, Benham CD, Droogmans G, Nilius B. Heat-evoked activation of TRPV4 channels in a HEK293 cell expression system and in native mouse aorta endothelial cells. J Biol Chem. 2002 Dec 6;277(49):47044–51.

Weidemann F, Sanchez-Niño MD, Politei J, Oliveira J-P, Wanner C, Warnock DG, et al. Fibrosis: a key feature of Fabry disease with potential therapeutic implications. Orphanet J Rare Dis. 2013 Aug 6;8:116.

Wilcox WR, Oliveira JP, Hopkin RJ, Ortiz A, Banikazemi M, Feldt-Rasmussen U, et al. Females with Fabry disease frequently have major organ involvement: lessons from the Fabry Registry. Mol Genet Metab. 2008 Feb;93(2):112–28.

Wittmann J, Karg E, Turi S, Legnini E, Wittmann G, Giese A-K, et al. Newborn Screening for Lysosomal Storage Disorders in Hungary. JIMD Rep. 2012 Mar 21;6:117–25.

Wouters MM, Balemans D, Van Wanrooy S, Dooley J, Cibert-Goton V, Alpizar YA, et al. Histamine Receptor H1-Mediated Sensitization of TRPV1 Mediates Visceral Hypersensitivity and Symptoms in Patients With Irritable Bowel Syndrome. Gastroenterology. 2016 Apr;150(4):875-887.e9.

Wraith JE, Tylki-Szymanska A, Guffon N, Lien YH, Tsimaratos M, Vellodi A, et al. Safety and efficacy of enzyme replacement therapy with agalsidase beta: an international, open-label study in pediatric patients with Fabry disease. J Pediatr. 2008 Apr;152(4):563–70, 570.e1.

Wu L-J, Sweet T-B, Clapham DE. International Union of Basic and Clinical Pharmacology. LXXVI. Current progress in the mammalian TRP ion channel family. Pharmacol Rev. 2010 Sep;62(3):381–404.

Xu F, Satoh E, Iijima T. Protein kinase C-mediated Ca2+ entry in HEK 293 cells transiently expressing human TRPV4. Br J Pharmacol. 2003 Sep;140(2):413–21.

Yam GH-F, Zuber C, Roth J. A synthetic chaperone corrects the trafficking defect and disease phenotype in a protein misfolding disorder. FASEB J. 2005 Jan;19(1):12–8.

Yamamoto M, Nishiyama M, Iizuka S, Suzuki S, Suzuki N, Aiso S, Nakahara J. Transient receptor potential vanilloid 1-immunoreactive signals in murine enteric glial cells. World J Gastroenterol. 2016 Nov 28;22(44):9752-9764.

Yamashita T, Wada R, Sasaki T, Deng C, Bierfreund U, Sandhoff K, et al. A vital role for glycosphingolipid synthesis during development and differentiation. Proc Natl Acad Sci USA. 1999 Aug 3;96(16):9142–7.

Yiangou Y, Facer P, Dyer NH, Chan CL, Knowles C, Williams NS, et al. Vanilloid receptor 1 immunoreactivity in inflamed human bowel. Lancet. 2001 Apr 28;357(9265):1338–9.

Young HM, Bergner AJ, Müller T. Acquisition of neuronal and glial markers by neural crest-derived cells in the mouse intestine. J Comp Neurol. 2003 Jan 27;456(1):1–11.

Young HM, Furness JB. Ultrastructural examination of the targets of serotonin-immunoreactive descending interneurons in the guinea pig small intestine. J Comp Neurol. 1995 May 22;356(1):101–14.

Zagorodnyuk VP, Chen BN, Brookes SJ. Intraganglionic laminar endings are mechano-transduction sites of vagal tension receptors in the guinea-pig stomach. J Physiol (Lond). 2001 Jul 1;534(Pt 1):255–68.

Zagorodnyuk VP, Chen BN, Costa M, Brookes SJH. Mechanotransduction by intraganglionic laminar endings of vagal tension receptors in the guinea-pig oesophagus. J Physiol (Lond). 2003 Dec 1;553(Pt 2):575–87.

Zagorodnyuk VP, Kyloh M, Nicholas S, Peiris H, Brookes SJ, Chen BN, et al. Loss of visceral pain following colorectal distension in an endothelin-3 deficient mouse model of Hirschsprung's disease. J Physiol (Lond). 2011 Apr 1;589(Pt 7):1691–706.

Zagorodnyuk VP, Lynn P, Costa M, Brookes SJH. Mechanisms of mechanotransduction by specialized low-threshold mechanoreceptors in the guinea pig rectum. Am J Physiol Gastrointest Liver Physiol. 2005 Sep;289(3):G397-406.

Zarate YA, Hopkin RJ. Fabry's disease. Lancet. 2008 Oct 18;372(9647):1427–35.

Zar-Kessler C, Karaa A, Sims KB, Clarke V, Kuo B. Understanding the gastrointestinal manifestations of Fabry disease: promoting prompt diagnosis. Therap Adv Gastroenterol. 2016 Jul;9(4):626–34.

Zhao H, Sprunger LK, Simasko SM. Expression of transient receptor potential channels and two-pore potassium channels in subtypes of vagal afferent neurons in rat. Am J Physiol Gastrointest Liver Physiol. 2010 Feb;298(2):G212-221.